Spring 1-1-2013

A Proposal for a Unified Process to Improve Probabilistic Ground Snow Loads in the United States Using SNODAS Modeled Weather Station Data

Michael Robert DePaolo
University of Colorado at Boulder, mdepaolo7596@gmail.com

A PROPOSAL FOR A UNIFIED PROCESS TO IMPROVE PROBABILISTIC GROUND SNOW LOADS IN THE UNITED STATES USING SNODAS MODELED WEATHER STATION DATA

By:

MICHAEL ROBERT DEPAOLO

B.S. Civil Engineering, Florida Institute of Technology, 2009

A thesis submitted to the

Faculty of the Graduate School of the

University of Colorado in partial fulfillment

of the requirement for the degree of

Master of Science

Department of Civil, Environmental, & Architectural Engineering

2013

This thesis entitled:

"A Proposal for a Unified Process to Improve Probabilistic Ground Snow Loads in the United States Using SNODAS Modeled Weather Station Data"

written by Michael Robert DePaolo has been approved for the

Department of Civil, Environmental, and Architectural Engineering

_____

Abbie Liel (Advisor)

_____

George Hearn

_____

James Harris

Date: _____

The final copy of this thesis has been examined by the signatories, and we find that both the content and the form meet acceptable presentation standards of scholarly work in the above mentioned discipline

DePaolo, Michael Robert (M.S. Department of Civil, Environmental, & Architectural Engineering)

A Proposal for a Unified Process to Improve Probabilistic Ground Snow Loads in the United States Using SNODAS Modeled Weather Station Data

Thesis directed by Professor Abbie B. Liel

ABSTRACT

Snow loads govern roof design in many parts of the United States. These loads are largely prescribed by the American Society of Civil Engineers ASCE 7 Standard for minimum design loads. Where ASCE 7 does not specify snow loads due to extreme local variability, such as in the West, many state jurisdictions have developed individual roof snow load documents and maps. However, among the western states border discrepancies and a general lack of uniformity in the methodology for developing such loads indicates a need for a unified approach.

This paper proposes a methodology to develop ground snow loads for the western United States, the application of which is illustrated for the state of Colorado. An innovative approach is taken which utilizes a hydrological snowpack model, Snow Data Assimilation System (SNODAS), developed by NOAA. This model provides estimates of ground snow depth and snow water content, easily convertible into loads, at 588 SNODAS weather stations in Colorado. The methodology proposed here then incorporates statistical techniques such as principal component analysis (PCA) and multivariate cluster analyses to regionalize the SNODAS stations by key shared properties. Several types of cluster analyses are evaluated including agglomerative hierarchical clustering (AHC), k-means, and a PCA-based method. Using various statistical and practical measures of quality, a step-wise hybrid method combining both AHC and k-means techniques is found to be the most statistically sound and robust clustering method. A relation-

ship is then developed between ground snow depths and ground snow loads for each cluster of SNODAS weather stations.

This paper proposes the following additional steps. A database of National Weather Service CO-OP stations with snow depth only measurements is gathered for the state of interest. The 50-year ground snow depths are extrapolated by testing the goodness-of-fit of several probability distributions. The ground snow depth-load relationships for each cluster produced by the hybrid method are then coupled with these 50-year ground snow depths to produce 50-year ground snow loads. Finally, these ground snow loads are mapped in GIS software using a Kriging geostatistical interpolation method to create continuous snow load isolines.

ACKNOWLEDGEMENTS

First and foremost, I would like to express my gratitude for the support my family provided during the writing of this thesis. I constantly relied upon their unyielding encouragement and guidance through some of the trying times of the past year. This work would not have been possible without them. I am truly blessed to have you all as my family. I love you mom, dad, Joey, and Michelle. Thank you for your continued love and support.

Secondly, I would like to thank my research advisor, Dr. Abbie Liel for her tremendous support and guidance throughout this entire process. Her experience and knowledge in snow engineering as well as her professionalism helped me to produce a quality product of which I am extremely proud. I am grateful to have had the opportunity to work with her on this research project and also to contribute to the scientific and engineering communities.

Finally, I would like to thank the members of the Snow Load Committee of the Structural Engineering Association of Colorado. Their contributions, ideas, and general experience with snow loads inspired the development of many components of this work. Specifically, I would like to acknowledge Richard Cunningham for his support and dedication. Working alongside him on this research project as well as current research for the Colorado state snow loads I have learned an incredible amount. I appreciate his generous contributions and advise that were highly influential.

Thank you all for your support in whatever capacity it was provided. It is my hope that this work will lead to great changes to the development of snow loads and eventually improve the safety of infrastructure.

TABLE OF CONTENTS

LIST OF TABLES

LIST OF FIGURES

1.0 DESIGN SNOW LOADS

1.1 Current State of Design Snow Loads

Snow loads govern roof design in many parts of the United States, from the Northeast to the high-elevations of the Mountain and Pacific West. The Midwest and West are particularly critical, however, due to extreme variability in snowfall depth and density coupled with the scarcity of snow load research and measurements compared to the Northeastern part of the country.

In the United States ground snow loads, which are the basis for the computation of design roof snow loads, are largely prescribed by a code-adopted standard, ASCE/SEI 7, authored by American Society of Civil Engineers' Structural Engineering Institute. At the time of writing, the current version is the ASCE 7-10 publication. The International Building Code (IBC) published by the International Code Council, which is widely referenced by jurisdictions in the United States, also prescribes ground snow loads among many other building design requirements. Section 1608 of its current version, IBC 2012, refers its user to the ASCE 7 Standard and simply duplicates its ground snow load maps which are used in the computation of roof snow loads (IBC 2009). Therefore, ASCE 7 is the primary national reference for snow loads in the country. State-produced snow load publications will be discussed in Chapter 1.2.

The ASCE 7 ground snow load maps read absolute load in pounds per square foot discretized into regions of loading at designated elevations (ASCE/SEI 2010). Roof snow loads are generated by factoring the ground snow load value to account for roof exposure, roof thermal conditions, slope and other effects. Due to the potential effects of wind, unbalanced snow loads, partial loading, snow drifts, and extra loads from rain on snow, additional modification factors may be required. The resulting roof load is incorporated into applicable load combinations for structural design of roofs. The governing load combination for roof snow loads, per Chapter 2 of

ASCE 7, apply a load factor of 1.6 to the roof snow load for use with LRFD (strength) design such that the ultimate snow load for the design life of the roof is 1.6 times the nominal roof snow load determined from Sections 7.3-7.10. The overall foundation of design roof snow loads, however, hinges on the initial ground snow load values that are modified to obtain these roof loads.

There are various issues with the construction of the ground snow load maps of ASCE 7, particularly for the western United States. A close examination of the snow load maps reveals some peculiarities in the arrangement of ground snow load regions; a portion isolating the state of Colorado is shown in Figure 1.1 (refer to Appendix A for the map in its entirety). As it can be seen, snow load boundaries seem to trace irregularly through the state sometimes resulting in adjacent regions where prescribed loadings are double in value (indicated by the arrow in Figure 1.1). By contrast the ground snow load map of the eastern United States has smooth, continuous contours of increasing load consistent with increasing latitude and elevation (particularly for the Appalachian Mountain Range). According to ASCE 7, the snow loads depicted on the map are only valid at or below the denoted elevation. This specified elevation, shown in parentheses on the map, creates confusion to engineers trying to understand its implications on roof design. Since the topography of many western states is dom-

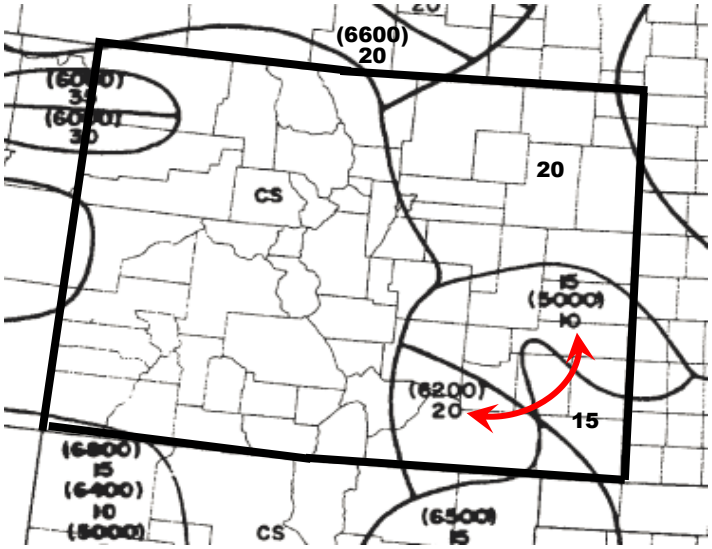

Figure 1.1: Ground Snow Load Contour Map for Colorado (Excerpted from ASCE 7*, Figure 7-1)*

inated by mountain ranges of the West, local elevation variations are prevalent. Therefore within a single snow load region, sites considerably below the specified elevation may be subject to inflated ground snow loads per ASCE 7. For sites above the specified elevation, ASCE 7 requires site-specific case studies to develop ground snow loads. Additionally, the map designates several regions that are labeled 'CS' indicating that extreme variability of snow depths and loads has precluded the official mapping of such regions. In these regions, case studies are also required to develop ground snow loads (ASCE/SEI 2010). Of all the 'CS' regions on the map, the vast majority is in the Mountain and Pacific West.

There are other issues with the construction of the snow load map related to the statistical analysis of the snow load data that supports it. The ASCE 7 commentary on the snow loads section details the measures taken to quantify the mapped ground snow loads. First, concurrent measurements of maximum annual snow depth and snow load were gathered from 204 weather stations where both had been measured for at least 11 years between 1952 and 1992. The same lognormal probability model was used for all stations. At each station, a lognormal distribution was fit to the annual maxima data to determine ground snow depths and a ground snow loads each with a two-percent probability of being exceeded. These two-percent depths and two-percent loads from each station were then plotted together and a nonlinear equation was fitted to them (ASCE/SEI 2010). This equation, developed by Tobiasson and Greatorex (1996), is shown in Eq.(1).

$$P_g = 0.279 \times {h_s}^{1.36} \tag{1}$$

where P_g is the two-percent ground snow load in pounds per square foot and h_s is the two-percent ground snow depth in inches. This equation was used to derive snow loads at approximately 9,200 other weather stations where only snow depth had been recorded. At these stations, the

two-percent ground snow depths were first estimated using the lognormal distribution. These two-percent depths were converted to loads using Eq. (1). Thus, the mapped ground snow loads are all based on a 50-year mean recurrence interval (MRI), equivalent to a two-percent annual probability of being exceeded. Both sets of snow load data (actual measurement sites and derived sites) were plotted on a map of the United States. Regions of equal snow load were drawn by connecting points of equal snow load. Although the ground snow load map represents statistical values, the maximum load at each of the 204 stations was used in *positioning* snow load isolines so as to be representative of most of the encompassed stations (ASCE/SEI 2010). Positioning the ground snow load isolines using the *maximum* values helped to ensure that the map reflected most of the statistical station load values of each snow load region.

According to the commentary, the snow load map is a revision of that published by the 1993 edition of ASCE 7 but has not been changed since the 1995 edition. The snow loads derived at the 9,200 depth-only stations and those measured directly at the 204 weather stations were generally in agreement and all stations had an average of 33 years of records (ASCE/SEI 2010). Where discrepancies did arise, the actual measurements from the 204 weather stations governed. While the general agreement of the two sources does give merit to the snow load development process as a whole, numerous issues can be expected when a single probability model is used throughout the entire country. These issues stem from local meteorological variations throughout the country. These known variations have led many jurisdictions to perform their own case studies of ground snow loads to provide a more detailed analysis for comparison to the mapped ASCE 7 values.

Tobiasson and Greatorex (2000) performed a statewide snow load case study for New Hampshire.[1] A majority of the towns in New Hampshire are within 'CS' regions, so this effort was required to produce ground snow load for those towns. The authors, in association with the Cold Regions Research and Engineering Laboratory (CRREL), collaborated with Structural Engineers of New Hampshire (SENH) to independently develop snow load case studies for every town (Tobiasson, Buska and Greatorex 2000). The engineers performing the case studies first established geographic centers for each of the 140 towns studied along with elevations representative of the tallest building in each town. Six other descriptive elevations within each town were also determined to help develop an elevation-load correction. Data analyzed in the investigation included snow load data from official and non-official sources (*i.e.* airport and voluntary observer stations, respectively), of varying record lengths. The case studies consisted of analyzing graphs of maximum recorded snow load vs. elevation plotted from all available records. For each town two graphs of snow load vs. elevation were analyzed: 1) a plot including only the nearest six to eight snow measurement stations and 2) a plot of all stations within 25 miles plus an official weather station. A snow load-elevation relationship was derived at each town by subjectively evaluating the validity of the two plots and selecting one judged to be representative. Separate teams of engineers from both CRREL and SENH worked on each town, creating linear best-fit relationships between elevation and snow load based on both graphical and analytical methods. The case study forms allowed for individual judgment on several issues such as whether or not to include stations with short records or stations with unusually high recorded maximum snow loads. The results of the study were tabulated values of snow load for each town

[1] Tobiasson and Greatorex (2000) have significantly contributed to ASCE 7 ground snow load maps.

with a corresponding snow load correction factor for high-elevations. Upon completing the case studies, the authors compared the prescribed ASCE 7 mapped ground snow loads, P_g, to the highest snow loads that were ever recorded at each town, P_{max}. The authors noticed several towns with either markedly high or low ratios of P_g to P_{max}. After constructing probability plots for the towns with the high and low ratios, it was clear that the ground snow loads in these towns were being over and under predicted, respectively. After the analysis of the data, the authors described how the lognormal distribution poorly predicted such extremes at either end (Tobiasson, Buska and Greatorex 2000). Since the national map is based on this distribution, this finding calls into question the universal applicability of the ASCE 7 ground snow load map.

1.2 Snow Load Design in the West

Due to the aforementioned 'CS' regions in the western U.S. where ground snow loads are not officially prescribed by ASCE 7, many western states perform individual studies to determine appropriate ground snow loads. In these western states, inclusive of Colorado, Wyoming, Montana, Arizona, Nevada, Utah, Idaho, California, Oregon, and Washington, the Structural Engineering Associations within each state produce their own ground snow load maps with accompanying reports. These state engineering associations use locally available snow data from measuring stations that vary in record length from state to state. Also, each state may have a unique philosophy for extrapolating 50-year ground snow loads including the choice of probability distribution type to fit the data, sources of such data, and consideration of elevation. The following section details the basic methodology used by the western states to determine ground snow loads with an emphasis on the state of Colorado, which is the case study for this investigation.

1.2.1 Ground Snow Loads for Colorado

The Structural Engineers Association of Colorado (SEAC) develops ground snow loads for Colorado. The current version of the snow load report for the state is the 2007 version entitled "Colorado Ground Snow Loads" (SEAC 2007). The information summarized in this section is adapted from that report. SEAC also produced an accompanying ground snow load map, a portion of which is illustrated in Figure 1.2. The ground snow load map in its entirety is available in Appendix B. The minimum state ground snow load is 20 pounds per square foot, which has been incorporated into the analysis and the map construction.

In order to determine ground snow loads, SEAC analyzed numerous sources of ground snow data. SEAC used data from nearly 800 statewide weather measurement stations with at least 12 years of records. These stations include those which only record snow depth as well as those which record concurrent measurement of snow depth and snow load. Weather stations whose records showed predominant snow depths less than 20 inches were eliminated from the analysis since such values generally do not produce loads that are above the minimum state snow load of 20 psf. For analysis, the weather stations were divided into regions above and below an elevation of 8,000 feet, in order to represent both compacted and settled conditions, respectively. Compacted conditions result from several snow events where snow depth accumulates throughout the winter season, while settled conditions result from single snow events with near complete melting in-between. The reason for the division between these regions lies in the mechanics of snowfall and also the seasonal processes of snow accumulation that influence snow density and thus weight. Most notably, compaction due to self-weight of several snow layers from successive storms is the most crucial process that influences density; this process is prevalent in compacted regions and almost nonexistent in settled ones.

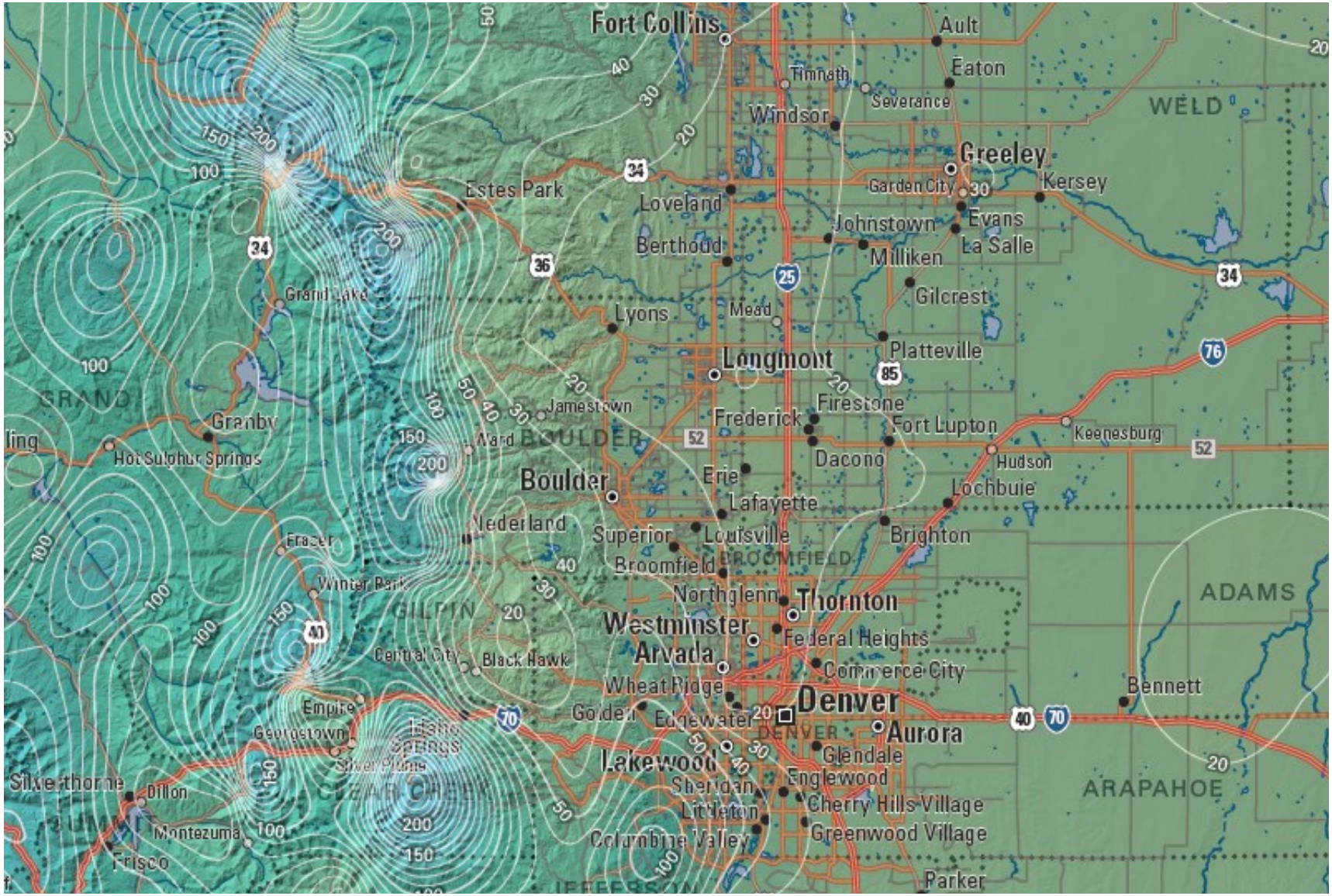

Figure 1.2: Ground Snow Load Map for Colorado: Portion Showing Fort Collins, Boulder, Denver and Vicinity (minimum state ground snow load is 20 psf where not indicated) (SEAC 2007)

For regions of the state where settled snow conditions exist, such as the plains east of the foothills of the Rocky Mountains, the following methodology was used by SEAC. Snow depth data was gathered from roughly 440 NWS CO-OP stations and concurrent snow depth and snow load data was gathered from NWS First Order stations in Denver, Grand Junction, and Pueblo (these station types are defined in Chapter 2.2). The station record lengths for all stations ranged from 1-110 years. The analysis was then divided into two phases: 1) analysis of the snow depth data from the CO-OP stations, and 2) analysis of the concurrent measurements from the First Order stations. For the CO-OP stations, an annual series distribution of maximum snow depths was then extracted, eliminating those with a significant amount of missing data or less than 12 years of measurements. After testing the goodness-of-fit of several probability distribution functions, the Generalized Pareto Distribution (GPD) was chosen to be the best fit for the annual maxima data. Specifically the GPD fit was tested using the Denver station data since this provided the longest record at the time (110 years). Further statistical tests of the GPD revealed that it was the most suitable distribution to use. Using this distribution, 50-year MRI ground snow depths were determined at all of the CO-OP stations.

The NWS First order stations were analyzed to determine a snow depth-snow load relationship. Two of the original three stations (Grand Junction & Pueblo) were eliminated due to absence of sufficiently large snow events in the station records (*i.e.* snow events with greater than 20 inches) leaving the Denver First Order station as the only station used in the analysis. The Denver station has nearly 60 years of simultaneous snow depth and load measurements. A nonlinear power curve was fit to the Denver data using linear regression. The resulting power equation has the following form.

$$P_g = 0.267 \times {h_s}^{1.32} \quad (2)$$

In Eq. (2) P_g is a 50-year ground snow load and h_s is a 50-year ground snow depth.

Eq. (2) was then compared to that used by the ASCE 7 to produce the national ground snow load map, referenced in Eq. (1). Due to the similarity of the two equations, and the more conservative nature of the ASCE 7 depth-load relationship (*i.e.* predicting higher loads for the same depth), the ASCE-7 power equation was chosen. However, the form of the equation was transformed into a format widely used by European snow load committees, namely that used by the Joint Committee for Structural Safety (JCSS). This equation is has the following form:

$$\mathrm{P_g} = \gamma_{\mathrm{s.max}} \times \mathrm{d} \times \ln\left[1 + \frac{\gamma_{\mathrm{s.min}}}{\gamma_{\mathrm{s.max}}}\left(\exp\left(\frac{\mathrm{h_s}}{\mathrm{d}}\right) - 1\right)\right] \quad (3)$$

In Eq. **(3)** $\gamma_{s.\mathrm{min}}$ and $\gamma_{s.max}$ are the minimum and maximum snow densities of the dataset in pounds per cubic foot, respectively. Also, d is a depth parameter determined, along with the density parameters, by using regression analysis of the depth data. The JCSS equation was chosen for its inclusion of site-specific variables such as minimum and maximum snow density. SEAC fit the JCSS equation to the ASCE 7 power equation and the above parameters were estimated using regression analysis. This equation was then applied at all of the CO-OP stations (whose 50-year ground snow depths had been extrapolated using the GPD) in order to compute 50-year ground snow loads at these locations.

For regions of the state where compacted snow conditions exist, such as mountainous regions of the state, the following methodology was used by SEAC. In these regions, SNOTEL

and Snow Course sites provided concurrent snow depth and equivalent snow load measurements[2]. For the analysis of the SNOTEL and Snow Course stations, a relationship between the 50-year depths and 50-year loads was developed, similar to that for the settled snow regions. However, compared to the single First Order station used in that analysis, there are more numerous SNOTEL and Snow Course stations in compacted regions. The same GPD was employed here because it also fit the data well. A nonlinear power curve was then fit to the 50-year loads and depths using linear regression; the resulting relationship is shown in Eq. (4):

$$P_g = 0.971 \times {h_s}^{1.16} \tag{4}$$

This equation, being different than that for settled snow regions, in that it predicts markedly higher snow loads for the same depth, validates the application of two distinct relationships for each region. Again, the same transformation was made to this equation so that it resembled the JCSS relationship depicted in Eq. (3). The parameters of this equation for compacted snow regions were also determined by regression analysis. Both sets of parameters for Eq. (3) are presented in Table 1.1. CO-OP stations scattered throughout the mountains provided snow depth only measurements. The 50-year ground snow depths were extrapolated from these stations using the same GPD. Finally, ground snow loads for compacted sites were obtained by applying Eq. (4) to all of the mountainous CO-OP stations. For the SNOTEL and Snow Course stations, 50-year ground snow loads were extrapolated from the snow water equivalent data.

The final step was to construct the ground snow load map. Using Geographic Information System (GIS) software, the latitudes, longitudes, and two-percent ground snow loads for

[2] SNOTEL and Snow Course stations record snow water equivalent. Refer to Chapter 2.2 for a description of these stations and Chapter 4.1 for a conversion to ground snow load.

each station were overlaid on a topographical map of Colorado. Finally, isolines were drawn connecting regions of equal snow load.

A comparison of the ASCE 7-10 and the SEAC mapped Colorado ground snow loads reveals some major discrepancies in prescribed snow load values. The only portion that is comparable between the two maps (*i.e.* non-CS regions) is at approximately the 104° longitude, parallel to the eastern border of Wyoming. For this eastern portion of Colorado, there are some regions where the SEAC mapped ground snow loads are more than double those from ASCE 7 (*e.g.* 50 psf vs. 20 psf in the southeastern potion of the state). These "hot spots" appear to coincide with locations of CO-OP stations used in the SEAC study. The reason for such a deviation from ASCE 7 prescribed ground snow loads is most likely due to the CO-OP snow depth records used in the SEAC study that include several recent extreme winter snow storms such as the March 2003 storm that brought as much as three feet of snow to the Colorado plains.

Table 1.1: Variables Used to Define Ground Snow Depth-Load Equations for Colorado (SEAC 2007)

Type of Variable	Compacted Snow Regions	Settled Snow Regions
$\gamma_{s.max}$	31.4 pcf	30.5 pcf
$\gamma_{s.min}$	18.0 pcf	10.0 pcf
d	44.1 in	48.2 in

1.2.2 Ground Snow Load Summaries for Other Western States

The aforementioned western states have their own Structural Engineering Associations that prescribe statewide design snow loads. The methodology used varies significantly from state to state. Table 1.2 summarizes the philosophies of each methodology, including the major differences between the developed snow load maps. As noted, for many of these states ground snow loads are explicitly related to elevation; usually ground snow load is positively correlated

to elevation. Also, there is some consensus in the general usage of some sort of snow density relationship which is applied to records of snow depth to determine loads. Nonetheless, there is considerable variation in the exact parameters and form of the ground snow depth-load relationship and type of probability distribution chosen by each state, particularly which will predict a two-percent ground snow depth.

Table 1.2: Basis of Design for Ground Snow Loads for Western U.S. Adapted from R. Sack (2012)

State	No. of Stations	Snow Depth-Load Relationship	Probability Distribution	Year Last Updated	Remarks
Montana	712	Elevation-Based	LP-III, LN	2004	Snow loads prescribed for 6 different regions, 4 different elevation ranges
Arizona	89	Elevation-Based	N/A	1981	Snow loads prescribed for 5 different regions based on elevation
Utah	413	RMCD†, Elevation	LP-III	1992	Rocky Mountain Conversion Density for snow depth-snow load
Idaho	514	RMCD†	LP-III	1986	Ground snow loads are mapped statewide, normalized by elevation
Northern California	32	Elevation-Based	N/A	1964	75% of maximum recorded ground snow load as basis of design
Oregon	689	Snow Density Prescribed for East/West	LN	2011	PRISM†† computer algorithms used to produce state map
Washington	N/A	RMCD†, Elevation	LP-III	1995	Rocky Mountain Conversion Density for snow depth-snow load

† Rocky Mountain Conversion Density
†† Parameter Regression on Independent Slopes analysis program
LN = Lognormal; LP-III = Log-Pearson Type III; N/A = Information not available

A number of states employ what is known as the Rocky Mountain Conversion Density (RMCD) to convert their records of ground snow depth measurements to ground snow loads. This relationship was developed at the University of Idaho by Sack and Sheikh-Taheri in order to

produce ground snow loads for Idaho (1986). This relationship was developed using ground snow depth and load measurements from nearly 3,000 Snow Course stations throughout the West with at least five years of records. A Log-Pearson Type III distribution was considered in the development of the RMCD. Using regression techniques, a bi-linear equation was fit to the plotted 50-year snow load vs. 50-year snow depth data. For this equation, two ground snow specific gravities were chosen for the bi-linear fit: one representative of greater snow depths and one representative of shallow snow depths. Eq. (5) was the result of the effort, along with the design snow load document that is still in use in Idaho (Sack and Sheikh-Taheri 1986). This equation is still widely used today in the noted western states listed in Table 1.2.

$$\begin{aligned} P_g &= 0.9 \times h_s && [h_s \leq 22\ in.] \\ P_g &= 2.36 \times h_s - 31.9 && [h_s > 22\ in.] \end{aligned} \tag{5}$$

The above mentioned RMCD depth-load relationship in addition to the ASCE 7 and the two SEAC relationships are plotted together in Figure 1.3. This plot provides a visual comparison of all the ground snow depth-load relationships and highlights some of the differences between all of them. Figure 1.3 illustrates that the RMCD always predicts higher snow loads than the ASCE 7 power equation for the same snow depth. This is expected since the data supporting the RMCD originates from high-elevation sites with generally higher density snowfall. As it can be seen, the SEAC depth-load equation for settled sites has been fitted to the ASCE 7 equation since the latter provided a more conservative estimate of ground snow loads as previously mentioned. The SEAC density equation for compacted sites, however, predicts much greater ground snow loads for the same depth than both ASCE 7 and the RMCD depth-load relationships. This highlights the need to update the ground snow load development methodologies in order to align them more closely.

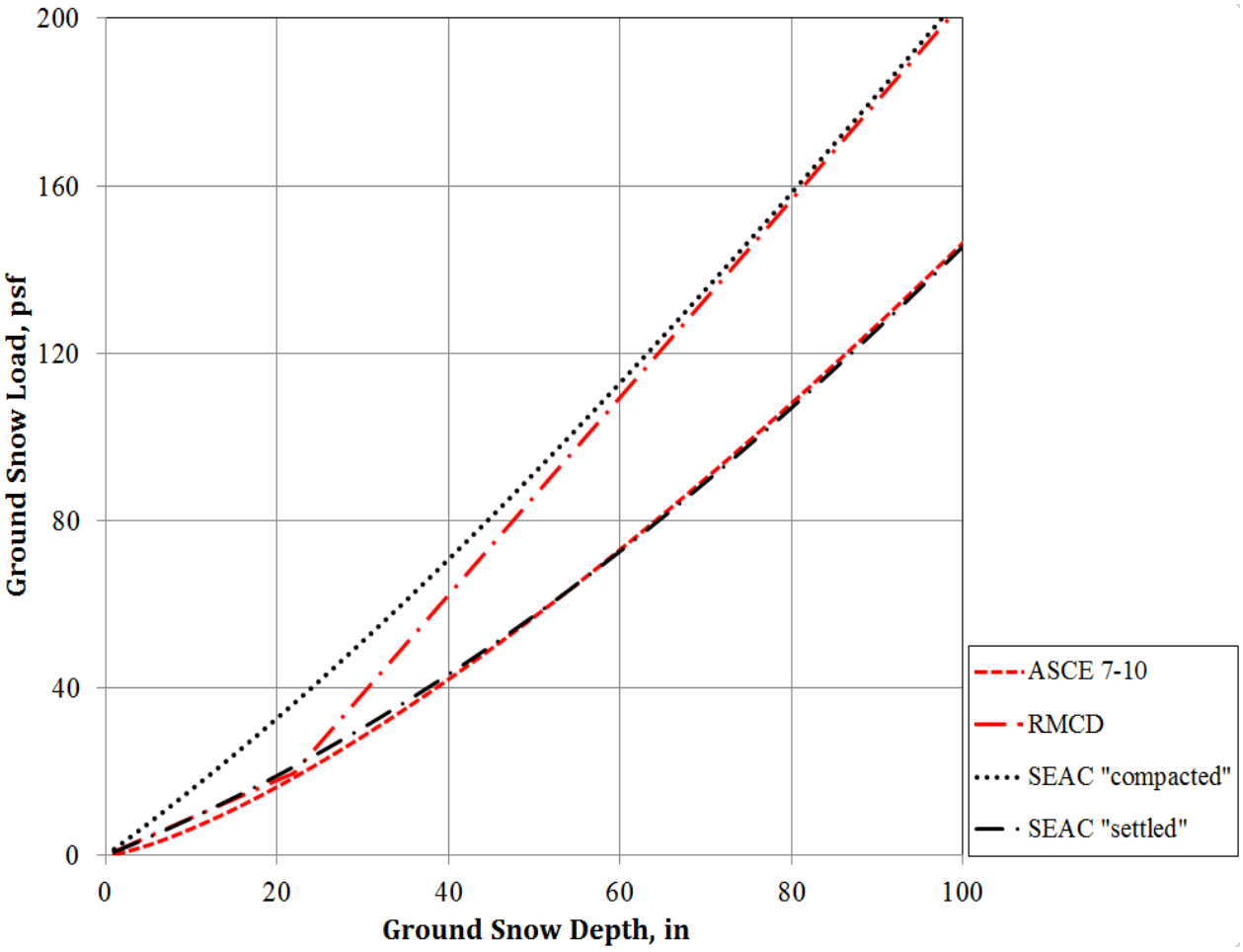

Figure 1.3: Comparison of RMCD, ASCE-7, and SEAC Ground Snow Depth-Load Relationships

1.3 The Need to Unify State Ground Snow Load Methodologies

The different philosophies adopted by all of the states in the West to determine 50-year ground snow loads have created a subtle yet unsettling dilemma. Mapped ground snow loads at the boundaries of all the western states do not coincide in value at most state borders. This is the case for several state borders such as that of Washington-Idaho, Oregon-Idaho, Idaho-Montana, Idaho-Utah, and Utah-Colorado. A few of the significant border differences in ground snow loads are discussed in detail below. The following discussion references R. Sack who originally amassed the values for comparison (2011).

A significant border discrepancy exists at the border of Washington and Idaho near the 48° latitude, where there is a significant deviation in nominal 50-year ground snow load predicted by the Structural Engineers Association of Washington (SEAW) and the Structural Engineers Association of Idaho (SEAI). About 14 miles west of the boarder, the SEAW nominal ground snow load is 34 psf for the cities of Dishman and Opportunity, WA. Proceeding east, in Idaho right on the border the 50-year ground snow load predicted by SEAI is 53 psf for State Line, ID and 56 psf for Post Falls, ID (five miles east of the border). Figure 1.4 illustrates a topographical map of the vicinity of these four cities annotated with the associated ground snow loads. Major ground elevation isolines bracketing the mountains and foothills to the north and south are also denoted with elevation in feet. As it may be seen, there is only about a 100-ft elevation difference between all four of the cities. Yet, the ground snow loads between Opportunity and Post Falls is some 19 psf apart, a difference of nearly 55%. That the ground snow loads are so different, considering the negligible elevation difference and a spatial difference of less than 10 miles, indicates a serious problem with how information is shared among states and how different the ground snow load methodologies are.

This same issue is encountered across other state borders, such as the border of Utah and Idaho, on the western edge of Bear Lake, which overlaps both states. The affected cities are St. Charles, ID which is approximately eight miles north of the border and Garden City, UT, approximately five miles south of the border. A topographical map of the vicinity of these two cities in Figure 1.5 is annotated with the associated ground snow loads (Figure 1.4 and Figure 1.5 were created with ArcGIS 10.1). Major ground elevation isolines are denoted for the Wasatch and Bear River Mountain Range to the west of both cities. The Structural Engineers Association of Utah (SEAU) prescribes a ground snow load of 50 psf for Garden City, UT whereas 13 miles

north SEAI prescribes a ground snow load of 90 psf for St. Charles, ID. As apparent from the elevation isolines, both cities are just below 6000 feet in elevation and both cities are just west of Bear Lake. The location relative to the lake is significant because it eliminates the phenomenon of lake-effect snow as an explanation for the vastly different ground snow load values.[3] Since the prevailing direction for snow storm systems in this region is west-east, lake-effect snow does not explain the difference in ground snow loads, leading to the conclusion that the difference in prescribed design ground snow loads are therefore methodological. There are many other similar situations between other states where ground snow loads do not agree at the border. The magnitude of the disparities in ground snow loads at state borders speaks to the gravity of the problems with state approaches to ground snow loads.

In addition to the discrepancies at state borders, there are significantly different methodologies used by the Structural Engineering Associations. Some of these methodologies were developed several decades ago and are in need of updating. These issues point to a major shortcoming of the systems by which states determine their snow loads. All of these states are in the same region of the United States and they all experience the effects of the same winter storm systems. These challenges point to a need for a close inter-state relationship between the committees that govern snow loads. Also lacking is a unified methodology which all state engineering associations follow to develop ground snow loads. This unified process, independent of local climatology or type of snowfall experienced, should set a standard that can be adopted in jurisdictions where aging snow load documents need updating or be used as a tool for evaluating ex-

[3] Lake-effect snow generally deposits heavier snow on the far edge of a body of water from where the cold air mass originates, due to the absorption of moisture from the body of water that condenses as snow on the leeward side (Eichenlaub 1970)

isting state ground snow loads. Ideally, the methodology should embrace the advantages of modern technology such as advances in weather monitoring equipment and computational abilities and utilize resources from other disciplines of the fields of science and engineering. This methodology can ignite the type of inter-state collaboration needed in this field and serve as a platform for future development and improvement. This thesis proposes such a unified process for determining probabilistic ground snow loads, using modern statistical tools and resources from the fields of hydrology and climatology. It will be robust, statistically sound, and one that can be integrated easily into the current ground snow load regimes of the western states.

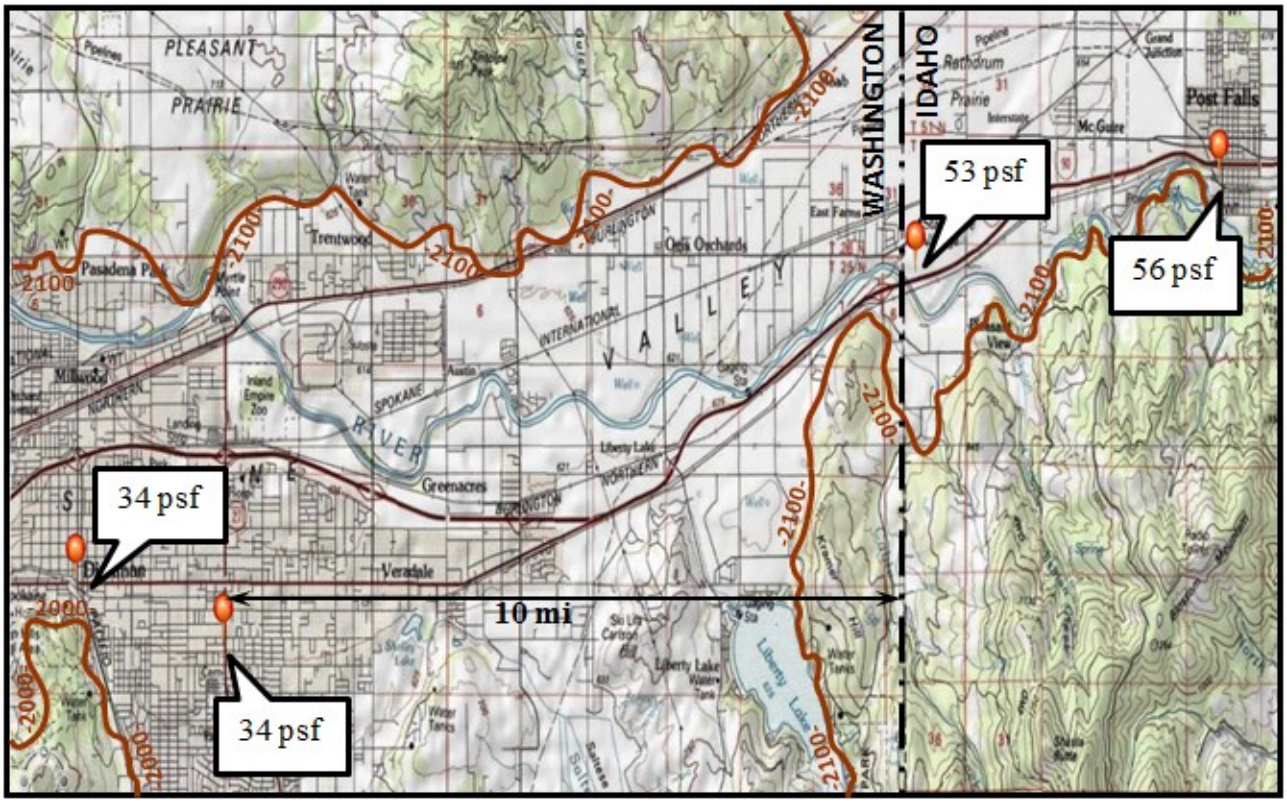

Figure 1.4: Topographical Map of the Washington-Idaho Border at Latitude 48 (west to east, ground snow loads shown for Dishman, WA, Opportunity, WA, State Line, ID, and Post Falls, ID)

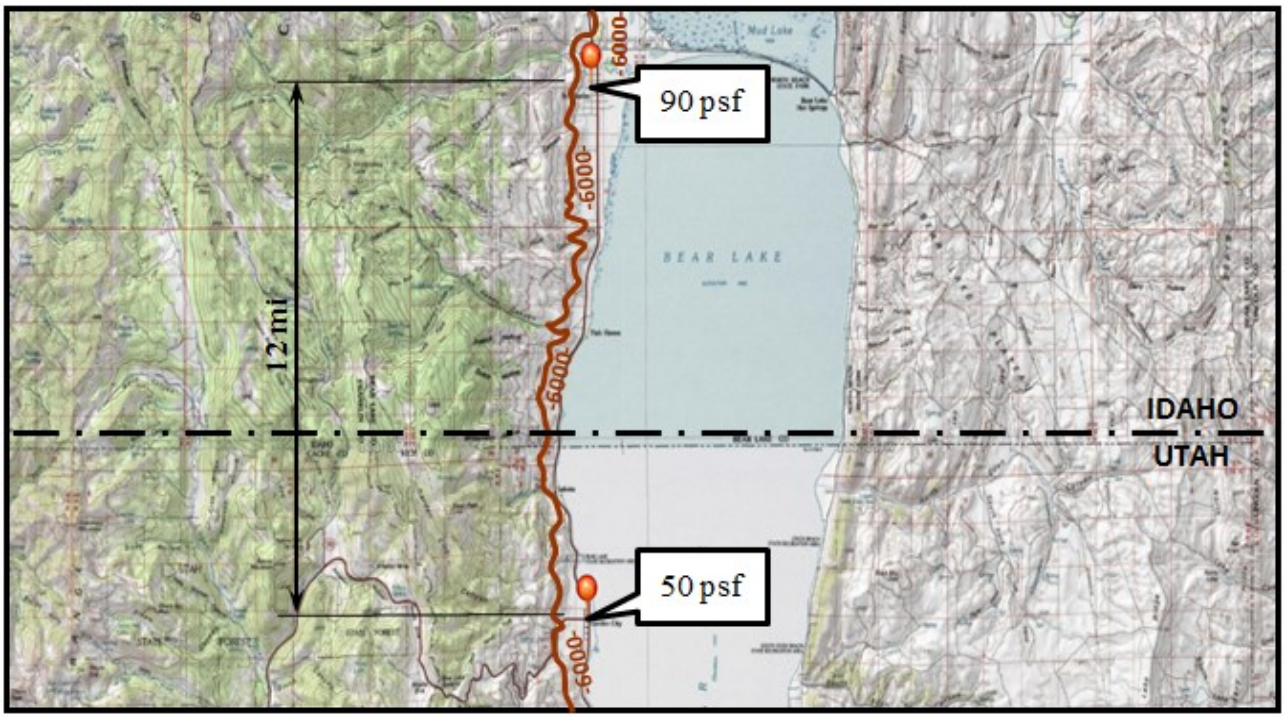

Figure 1.5: Topographical Map of the Idaho-Utah Border (south to north ground snow loads shown for Garden City, UT, and St. Charles, ID). Maps created using data from Sack (2011).

2.0 WEATHER STATIONS & CLIMATOLOGICAL DATA

2.1 Background

The data measured by weather stations across the United States is of great use in forecasting not only major weather events, but also patterns of major snow events and climatological trends that coincide with these snow events. In this chapter a brief description of the history and development of various types of weather stations is discussed. The data recorded from these stations will be used in the development of probabilistic ground snow loads.

The history of systematic collection of weather and climatological data in the United States dates back nearly to the founding of the country itself. In 1870, President Ulysses S. Grant signed into law a proposal establishing an agency responsible for the widespread collection of weather observations across the United States (NWS 2012b). This agency became known as the National Weather Service (NWS). The primary motivation behind the establishment of the NWS, initially responsible for taking basic meteorological observations and reporting of *major* storm systems, was the safety of maritime vessels along the seacoast and in The Great Lakes (NWS 2012b). Similar agencies such as The United States Coast and Geodetic Survey (formed in 1807) and the Bureau of Commercial Fisheries (formed in1871) helped to define the scientific heritage of the country (NOAA 2006).

Together, these three historic agencies were united in 1970 under a declaration to Congress by President Nixon who wanted to "protect life and property from natural hazards [and]…better understand the total environment" (NOAA 2006). This agency, the National Oceanic and Atmospheric Administration (NOAA) realizes that mission by researching and monitoring all natural phenomena. NOAA is the parent government agency under whose authority the NWS and the National Climatic Data Center (NCDC) now operate. The current responsibilities

of these divisions of the NOAA are to research and monitor a wide range of meteorological events in the United States (the role of the NWS) and to analyze and archive such data (the role of the NCDC) (2012b). The data and services produced by NWS and archived by NCDC will be relied on heavily in this paper; refer to Chapter 2.2 for further discussion.

Weather monitoring and research, however, is not solely of interest to government agencies that endeavor to study the environment and protect society from natural hazards. A rather different need to research and monitor the climate emerged from the demands of the agriculture economy of the United States. Formally established in 1862, the USDA is primarily responsible for protecting the viability and safety the nation's food and agricultural sectors, as well as developing sound public policy in these areas and natural resource and forest conservation (USDA 2012). The farming industry in the mid-19th century was steadily growing, becoming the primary livelihood for nearly half of Americans at the time of the census (Kennedy 1864). Therefore, the USDA's initial role was to sustain the future of the agriculture industry and protect farmers from the devastating effects of drought. This is a very real concern in the Mid-West and Pacific Western regions of the U.S., where much of the region is semi-arid or arid. In these dry regions, a small number of winter weather systems provide most of the yearly precipitation; as a result, anywhere from 50-80% of the region's potable water supply comes from spring melt off of mountain snowpack that gets allocated either east or west of the Great Divide (NRCS 2009). Although these states have water management agreements that stipulate which state or municipality is entitled to the outflows of each catchment, a centralized organization with the resources and technical capabilities was needed to provide specific water resource forecasting for these states. The National Resource Conservation Service (NRCS) was created within the USDA as a focused department dedicated to helping agricultural producers sustain the health of their crops

and conserve precious natural resources (NRCS 2012). Specifically of interest to this paper are the programs NRCS has implemented to forecast water supply, such as the SNOTEL stations and products; they are defined in Chapter 2.2.

Since the inception of the historic agencies described above, the use of weather measurements of all kinds has pervaded every discipline of the engineering and applied science communities. For instance, one discipline that has benefited significantly from advancements in weather measurements is the field of hydrology. Manual and more recently automated snow surveys are being collected with increasing frequency as a means for forecasting water supply derived from snowmelt (NRCS 2012). These measurements are used directly to predict outflows from rivers into basins and thus the availability of water to municipalities. These forecasts allow federal, state, and local governments to produce legislation directed at maintaining the availability of potable water, sustaining the health of ecosystems, mitigating the effects of flood scenarios and also improving general water management policy (NRCS 2012). More recently, surveys and other related climatological observations have become invaluable to other scientists and engineers. The scope of this investigation is limited to applications to the structural engineering community and the preclusion of snow-related roof collapse and casualties. The use of snow surveys and other measured climatological variables now plays a critical role in such an endeavor.

The sections to follow detail three main classifications of acquired climatological data and their associated instrumentation, relevance, and validity. Each source of data comes with its own advantages, limitations, and bias; however when combined properly the limitations and biases can be mitigated.

2.2 Observed Ground-Based Measurements

Ground-based measurement of climatological data can be defined broadly as any firsthand, physical collection of the data of interest. These types of measurements are the most accurate forms of collecting data since they do not rely on indirect inferences from other measurements. As the name implies, the instruments associated with such measurements are located on the ground. One of the most ubiquitous ground-based devices is the weather station. The photo on the right of Figure 2.1 is an example of an Automatic Surface Observation Station (ASOS). A network of thousands of ASOS stations monitor and record weather at airports

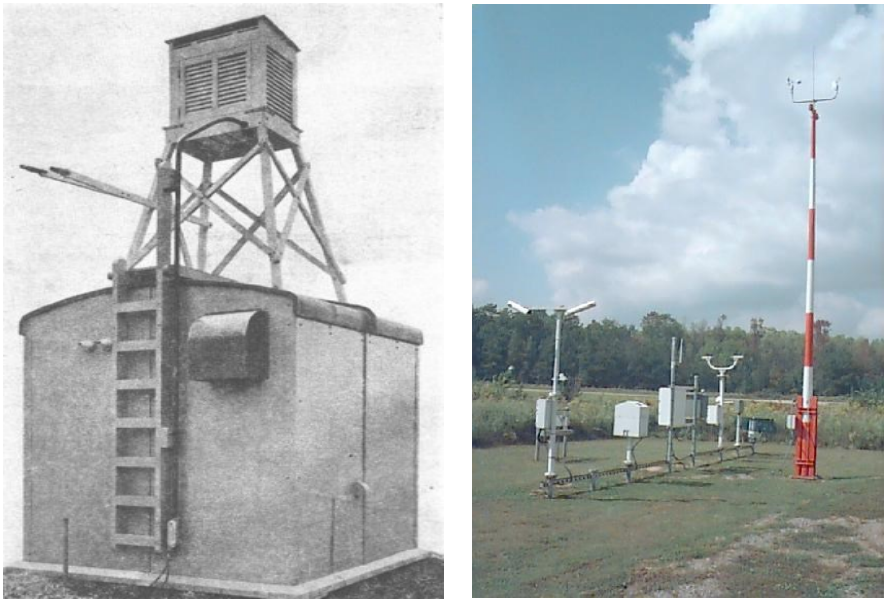

Figure 2.1: Then and Now: First Automatic Weather Station, left (Wood 1946) and Modern ASOS Weather Station, right (NWS 2012b).

(NWS 2012b). Ground-based measuring stations such as these are permanently fixed to the ground and contain several instruments for recording real-time measurements of weather in the immediate vicinity of the station. Wind speed and direction are measured via anemometers, temperature readings via shielded thermistors, and relative humidity via chilled mirror hygrothermometers, though additional features may be available.

ASOS and other similar stations are descendants of the original weather stations, shown on the left of Figure 2.1. These original automatic weather stations (AWS) were first implemented in 1941 under the direction of the Bureau of Aeronautics, U.S. Navy. Advancements in radio broadcasting technology quickly led to the capability of these stations to transmit data to weather offices around the world (Wood 1946). The limited technological capabilities of the 1940's forced these stations to be designed around ease of installation and maintenance. A technician could easily perform these tasks on a device accessible from the ground. The first of these stations was quite bulky and required an internal power plant to drive the internal components and measurement devices. This enabled the collection of atmospheric pressure, temperature, relative humidity, wind direction and speed, and rainfall (Wood 1946).

U.S meteorological measurements are based on two primary sources: a network of 274 NWS "First Order" weather stations and 32,000 NWS Cooperative Observer (CO-OP) Stations (NCDC 2012b). However, several other agencies exist that are responsible for many other types of weather stations. First Order is the term the National Weather Service gives to the class of manned, official weather stations which offers a suite of measurements including: temperature (daily max., min., avg.), snow depth, snow water equivalent (in. of water), precipitation, barometric pressure, sky cover (using cloud radar data), and several wind speed and direction statistics. These measurements are taken 24-hours per day, year-round by certified NWS-trained observers (Quayle 2013). Snow water equivalent (SWE) is defined in Chapter 4.0; a concise description here is that it is a measurement of the amount of water in snow. Figure 2.2 shows a certified NWS observer recording the official snow depth at a weather forecasting office. In contrast to First Order stations, CO-OP stations are technically not stations but rather residences,

farms, commercial facilities, etc. where individuals have agreed to voluntarily record measurements of temperature, precipitation, barometric pressure, and sky cover (NWS 2012a).

Figure 2.2: Trained NWS Staff Recording Official Snow Depth at First Order Weather Station (NWS 2012b).

Another substantial network of cooperative observer stations comes from the Community Collaborative Rain, Hail, and Snow Network (CoCoRaHS) which was created in response to a devastating flash-flood in Fort Collins, CO in 1997 (Cifelli, et al. 2005, CoCoRaHS 2011). The CoCoRaHS network now comprises nearly 44,650 volunteer stations nationwide, 331 of which are in Colorado. Volunteers record and report precipitation (liquid and solid) and hail quantities to the CoCoRaHS website (www.cocorahs.org). Several other maps and types of data are available such as significant weather reports, drought impact reports, and water year summaries for each station. A high level of measurement quality is maintained since all stations receive standard equipment including 4-in. rain gauges and hail pads. These combined qualities have made the CoCoRaHS network an invaluable source of climatological data.

Finally, there is the GHCN database, compiled by the NCDC, which combines numerous surface weather station databases such as:

(1) United States Collection: composed of several datasets archived at NCDC that originate from U.S. Forts, Air Force installations, and Observer Stations
(2) International Collection: composed of roughly 20,000 global weather stations from 100 different countries
(3) Government Exchange Collection: composed of records obtained by bilateral agreements with federal weather reporting offices from 76 different countries

The types of measurements taken vary widely from station to station, and the database consists of several types of stations. However, common baseline measurements taken by all GHCN stations include liquid precipitation, snow depth, and temperature. These datasets are subjected to a rigorous set of quality control processes including a screening phase to ensure all required data fields are present; an assimilation phase to remove duplicates, prioritize certified source stations, and homogenize reporting frequency; and a final quality control phase where checks for unusual streaks, world records, and gaps are made (NCDC 2012a). While the GHCN database consists of international sources, the NWS First Order and CO-OP stations are all United States-based and are not subject to as tight scrutiny of the data as the GHCN database. There are no duplicate stations between the NWS First Order and CO-OP networks, and GHCN station databases; however, records are maintained separately to varying levels of quality control.

One of the main sources for ground-based measurements of *snow properties* comes from a proven method for measuring descriptive snow properties in mountainous areas. Snow Courses have been around since 1906 and are permanent mapped locations in mountainous regions where professionally trained Snow Course personnel ski to and manually record snow depth and SWE (NRCS 2012). The instruments used to record snow course measurements at are not high-

tech, nor even digital, yet the quality of the data has made the method a benchmark in the field of hydrology. In fact, it was a Congressional mandate in the mid-1930's to measure snowpack in the mountains and forecast the water supply, motivating the installment of Snow Courses. Figure 2.3 illustrates the proper technique used to obtain the SWE measurement, adapted from the Snow Survey Sampling Guide (Soil Conservation Service 1984). First, a hollow aluminum measuring rod is inserted into the snowpack and removed with a core of snow plus a cork of sod at the end. Then, using a spring scale calibrated with the rod empty weight, the filled rod is weighed (less the cork of soil that must be removed). The spring scale reads inches of water directly, so no calculations are required by the observer. A typical Snow Course consists of 10 permanently labeled sampling sites stretched across roughly half of a mile of mountainous terrain, in an effort to decrease the effect of local variations in measurements (NRCS 2012). The data obtainable from Snow Courses is very valuable to structural engineering much like that from NWS First Order weather stations, since SWE is directly recorded.

As the need arose to forecast water supply at an increasing level of certainty, especially in the arid western parts of the country, specialized stations were designed for remote, mountainous regions of the western United States. These SNOTEL stations (short for SNOwpack TELemetry) were introduced by the NRCS in 1978 (NRCS 2009). Unlike NWS First Order stations, these stations only measure a few climatological properties related to precipitation. The standard configuration of SNOTEL stations includes instrumentation to measure air temperature (shielded thermistor), liquid precipitation (rain gauge), snow water content (snow pillow, pressure transducer), and snow depth (sonic sensor). These stations are part of a comprehensive system that is operated and maintained by NRCS, encompassing the states of New Mexico, Colorado, Wyoming, Montana, Idaho, Utah, Arizona, Nevada, California, Oregon, Washington, and Alaska.

Figure 2.4 illustrates the current sites of operational SNOTEL stations in the western U.S. as of 2012. The sites are clustered in the peaks of the Cascades, Rocky Mountain, and Sierra Nevada Mountain Ranges. The central feature of these stations that allows them to efficiently transmit such valuable data from such remote mountainous sites is remote telemetry via meteor burst technology. Meteor burst technology is a reliable means of transmitting data by means of VHF radio frequencies that are bounced off an ever-present band of ionized gas in the Earth's atmosphere (NRCS 2009). Consistent records of SNOTEL measurements are available from the early 1990s through the present, although scattered interruptions in records may exist due to stations being decommissioned or upgraded from snow courses.

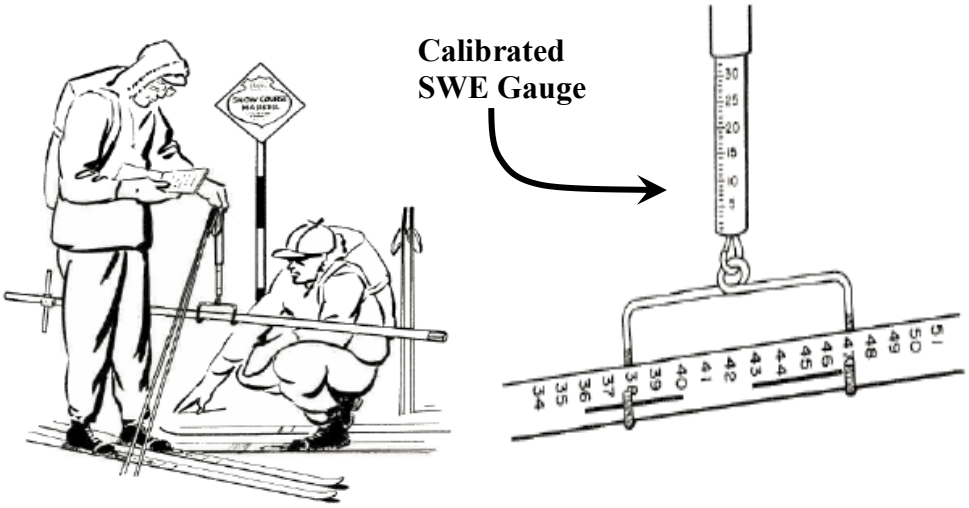

Figure 2.3: Proper Technique for Measuring SWE at Snow Courses from the Snow Survey Sampling Guide (Soil Conservation Service 1984)

The most important of the measurement capabilities of SNOTEL stations is water content of snowpack and it is measured via a snow pillow platform upon which snowfall accumulates. The snow pillow, filled with an anti-freeze solution and pressure transducers, measures average pressure along its surface and back calculates the equivalent water content (NRCS 2009). A ground snow depth measurement is made with a sonic device. According to NRCS, the accura-

cy and percentage of time operational is usually around 99%. For this investigation, the station records obtained are invaluable to describing properties of the snow in the highly variant mountainous terrain. Their application is discussed in Chapter 3.0.

Figure 2.4: SNOTEL Site Locations Operated and Maintained by NRCS (2012)

A current catalog of all ground-based weather stations including governing agencies and active station counts is available from the NCDC Historical Observing Metadata Repository (HOMR) website (NCDC 2012c). Table 2.1 lists all of these active U.S. weather stations plus active Snow Course and SNOTEL stations, with associated statistics such as governing agency, station description, station count, year of establishment, and measurements recorded.

Table 2.1: Ground-Based Weather Station Descriptive Information (NCDC 2012b)

Station Type	Agency	Description	Station Count	Active Since	Meas.
CO-OP	NWS	National Weather Service Voluntary Cooperative Observer Program	32,000	1900†	E,T,P,S
LCD	NWS	National Weather Service (First Order) Local Climatological Data Program	274	1903†	C,P,T,S SWE
CoCoRaHS	CCC, NOAA	Community Collaborative Rain, Hail, and Snow Network	44,644	1998	H, P
GHCN-D	NCDC	Global Historical Climatology Network Daily (database)	80,000	1763††	T,P,S
AWOS	FAA	Automated Weather Observation Stations (airports)	700+	1987	C,P,PR, S,V,W
ASOS	NWS	NWS/FAA/DoD Operated Automated Surface Observation Stations (airports)	900+	1990	C,P,PR, S V,W
USCRN	NOAA	U.S. Climate Reference Network (database)	120+	2002	T,P,RH SR,W
USRCRN	NOAA	U.S. Regional Climate Reference Network (database)	60+	2002	T,P,RH SR,W
USHCN	NOAA	Subset of NWS CO-OP Stations (long records)	1,219	1980s	T,P
SC	NRCS	Snow Course Manual Ski Stations (mountains)	1,200	1906	S,SWE
SNOTEL	NRCS	Snowpack Telemetry Automated Stations (mountains)	750	1978	T,P,PR, S,SWE

† date is best available estimate
†† earliest available record globally
C = cloud cover; E = snow evaporation; H = Hail; P = precipitation; PR = air pressure
RH = relative humidity; S = snow depth; SR = solar radiation; T = temperature
V = visibility; W = wind speed/direction; SWE = snow water equivalent
CCC = Colorado Climate Center

The future of snow measuring instrumentation is depicted in Figure 2.5. This modern GPS snow gauge is intended for snow-related measurements in high, mountainous environments. It receives GPS signals from different satellites and uses them to measure descriptive properties of the snow (such as depth and water content). Aside from providing technological gains over

the standard weather station, this technology offers solutions to data processing issues facing ground-based observations such as sampling bias due to scatter in the location of weather stations. According to the owner and developer of the GPS snow gauges, the National Center for Atmospheric Research (NCAR) located in Niwot Ridge, CO, the new GPS gauges are capable of measuring the noted snow properties for 100 by 100 meter region of ground around the station (2011). When fully implemented on a larger scale, these stations will be able to provide area measurements of snow properties, offering improved interpolations between adjacent stations over point measurements from standard weather stations. While data from these stations will not be used in this study, future research in this field can benefit from the data obtained from these gauges.

Figure 2.5: Modern GPS-Enabled Snow Gauge at Niwot Ridge, CO (NCAR 2011)

2.3 Observed Remotely-Sensed Measurements

Recent advancements in satellite imagery and microwave scanning technologies have led to new methods of taking measurements of various atmospheric and climatic variables. These

are obtained from the field of remote sensing. In the scope of this investigation, remotely-sensed observations are defined as expansive measurements taken from great distances. Measurements from these distances rely on correlations to other known variables. A simple example of remote sensing is temperature measurement using an infrared (IR) temperature gun, which is widely used by geologists and firefighters. IR temperature guns detect the amount of infrared energy radiating from a warm body; coupled with the estimated emissivity of that body, they can calculate the temperature (Zhang, Tsai and Machin 2010). Since an estimation of emissivity is required to calculate the desired temperature, the reading of IR energy alone cannot determine the temperature. In this sense, remote sensing can be considered inferred measurements and are highly dependent on the quality and certainty of other variables. The following are examples of remotely-sensed measurements related to snowpack properties.

The first type of remotely-sensed snow measurements is satellite imagery analysis, which includes obtaining high-resolution digital imagery and subsequently processing it to obtain snowpack properties. This process, known as passive microwave remote sensing, involves reflecting microwave energy from satellites off the Earth's surface and measuring the reflectance. One example is the Moderate Resolution Imaging Spectroradiometer (MODIS) system (Parajka 2012). Using two NASA satellites, Terra and Aqua, MODIS is capable of producing daily, 8-day and monthly estimates of snow cover. The input data is high resolution, digitally-encoded imagery with coded values assigned to individual pixels based on color. This data is fed into the MODIS computer algorithms that can discern between clouds and snow using 36 different bands of spectral energy emitted by the two scanning satellites. The quality of this product depends somewhat on the clarity of the sky at the time the images are taken. To overcome this dependency, MODIS incorporates a technique wherein multiple images for the same location are

taken and each pixel value is scored to best represent the true snow cover at that location (Parajka 2012). The score is based on quality of the image, solar effects, angle of imagery, and several other properties. This practice is intended to eliminate the bias from any one image where cloud cover could be mistaken for snow.

Applications of MODIS are widespread, but are mostly based on some form of hydrologic watershed modeling. Several local studies have incorporated its output into snow cover mapping while global initiatives have incorporated its output as input for major climate models. For instance, the ambitious Snow and Sea Ice Global Mapping Project, under the management of the National Snow and Ice Data Center (NSIDC), implements several MODIS products to produce global snow and ice coverage maps (NASA 2012). Beyond snow coverage, research using MODIS products has shown promise in the reconstruction of SWE at a watershed for previous seasons, explored by Durand et al. for the Rio Grande basin in the U.S. (Durand, Molotch and Margulis 2008). As well spatial interpolation of SWE is possible and practical, as shown by the efforts of Bocchiola in the Italian Alps (Bocchiola and Groppelli 2010).

Despite the promising results from such applications of MODIS its interpolations of SWE present bias when compared to ground-based measurements. Recently De Lannoy et al. compared SWE observations from remote sensing to CO-OP and SNOTEL datasets during a study of SWE in the Northern Colorado Rockies (2012). The study compared SWE interpolation from ASMR-E combined with snow cover fraction (SCF) products produced by MODIS against in-situ measurements at the ground-based stations.[4] In this study, the MODIS output provided only data regarding the physical extent of snow covered regions while the ASMR-E data provided

[4] ASMR-E is a remote-sensing technology that uses microwave energy to interpolate SWE directly.

SWE interpolations. Daily datasets for both the remotely-sensed and ground-based observations through eight winter seasons from 2002 to 2010 were analyzed. Even after assimilating MODIS and ASMR-E, equalizing the spatial output scaling (down to 1 km), and applying data filters the interpolation of SWE was found to be inaccurate at locations with patchy and deep snowpack. In general, interpolating SWE from the SCF output from MODIS alone experienced problems which were only slightly mitigated with assimilation of the ASMR-E data.

A second type of remote-sensing that also uses imaging is the suite of GOES (Geostationary Operational Environmental Satellite) satellites that have been in service 1994 (Olsen 2007). GOES satellites have provided key monitoring products such as tracking of major weather systems, cloud coverage analysis, wind speed/direction, surface and atmospheric temperature profiles, and atmospheric water content analysis. The first two of its products are aimed at monitoring images taken of the earth, performed by onboard optical equipment similar to that of MODIS. The more complex products, such as temperature profiles, cloud height, atmospheric water content, and wind speed/direction at various atmospheric altitudes are performed using specific sensors coupled with highly sophisticated analysis. For instance, the interpolation of cloud temperature and atmospheric water content requires an EM (electromagnetic) emitter capable of radiating five wavelengths (from 0.65μm to 12.0 μm) (Olsen 2007). For interpolation of water content, a specific wavelength of EM is chosen which liquid water in the atmosphere absorbs. The energy absorbed by the water in the atmosphere may not be reflected back to the GOES receivers, or may be reflected back partially depending on the amount of water in the atmosphere. GOES detects this reflection and relates the returned energy to the amount of water that must be present in the atmosphere.

The most useful applications of predicting snowpack properties using GOES data involve relationships between the snow cover properties obtained from remote measurements to determine snow depth. Some of these studies also incorporate land cover and vegetation to refine the measurement of snow depth. An investigation into establishing such a relationship between snow reflectance and ground snow depth using GOES output was made in 2004 for a study area including the U.S. Great Plains and the Canadian prairies (Romanov and Tarpley 2004). The relationship developed contrasted the reflectance – or energy reflected back to GOES – of the ground against the known reflectance of snowpack. This difference was used to determine depth of snow for 12 km square grid cells throughout the study area. Comparisons of the predicted ground snow depths to observed ground snow depths (at over 1400 snow depth measuring weather stations in the study area) produced varied results. Provided that observed ground snow depths were below 30 cm, the relationship developed produced errors less than 30%. The results indicated limited usefulness for greater snow depths. Since ground snow depths in mountainous regions frequently exceed hundreds of centimeters, the model produced by Romanov and Tarpley is not useful at all to this investigation. Moreover, since the output spatial resolution was so coarse its usage in this study doesn't agree with regional scale interpolations. Therefore, the concept of ground snow depth derived from satellite data alone is not mature enough to be used alone.

Active remote sensing, such as radar, is a promising remote sensing technology that predicts SWE directly from the obtained measurements, instead of relating fractional snow cover or snow depth, first to estimate SWE (Nolin 2010). Therefore, radar is not subject to the secondary sources of error in the interpolation of SWE. Radar remote sensing of snowpack whether by plane or by observing satellites also has the advantage of finer spatial resolutions (closer to 1km).

Basically, radar devices used in remote sensing of snow detect the difference in scattering of reflected energy (known as backscatter) between snow and non-snow bodies across different bands of wavelength. This is illustrated by Figure 2.6 which depicts radar interference graphs created by two bands of energy (L- and C-band). While usually used to obtain topographical elevation models, this technology can also be adapted to interpolate values of SWE in snowpack provided the radar is calibrated to experimental testing (Olsen 2007). Relationships between the difference in backscatter and the SWE of the snowpack can be constructed, resulting in spatial interpolations of SWE.

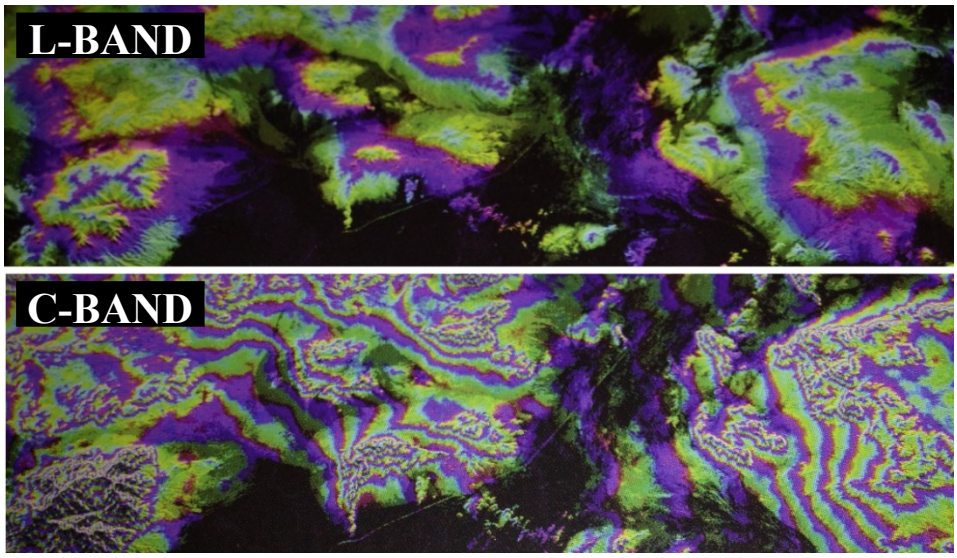

Figure 2.6: Interference Patterns of L-Band and C-Band Obtained from SAR Flown Radar over the Mojave Desert, CA (Olsen 2007).

Estimating properties of snowpack derived from radar, microwave emission, or processed satellite imagery has great potential in supporting the prediction of ground snow depth and SWE. Considering the simplicity and advantages over other technologies, radar would appear to be the standard for remote sensing of snowpack properties. However, radar is subject to the same sources of error that troubles all remote sensing technologies. Many bands of radar are particularly prone to problems distinguishing snow backscatter from non-snow backscatter when the

density is very low and the snow is very dry (Nolin 2010). In these instances, the radar energy passes through the snow layer too easily and the measured reflectance is only a function of the properties of the ground surface. Also, radar backscatter is related to SWE in a nonlinear relationship that varies with climatic and also geographic variables (*e.g.* humidity, type of underlying soil reflecting radar energy). This increases the estimated error in predicting SWE over large regions. In general, remote sensing technologies cannot yet overcome the inherent errors in measurement such as backscatter issues associated with radar, coarse resolution issues associated with GOES, and cloud interferences associated with MODIS. Consequently, remote sensing should be coupled with more reliable but perhaps less informative types of measurements such as snow depth. This is discussed further in the next section.

2.4 Evaluation of Ground-Based and Remotely-Sensed Observations for Structural Engineering Applications

The sources of climatological data described in Chapters 2.2 and 2.3 provide valuable data, the utility of which depends on the application. For ground-based weather measurement stations such as NWS First Order and CO-OP stations, the intended users are weather forecasting offices around the country. For SNOTEL and Snow Course stations the intended users are hydrologists and water forecasting officials. Lastly, remote sensing is tailored to scientists studying climate changes on a global scale. While none of this data is tailored specifically to the structural engineering community, many pieces can be extracted which are useful when combined together. A few of the strengths and limitations of each source are described below, along with recommendations on how to mitigate these limitations for the specific applications of this thesis.

Out of all the station types that provide firsthand snow measurements, the network of NWS First Order stations provides data that is most meaningful to the structural engineering community since these stations record SWE. A measurement of SWE can be conveniently trans-

lated into a ground snow load. The utility of these stations is even greater considering regular ground snow depth measurements are concurrently recorded. The caveat, however, is that these stations are rather sparse in comparison to the related NWS CO-OP stations that record snow depth (among other measurements). The only current NWS First Order stations in Colorado are Alamosa (ALS), Colorado Springs (COS), Denver (DEN), Grand Junction (GJT), and Pueblo (PUB) (NCDC 2012c). Furthermore, several studies (Robinson 1989, Schmidlin 1990) have indicated the existence of observer error at various NWS stations wherein zero-depth measurements were recorded at stations where analysis revealed significant snow accumulation at nearby stations. Missing entries and assumed snow depth or density are also common. Unfortunately the uncertainty in the extent of these errors complicates any corrective measures.

The networks of the NWS CO-OP and CoCoRaHS programs boast quantity of stations and significantly increased spatial coverage of the country compared to any other weather station network. This is especially useful from a statistics point of view, although the usable data from these stations for this investigation are limited to ground snow depth measurements. Nevertheless, station data from these programs cannot be disregarded. The strength of their spatial coverage makes them important for the development of ground snow load maps.

The other sources of climatological data have roughly equal strengths and weaknesses. The GHCN database is significantly larger in station count than either NWS First Order or CO-OP, but lacks informative measurements (only records of temperature and precipitation are available). Data originating from Snow Course and SNOTEL products are very reliable and consistent due to proven history and automation, respectively. However, data obtained from these two sources can only shed light on snow properties in a small subset of relatively remote, mountainous regions of the country. Finally, remote sensing techniques are useful in describing

characteristics of very broad regions and are able to produce continuous digital maps, something not possible through analysis of any other source of weather station data. Their limitations have been discussed but most of them stem from the long distances between the source and the equipment.

In order to achieve optimum data fidelity and objectivity all sources must be incorporated into an analysis that attempts to model snow loads from the available data. All of these sources should be incorporated in a manner that permits a type of check and balance so that the strengths of one dataset overcome the weaknesses of another. Historical archived datasets from *all* of the sources in Chapters 2.2 and 2.3 are therefore employed in this analysis of ground snow loads. Specifically all such weather stations within Colorado, as well as other types of measurements, are used in the development of a case study for the state. These stations are assimilated into a sophisticated computer snowpack model, introduced in the next chapter.

3.0 SNOW DATA ASSIMILATION SYSTEM (SNODAS)

3.1 Objectives of the SNODAS System

The National Operational Hydrologic Remote Sensing Center (NOHRSC) of NOAA has developed a climate prediction computer model that utilizes and assimilates various types of measured data. SNODAS, or Snow Data Assimilation System, produces modeled estimates of snowpack and associated properties/variables. These estimates are used to support national hydrologic analysis (Barrett 2003). The SNODAS system accepts a variety of meteorological data as input, combining different sources, conducts quality control of the data, and produces a computer-based snow model with several snow-related variables as output. SNODAS input includes measurements from ground-based sources (as described in Chapter 2.2), satellite and airborne sources (as described in Chapter 2.3) and numerical weather prediction models. SNODAS output are mapped values of snowpack variables for the conterminous U.S. It is advanced at six hour intervals under the direction of analysts and meteorologists who decide which sources to use during each interval. The current output is available at a spatial resolution of 1km and temporal resolution of 1hr. Spatial resolution refers to the size of the geographic square plot of land for which output is modeled; temporal resolution indicates how frequently the output is produced. These plots of land within the model are referred to as grid cells that collectively form a complete grid of the U.S.

3.2 Variables Modeled by SNODAS

There are three basic types of variables that are used by the SNODAS computer snow model: driving, state, and diagnostic (Barrett 2003). These variables quantify descriptive properties of the atmosphere, snowpack, or precipitation. Table 3.1 lists the major variables modeled

and describes the general role of each on the produced output. Only the major contributing variables are shown; some have been omitted for conciseness. The initial parameters are somewhat site-dependent properties and are necessary for the spatial interpolation of modeled variables between observation points. Driving variables are climatological factors which directly affect each state variable – descriptive properties of snowpack at each output interval. Finally, the diagnostic variables are modeled to cross-reference other driving and state variables. They are used to assist the analysts in deciding which data to include/exclude each time the model is advanced, and are also important for validating the correctness of the model.

Table 3.1: SNODAS Model Parameters and Variables (Barrett 2003)

Type of Variable	**Variable**	**Properties/Processes Influenced**
Initial Parameters	Forest Cover Fraction	Site-specific thermal properties
	Soil Bulk Density	Water transport properties
	Soil Plasticity	Thermal/mechanical properties
Driving Variables	Surface Zonal Wind	Snowpack sublimation losses
	Surface Air Temperature	Snowpack composition/melting
	Surface Relative Humidity	Snowpack composition/melting
	Snow/Non-Snow Precipitation	Affects snow water equivalent
	Solar Radiation	Affects snowpack melting
State Variables	Snow Water Equivalent**	Water yield of snowpack
	Snowpack Thickness**	Water yield/thermal properties
	Snowpack Average Temperature	Snowpack composition
Diagnostic Variables	Snow Sublimation Rates	Mass-energy balance
	Conductive/Latent Heat Flux	Validate average temperature
	Snowpack Melt Rate	Mass-energy balance
	Long Wave Radiation Flux	Compare with solar radiation/flux

* This list of model parameters/variables is only partial; some have been omitted for conciseness.

The number of input variables listed in Table 3.1 demonstrates the complexity of the SNODAS climate modeling platform. This complexity reflects the complicated climatic processes that affect snowfall properties. Due to the large number of variables that impact the output, no single variable carries significant weight such that an outlier in a particular variable (*e.g.*

abnormally high, erroneous temperature measurement) would drastically alter the output. Also, since diagnostic variables are also produced as output, they are used validate the other variables and ensure the model is working properly. The variables denoted with asterisks in Table 3.1 are of particular importance in this investigation and are the principal output variables that will be gathered for selected grid cells in Colorado for developing ground snow load maps. These variables, SWE and snowpack thickness (depth), directly affect the density of the snowpack at each grid cell and are useful for determining probabilistic ground snow loads in the state.

3.3 Identification of SNODAS Input

The SNODAS snowpack model assimilates various different sources of weather station data that are otherwise not compiled together. Specifically, SNODAS input includes all of the types of measurements described in Chapters 2.2 and 2.3; weather station input comes from most of the stations listed in Table 2.1. SNODAS uses a unique weather station identification system to archive its modeled output. The numerous agencies which operate and maintain the weather stations that are inputs to SNODAS have unique identification systems as well. These station identification systems are distinct, so a weather station identified by one system might possess a completely different name associated with its SNODAS modeled output. A brief explanation of the SNODAS weather station identification system is presented. Also, all SNODAS weather stations within Colorado that are used in this investigation are identified.

3.3.1 SNODAS Station Identification System

The NOHRSC branch of the National Weather Service has created a unique exchange format for storing modeled or observed meteorological data. This format allows interoperability and exchange of data across computer platforms and agencies, through a format known as SHEF or Standard Hydrometeorological Exchange Format (NWS 2012c). The SHEF format is applied

to all assimilated weather station data that SNODAS uses and it serves as a method of standardizing data that may have originated from numerous sources. While the coding and features of this format is not of interest here, the application of the SHEF format reduces all assimilated weather station identifiers into a string of five alphanumeric characters. The SHEF format adopts the naming convention of the NWS meteorological and climatological programs. This naming convention incorporates the first three letters of the city or town in which the station resides plus a two character 'SID Code'. The SID Code is an alphanumeric code assigned by NWS to represent the state or regional area. The SID Code for Colorado, for instance, is 'C2'. An example of a SNODAS station SHEF ID is the station at the Arkansas River in Granite, CO named 'ARGC2'.

To visualize the spatial coverage of stations included in the SNODAS model, Figure 3.1 displays all of the 588 stations modeled by SNODAS and considered in this investigation. They are plotted by their geographical coordinates on a topographical map of Colorado. Note that the weather stations plotted in Figure 3.1 do not represent the complete inventory of weather stations for which SNODAS models output; this investigation only considers SNODAS stations in Colorado with complete records from water year (WY) 2003 through 2012.[5] Refer to Chapter 6.3 for more details on the procurement of station data. A partial inventory of SNODAS stations used in this investigation is presented in Appendix C. To supplement this, a table which lists concise descriptions of each SNODAS station type is presented in Appendix D.

[5] A hydrological water year begins on October 1st and ends on September 30th of the following year.

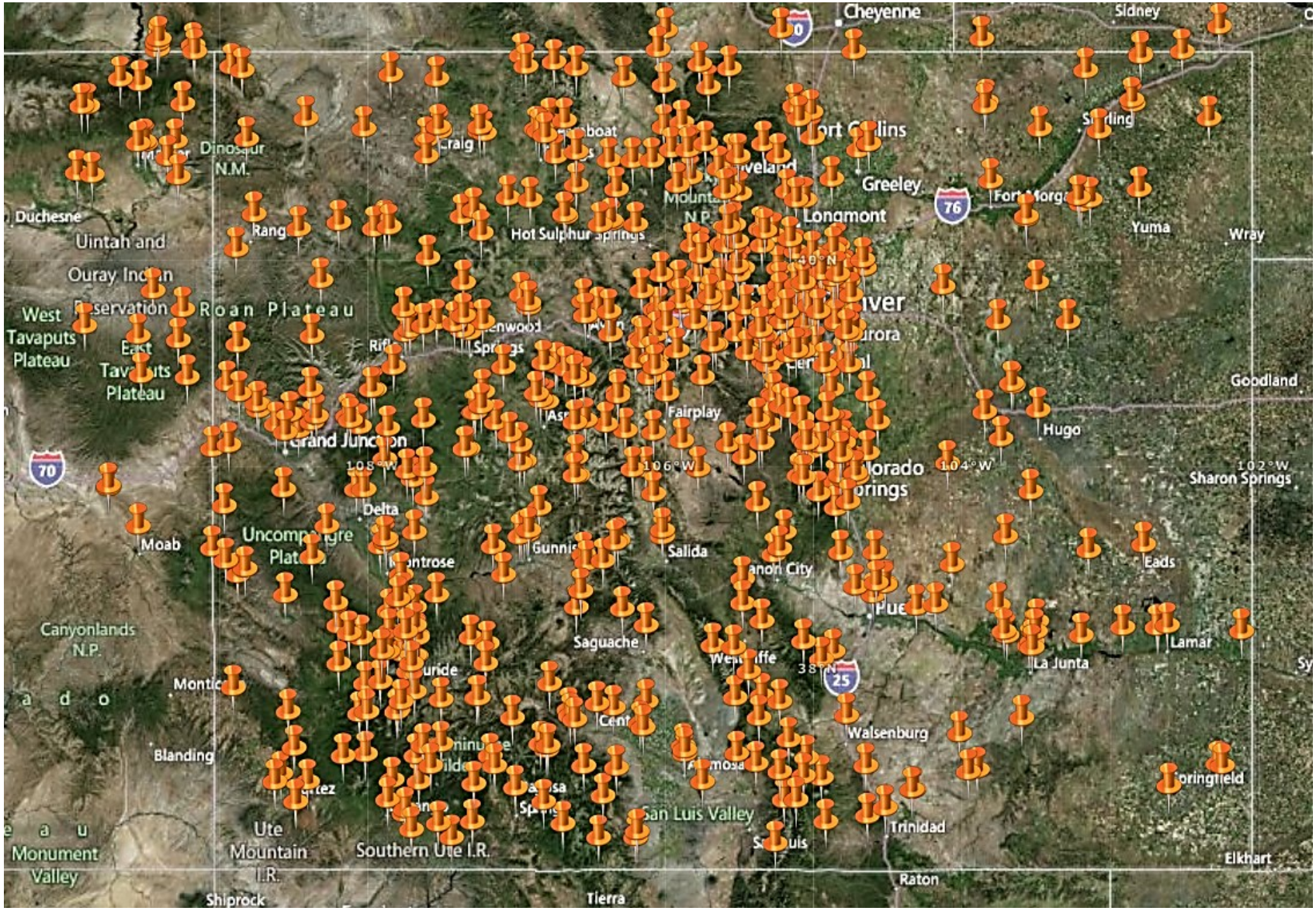

Figure 3.1: Weather Stations in Colorado and Vicinity Modeled by SNODAS Snowpack Model and Considered in this Investigation (stations shown have complete modeled records from WY 2003-2012). ArcGIS 10.1 was used to produce this topographical map.

3.4 SNODAS Data Assimilation

As previously mentioned, SNODAS assimilates various types of measured climatological data from ground-based, satellite, and airborne sources. All of these sources are either manually assimilated by trained analysts or numerically assimilated by the model algorithms. Data assimilation involves regulation of spatial and temporal variations in the source data as well as resolving discrepancies between modeled versus observed values. As introduced by Figure 3.1, each of the pins represents a station whose modeled SNODAS output is utilized in this investigation.

The main challenge for SNODAS is that ground-based sources provide *point* spatial observations while remotely-sensed observations provide *gridded* estimates (which is also the form of the final SNODAS output). All input, ground-based data are assimilated into SNODAS and each point source is responsible for the nearest grid cell or group of grid cells (Barrett 2003). This depends on the spatial distribution of the weather stations. Airborne or remotely-sensed data naturally produces gridded observations, so their coordinate systems need only be aligned with that of the SNODAS model. The SNODAS documentation does not describe in detail the process of combining point or areal source data into the grid cells, specifically in the event of uneven spatial distributions of weather stations. However, all sources are eventually assimilated into a single gridded model. To represent land cover, it incorporates a digital elevation model and also terrain features such as forest cover fraction and vegetation properties available from satellite and radar data (Barrett 2003). These site-dependent properties facilitate model interpolation between grid cells. An example of model input from satellite and radar that provides forest density and land use estimates of each station, vital to estimating the soil bulk density and other driving variables, is Landsat relief imagery. An example of a Landsat imagery analysis for station BOUC2 in Boulder, CO that feeds into SNODAS is available in Appendix E.

Another issue to consider is the selection of the temporal structure of the model, such as when model output is published and what timescales of the input sources are used. This is important since all sources of information do not publish data at the same time intervals. Also, establishing a standardized timeframe for reporting estimates is crucial since the time of the day significantly affects many output variables. Regardless of individual reporting times for all of the input sources such as ground-based and remotely-sensed, the model uses daily measurements/observations that coincide the closest to 6:00 UTC, or coordinated universal time (Barrett 2003, NOHRSC 2012). Despite the fact that SNODAS produces hourly modeled data, most of the snowpack properties such as snow depth and SWE are only updated once a day at this time. This standardized time roughly coincides with the beginning of the day for the central U.S. which eliminates measurement or observation errors that may arise from increased temperature and humidity during the daytime.

SNODAS may produce estimates of snowpack properties that differ slightly from the observations at the input stations. Modeled estimates must be balanced with observations from all of the sources of data in order to produce the most accurate output. The manner by which SNODAS handles discrepancies between modeled versus observed values is described in the next section. The general structure of the modeling procedures is first described.

3.5 SNODAS Snowpack Model Structure

SNODAS is a multi-layered, mass-energy balance snowpack model which is spatially distributed but uncoupled (Barrett 2003). This means that the redistribution of energy and mass inputs/outputs from one grid cell to another, due to snow drifting for instance, is not considered by the model. Energy inputs include radiation fluxes, surface temperatures, *etc.* while mass inputs include snow depth, modeled precipitation, SWE, *etc.* The snowpack model is most accurate

when used to estimate the current or previous properties of the snowpack; however, it has the ability to forecast at least one week into the future (NOHRSC 2012). The model is intended to provide the best estimate of snow cover and snowpack properties for prediction of hydrological modeling and water forecasting. However, between all of the driving, state, and diagnostic variables the model is capable of producing much more. The model can handle and incorporate a wide variety of meteorological conditions such as rain-on-snow, discrete snowfall accumulation, and freeze-thaw cycles while accounting for other phenomenon such as water transport, taking into account absorption and transpiration. Other processes such as the compaction of snow and its metamorphosis after deposition on the ground are also considered in the model.

The core of the SNODAS snowpack model is a set of governing differential equations that are based on the laws of energy balance and thermodynamics, which allow the preceding meteorological processes discussed above to be modeled (CRREL 1991). Due to the complexity of the constituents involved, which include snow and soil layers of spatially varying composition with properties (thermal conductivity, density, porosity, *etc.*) that vary with depth, the model is divided into layers of snow and soil. This allows computationally intensive equations to be solved incrementally with time and simultaneously for each layer.

There are three snow layers and two soil layers considered in the model (Barrett 2003). The snow layers define those representing the atmosphere-snow boundary layer, the insulated snow later, and the soil-snow boundary layer. The two soil layers reflect porosity and density variations, differing with depth, that affect water transport. The top soil layer is subject to thermodynamic fluxes while the deeper soil layer is isolated from such fluctuations. SNODAS uses this model of the soil-snow layers and applies horizontally infinite control volumes around them. These control volumes behave similar to Gaussian surfaces. Figure 3.2 illustrates the fractional

volumes of soil and snow which the model considers. Since air represents less than one percent of the mass of the soil or snow mixture, the layers that include fractions of air are excluded from the model equations (Figure 3.2 illustrates these two additional layers, however). The five-layer concept and control volume approach is coupled with the application of governing heat and mass conservation equations that are adapted from thermodynamics (CRREL 1991). Mixture theory, a specific branch of thermodynamics, is used here to account for the different layers which comprise matter of both different phases and different constituents (liquid and solid precipitation, plastic and frozen soil matrix).

Thus, a large set of equations are imposed on each layer and boundary conditions are set. These boundary conditions originate from the driving variables listed in Table 3.1 in addition to data assimilated from numerical weather prediction models (Barrett 2003). An example of a weather prediction model that is incorporated into SNDOAS is the RUC2 model used by meteorologists in near-term weather forecasting. The output from this model provides the driving variables of temperature, wind, relative humidity, air pressure, and precipitation that help the model initiate. By imposing the boundary conditions around the control volume and applying the conservation equations, a set of solvable differential equations is produced. These equations rely on the premise that the time rate of change of the state variables must equal their net flow across the boundary surface of the control volume, plus any internal production (CRREL 1991). The equations themselves are complex and require considerable background in advanced thermodynamics, fluid flow, and mixture theory. Thus, a detailed description of them is omitted for this paper. However, a brief discussion of the solution procedure is presented later.

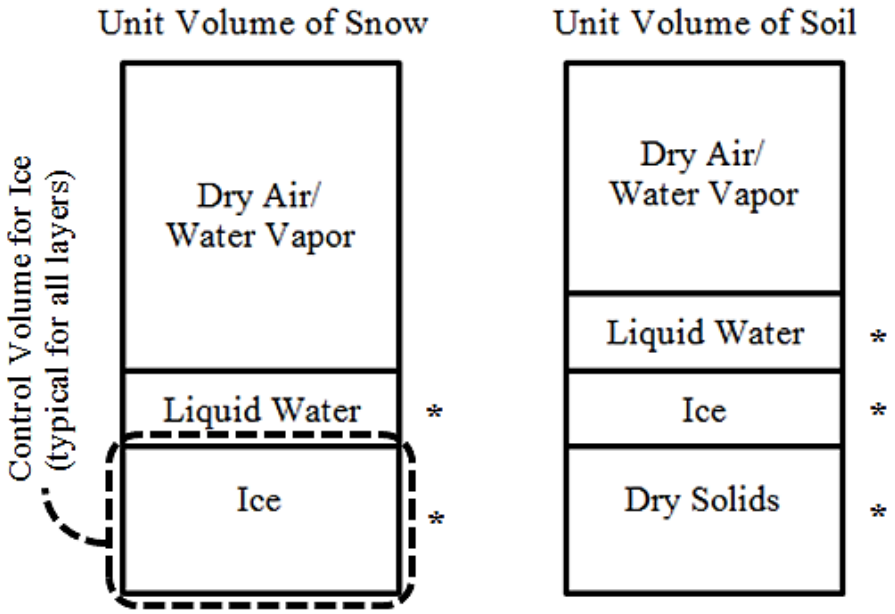

Figure 3.2: Phase Diagram Illustrating Five Soil/Snow Layers Incorporated into SNODAS Model. The five layers considered in model equations are denoted by asterisks. Adapted from CRREL (1991).

SNODAS output variables are modeled for discretized square grid cells of the Earth measuring 30 arc-seconds of length in latitude and longitude which roughly equate to a 1km × 1km model grid (Barrett 2003). Model output from SNODAS is estimated at the center of each grid cell. The coordinates of each grid cell and their boundaries are known from geophysical relationships, so they can be mapped internally within the model. These mapped grid cells are integral since they essentially represent control volumes themselves; their boundaries define which nearby sources are considered.

The general process of the SNODAS snowpack model is as follows (Barrett 2003):

(1) The model is initiated with the RUC2 numerical weather model using *Driving Variables*.
(2) At each grid cell, a mass-energy balance is computed in order to produce *State Variables.*
(3) All available ground-based station data are input and assigned grid cells in the snowpack model [UPDATE *State Variables*].

(4) All available airborne or remotely-sensed observations are input and aligned with the SNODAS grid, then assigned grid cells in the snowpack model [UPDATE *State Variables*].
(5) Difference fields are calculated between all observed vs. modeled quantities, in other words items (3), (4) vs. item (2).
(6) Difference fields are analyzed manually to determine if regions should or should not be updated with observations.
(7) Difference fields deemed necessary to update are interpolated through the entire gridded model.
(8) Model 'nudging fields' are created by dividing difference fields over a 6-hour period.
(9) Finally, SNODAS is re-run for the preceding 6 hours and 'nudging fields' are applied to the model to produce final *State Variables*.

In the preceding description of the SNODAS model process, the notation [UPDATE] denotes periods where state variables from ground-based and remote sources are introduced into the model. While not explicitly mentioned, the diagnostic variables are used throughout the entire process to validate proper operation of the model. During the model updating, any observation from ground-based or remotely-sensed sources from the preceding 18 hours is a candidate for the model run. If none exist or only a sparse distribution of update sources is available, a decision is made by the model analysts on which sources to include. Also, satellite imagery is incorporated into item (6) to determine regions that require updating; cloud cover usually indicates which remotely-sensed observations are to be included (usually only when mostly clear skies are present). Items (5) through (9) require a specialized process that is essentially the basis of the SNODAS model. These steps involve an assimilation procedure known as Newtonian Nudging, hence the term 'nudging fields' in (7) through (9). This assimilation procedure specifically addresses the disparities that can arise between the different sources, both spatially and temporally.

Newtonian Nudging or Relaxation is a four-dimensional assimilation process whose aim is to drive (or 'nudge') model-based output variables towards observed ones by taking into ac-

count spatial and temporal influences (Paniconi, et al. 2003). It can be performed on any model where various observation sources, such as grid-based (*i.e.* remotely-sensed) and scattered (*i.e.* ground-based) sources, need to be transformed and standardized so that they can all be incorporated into the model. The transformation includes forcing the model state variables towards observations by adding an additional forcing function to the model equations. This forcing function has the following form (Paniconi, et al. 2003).

$$\frac{\partial v}{\partial t} = F(v, \mathbf{X}, t) + G \cdot W(\mathbf{X}, t)\, \epsilon(\mathbf{X}) \cdot (v_{\mathrm{o}} - v) \qquad (6)$$

In Eq. (6), v is the assimilated state variable of interest and its subscript 'o' denotes observed quantities while the nominal form denotes model estimates. Also, $\mathbf{X}$ and t are the spatial and temporal coordinates of the state variable and thus the first term F represents the *model* forcing of the state variables from step (1) in the model process description. This forcing is for a particular variable at a particular point in space and time. The term G is a strength term applied to the weighting function, W, which varies spatially and temporally for each ground-based station. This weighting function determines the influence of nearby sources. Finally, ϵ is the usual error term that explains measurement error and reliability of the various sources. Since difference fields are determined first at observation points (*i.e.* ground-based weather stations) the Newtonian Nudging process is performed first at the ground-based stations. The rightmost term in Eq. (6) comprises the 'nudging' term or forcing. This equation is applied over all of the state variables at all SNODAS stations in order to create the nudging fields in step (8) of the process description. The weighting functions described above vary in form based on the philosophy chosen to account for spatial inconsistencies in observation points, as noted in Figure 3.1. Although the SNODAS documentation does not divulge the specific type of weighting function incorporated

in the Newtonian Nudging process, it is assumed to be Cressman-type or distance-weighted since these methods are very common in hydrologic modeling. A form of Eq. (6) specifically designed to handle unevenly distributed observation points, particularly for situations where values are not available at every point, was developed by Houser et al. (Paniconi, et al. 2003). This variant is not specifically discussed in this paper.

The SNODAS modeling process can be concisely summarized as follows. For a given six hour window of estimation, the model is initiated using numerical weather prediction models. Then, the model is updated with observations from both ground-based and remotely-sensed sources. Differences between model estimates and observations are computed at the ground-based stations. Difference fields are analyzed by meteorologists and model analysts to determine which regions to update. These differences are pushed or interpolated through to the entire gridded model. Hourly averages of these differences are computed and then forced into the model using Newtonian Nudging. This nudging process is performed at the ground-based stations first, then interpolated through the entire gridded model. The entire SNODAS model is then re-run and nudged at hourly increments for the preceding six hour window. This process is repeated every six hours, producing hourly modeled output.

3.6 Modeled Output Variables

The SNODAS model produces output available hourly for all stations with a SHEF ID (refer to Chapter 3.3). For each SNODAS station there are eight plots of modeled output produced, each of which plot several related snowpack model diagnostic and state variables. Table 3.2 lists the output plots and various diagnostic and state variables included in each.

Table 3.2: Output & Plots for Each SNODAS Station Available from SNODAS Snowpack Model (NOHRSC 2012)

Plot	Title of Plot	Diagnostic & State Variables Presented
1	Snow Water Equivalent, Snow Depth and Snow Melt	DEN,MLT,SD,SWE
2	Precipitation, Snow Water Equivalent and Snow Depth	P,SD,SWE
3	Time Window Cumulative Precipitation	P,SD
4	Snow Pack Temperature and Density by Layer	DEN,LD,T
5	Snow Surface, Mean Snow Pack, and Air Temperatures	MST,T,TS
6	Snow Melt, Sublimation, and Weather Forcing	MLT,RH,SUB,W
7	Snow Surface Energy Exchanges	HF,LF,SF
8	Snow Surface Radiation Fluxes	Net SF, Net LF

DEN = snow density; HF = heat flux; LD = snow layer depth; LF = longwave flux
MLT = snow melt; MST = mean snowpack temperature; P = precipitation (liquid/solid)
RH = relative humidity; SD = snow depth; SF = shortwave flux; SUB = snow sublimation
SWE = snow water equivalent; T = air temperature; TS = snow surface temperature

Out of the available data and plots produced by SNODAS, plots 1 and 2 are the most valuable for the purposes of this study because they include the two important output variables: SWE and snow depth. The SNODAS station BURC2 (a SNOTEL station) is geographically illustrated in Figure 3.3 with its output for WY 2005-2006 (plot 2) shown in Figure 3.4. This station is at an elevation of roughly 2850 meters, or 9350 feet. This station also provides input to the model, so both modeled and observed output are available and plotted. As it can be seen in Figure 3.4, the observed data and modeled data are remarkably close. The SNODAS model is intelligent enough to neglect the extreme outliers of observed snow depth (teal squares) when computing the time series of the plotted data. These outliers most likely represent erroneous readings due to rain on snow or some object obstructing the SNOTEL snow pillow. It is also worth noting that the plots for SWE and snow depth in Figure 3.4 accurately reflect the typical accumulation of both in high mountainous terrain during the winter months, with a sudden melt-off period starting in April and lasting until sometime in June (Doesken 2012). This provides

some validation of the model performance. The other available plots provide useful information for forecasting or monitoring a variety of climatological measurements. Notice that in Figure 3.4 the modeled time series for ground snow density appears to deviate considerably from the observed densities at the end of the water year. It is apparent that SNODAS encounters difficulty in predicting snowpack density at this time. This issue is likely associated with the larger variability and inconsistencies with snow density as a function of snow depth or SWE, as discussed in Chapter 4.3. Therefore, to avoid such issues with inaccuracy in modeled snow density, its output is avoided in this investigation.

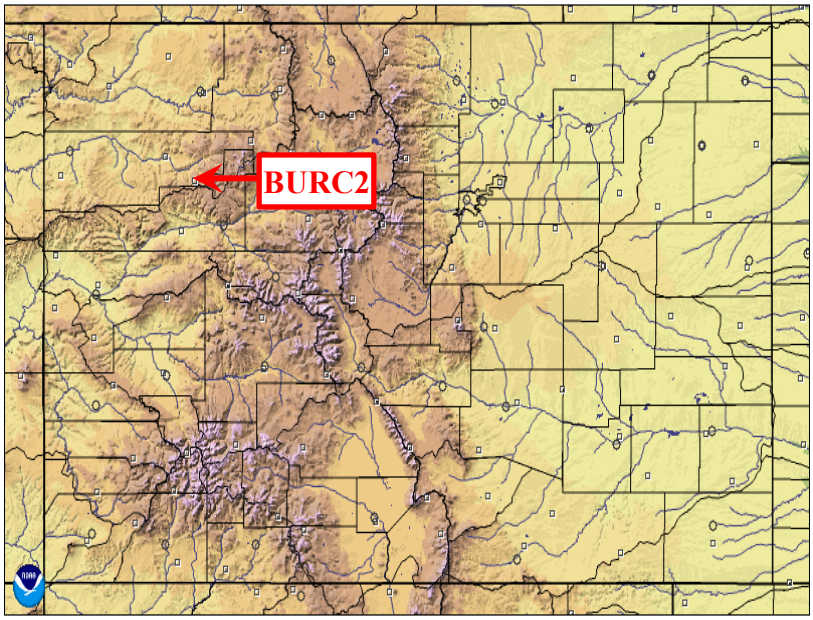

Figure 3.3: Location of SNODAS Station BURC2 in Colorado (NOHRSC 2012).

Examples of the other plots listed in Table 3.2 for SNODAS station BURC2 are available in Appendix F. Due to the elevation and most likely the heavy forested nature of the station, complete melt-off of the snowpack does not usually occur until late in the April-June timeframe since temperatures before that time period remain at levels below that needed to initiate melting. Temperature is not solely responsible, however, for melting of the snowpack; radiative energy from whatever sunlight the station sees also plays a role (Doesken 2012). A particularly interest-

ing observation made from scanning the plots in Appendix F is that the peak intensity of snowpack melting modeled by SNODAS in plot 1 (April-May) corresponds to the peaks of both the longwave and latent heat fluxes of the snowpack (Plot 7). These heat fluxes are indicators of energy absorption of the snowpack from radiative energy from the sun, which ultimately lead to melting. As well, this peak in melting also corresponds to the period of time when the daily average *observed* high temperature recorded by the SNOTEL exceeds 10-12 degrees C (50-54 degrees F), noted in Plot 5. This is consistent with temperatures necessary for moderate snowpack melting (Doesken 2012).

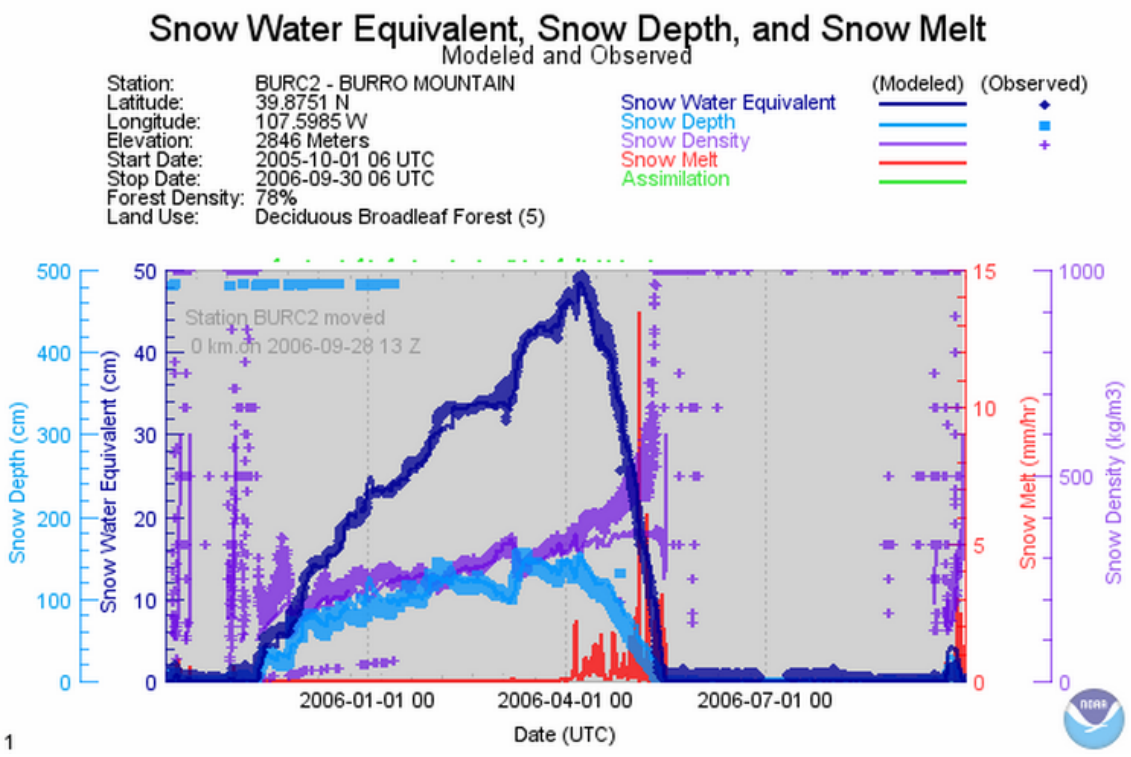

Figure 3.4: SNODAS Model Output Plot Showing Precipitation, SWE, and Snow Depth for Station BURC2 for WY 2005-2006 (NOHRSC 2012)

The variables graphed in the various plots of Appendix F are very useful to provide not only a means of validation of the output but also to indicate significant meteorological and physical processes that correspond to snowpack accumulation, melting, as well as those that possess

seasonal characteristics. Variables such as radiative fluxes, air temperatures, and wind speed may be used in the future as alternative means of correlating ground snow depth to density or water content.

3.7 SNODAS Modeled Output Validation

Validation of SNODAS output accuracy is difficult since the modeled output has only been available for roughly nine years to-date. According to the SNODAS documentation produced by the NSIDC, tens of years of data will be needed in order to make a proper evaluation of model output using observations available on the ground (Barrett 2003). This evaluation is complicated by the fact that the data sets that would normally be used to validate SNODAS output are actually model inputs. It is also not likely that independent validation data sets are available at the same spatial or temporal resolution as SNODAS (which should be aligned with validation data). However, a possible way to compare the output would include using records of data from stream gauges or other similar hydrologic instrumentation whose data is not currently assimilated into the model. Then, the simulated runoff interpolated from SNODAS output could be compared to the observed stream gauge data, for annual timescales (Barrett 2003).

This type of effort has recently been made in a region of the Rocky Mountains Range that lies within Colorado, using an independent dataset provided by the U.S. Geologic Survey (USGS) (Clow, et al. 2012). The study area included the roughly 660 hectare Loch Vale drainage basin located near the southern portion of the Rocky Mountain National Park, CO, illustrated in Figure 3.5. The basin area encompassed forested, subalpine, and alpine environments. This particular basin was chosen due to its involvement with ongoing research directed by the USGS related to hydroclimatic research, and the availability of independent data with which to validate SNODAS.

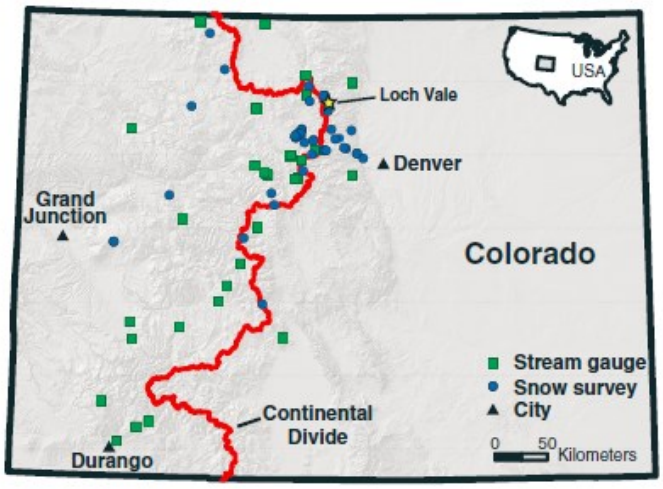

Figure 3.5: Loch Vale Watershed Study Area Used by Clow et al. for SNODAS Model Validation (2012).

Data to be evaluated in the study included gridded model output from SNODAS from January 2007 through July 2007. Utilizing GIS software, modeled estimates from SNODAS such as SWE and precipitation at the center of each grid cell were plotted along with basin boundaries. Modeled water-balance calculations were performed at the center of each grid cell. The calculations determined the differences between modeled April 1st SWE outflow minus sublimation, transpiration, and ground transportation, totaled for the entire basin.

Independent validation data came from snow surveys conducted by the research team and water-balance calculations performed at the 31 headwater gauges in the watershed. The snow surveys closely followed current snow course standards for extracting observed SWE measurements. Sites were chosen that correlated to roughly the center of each grid cell SNODAS models for the Loch Vale watershed. The independent validation water-balance calculations came from a USGS watershed model developed specifically for the Loch Vale watershed. These water-balance calculations were compared to interpolated water-balance estimates as modeled by SNODAS.

The results of the comparison indicated that SNODAS performed quite well in most forested regions. The correlation coefficient between the measured SWE and snow depth and SNODAS modeled SWE and snow depth in forested regions was 0.77 and 0.72, respectively. However, for alpine regions within Loch Vale SNODAS accuracy suffered, with correlations between measured and modeled SWE and snow depth reducing to 0.30 and 0.16, respectively. The modeled water-balance correlated relatively well to the runoff calculations at the headwater gauges. For these calculations, the correlation between actual and modeled water-balance was acceptable ($R^2 = 0.52$) with a root mean square error of only 9.5 cm of SWE. Alpine regions with poor correlation were included in the overall estimates of modeled runoff by SNODAS, reducing the overall correlation to actual runoff.

The study determined a method for correcting the SNODAS model estimates in the alpine regions where correlation to actual measurements was poor. Since the results indicated that wind redistribution of snow in alpine regions most likely resulted in the poor performance of the model in these areas, an error correction was applied in the alpine regions of modeled output. Recall that since the model is spatially uncoupled, redistribution of any mass variable is not considered, so this is a viable concern. Using a 'wind index' derived from the terrain slope in the upwind direction as a predictor, a multiple regression analysis was performed on the model errors in alpine regions. The corrected SNODAS estimates resulted in significant improvement to model performance for the averaged results of all sites. Averaged SWE and snow depth correlations increased by 0.67 and 0.37, respectively. Root mean squared errors were nearly cut in half after model adjustments were applied. The unadjusted and adjusted comparisons of measured versus modeled SWE are illustrated in Figure 3.6.

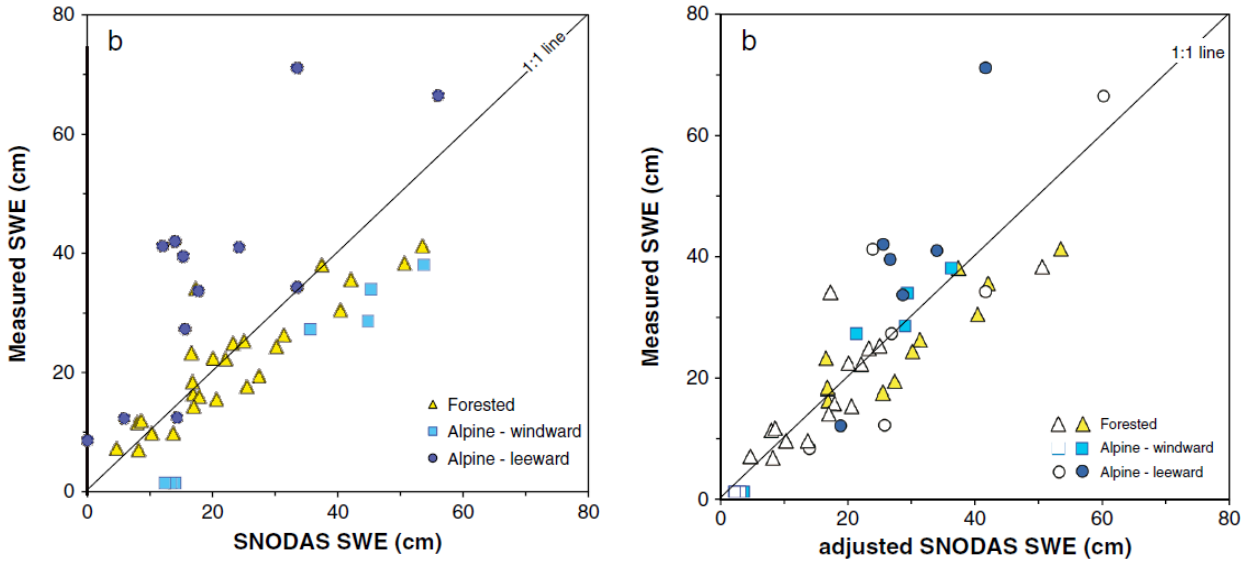

Figure 3.6: Comparison of Measured SWE to SNODAS Modeled SWE, Before Model Adjustments, left, and After, right (Clow, et al. 2012).

The study did validate usage of SNODAS in forested areas, which account for the majority of the stations in Colorado. A criticism of the study, however, is that for the watershed runoff water-balance correlations, the spatial resolution of the validation set was much finer than that of SNODAS. As previously mentioned, these spatial resolutions should be aligned since SNODAS was not designed to predict such localized estimates of SWE and runoff. Second, it is not feasible to assess the efficacy of the SNODAS model using less than one year of data from one source. However, the adjustment methodology is noted as a viable way to correct SNODAS estimates in extremely unprotected, alpine regions. Overall, the results of this study indicate good performance of SNODAS on the regional level, which is in accordance with its usage in this investigation.

Another widely-used snowpack assimilation model is the NOAH LSM/HRLDAS (Land Surface Model/High Resolution Land Data Assimilation System) model (Barlage, et al. 2010). This coupled system, referred to simply as NOAH, is very similar to SNODAS. It also utilizes a mass-energy balance in its model to estimate snow state variables, assimilates input from a varie-

ty of sources, and initiates with a Weather Research Forecast (WRF) model similarly to the weather prediction model used by SNODAS. A significant difference between NOAH and SNODAS is that the former is quite less complex in terms of its model algorithms. It only considers a single layer of mixed soil/snow, and lacks the capability to model snow grain metamorphism, multi-dimensional snowmelt factors, or water retention among other differences. SNODAS incorporates all of these elements into its snowpack model. This lack of complexity has likely resulted in the under prediction of snowpack accumulation/ablation and SWE by NOAH. Recently, the SNODAS snowpack model was used as a validation to the coupled model.

Barlage et al. (2010) used an independent dataset composed of SNODAS output as well as SNOTEL ground-based station data to validate and help improve the temporal prediction of SWE by the NOAH model. They considered several model modifications such as the adjustment of solar radiation for varying terrain slope and aspect, the addition of time-varying snow albedo (reflective coefficient), and other enhancements to improve snow/soil boundary layer processes (Barlage, et al. 2010). To test their effects, individual model modifications were successively implemented, in addition to a final trial with all modifications, and compared with the SNOTEL and SNODAS output/observations.

The SNOTEL station dataset used as verification was independent from that used as model input. Validation with both SNODAS and SNOTEL was performed separately for the timeframe between November 2007 and August 2008. In each effort, elevation was used to separate out groups of validation output points (for SNODAS) or stations (for SNOTEL); four to five elevation groups were created for comparison to NOAH model output.

The modifications to the NOAH model resulted in significant reductions in SWE under prediction when compared to SNOTEL and SNODAS data, when all modifications were imple-

mented (Barlage, et al. 2010). The reductions were nearly identical for the comparison of the model to either SNOTEL (36% reduction) or SNODAS (34% reduction). When *snow cover* predictions were compared to MODIS and SNODAS, agreement between both of those models and NOAH was generally greater than 80% after the implementation of the modifications.

In relation to this investigation, the results of this study give merit to SNODAS as a snowpack model. The nearly identical performance gains between NOAH and both SNOTEL and SNODAS implies some sort of relationship between the latter two. The high reliability of SNOTEL data and its usage alongside SNODAS in a validation capacity furthers the reliability of SNODAS. Furthermore, the modifications made to the NOAH LSM/HRLDAS model which resulted in significant performance gains are already implemented into the SNODAS platform. Finally, the fact that SNODAS is being used as validation for other less-developed snowpack models speaks to its own strength as a modeling platform.

4.0 APPLICATIONS OF SNOW WATER EQUIVALENT AND SNOW LOAD RESEARCH

4.1 Snow Water Equivalent

The parameter of interest for this investigation is a ground snow load that can be determined and mapped at all locations in Colorado. However, even at specialized stations such as SNOTEL, Snow Course, First Order NWS, and modeled SNODAS stations, a measurement of ground snow load itself is not obtained directly. What is directly measured (or modeled in the case of SNODAS output) at the aforementioned stations is a particularly useful measurement of the snow water equivalent (SWE) of the snowpack. A value of ground snow load can easily be obtained with this quantity, as discussed in the following sections.

As briefly defined in Chapter 2.2, SWE is a measurement of the equivalent water content of the snowpack. More specifically, a measurement of SWE is a depth of water that would result from melting a column of snow with a unit cross-sectional area (Schmidlin 1990). It is directly related to snow depth and density via the following relationship:

$$SWE = h_s \left(\frac{\rho_b}{\rho_w}\right) \tag{7}$$

In Eq. (7), *SWE* is typically reported in inches, h_s is the depth of the snowpack in inches, ρ_b is the bulk density of the snowpack in pounds per cubic foot, and ρ_w is the density of water (Sturm, et al. 2010). By inspection, the weight of the snowpack can be directly calculated by re-arranging Eq. (7) and solving for $\rho_b h_s$, the ground snow load, P_g. Thus, for stations where SWE and snow depth are directly measured, the ground snow load can be computed by multiplying the measured SWE by the unit weight of water. Since the ratio $\left(\frac{\rho_b}{\rho_w}\right)$ is unit-less, *unit weights* can be

substituted in place of densities in Eq. (7) in order to arrive at a ground snow load per unit area. Equations (8) and (9) below illustrate this (specialized for English units):

$$P_g = SWE \times \gamma_w \tag{8}$$

$$P_g\ (psf) = \frac{SWE\ (in)}{12\ (^{in}/_{ft})} \times 62.4\ (pcf) = 5.2 \times SWE \tag{9}$$

Where SWE is not directly obtainable it must be implicitly determined in order to derive a ground snow load using Eq. (9). Recall from Chapter 1.2 that SEAC performed an analysis of annual records from SNOTEL and NWS First Order stations. That analysis included translating the SWE measurements at these stations into ground snow loads using Eq. (9). A relationship between this ground snow load and the recorded ground snow depth was then made and applied to other stations throughout the state where only depth was recorded. Recent research regarding the estimation of SWE using climatological and meteorological data has been conducted by numerous federal agencies within the United States as well as international agencies throughout the world. This research could perhaps be adapted and applied to weather stations where ground snow loads or SWE are not directly measured. The research performed here will build on such previous work outlined below.

4.2 Mechanics of Snowfall that Affect its SWE, Density, and Load

Snow precipitation varies greatly in water content (SWE) and density, depending on various atmospheric factors and processes before snowfall and after deposition on the ground. These factors greatly affect the supersaturation of water and density of the snowfall (Judson and Doesken 2000). Immediately after its formation within clouds, the quantity of SWE in the snow crystals will typically remain constant unless the crystals encounter warm moist atmospheric layers. Conversely, the density of the snow is greatly affected by the atmospheric temperature and

pressure as it falls. After deposition on the ground, both the SWE and density of a unit volume of exposed snow are products of numerous time-dependent factors. Since both SWE and density are closely related to ground snow load, the mechanics of snowfall and the factors that affect these snow properties are of significant interest to this investigation. The composition of snow and its subsequent metamorphosis both prior to and after deposition on the ground is discussed.

Snow begins as droplets of supercooled water in clouds that condense in the cold atmosphere, nucleate around dust particles, and form smooth plates of ice (Caltech 1999). The habits, or shapes, of the ice crystals during formation have been studied extensively (Baxter 2005). Four main habits of ice crystals have been identified that depend on the temperature during crystal formation and the water supersaturation within clouds. These configurations include dendrite, plate, column, and needle habits, as depicted in Figure 4.1. The most familiar shape of snow crystal is the ubiquitous snowflake which assumes a plate or dendrite habit. Various other configurations which are permutations of these basic habits are possible as well.

The habit is of particular interest because it determines the amount of pore space (or entrapped air) within the newly formed crystal (Judson and Doesken 2000). This pore space dictates the initial density of the snow as it is falling. For instance, when ice crystals of snow form at colder temperatures they typically form smaller, less dense habits as illustrated by the right hand side of Figure 4.1. Thus, the habits formed at these conditions are smaller, less dense, and usually of the dendrite variety which has a higher surface area to volume ratio. Conversely, warmer and thus moister conditions are associated with the more dense needle and solid column habits. Between ice crystal formation and deposition on the ground, riming or crystal growth by accretion of supercooled water droplets can greatly affect the snowfall's initial density or water content (Alcott and Steenburgh 2010). The degree of riming is largely dependent on weather

patterns, presence of warm atmospheric layers, or updrafts and most often highly variable. Lastly, a factor that greatly affects both density and SWE during formation is the storm track taken by winter snow events. Storm tracks in which low pressure systems originate from the Gulf of Mexico and travel northeast differ greatly from those that originate in the Arctic and travel southeast across the Plains of the United States (Baxter 2005). Winter storms taking the former track tend to carry more warm moisture from the Gulf while those taking the latter tend to be drier and colder. Colorado is situated in a longitude range where both types of systems impact the state; however, this varies throughout the winter season.

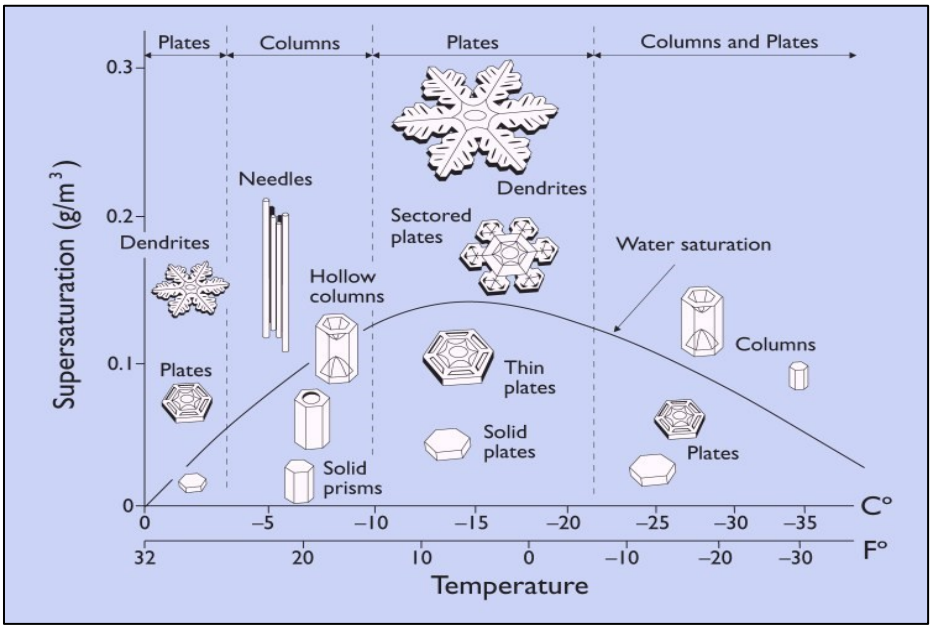

Figure 4.1: Types of Snow Ice Crystal Habits as Functions of Temperature & Supersaturation (Caltech 1999)

A study performed by Judson and Doesken[6] (2000) examined the density of snowfall in the Central Rocky Mountains, from sites across Colorado and Wyoming. Thus study provided insight into the mechanics of snow after it has been deposited. This study investigated the evolu-

[6] Dr. Nolan Doesken is the State Climatologist of Colorado.

tion of several properties of snowfall during the most crucial timeframe after snow falls (1 to 24 hours). Data was collected from daily snow core sample measurements taken from 11 sites of varying type (avalanche research facilities, snow research institutes, *etc.*) through four winters. The measurements were taken on standardized National Weather Service snow boards and SWE measurements were obtained using official sampling tools. Throughout the four winters sampled from each site, the range of densities of all the snow cores was between 10 and 257 kg/m^3 (0.624 to 16.0 lb/ft^3) with a standard deviation of as high as 41 kg/m^3 (2.56 lb/ft^3). This underscores the variability of the type of snowfall experienced throughout Colorado, where the majority of the study sites were located.

An additional component of the Judson and Doesken (2000) study was the investigation of overburden effects (compaction due to self-weight) on snow density. The analysis of snowfall events with moderate accumulation (greater than 30 cm) at five sites in the Central Rockies revealed that a subset of the data (events with a minimum of 2.5 cm SWE) indicated very high densities at the 24 hour mark. These densities were on average 16% higher than average densities for shallow snowfalls (less than 15 cm); some sites had densities 200% higher than the shallow sites. These data reaffirmed that compaction (and densification) due to self-weight is a prominent process even for snowfalls with relatively low water content.

Judson and Doesken (2000) also studied spatial variations in snowpack properties. From Colorado stations excerpted from the dataset, they determined the correlation of SWE data between pairs of stations with varying separation distance. The correlation coefficient as a function of separation distance was then plotted on a graph as seen to the right of Figure 4.2. The authors noted that beyond 10 km of separation, the correlations of any two stations fell uniformly below 0.7. Much further than this, the correlation was of little statistical significance.

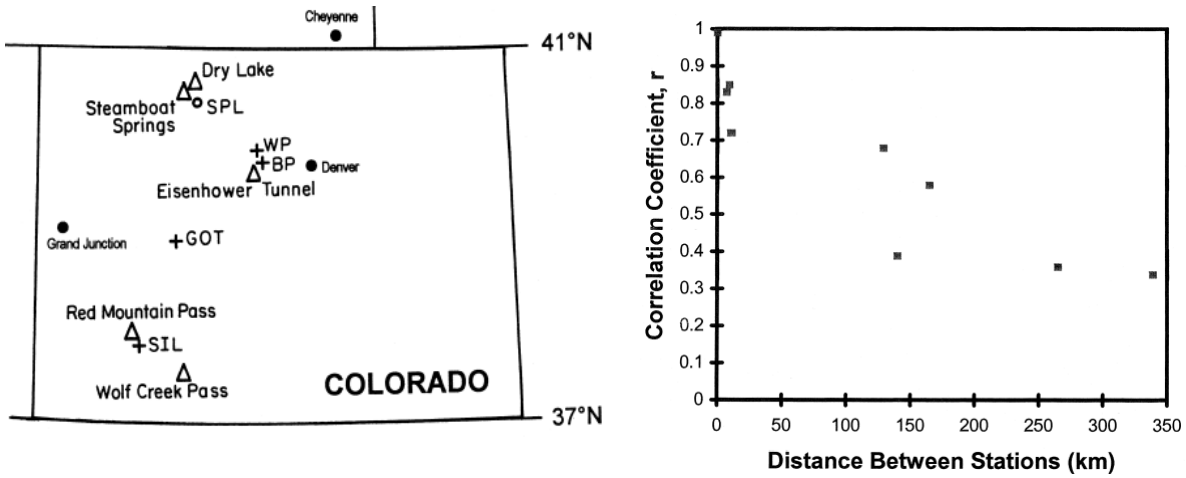

Figure 4.2: Weather Stations in Colorado Used by Judson and Doesken and Corresponding Plot of Correlation Coefficient vs. Station Separation for the Dataset (2000).

Overall the study showed that there were sizeable spatial variations in the daily fresh snow densities at the analyzed sites (Judson and Doesken 2000). Two main observations were that temperature was positively correlated to snow density for fresh snow and that compaction due to self-weight of the snowpack generally led to increased density. However, since the authors could not find a correlation of statistical significance for either assertion, they concluded that extreme spatial and temporal variations in density and SWE precluded such relationships. Therefore, in the Central Rockies snowpack density, SWE, and subsequently snow load are properties largely the result of highly variable weather and climatic processes that are not fully understood. This last statement was also confirmed by a separate study of long-term annual snowpack patterns across the entire Rocky Mountain Range (Changnon, McKee and Doesken 1993). In that study, various seasonal climatic patterns were discovered from more than 30 years of snowpack measurements at snow course sites from 1951-85. They discovered three predominant climatic patterns affecting snow pack properties: (1) abnormally wet or dry seasons for the entire region, (2) abnormally wet or dry seasons for the northern/southern Rockies, or (3) nor-

mally wet or dry seasons for the entire region. The high spatial and temporal variability of these patterns precluded the development of any trend or forecast of the patterns, be it spatial or temporal. The authors could, however, explain the climatic mechanisms behind them.

4.3 Recent Research on Ground Snow Depth-SWE Relationships

4.3.1 Development of a Model for SWE

The field of applied meteorology is saturated with research work concerning snow water equivalency in mountain snowpack. As defined in Eq. (9), a model to predict SWE is mathematically equivalent to one for ground snow load. A massive project was recently undertaken involving both the U.S. Army Cold Regions Research and Engineering Laboratory (CRREL) and NRCS, among other international organizations, which attempted to estimate density at a given site using inputs of snow depth, day of the year, and climate class (Sturm, et al. 2010). This study used a statistical model, grounded in Bayesian methods, trained by a set of 25,688 records of snow depth, density, and SWE obtained from weather stations in the United States, Canada, and Switzerland (Sturm, et al. 2010). The climate classification of each station was based on physical attributes of snowpack (depth, density, and type of snow layers) as well as information on vegetation, scrutiny of aerial photographs, and location (Sturm, et al. 2010). After an exhaustive effort to narrow down potential predictor variables, regression analyses yielded models that predicted density from the aforementioned inputs; an independent blind verification dataset confirmed the robustness and validity of the model. An interesting decision made by the research team here is to attempt to model bulk density of the snowpack (instead of SWE itself), and then convert that to SWE, presumably by the direct relationship indicated by Equation (9). Figure 4.3 illustrates the underlying reasoning for estimating bulk density. There is simply a smaller range of values for density as opposed to SWE. By studying the range of dependent variables in the

two plots, it is clear that the range of bulk density is several orders of magnitude smaller than the range of SWE. Thus, even though there is a very good correlation in the lower range of the Depth-SWE plot in Figure 4.3, an attempt to estimate SWE directly from depth would invariably incur more error in estimation than one in which density is first estimated from depth simply due to the substantial range of values for SWE. With that said, the correlation of snow depth to density is still quite poor although not explicitly noted in Figure 4.3.

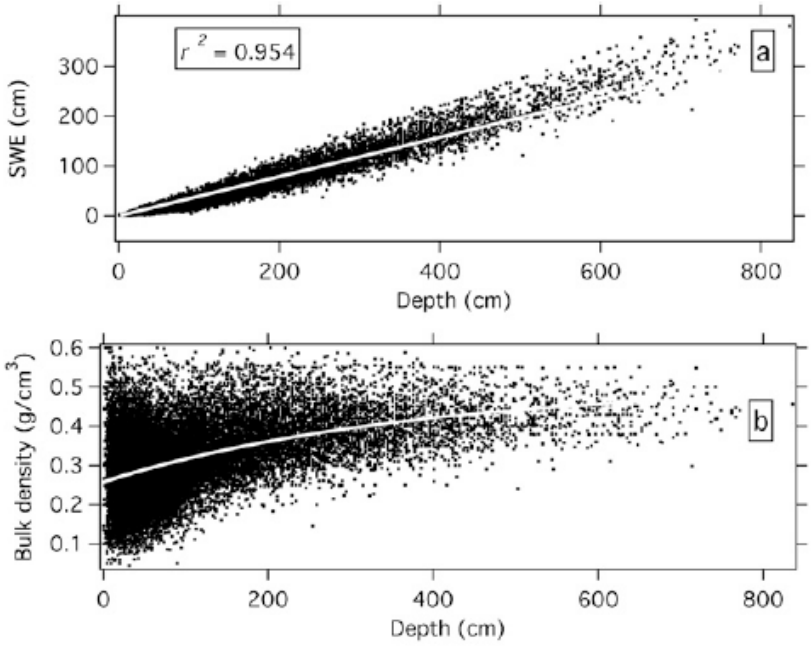

Figure 4.3: Depth-SWE and Depth-Bulk Density Relationships from Station Data (Sturm, et al. 2010)

Overall, the research by Strum et al. yielded a relatively good model to predict SWE from depth and relatively few inputs. The required inputs (snow depth, day of year, climate class) are readily available at most weather monitoring stations dating back to historic time periods. However, despite the large sample size, it did not encompass a variety of snow types and densities and hence was not truly a random sampling. As it can be seen by Figure 4.4, numerous sites are clustered in northern Alaska and the northern part of the Rocky Mountain Range. Furthermore,

according to the data presented, a disproportionate percentage of both the model training data set and the blind verification training set favored the same climate region (Sturm, et al. 2010). Lastly, while the climate classes (indicated by the key in Figure 4.4) were assigned by studying climate and topographical patterns, the class assignments is not supported by quantitative evidence. The authors do not discuss the assignment of stations where two or more classes are viable choices. This is generally problematic in that reproducibility of this effort would likely produce different climate class assignments.

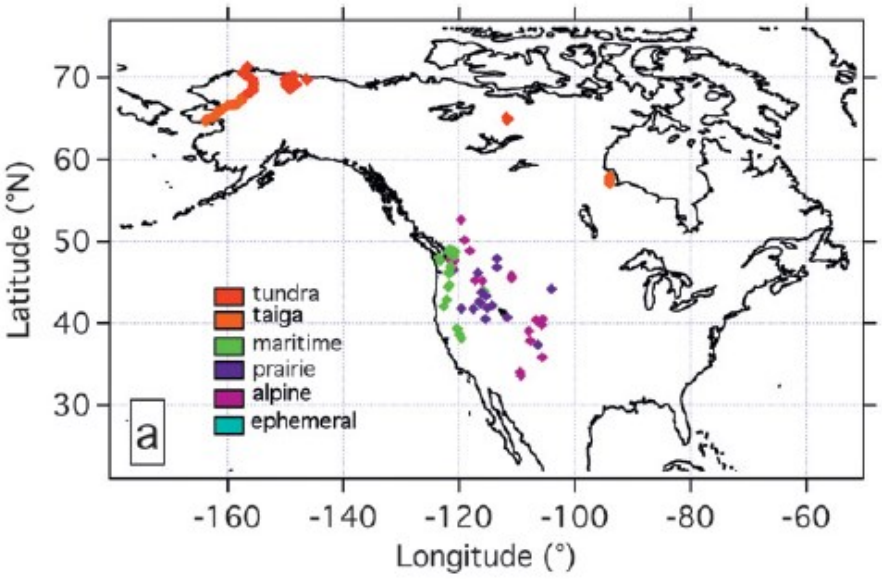

Figure 4.4: Locations of U.S. and Canada Stations Used by Sturm et al. (2010)

4.3.2 International Research on Depth-SWE Relationship

Similar research performed in the Swiss Alps attempted to combine the strengths of Sturm et al. with additional research interests and safeguards against sampling bias. A recent study performed in coordination with the WSL Institute for Snow and Avalanche Research in Davos, Switzerland attempted to estimate the spatial and temporal distribution of SWE in the Swiss Alps. The objective was to determine a relationship between snow depth and snowpack density that included both a time and location component, and later use this depth-density rela-

tionship to calculate SWE using the methods similar to Sturm et al. The Jonas et al. (2009) dataset used to produce the model was also quite large (11,147 records), as well as statistically robust (average 35 years of record per site). The records consisted of snow cores sampled bi-weekly since 1960 by trained personnel at the Swiss Federal Institute of Technology, equivalent in measurement type to Snow Course practices in the U.S. described in Chapter 2.2. Tight control of the standards and quality of measurements was available considering that a single regional entity was responsible for the data, and also since all measurements were snow cores and not mixed types.

Through descriptive statistics and preliminary temporal analysis of the site data, the authors were able to narrow down four factors which had a notable effect on density: (1) season, (2) snow depth, (3) site altitude, and (4) region (Jonas, Marty and Magnusson 2009). Factors (2) and (3) are intuitively linked to snowpack density since increasing snow depth inevitably results in increased compaction and also because elevated, colder mountain peaks generally experience greater snow accumulation. With regard to item (4), the snow core sites scattered throughout the Swiss Alps were apparently segregated into regions according to the basin or catchment in which they resided; however, the article did not precisely describe how sites were assigned to classes. Figure 4.5 illustrates the assigned regions with dark lines representative of region boundaries that appear to trace mountain ridges and valleys, indicative of typical basin catchments. A total of seven snow-climate regions were established, which ranged from wet-alpine to dry-alpine, also encompassing a range of nearly 1800 meters in elevation gain from the highest to lowest site (860 m. – 2690 m. asl.). The results of the investigation, after formulating a snow density model, indicated that season and snow depth were the two most important ones. Several experimental trials of model performance were conducted, varying the included factors (1) through (4) above.

The authors compared each trial model to an independent validation dataset. When season and snow depth were excluded the greatest model bias and root-mean-square error (RMSE) was observed (RMSE of nearly 38 inches of SWE). In contrast, the baseline model with only season and snow depth only had a RMSE of approximately 3 inches of SWE. Overall, the most important finding from this research is that temporal variations in addition to snow depth affect the depth-density relationship (Jonas, Marty and Magnusson 2009).

The model as created by Jonas et al. reportedly presented difficulties with low-altitude, early season, and shallow snowpack – a significant drawback for snow research in non-alpine regions, such as Colorado. Nonetheless, the effort to regionalize the stations is significant and should be taken into consideration for this investigation.

A similar study performed in the Italian Alps supported the concept of weather station regionalization by studying the spatial distribution of SWE in the Alps (Bocchiola and Rosso 2007). The initial objective of the research was to determine the statistical distribution that best described observed patterns of SWE. The dataset included 14 years of SWE measurements that were spatially distributed and covered the majority of the Italian Alps. The results of this study were that the scaled values of SWE showed homogeneity of the coefficient of variation in space, indicating a significant spatial variation of SWE. Bocchiola and Rosso therefore recommended a regional approach (*i.e.* one where stations were grouped prior to a statistical analysis) for frequency estimation of SWE (2007).

Figure 4.5: Map of Snow Course Sites Throughout the Swiss Alps Used by Jonas et al. (2009)

4.3.3 Early Approaches to Regionalization of Weather Stations

The regionalization of weather stations has been studied for decades. A study performed in the northeastern U.S. in the early 1990s attempted to create a simplified model to predict SWE using only a few input variables. The study was performed prior to the era of sophisticated weather instruments, so basic model inputs were necessary. The model, developed by Samelson and Wilks, was designed to predict SWE at 15 NWS First Order stations in the Northeast U.S. using basic inputs that could also be obtained at CO-OP stations (1992). Such inputs included daily snow depth, precipitation, and temperature readings. The 15 NWS First Order stations had between 33 and 35 years of SWE records that were used as model validation. After evaluating various test models, the authors narrowed down four variables reasonably correlated to snow-pack SWE. These variables included both quantities readily available at CO-OP stations in addition to derived variables that are simply reconfigurations of the original ones. For instance, one of the derived predictor variables used in the final model represented the number of consecutive days where the station recorded a maximum temperature below freezing. This predictor was de-

rived from temperature readings taken during the month. Other predictor variables used in the final model included the prior day's precipitation, the prior day's snowfall, and the square root of the current day's snow depth.[7] Due to the nature of the inputs, the model was designed to predict SWE daily.

The analysis first determined regression coefficients that defined prediction models relating the four aforementioned predictor variables to SWE at each of the 15 First Order stations. The four-variable model was then compared to daily historical records of SWE at the First Order stations. Statistical testing revealed a sizeable range of coefficients of determination, R^2, between the model and each station (0.43 to 0.88) but only a modest range of RMSE (0.13 to 0.27 inches of SWE) (Samelson and Wilks 1992). The authors refined the models by combining groups of stations together subjectively by climatic region. Four climate regions ("coastal", "mountain", "western New York", and "total") were created. Then, regression models for each climate region were developed by determining the model coefficients that best fit all of the members within the region. The results showed improvement in R^2 for each group (0.62 at the lowest) with virtually no change in the RMSE.

Using an independent set of verification data available in the form of Snow Course data at nearby sites (which provided useful SWE datasets), the models were assessed. The results of this validation revealed that the developed models predicted SWE reasonably well at higher values. Approximately 67% of all estimated SWE values fell within 50%, 25%, and 15% of observed SWE when the estimated values were 2.5, 12.7, and 25.4 cm, respectively (Samelson and

[7] Previous work by Neter et al. (1985) had illustrated that the square root of snow depth was a better predictor of SWE than snow depth, so the authors incorporated this finding into their analysis.

Wilks 1992). In other words, the model accuracy increased with increasing values of SWE. Overall, this study demonstrated the value of regionalization of weather stations and underscored the importance of retaining model simplicity.

4.4 Recent Snow Load Research

Recent research efforts to modernize and standardize the Eurorode have resulted in significant improvements. The Eurocode is a globally respected building code specifically adopted by the 31 European countries that comprise the European Committee for Standardization (CEN) (Gulvanessian, Calgaro and Holickây 2002). The Eurocode is also widely promoted outside the EU. The latest version of the code contains 10 separately published sections which govern the basis of design and the actions imposed on all structures (EN1990 & 1991), material specific requirements (EN1992-1996, 1999) and geotechnical and seismic requirements (EN1997 & 1998). Snow load provisions are covered under EN1991: Actions on Structures. Within it, there are now 10 'homogenous' climatic regions whose geographic snow load maps are presented in Annex C of the code. The methodology behind the development of snow loads of the Eurocode is important to this investigation due to the broad endorsement of the Eurocode by the CEN and the recent research efforts focused on improving its snow load provisions. Therefore, any applicable philosophy that can be drawn from EN1991 regarding ground snow load analyses should be considered in this investigation.

Prior to the research efforts the code was absent of standardization of the snow load maps. There was no comprehensive European ground snow load map with individual country regions discretized. Therefore, various countries chose different approaches for statistical analysis, including different distributions to describe snow loads such as Gumbel, Weibull, and Log-Normal (Formichi 2008). Finally, much like the problems that plague the U.S. state-produced

snow load maps the national maps constructed by the Eurocode had inconsistencies at country borders. After the updating efforts the European region increased its database of snow loads for analysis, standardized the usage of a Gumbel Type I cumulative distribution function, and regionalized the CEN area into the current 10 climate regions. Nearly 2600 weather station datasets are included in its current version, which were used to develop snow load vs. elevation relationships for zones established within each region. These regions are illustrated in Figure 4.6 alongside a sample plot of snow load vs. elevation for the Alpine region, produced by Formichi (2008). The wide acceptance of the Gumbel Type I distribution was based on the evaluation of the three aforementioned distributions; the Gumbel distribution fit the dataset the closest after a comparison of correlation coefficients. The code recognizes the issue where some regions experience winters with significant accumulation followed by no-snow winters, and has thus analyzed these regions according to a mixed distribution approach, initially proposed by Thom in 1966. In the development of the ground snow load relationships within each zone of each region primary consideration is given to altitude, believed by the CEN to be the most crucial component. Other contributing factors to ground snow load have been studied on the international level. These studies introduce other variables while maintaining the significance of regionalized climate classes as in the Eurocode.

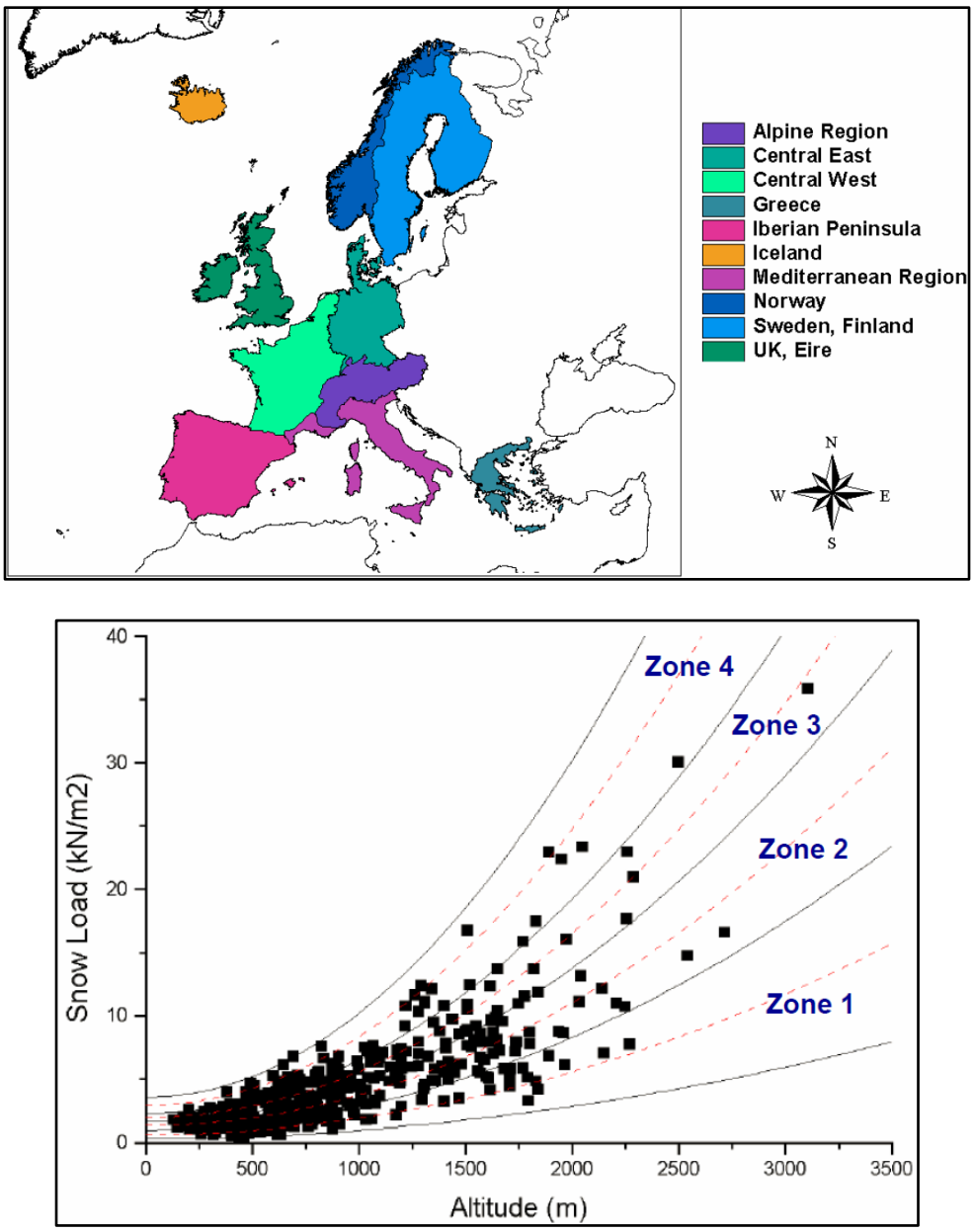

Figure 4.6: Ten Climate Regions Established in Eurocode EN1991-1-3, top and Partitioning of Alpine Region into Zones 1-4 Showing Load-Elevation Relationship, bottom (Formichi 2008).

A research effort in the United States in 1982 by Ellingwood and Redfield examined extreme annual ground snow loads at weather stations throughout the Northeast (1983). Ellingwood and Redfield performed a statistical analysis of extreme ground snow water equivalents in an attempt to suggest an appropriate type of probability distribution to describe these extreme events. The research was performed just after the publication of ASCE 7-82; the objective of the

study was to prepare for modifications to the next publication of the standard, ASCE 7-88. The study area included 76 NWS First-Order weather stations in the Northeast that had at least 10 years of data, covering the winters of 1952-1980. The two most widely accepted distributions in the literature at the time of the study, the lognormal and the Type 1 extreme value (Fisher-Tippet) distributions were analyzed. A third, the Type II extreme value distribution, was also considered. These represented three probability distributions with considerable differences in the spread and upper tails of the density functions.

In order to determine the appropriate probability distribution, goodness-of-fit was evaluated using the maximum probability plot correlation coefficient (MPPCC) criterion (Ellingwood and Redfield 1983). For each station, the dataset of water equivalents were rank-ordered and plotted on probability paper, and then an equation was fit by linear regression. If the equation was approximately linear and the MPPCC was close to unity, then the probability distribution that produced the results was chosen as representative for that station. The results of the analysis showed that 50 of the 76 stations were best fit by a lognormal probability distribution. The Type II provided the best-fit at so few stations that the next best choice, the lognormal distributions, was selected as the best-fit at these stations.

The influence of limited sample size (*i.e.* less than 28 years of data) was also evaluated to see if the results were biased due to small historical records (Ellingwood and Redfield 1983). Simulations of snow water equivalents were produced at 38 selected stations using a Monte Carlo analysis. After testing the hypothesis that the Type I distribution was the best for describing annual extreme water equivalencies at the 5% significance level, the probability that it was the best fit was determined to be negligible (10^{-9}).

The results of the research suggested that the lognormal probability distribution was the best fit for all of the data. These results were further supported by the results of a similar study of probability models of annual extreme SWE, performed the following year, which Ellingwood and Redfield also authored (1984). These efforts were largely influential in the development of the ASCE 7-88 standard in which the same probability distribution was selected for the entire country. Subsequent editions of the Standard, up to the recent ASCE 7-10, have adopted the same methodology and probability distribution. However, a criticism of these research efforts is that they only considered a very limited region of the United States with very similar climatology. The best-fit distribution for the Northeast surely would not be the best-fit for the entire country. The narrowing of the data to the northeastern quadrant of the country was necessitated due to limited availability of ground snow depth and snow water equivalency data for the western portions of the country, at the time of the study. A solution to this issue is developed in this paper and discussed further in the following chapters.

5.0 PROPOSED METHODOLOGY FOR QUANTIFYING GROUND SNOW LOADS

The primary objective of this investigation is to develop a methodology for establishing ground snow loads that leads to mapped values for use in roof structural design. The ground snow load map itself is the main product from which the potential end users, such as designers and engineers, will benefit. The methodology described below focuses on those processes that collectively represent the transformation of raw snow data into a form that is suitable for constructing a snow load map.

The first component in this methodology is procurement of weather station measured data to be used in the analysis. Station data used in this investigation includes historical station records (snow depth, SWE, *etc.*) as well as station properties (location, elevation, ground slope *etc.*). Additionally, the procurement process covers the selection of the appropriate number of years of data, the data mining, and establishment of a local organizational system. A key innovation here is the use of modeled climatological data from SNODAS that provides a continuous field of output data. The SNODAS output used here is from nearly 600 modeled stations which represent all the different climate regions of the state. In addition, the SNODAS snowpack model is capable of producing continuous output fields that can be interpolated down to the 1km scale. This possesses significant advantages in spatial coverage over the much less dense point source datasets of both snow depth and SWE currently used in various state snow load analyses. The data procurement process is described in further detail in Chapter 6.0.

After the data has been procured, data processing can begin. This includes several initial items such as file organization and data cleaning to facilitate the statistical analysis. Statistical analysis of the data begins with preparation of the stations themselves, which includes perform-

ing a principal component analysis to separate out the key station properties (and groups thereof) that greatly influence the data. A critical aspect of the statistical analysis is the grouping of stations by similar climatology and topography so that members of each group can be expected to receive similar patterns of snowfall and snow loads. This is accomplished through various multivariate clustering techniques that incorporate the results of the principal component analysis. Techniques are then employed to improve the quality of the clusters, such as the standardization of the variables by z-score. This innovative approach to regionalizing station data is both robust and statistically grounded, resulting in highly reliable regions of similar stations. Once groupings of stations are established, relationships between snow depth and snow load are developed for each newly created cluster through nonlinear regression. These nonlinear relationships are tailored to each cluster and thus ensure that the relationship between ground snow load and depth accounts for the topography and climatology of each region.

These relationships are then used in conjunction with observed snow depth data at CO-OP stations to relate snow depth to snow load. At this stage, a probability distribution is fit to the snow depth data from CO-OP stations that reside in each cluster. Several distributions are investigated for each station; the one with the best statistical measure of goodness-of-fit within a cluster is then chosen for all stations in that cluster. Once a probability distribution is selected, a ground snow depth at a target MRI can be estimated for each station. This target MRI, historically taken to be 50 years, ideally is based on a reliability analysis as was done by ASCE 7. Finally, the target MRI snow depths are paired with the associated snow depth-load relationship for that cluster to yield ground snow loads with that target MRI. This process is described more thoroughly in Chapter 7.0.

The methodology proposed in this paper attempts to standardize and improve the overall process for determining *and* mapping ground snow loads. Therefore, once the desired snow loads at each SNODAS station location are determined, the next logical step is to plot these points on a topographical map and perform some spatial analysis to produce accurate snow load isolines. This spatial analysis is performed via geospatial information system (GIS) software. Several tools are available in GIS software packages that allow isoline and contour creation through the use of Kriging, inverse distance weighting, or nearest neighbor methods which provide spatial interpolation of values in regions where none exist. Alternatively, a grouping analysis using neural networks or a classification analysis, coupled with rolling-average mapping techniques can improve snow load mapping. Since various methods employ quite different algorithms to interpolate between the input point data, the results will be different. The robust analysis of ground snow loads performed in Chapter 7.0 would be undermined if an arbitrary method was used to map them. Therefore an established method for spatial interpolation is recommended here. Construction of a ground snow load map using spatial interpolation and GIS is described in detail in Chapter 8.0.

Figure 5.1 maps the entire process described above in the form of a flowchart. The flowchart progresses from the procurement of the datasets through to the final activity of producing a snow load map (in the flowchart, 'SD' and 'SWE' denote snow depth and snow water equivalent, respectively).

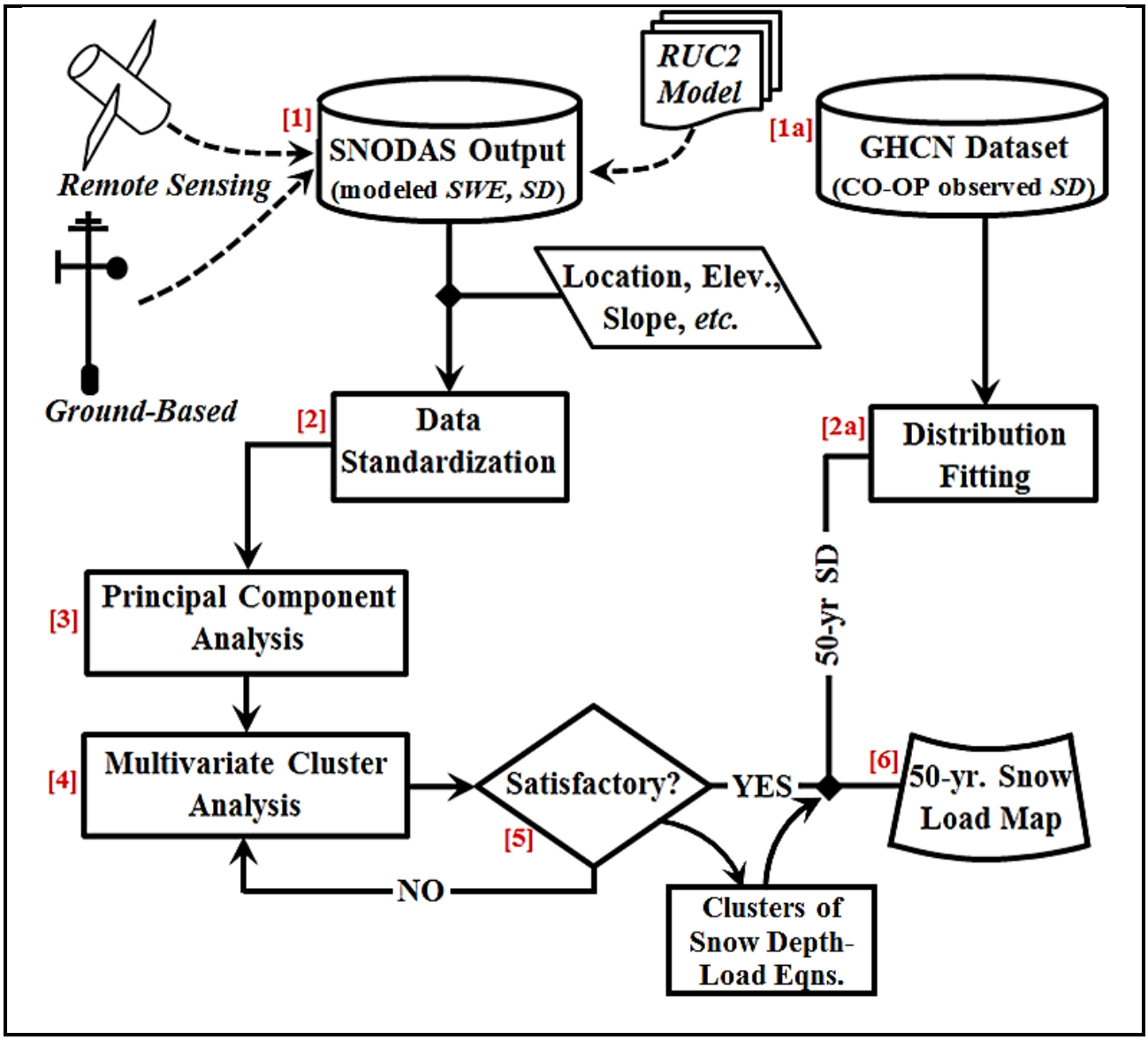

Figure 5.1: Process Flowchart for Ground Snow Load Analysis

6.0 WEATHER STATION DATA PROCUREMENT

6.1 Introduction

The data procurement phase includes acquiring all of the station records necessary for analysis and post-processing. The data collected for use in this investigation are composed of:

(1) Descriptive properties of each SNODAS station
(2) *SWE* and *snow depth* output from the SNODAS snowpack model
(3) *Snow depth* records from National Weather Service CO-OP stations

These sources alone are sufficient to accomplish the objectives laid out in Chapter 5.0. Item (1) above includes the input variables to flowchart element [2] from Figure 5.1. Items (2) and (3) are used for the ground snow load and ground snow depth analyses, and reference flowchart elements [1] and [1a], respectively. Since the SNODAS snowpack model readily assimilates SNOTEL, Snow Course, NWS First Order, and CoCoRaHS station datasets into its snowpack model, from a procedural perspective there is no need to consider these sources separately. Records for CO-OP stations are available from the Western Regional Climatic Center (WRCC 2006), although a more comprehensive and trustworthy archive is available from the GHCN database through the National Climatic Data Center web page.[8] The GHCN source of CO-OP station data is used in this investigation. Recall that the GHCN database receives a thorough review of its data to ensure accuracy and consistency of records (minimal missing data, data verification, *etc.*). Records of model output for all of the SNODAS stations used in this investigation are available from the NOHRSC web page.[9] Since SNODAS is under the jurisdiction of NOAA's National Weather Service, its modeled station data is associated with a weather fore-

[8] The NOAA NCDC web page: http://www.ncdc.noaa.gov/cdo-web/datasets/GHCNDMS/locations/FIPS:08/detail
[9] The NOAA NOHRSC web page: http://www.nohrsc.noaa.gov/shef_archive/wfo_stations.html

casting office (WFO). For the state of Colorado, the NWS maintains three: a Boulder-Denver office (BOU), a Grand Junction office (GJT), and a Pueblo office (PUB). Station output is queried using the WFO at the NOHRSC website.

6.2 Procurement of NWS CO-OP Station Data

The NWS Cooperative Observer (CO-OP) weather stations provide data that is used directly in the snow depth analysis. Of the NWS stations, both the First-Order and CO-OP station data are inputs to the SNODAS snowpack model, so both indirectly affect the output. However, CO-OP stations also provide valuable, lengthy historical records not available by the SNODAS snowpack model. Also, these numerous stations provide valuable data points that facilitate the creation of a ground snow load map, discussed later. Historical records from CO-OP stations are first acquired from online archives, filtered to eliminate invalid entries or stations with too short of a measurement record, and lastly processed to minimize inconsistencies such as duplicate stations or station relocations. Figure 6.1 shows a map of Colorado with all of the CO-OP station locations superimposed as squares. There are a total of 331 NWS CO-OP stations in Colorado or in the nearby vicinity.

The complete inventory of Colorado CO-OP stations is available on a separate web page.[10] This inventory includes pertinent descriptive information about every CO-OP station such as its unique station ID number, location, name, timeframe of measurement, and location information (latitude, longitude, elevation). A key piece of information provided, aside from the geographical location information, is the unique COOP number assigned by NWS that enables identification of each station. The list is comprehensive and includes every documented instance

[10] The WRCC inventory of CO-OP stations web page: http://www.wrcc.dri.edu/inventory/sodco.html.

of creation, relocation, or decommissioning of a CO-OP station. For example, there are seven entries for the 'AKRON 4E' station located in Washington, CO each with a beginning and end date of measurement for the six times the station moved. Most of these relocations, on average, involved distances of less than one minute of latitude (less than one mile). However, each entry for the same station must be assembled into one record so that no historical data is lost.

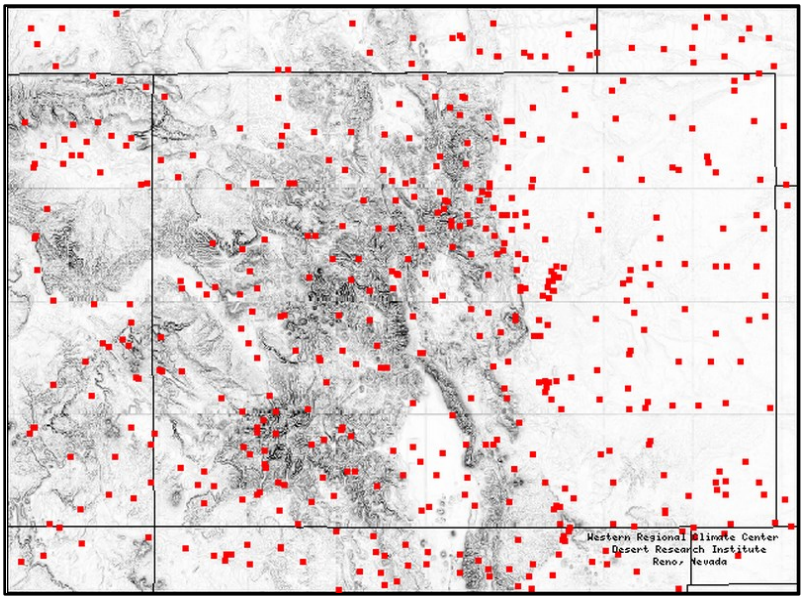

Figure 6.1: Map of NWS CO-OP Weather Stations of Colorado and Vicinity Used in Ground Snow Load Analysis (WRCC 2006)

For each CO-OP station, the NCDC offers various forms of datasets for these stations such as the annual summary, monthly summary, daily summary, 15-minute summary, or normal (averages) for the above timescales of temperature, precipitation, and ground snow depth. Of the products available for each station, the monthly data summaries are the most useful for this analysis. This is because the 2007 Colorado snow loads analysis and report published by SEAC analyzed station data with the same timescale. Moreover, the daily summary format contains extraneous detail which may be full of missing values and the annual summary format does not provide sufficient detail for an analysis. Since these stations are CO-OP stations they measure temperature, precipitation, and ground snow depth (refer to Table 2.1). The NCDC CO-OP web

page mentioned in Chapter 6.1 directly leads to station data access for Colorado. Data can be obtained by submitting a data request (the 'add to cart' hyperlink) free of charge. On the following web page the output date range, or start and end dates, is selected for the data of interest. As far as the requested output format, the most convenient is a Comma Separated Values (CSV) file type, which can be easily opened in a variety of software packages such as MS Excel. CSV files are composed of text strings with commas delineating separate types of entries that would normally be organized into columns of data. The data can be downloaded directly, or in some cases must be sent via a large file transfer service from NCDC for lengthy date range requests.

The CSV file contains a single header line describing the content of each column of data. The content includes the following: station (unique CO-OP ID number), station name (location, nearby city, *etc.*), elevation (feet above mean sea level), latitude, longitude, date on which measurement was recorded (year and month), EMXP (extreme maximum precipitation within month, hundredths of inches), MXSD (maximum snow depth for the month, inches), TPCP (total precipitation for the month, hundredths of inches), and TSNW (total snowfall for the month, tenths of inches) (NCDC 2013). At the present time, the fields EMXP, TPCP, and TSNW are not used in this investigation; however, it is possible that future efforts may find a use for precipitation or snowfall measurements. For the measurement fields, values of '9999' indicate that either missing values could not be reconciled or there was no data measured for that entry. NCDC does attempt to correct missing or erroneous entries by cross-referencing duplicate stations or using weighted averages of similar adjacent stations (NCDC 2012a). See Table 6.1 for an example of CO-OP station AKRON, which lists these tabulated values for selected dates where the station relocated. AKRON is located approximately 30 miles east of Fort Morgan, CO in the upper northeast quadrant of the state. The city Akron, CO is at an average elevation of 1,400 m.

Upon reviewing the data, it is clear that some data cleaning is necessary. First of all, there are instances of duplicate CO-OP stations that have resulted from station relocations. At first glance there is no obvious way to distinguish true duplicate stations from relocated stations. Duplicate stations are those very close to one another that share the same CO-OP ID, while relocated stations are those with the same CO-OP ID that have moved considerably far away. One method would be to use the unique CO-OP station identification numbers to separate the duplicates from mere relocations (since relocated stations sometimes are assigned new CO-OP IDs). However, this does not always resolve the issue. This issue is important due to its implications on the snow depth analysis. Say, for instance, a CO-OP station *appeared* to represent several distinct stations which possessed unusually high records of ground snow depths. In performing the statistical analysis on the ground snow depths to determine the target MRI depth, the result would be artificially inflated due to the effects of an outlier that was essentially more heavily weighted. Therefore, it is ill-advised to split a "single" station into two distinct stations. Likewise, it is also dangerous to consider several separate stations as one, based solely on the CO-OP station ID number.

Table 6.1 shows a portion of the dataset from the AKRON CO-OP station. This station possesses two separate station IDs throughout its existence, suggesting it represents two distinct stations each with historical records. The full dataset for AKRON includes all of the monthly entries for the station, most of which have been omitted. As it can be seen in Table 6.1, stations 50114 and 50109 are two distinct stations according to the National Weather Service. However, in both cases the latitude and longitude of the sites differ by less than a tenth of a degree. Most importantly, the elevation differs by less than 50 feet. Therefore, the identification of distinct stations according to CO-OP ID is misleading; these instances represent localities that experience

the same weather patterns. For this reason, the dataset of CO-OP station records must be carefully scrutinized and several metrics established to test whether separate station entries actually represent the same locality or vice versa.

Table 6.1: Historical Records for CO-OP Station AKRON Obtained from the NCDC Global Historical Climatological Network Database†

ID No.	Station Description	Elev. (m)	Lat. (deg-N)	Long. (deg-W)	Date of Measurement (yyyy)	(mm)	EMXP (in)	MXSD (in)
50114	AKRON WASH. CO AIRPORT	1384	40.157	-103.144	1937	03	9999	9999
50114	AKRON WASH. CO AIRPORT	1398	40.117	-103.167	1947	12	9999	9999
50114	AKRON WASH. CO AIRPORT	1423	40.167	-103.217	1960	07	93	0
50109	AKRON 4 E CO	1384	40.150	-103.150	1982	01	10	2
50109	AKRON 4 E CO	1384	40.155	-103.150	1990	08	180	0
50109	AKRON 4 E CO	1384	40.157	-103.144	1996	09	178	0
50109	AKRON 4 E CO	1384	40.155	-103.142	2002	02	2	1

† Table shows only selected entries where station AKRON appears to relocate; many monthly measurement entries and some columns have been omitted for conciseness.

To deal with the duplicate stations, first, the entire dataset sorted alphabetically by the station description field and then chronologically by date of measurement. If station duplicates exist, they would reside in the same city and so the first part of the station description would be the same. This step arranges the groups of station duplicates (if they exist) so that they are listed near each other chronologically. Then, a code is written in MS Excel to test if the individual station entries within each group differ in latitude or longitude by 0.05 decimal minutes. This represents approximately 6 km of distance on the Earth at approximately the 40° latitude, near the center of Colorado (NWS 2010). Specifically, it corresponds to instances of station relocations where there was also a significant elevation deviation (>30 meters). This threshold distance has

been chosen after several trials of applying various cut-off distances and observing the effects on 1) the total number of statewide stations produced, and 2) the maximum elevation differences between entries of a single station after each test. It is desired to keep the elevation differences below 50 meters, which resulted in the selection of 0.05 decimal degrees.

To deal with relocated stations presenting as singular stations, a second code is then written in MS Excel to test whether stations, separated by more than 0.05 decimal degrees latitude or longitude, possess a single station ID. Station instances separated by more than the threshold distance, regardless of station name, are considered unique. The results of these tests are implemented by aggregating or separating station entries accordingly.

The next operation performed on the dataset is to remove all entries where data is missing (*i.e.* where a value of '9999' exists in the measurement field for snow depth). Although NCDC performs quality checks on the GHCN database to correct missing values, not all of them can be replaced with data if, for instance, there are lengthy gaps of missing measurements. In this case, the data is neither functional nor desirable. Therefore, entire rows of data where the value '9999' exists for the maximum snow depth are removed.

The last operation performed on the dataset is a manual screening of the final list of CO-OP stations that have been distilled. The previous operations did not consider the possibility of missing station values such as elevation, latitude, and longitude that are needed for the later analysis of the dataset. Therefore, the dataset is then reviewed for such missing values and the appropriate values of these parameters (*i.e.* elevations, latitudes, or longitudes) are replaced. Adjacent entries with exactly matching station descriptions are used to replace the missing values. Station descriptions are lengthy and rather unique so they provide a reliable source for matching missing values. Now that the data cleaning has been performed, the stations are separated so that

their records can be analyzed later for extraction of target MRI snow depths. The statistical analysis of snow depths is detailed in Chapter 7.10.

6.3 Procurement of SNODAS Modeled Station Data

Access to the SNODAS model output is provided by the NOHRSC and NSIDC, who have a joint agreement to produce and archive all historical output from the model. Therefore, all data derived from SNODAS references these two sources (NOHRSC 2012, NSIDC 2004). Access to SNODAS resources is available by visiting the NOHRSC snow model output web page listed in Chapter 6.1. This web page serves as the home page and hub for all modeled output station web pages. By entering each station's SHEF ID into the 'Station Query' navigation pane, the browser is redirected to each station's main web page. There, station descriptive properties (elevation, latitude, longitude) as well as the modeled output variables (SWE, snow depth, precipitation, *etc.*) are accessible. The procurement of SNODAS modeled station data includes acquiring both of these types of data for each station. The procurement process for the above variables is described in the following sections.

6.3.1 Modeled Output from Each Station

The output variables SWE and snow depth from the SNODAS snowpack model are of particular interest to the analysis of ground snow loads in this investigation. These variables plus precipitation are provided in plot 2 of the NOHRSC as listed in Table 3.2. Therefore, the modeled output from plot 2 is obtained for all 588 SNODAS stations considered in this investigation. While graphical representations such as plot 2 are useful for displaying general trends and visually observing model performance, the assimilated model data behind the plots are much more useful for the statistical analysis.

The assimilated SNODAS output data in the NOHRSC plots is also available in downloadable a CSV file format, located at each SNODAS station's webpage. There are eight CSV files that correspond to plots 1 through 8, which contain output data directly from the SNODAS model. Each file contains the hourly modeled SNODAS variables for a user-specified model timeframe. This timeframe designates the start and stop dates as well as time of day for each. The start and stop dates of modeled output for each station encompass a single year and correspond to October 1st and September 30th, respectively. This ensures that the data is consistent with the hydrologic water year. Due to the design of the SNODAS model, specifically how it processes input data, the start and stop time of day is consistently chosen to be 6:00 AM. The measurement format chosen for all output are English units.

The CSV file download option provides the most flexibility for statistically analyzing the data on a local computer, as opposed to the web-based graphical output similar to Figure 3.4. However, with 588 individual stations and nine water years for which to obtain data, this task is too cumbersome for manual extraction. Therefore, Microsoft Visual Basic (VB) code is written to automate the data mining task. Specifically, a 'WGET' function is written in VB that successively parses through the NOHRSC station web pages for all of the 588 SNODAS stations. This code takes advantage of the archival structure of each station's modeled output data and the fact that each CSV file resides at a unique internet address. Therefore, the VB code only needs to open each of the 588 station webpages, specifically hyperlinked to the each respective CSV file, to initiate the downloads. A blank template of an internet protocol used with this Visual Basic WGET function is provided below:

> http://www.nohrsc.noaa.gov/interactive/html/graph.html?station=***STATION***&w=600&h=400&o=a&uc=0&by=***Y1***&bm=***M1***&bd=***D1***&bh=6&ey=***Y2***&em=***M2***&ed=***D2***&eh=6&data=12&units=2&region=us

In the above template internet address, "STATION" refers to each SNODAS station's SHEF ID, and "Y1", "M1", "D1", *etc*. refer to the year, month, and day of the start date for which the CSV file will contain modeled output. The numbers 1 and 2 in the above address designate start and stop days, respectively. The year is in a four-digit numerical format and the month and day are both in two-digit numerical formats.

The WGET script cycles through all nine water years for each of the 588 SHEF IDs, downloading the associated CSV files into a hierarchical system of folders on a local computer. Each modeled water year from 2003 to 2012 for each station is archived into a separate folder. SNODAS stations that reside within the same WFO are also organized together in a larger folder. A sample of the downloaded CSV file for station BURC2, including modeled SWE and snow depth, for water year 2005-2006 is available in Appendix G.

6.3.2 Descriptive Properties of Each Station

SNODAS Station descriptive properties are relevant for distinguishing every station from neighboring stations and providing unique characteristics about the topography and climate predictors of the station vicinity. Thus, regional patterns or differences in modeled output variables can be explained given an understanding of such properties. For instance, major differences in historical records of modeled SWE and snow depth at two SNODAS stations in the Central Rockies (GRTC2 and JWGC2) separated by only 10 miles cannot be explained by location or separation distance alone, since they are so close. However, supplemental information such as the elevations of the two stations, 8,720 ft. and 11,417 ft. respectively, does explain such differences. This observed local increase in snow precipitation with increased elevation is due to the phenomenon known as the orographic effect (Daly, Neilson and Phillips 1994). The sudden and sharp peaks of mountain ranges causes a retardation of the air masses of frontal weather systems

that, coupled with forced updrafts, result in localized increases in precipitation at higher elevations. Therefore, increasing information about a station's topography leads to increasing understanding of local and regional variations in snowfall properties.

Basic geographic information of all stations such as elevations, latitudes, and longitudes of all stations are easily obtained through the individual SNODAS station webpages, listed on each station information page. These basic descriptors are all recorded for all 588 stations for use later in the statistical analysis. A list of these geographic properties for stations AGLC2 through BRTC2 is available in Appendix C. However, these are not the only significant descriptive station properties that affect snowfall and SWE. Various other properties that describe topography and hydrologic properties are crucial in accounting for spatial variation in SWE and snow depth.

The slope direction, or aspect of the terrain is the one of the most influential topographical features, second to elevation, that impacts the amount of snow precipitation that accumulates at a site. The aspect of a site is the direction of the steepest downhill path, projected onto the horizontal plane, provided as an azimuth angle from geodetic north as illustrated in Figure 6.2 (Leyk 2008). Aspect is very good predictor of snow accumulation because winter storm patterns that trace easterly over the West deposit most of their snow precipitation on high elevation mountain *west* facing slopes (Doesken 2012). While local conditions such as updrafts and wind disturbances provide snowfall to other facing slopes, those facing the west certainly see more pronounced snowfall and accumulation. Therefore, aspect is used in this investigation as a predictor for snow depth and SWE.

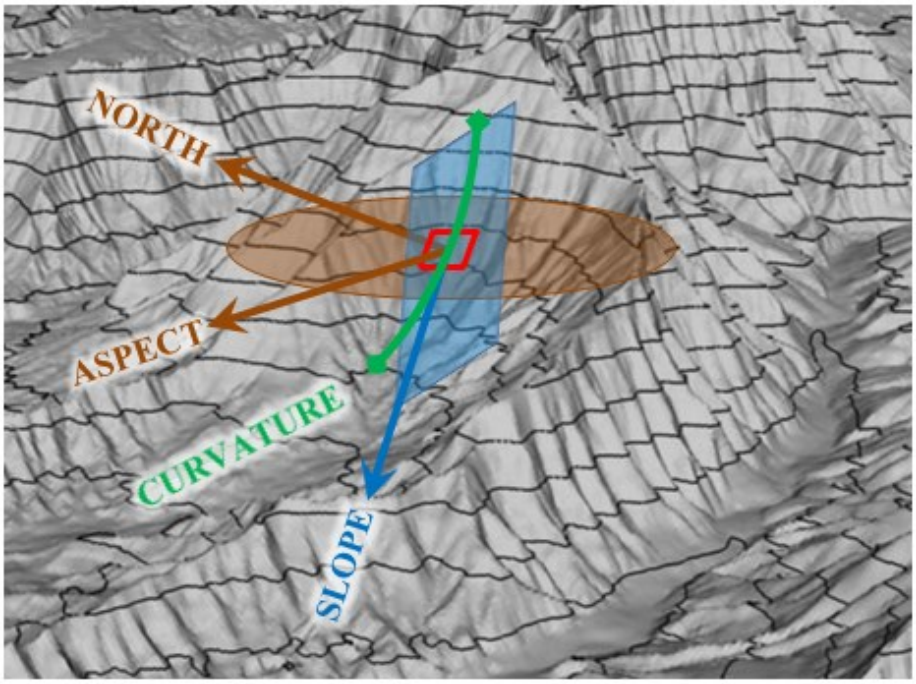

Figure 6.2: Graphical Representations of Slope, Aspect, and Curvature for a Grid Cell. Terrain model adapted from Leyk (2008).

Recently, a study performed by Kumar et al. demonstrated that the accuracy of snow cover forecasting models, like those that rely on MODIS remote sensing measurements, is greatly improved when terrain features such as aspect are included in the models (2013). The study area was the Colorado headwater region, which includes the majority of the state. From November 2007 to May 2010, MODIS snow cover predictions were compared to the ground-based SNOTEL stations located throughout the Colorado Rockies both with and without terrain corrections that included incorporating the aspect of the terrain. The authors theorized that since the aspect of the terrain greatly affects the amount of incident radiation from the sun absorbed into the snowpack, including it would assist MODIS in projecting true snow cover amounts. This hypothesis was confirmed by the results, which indicated that much as a 58% improvement in detecting true snow cover was seen once the aspect of the terrain was incorporated into MODIS

(Kumar, et al. 2013). Overall, this effort confirms the significance of terrain features such as aspect with respect to predicting snow properties.

The slope and curvature of the terrain are also very significant factors in determining the amount of snow precipitation that accumulates at a site. Slope and curvature of a particular site are topographical properties related to the inclination and shape of the terrain. Slope is defined as the ratio of the change in elevation to the change in horizontal run (Leyk 2008). The horizontal run is oriented in the direction of the aspect, defined above. Here, this ratio is referred to in shorthand as slope ratio. Slope can either be expressed as a percentage (slope ratio × 100) or in terms of degree of inclination, computed as $\tan^{-1}$(slope ratio). Mathematically, curvature is the derivative of slope; this same relationship applies to the geospatial properties of slope and curvature of terrain. Curvature describes the type of camber of the terrain at a site and can be expressed as convex or concave. Intuitively, concave terrain is indicative of valleys that are in the precipitation shadows of mountain peaks, while convex terrain is indicative of mountain peaks. Slope and curvature are both illustrated graphically in Figure 6.2 for a grid cell, outlined in red.

Slope has been studied extensively for its role in the accumulation, persistence, and ablation of snow depth in mountainous terrain. Particularly, a study performed within the Green Lakes Valley, located in the Arapaho-Roosevelt National Forest of Colorado, studied the effects various topographic features including slope on the effect of seasonal snow depth (Erickson and Williams 2005). The dependent variable snow depth was chosen to represent generally the persistence of snow accumulation. Specifically, the study investigated the effects of elevation, slope, incident radiation, and wind sheltering as potential predictors of the spatial variability of snow depth in the Green Lakes Valley. Using a type of geostatistical multiple linear regression technique known as complex mean geostatistical methodology, a geospatial model to estimate

the above parameters and their influence on snow depth was developed. Independent snow surveys were conducted by the research team for the winters between 1997 and 2003. The authors considered constant, linear, and non-linear spatial models to describe the effects of each predictor on snow depth. The analysis of the three models suggested that slope was the third most correlated predictor to snow depth, behind wind sheltering and elevation. A regression tree model analysis, however, resulted in slope being the best predictor (Erickson and Williams 2005). In either case, slope and curvature (by association) are very good predictors of snow depth. Numerous other studies have corroborated these findings, demonstrating slope to be a key component in hydrologic processes through the use of runoff models (Zhang, Drake, et al. 1997) as well as snowpack assimilation models (Barlage, et al. 2010). Intuitively, steeper slopes, such as those at the crests of mountains, cannot accumulate great amounts of snow due to gravitational runoff and wind effects in alpine regions. Conversely, flat terrain at the base of a peak likely accumulates great amounts of snow that drift downslope.

The Hydrologic Unit Catchment (HUC) number is a six-digit water resources region, assigned by the USGS, which delineates a region of land that drains to a single outflow (USGS 2013). In other words, all precipitation that falls within a given HUC drains to the same place, usually a major river. The continental divide in the Rocky Mountain Range divides all precipitation either to the Pacific Ocean or to the Gulf of Mexico, so the HUC assignments in Colorado are traced around the divide. There are many subdivisions of the HUC assignments, from broad water resources regions of the U.S. (2-digit watershed regions) to state and county-level units (8-digit cataloguing units). A map of the 2-digit water resources regions, charted by the USGS, is presented in Figure 6.3. Few studies have specifically investigated the use of HUC assignments as indicators of snowfall accumulation. The HUC assignments, however, provide contrast to the

other types of topographical variables such as slope and aspect; therefore, HUC assignments are valuable experimental variables used in this investigation.

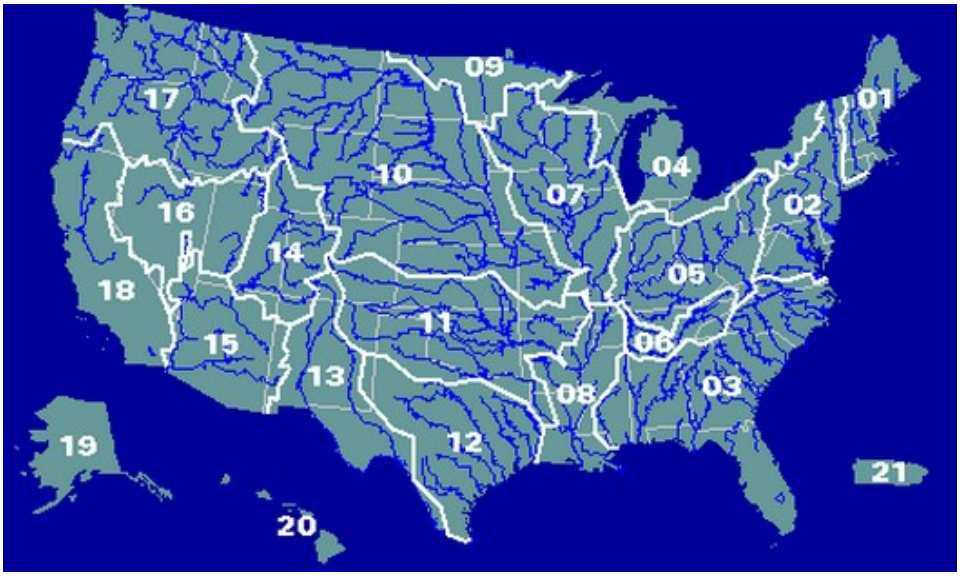

Figure 6.3: Map of 2-Digit HUC Regional Watersheds in the U.S. (USGS 2013).

The procurement of aspect, slope, and HUC assignment is facilitated by the GIS software utility ArcGIS 10.1. Using this software, GIS raster files that contain digitally encoded spatial values of the above are superimposed on a topographical map of Colorado. A KML file, encoded with the SNODAS station geographical coordinates is also inputted into ArcGIS. Then, using spatial analysis tools within ArcGIS, the encoded values are extracted at the SNODAS station points. Finally, the extracted values are exported to an MS Excel spreadsheet for some minor data cleaning.

For slope and aspect extraction, a digital elevation model (DEM) is superimposed on the topographical map of Colorado in ArcGIS. The incorporated DEM provides digitally encoded elevation values at a spatial resolution of 30-arc seconds of latitude and longitude. Based on this gridded DEM model, ArcGIS computes the slope using built-in algorithms, which is computed at

the center of each grid cell. This slope, constant throughout the grid cell, is extracted at each SNODAS station as a percentage of rise to run.

Aspect is also computed in ArcGIS using built-in algorithms and extracted at each SNODAS station as an angle from geodetic north, from 0-360 degrees. In an MS Excel spreadsheet, these angular measurements are translated into cardinal directions, specifically into four cardinal directions (north-facing, east-facing, south-facing, west-facing). For analysis of Colorado, any aspect orientation that contains an east or west component (*i.e.* NE, SE, NW, SW), within 45° of north or south, is assigned either 'east' or 'west' accordingly. This reflects the influence of east and west-facing slopes on snowfall accumulation. Each SNODAS station is assigned a number from 1 to 4, representing the four directions described.

For HUC assignment a raster file that contains encoded HUC regional watershed information, downloaded from NOHRSC [11], is imported into ArcGIS. The raster file is imported as a superimposed layer that contains a HUC assignment for every pixel on the topographic map. These HUC assignments are then extracted, using the spatial analyst tool, to each SNODAS station on the map and then imported into an MS Excel spreadsheet for later analysis.

Illustrations of the DEM, aspect, and slope relief imagery produced by ArcGIS spatial analyst tools for the extraction of values at SNODAS station is available in Appendices H and I. Colors on the relief imagery represent elevations for the DEM, azimuth angles from north for the aspect imagery, and percentage of rise/run for the slope imagery.

---

[11] NOHRSC webpage with GIS raster files for HUC regional watersheds: http://www.nohrsc.noaa.gov/gisdatasets/

7.0 STATISTICAL ANALYSIS OF WEATHER STATION DATA

7.1 Introduction

Analysis of weather station data begins after the receipt of the files acquired in Chapter 6.0. The initial files from each station must be consolidated and organized as well as summarized by descriptive statistics prior to any analysis of the data. Once the data is in a form that facilitates further evaluation, several statistical analyses and tests can then be performed which will ultimately lead to 1) the identification of clusters of stations, 2) relationships of ground snow depth to ground snow load within each cluster, and 3) the extraction of extreme probabilistic ground snow loads at all stations in Colorado.

7.2 Management of SNODAS Station Data

As stated in Chapter 6.0, the SNODAS model output was downloaded from the NOHRSC web-based archive to a hierarchical system of folders on a hard disk. These station outputs are organized first into weather forecasting office folders and then station name folders. The initial CSV format of the files needs to be converted into a more recognizable and user-friendly file type. Therefore, the industry standard software package Microsoft Excel is chosen as the platform for performing all analysis of the modeled output. It is capable of reading CSV files and saving them as native Excel files allowing them to be universally distributed and viewed.

The file preparation begins with consolidating each station's yearly data into a single Excel file so that each modeled SNODAS station record can then be assessed collectively. Recall that nine years (2003-2012) of modeled station records are currently available, each year aligned with the water year. Also, these records for each year reside in separate CSV files within nested

folders. Figure 7.1 illustrates the system of folders established to organize the 588 stations according to the appropriate weather forecasting office ('BOU', GJT', and PUB'). The first three modeled stations within the folder 'PUB' are visible on the left in Figure 7.1, with the nine CSV files of modeled output for each year at station AGLC2 visible on the right. These separate files are merged into a single file so that the nine years of model output could be collectively compared and summarized.

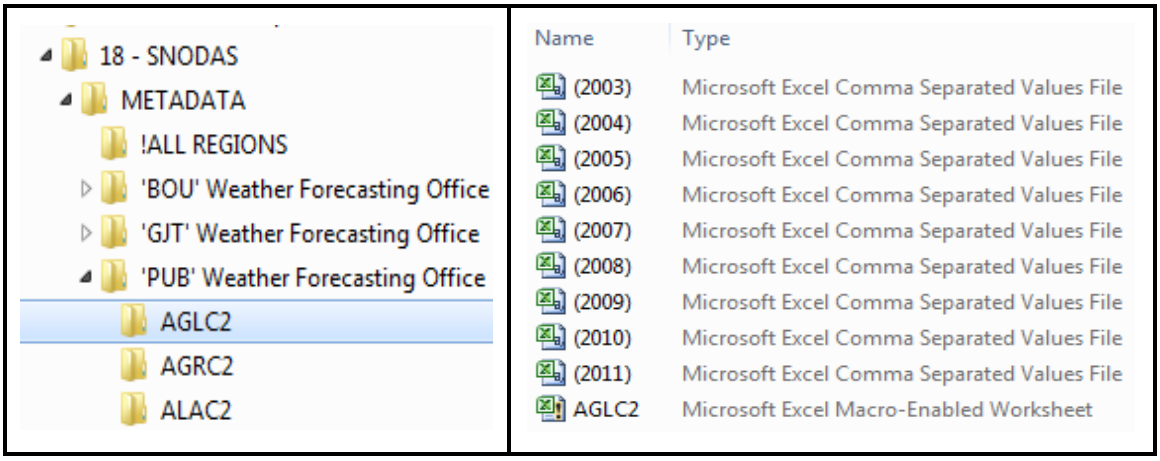

Figure 7.1: Hierarchical Organization of SNODAS Files and Folders, left, with Associated Excel and CSV Files, right.

To accomplish this, several Microsoft VB macros are written within Excel which automates the process. These macros reside in each station master files such as the one labeled 'AGLC2' on the right side of Figure 7.1. Once the macros are run, the master file contains all nine years of modeled data for a single station. This macro is then automated to repeat this for each of the 588 stations.

With all SNODAS station modeled output compressed into individual Excel files for each station, descriptive summaries and basic statistics of the modeled output can be created. Descriptive summaries for all nine water years of each station include the variables listed in Table 7.1. The derived snow load denoted by item (3) can be quickly determined using the relationship

established in Eq. (9). The annual maximum snow unit weight denoted by item (5) can be determined from the relationship established in Eq.(10), specialized for English units.

$$\gamma_{max}(\text{pcf}) = \frac{SWE_{max}}{h_s *} \times 62.4 \text{ (pcf)} \tag{10}$$

In this equation γ_{max} is the annual maximum snowpack unit weight, SWE_{max} is the annual maximum snow water equivalent, and $h_s *$ is the snow depth associated with the annual maximum snow water equivalent. Note that in Eq. (10) the units of both SWE_{max} and $h_s *$ must be similar, and usually are expressed in inches. This relationship is not explicitly used to convert SWE and ground snow depth data in this investigation. Item (6) will be discussed further in Chapter 7.10.2. It is an important scaling factor used to adjust the annual maximum ground snow depth.

Table 7.1: Descriptive Summaries of Each SNODAS Station for each Water Year (2003-2011)

Item	Descriptive Summary Variable
(1)	The annual maximum SWE
(2)	The annual maximum snow depth
(3)	The derived snow load from the annual maximum SWE
(4)	The snow depth at the date of annual maximum SWE
(5)	The maximum snow unit weight derived from (1) and (4)
(6)	The ratio of items (4) to (2)

Once the descriptive summaries for all years and all stations are gathered, some basic statistics are determined for each station to represent all nine years of data. These statistics are determined for each of the descriptive variables listed in Table 7.1. They help to describe general trends between different types of stations such as the variance of model output among stations at different elevations. Some will be evaluated for use in later statistical analyses. The descriptive statistics from each water year of each station include the mean, standard deviation, and variance. A sample sheet containing these quantities compiled for each year of modeled output for

SNODAS station 'AGLC2' is presented in Appendix J. Upon creating descriptive summaries and basic statistics, a separate VB macro is written which parses through each folder of each station and populates a brand new Excel file with values of SWE, snow depth, snow density, and the basic statistics for all nine years of all 588 stations. Now that the entire dataset is amassed in a single file the SNODAS stations are ready for the next phase of analysis in preparation for partitioning of them into statewide regions.

Prior to a clustering analysis, used to regionalize weather stations by similarities, the clustering variables themselves need to be prepared. These variables, which are obtained in the data procurement phase of Chapter 6.0, include properties related to the SNODAS station location, site topography, and modeled snow measurements. Table 7.2 lists all of the variables for each station used throughout the entire clustering process.

Table 7.2: Descriptive SNODAS Station Properties Incorporated into Cluster Analysis

Item	SNODAS Station Variable	Measurement Unit
(1)	Elevation Above Mean Sea Level	Length (feet)
(2)	Latitude (WGS 84)†	GPS Coordinate (Deg.-N)
(3)	Longitude (WGS 84) †	GPS Coordinate (Deg.-W)
(4)	USGS Basin HUC ††	6-Digit HUC (No.)
(5)	Slope of Terrain at Station	Elevation Increase (%)
(6)	Aspect of Terrain at Station	Cardinal Direction (Deg.)
(7)	Curvature of Terrain at Station	Inverse Length (1/feet)
(8)	Averaged Annual Maximum Snow Water Equivalent	Depth (inches)
(9)	Averaged Annual Maximum Snow Depth	Depth (inches)

† GPS Coordinates use the World Geodetic System of 1984

†† United States Geologic Survey – Hydrologic Unit Catchment Number

As it can be seen from the Table 7.2, the variables that are to be used in the cluster analysis do not carry the same units of measurement. Consequently, the magnitudes of the variables will vary significantly, especially for elevation and HUC basin number. If the clustering process

were to proceed with the variables as-presented in Table 7.2, then those with higher means and standard deviations would represent outliers in the clustering process and could highly skew the clustering (Tufféry 2011). Therefore, to avert such a situation, the variables must be both centered and reduced. The most widely used technique to accomplish this, which transforms the variables into unit less quantities with a mean of 0 and a standard deviation of 1, is standardization by z-score (Ferris 2008). The equation used to transform all of the variables into their respective z-scores is depicted in Eq. (11) below:

$$Z_x = \frac{X_i - \bar{X}}{\sigma_X} \tag{11}$$

where X_i is the i^{th} term of the set of terms in X, $\bar{X}$ is the mean of the set, and σ_X is the standard deviation of the set. Here, a *set* of terms refers to the 588 station values for each variable listed in Table 7.2. Therefore, there are nine sets of terms that are standardized by z-scores. A portion of the complete table is presented in Appendix K, which lists only stations AGLC2 through BRTC2 for conciseness. The variables, now centered and reduced, are ready for further analysis in preparation for clustering.

7.3 Principal Components Analysis

At this point, a number of variables describing each station have been identified, centered, and reduced. Altogether there are $p = 9$ variables (listed in Table 7.2). Also, there are $n = 588$ individuals of the population. The term individuals shall denote the SNODAS stations, each of which possesses distinct values for each variable p. Therefore, overall we have a 588×9 matrix of data points discretized into p-columns and n-rows. If graphed, the result *would* be a nine-dimensional plot with separate 'clouds of individuals' (Tufféry 2011). Obviously, this graphical representation becomes impossible whenever $p > 3$, so the amassed data here cannot be plotted

together. This inability to plot the entire multivariate dataset graphically suggests an inability to effectively manipulate the data. Also, clustering techniques are quite inefficient when dealing with the number of variables present here (Tufféry 2011). The multivariate clustering techniques used to regionalize the stations will be discussed in Chapter 7.5. For now, the data possesses too many dimensions to analyze in a practical manner. Therefore Principal Component Analysis (PCA) is employed to reduce the dimensions of this problem, effectively decreasing the number of input variables without significant loss of information. PCA is an important analysis that should be completed prior to a clustering (Jolliffe 2002, Tufféry 2011, Johnson and Wichern 2007). PCA can help determine which of the nine variables are the most crucial. Upon completing this analysis, a reduction down to the core contributing variables is seen, with which a cluster analysis can be performed.

The central purpose of PCA is to reduce the dimensionality of multivariate data, as previously mentioned, resulting in a *projection* of the original data onto a two or three-dimensional plane (Tufféry 2011). This objective is accomplished by finding 'axes of rotation' of the data, which are distinct and successive rotations of the data which minimizes the loss of information. In mathematical terms, these axes of rotation are linear combinations of the variables, which are smaller in number than the original set of variables. The criterion used to prevent significant loss of information is the concept of maximizing population inertia, *I*, to a level as close as possible to the original, unreduced dataset. The inertia of a set of data points is the weighted sum of squares of the distances from each point to the group center of gravity (or arithmetic mean). It is mathematically equivalent to variance. It can be expressed mathematically by Eq. (12):

$$I_X = \sum_{i=1}^{n} w_i \times dist(c, X_i)^2 \tag{12}$$

where *i* represents an index variable for the 588 individuals of the population, w_i is a weight assigned to each individual (usually $1/n$ for every *i*), *c* is the center of gravity of the population, and the function *dist* denotes the distance between the centroid and each individual *X* (Tufféry 2011). The centroids of centered and reduced (standardized) variables is zero, therefore c_i is zero. The concept of distance here refers to the simplest mathematical distance, Euclidean distance. For any two random variables, *X* and *Y*, Euclidean distance can be defined as follows.

$$dist(X,Y) = (X_1 - Y_1)^2 + (X_2 - Y_2)^2 \ldots + (X_n - Y_n)^2 \tag{13}$$

The expressions in Eq. (12) and (13) are applicable for univariate data in order to illustrate the central concept of PCA. In practice, and in this investigation, there are many variables on which to perform a PCA. Therefore, in order to apply the concept of PCA on multivariate data, a covariance matrix is constructed. A covariance matrix is appropriate since the act of maximizing population inertia effectively maximizes population variance. And since all of the variables used in the PCA have been standardized by z-score (*i.e.* their means are 0 and standard deviations are 1), the covariance matrix is mathematically equivalent to a correlation matrix. Recall that the linear correlation coefficient between two variables, $r_{XY} = \mathrm{cov}(X,Y)/(\sigma_X \cdot \sigma_Y)$ and that a value of covariance is equal to the scalar product of the two centered variables (Tufféry 2011). Thus, assembling this correlation matrix results in the following:

$$M_{CORR} = \begin{bmatrix} 1 & r_{12} & \cdots & r_{1p} \\ r_{21} & 1 & & \vdots \\ \vdots & \vdots & \ddots & \vdots \\ r_{p1} & r_{p2} & \cdots & 1 \end{bmatrix} \tag{14}$$

In the correlation matrix for this dataset the row and column labels represent the *p* standardized variables and the non-diagonal terms represent the correlations with each other. The correlation

matrix is always square and symmetric, with ones along the diagonal, since a variable is perfectly correlated with itself.

During a PCA, this matrix is populated with the correlation coefficients relating all of the pairs of variables. At this point the concept of maximizing population inertia is implemented on the multivariate dataset. The successive axes of rotation which maximize the inertia, I, of the correlation coefficients of the variables must therefore be found (Tufféry 2011). These axes are determined using techniques of linear algebra to solve for the eigenvalues and corresponding eigenvectors of the M_{CORR} matrix. The total sum of all of the eigenvalues equals the number of variables p. This plays a critical role during the application of PCA in Chapter 7.4. Finding the eigenvectors and eigenvalues maximizes both the correlation coefficients of the variables and the inertia of the individuals.

Once the directions of the axes (*i.e.* the eigenvectors) are determined, the concept of factor loadings is defined. There are p successive, orthogonal axes of rotation of the data, *i.e.* principal components (Jolliffe 2002). The first principal component possesses the highest inertia and explains most of the variance in the data. The next PCs possess inertias, *i.e.* variance, of decreasing value. Since p distinct PCs exist, each individual in the dataset (*i.e.* each standardized SNODAS station value) has some projection onto each. This projection is defined as a factor loading, F_i. Mathematically, the factor loadings of each PC are calculated as the scalar multiplication of each eigenvector with the square root of the associated eigenvalue. Conceptually, they represent the linear correlation of each variable with each principal component. They are usually represented in a $p \times p$ table with PCs displayed column-wise and the factor loadings for each variable displayed row-wise. A property of factor loadings is that the sum of squares of all of the

coefficients for a given PC (*i.e.* the sum of squares of the rows in the table) is equal to the eigenvalue of that PC.

$$\lambda_j = \sum_{i=1}^{p} r_j(P_j, F_j)^2 \tag{15}$$

In Eq. (15), $r_j(P_j, F_j)$ is the correlation coefficient at the intersection of the P_j row and the F_j column of the table (Tufféry 2011). An example of a factor loading table is presented with the PCA performed on the data in Chapter 7.4. A convenient usage of factor loadings is to square each coefficient and divide it by the eigenvalue of that PC. This results in the fundamental concept of variable contribution, in other words the percentage of influence each variable has on the given PC. Since each variable p theoretically should carry a weight $1/p$, logically a contribution of more than this would be significant. Quantifying the contribution of each variable helps to identify not only those variables which contribute the most to each PC, but also groups of variables which collectively contribute to the same PC. This can set the framework for understanding which variables should belong together in a clustering analysis, and which can be excluded through a reduction in dimensionality.

A final useful tool to introduce before applying these principles of PCA on the dataset herein is the idea of cumulative variance. Recall that the first few PCs are the most significant and explain the majority of the variation in the data. A logical question to ask is how many PCs are sufficient to explain the 'majority' of the variance. Eq. (16) provides a metric for helping to determine this cut-off (Johnson and Wichern 2007). Since the sum of all eigenvalues, one for each PC, equals p then it follows that:

$$\mathrm{var}(X_i) = \lambda_i / p \quad \rightarrow \quad \sum_{i=1}^{p} \mathrm{var}(X_i) = \sum_{i=1}^{p} \lambda_i / p = 1 \tag{16}$$

The total variance in the data, the sum of each eigenvalue divided by the p number of variables, should equal 1. This leads to a measure of cumulative variance that can be incrementally calculated which would indicate how many PCs (desirably < p) are required to reach a specified percentage of cumulative variance. Previous studies using PCA have established a rule of thumb which states that a cumulative variance of anywhere from 70% to 90% of the total variance is a sufficient cut-off point, depending on how many variables this reduces to and whether it is a practical amount with which to work (Jolliffe 2002, Varmuza and Filzmoser 2009, Johnson and Wichern 2007).

The applications of principal component analysis have pervaded every aspect of the fields of mathematics, engineering, computing, and the social sciences. In the field of structural engineering, PCA has offered a solution to the dilemma facing structural engineers trying to study and interpret acceleration and force data in the wake of seismic events. Particularly, PCA has been employed to compress accelerometer sensor data from buildings post-earthquakes for quicker and more effective means of data recording and transmission (Zhang, Li and Chae 2007). This area of building health monitoring has benefited from the ability to reduce the dimensionality of large amounts of monitoring signals so that only the most crucial pieces are captured, with minimal loss of information. Industrial processes, specifically those involving complex chemical reactions, have employed PCA to assist in process performance. Chemical polymerization reactors, for instance, utilize PCA to substitute expensive and time intensive quality control sampling techniques for monitoring critical outputs in the production of industrial and commercial compounds (*e.g.* polyethylene and polyvinylchloride) (Kayihan, Cinar and Palazoglu 2007). Finally,

PCA has been shown to be able to accurately predict the natural structure of a dataset (number of classes) and provide insight into the stability of clustering algorithms (*i.e.* sensitivity to normalization, types of clustering variables, choice of algorithm) when performed a priori; in this manner, PCA has greatly improved the analysis of gene expression in the field of human genomics (Ben-Hur and Guyon 2003).

7.4 Principal Component Analysis Performed on SNODAS Dataset

The principles of PCA previously described are now applied to the dataset of 588 SNODAS stations and the nine station variables listed in Table 7.2. The objective is to use the concept of cumulative variance as the criterion to define where to cut-off the analysis, thus excluding any further PCs. Then, the contributions of each variable (elevation, latitude, longitude, *etc.*) are used to obtain relationships among variables and thus determine which variables should be clustered together. The inputs to the PCA must first be assembled and organized. These are the centered and reduced SNODAS station variables of Table 7.2, tabulated for each station. Next, the principal component analysis is performed on this input table with the assistance of the software program *XLSTAT Pro* version 2013.1.01 (Addinsoft 2013). The results and interpretation thereof are discussed below.

The method of performing the PCA is chosen to be that developed by Pearson (1901) since it is widely understood to be the first and most widely used method of principal components analysis (Jolliffe 2002). Other PCA methods include those pioneered by Kendall and Spearman, which have applications for specific types of data. The first product of the PCA is the correlation matrix. Although a covariance matrix can be used to perform the analysis, the use of a correlation matrix reduces the effect of scale on the variables (Addinsoft 2013).

The Pearson correlation matrix for the dataset is shown in Table 7.3. The primary insight that the correlation matrix provides at this point is that SWE and snow depth are highly correlated, implying that an increase in snow depth leads to an increase in the water content in the snow. This logically follows from the concept of snow compaction discussed in Chapter 4.2. This matrix also shows correlations between SWE and snow depth, and elevation of the station. Clearly elevation seems to be an underlying factor affecting the properties of snow depth and water content, one that cannot be eliminated. Finally, longitude and basin assignment of each of the stations appear closely linked, albeit inversely related to one another. This relationship must be related to the fact that basin assignments in the state are generally segregated either east or west of the Great Divide.

Table 7.3: Pearson (n) Correlation Matrix for the Principal Component Analysis

	Elev.	**Lat.**	**Long.**	**Basin**	**Slope**	**Aspect**	**Curv.**	**SWE**	**Depth**
Elev.	**1.000**	-0.163	-0.261	0.268	0.041	-0.031	-0.036	0.717	0.762
Latitude	-0.163	**1.000**	0.020	-0.208	0.050	0.073	0.019	-0.019	-0.036
Longitude	-0.261	0.020	**1.000**	-0.781	-0.018	-0.007	-0.028	-0.200	-0.191
Basin	0.268	-0.208	-0.781	**1.000**	0.034	-0.002	0.000	0.312	0.309
Slope	0.041	0.050	-0.018	0.034	**1.000**	0.095	-0.038	0.138	0.130
Aspect	-0.031	0.073	-0.007	-0.002	0.095	**1.000**	0.174	-0.043	-0.038
Curvature	-0.036	0.019	-0.028	0.000	-0.038	0.174	**1.000**	-0.021	-0.021
SWE	0.717	-0.019	-0.200	0.312	0.138	-0.043	-0.021	**1.000**	0.990
Depth	0.762	-0.036	-0.191	0.309	0.130	-0.038	-0.021	0.990	**1.000**

Upon assembly of the correlation matrix, the eigenvalues and eigenvectors are computed, as reported in Table 7.4, Table 7.5 and Figure 7.2, where F_i indicates the i^{th} factor axis or principal component. This crucial phase of the analysis sets the stage for the determination of the most critical principal components and the exclusion of the rest. The computation of the eigenvalues allows the cumulative variance and factor loadings to be computed as well. Graphical representations of the eigenvalues facilitate an accurate interpretation of their significance. Scree plots

like Figure 7.2 consist of the plotted eigenvalues vs. principal components. They were originally developed for the purpose of finding the principal component cut-off graphically. Where there appears to be an 'elbow' on the Scree plot (point where the slope drastically changes from steep to shallow) is the optimal minimum number of successive PCs to consider (Johnson and Wichern 2007). However, data with a strongly dominating first PC would skew the line plot and render the graphical technique unreliable. Scree plots are no longer used for this purpose, but now serve as a visual aid to interpret the cumulative variance.

An important trait to take into account with regard to the eigenvalues and eigenvectors represented in Table 7.4 and Table 7.5 is that individual values of the coefficients by themselves provide little information for their interpretation. Also, the three significant-digit precision noted in the tables does not speak to the precision required for PCA, but rather a convention for presentation purposes. The relative absolute magnitudes among neighboring coefficients and their signs *are*, however, significant in any PCA. In other words, we look for high absolute magnitudes as initial indicators of relative importance. To clarify what is essential to infer from Table 7.5, coefficients whose absolute value is at least half of the maximum in each column are represented in bold text. This practice has been used in many applications of PCA to simplify the interpretation of the results (Jolliffe 2002).

With this in mind, Table 7.4 and Figure 7.2 indicate that the first principal component dominates the others, representing nearly 34% of all the variance in the data itself. This PC primarily represents the effects of SWE, snow depth, and elevation which are the main contributors to it. This is evident by relative magnitudes of their coefficients for F1 in Table 7.5. Longitude and basin assignment while significant do not carry as much weight. The next PC represents half of the variance as the first and only about 17% of the variance itself. This represents the effects

of longitude and basin, and as it can be seen, they are the only major contributors to PC2. Their corresponding coefficients in Table 7.5 have opposing signs, which indicates they have a similarly opposing relationship with one another.

Table 7.4: Eigenvalues and Variance for Each Principal Component of the PCA

	F1	F2	F3	F4	F5	F6	F7	F8	F9
Eigenvalue	3.02	1.49	1.22	1.04	0.940	0.783	0.350	0.159	0.007
Variance (%)	33.5	16.5	13.5	11.5	10.5	8.70	3.89	1.77	0.079
Cumulative (%)	33.5	50.0	63.6	75.1	85.6	94.3	98.2	99.9	100

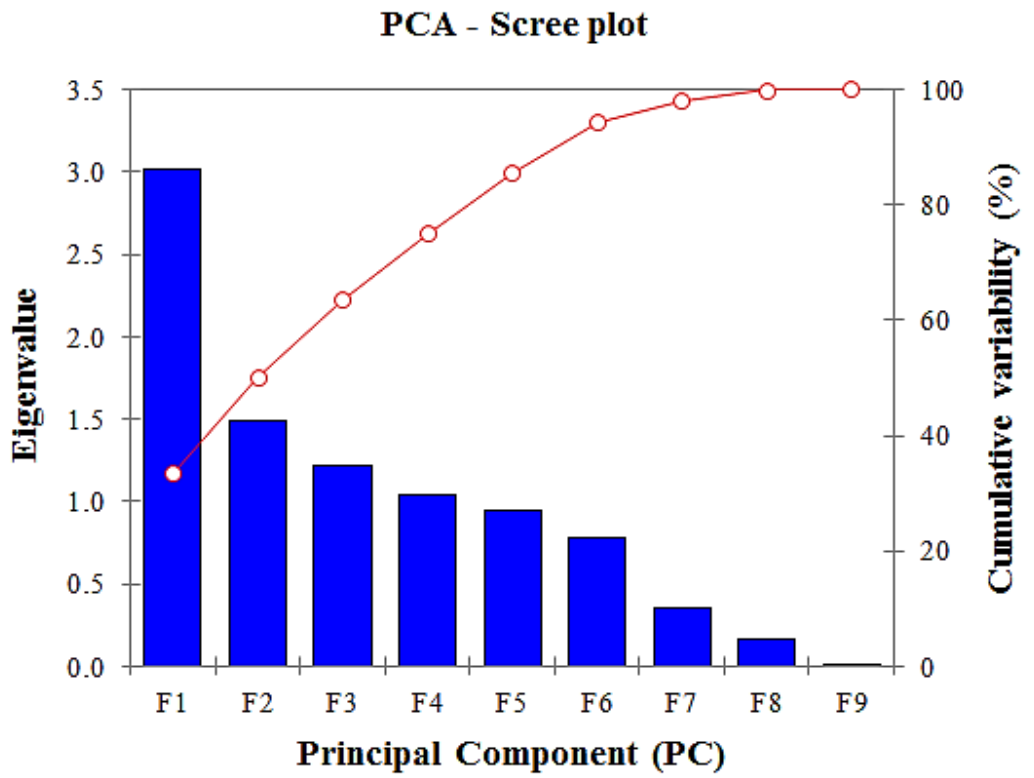

Figure 7.2: PCA Scree Plot of Eigenvalues and Cumulative Variability vs. Principal Component. Plot was created using XLSTAT Pro (Addinsoft 2013).

Table 7.5: Eigenvectors for Each Principal Component of the PCA

	F1	F2	F3	F4	F5	F6	F7	F8	F9
Elevation	**0.477**	0.190	-0.052	-0.157	-0.024	0.104	0.765	0.326	-0.079
Latitude	-0.091	0.184	**0.374**	**0.424**	0.771	-0.008	0.065	0.197	-0.002
Longitude	**-0.300**	**0.620**	-0.073	-0.176	-0.184	0.015	-0.281	0.613	-0.030
Basin	**0.350**	**-0.589**	-0.005	0.100	-0.007	-0.005	-0.327	0.642	-0.019
Slope	0.084	0.130	0.331	**0.625**	-0.542	-0.415	0.097	0.019	0.001
Aspect	-0.028	-0.048	**0.680**	-0.106	-0.248	0.678	-0.036	-0.023	-0.003
Curvature	-0.020	-0.095	**0.526**	**-0.591**	0.076	-0.598	0.023	0.027	-0.002
SWE	**0.518**	0.288	0.043	-0.029	0.073	-0.009	-0.370	-0.221	-0.674
Depth	**0.524**	0.295	0.036	-0.050	0.059	0.006	-0.278	-0.126	0.733

Beyond this, the next three PCs contribute roughly the same amount of accumulated variance (between 10.5% and 13.5% each). There is no need to look any further than the fifth PC since more than 80% of the overall cumulative variance has already been explained and also since the individual variance provided by the sixth is smaller than the theoretical weight of each variable ($^1/_p$ or 11.1%). Thus, the first four PCs emerge as prominent factor axes that play significant roles in describing the variance in the data. The fifth can be eliminated for practical reasons since it isn't entirely needed; without it the remaining four still represent 75% of the variance in the data. Furthermore, an additional variable to add to the clustering analysis will only complicate that analysis. Similarly, PC5 through PC9 will not be considered further.

Biplots are a useful visual tool for analyzing the results of a PCA. They consist of factor loadings for any two PCs plotted against one another; they are also known as factor planes (Tufféry 2011). A sample biplot illustrating factor axis F2 plotted against F1 is presented in Figure 7.3. The values in parentheses on each axis indicate percent contributions. As it can be seen, a circle of perfect correlation (r = 1.0) surrounds the plot, providing a visual indication of how much a variable contributes to a particular factor. Factor loadings are plotted as vectors all

drawn from the origin of the plot. The plot only indicates significant relationships between two variables *if* their plotted vectors on the biplot are reasonably close and near the circle of perfect correlation. There are many combinations of biplots (F1vs.F2, F1vs.F3, F2vs.F3 *etc.*) which are all important. The remaining biplots produced by the PCA are available in Appendix L.

The final useful products of the PCA are the factor loadings and subsequent variable contributions tables which provide definitive answers as to exactly which variables are critical for the next phase. Factor loadings and variable contributions for each principal component are provided in Table 7.6 & Table 7.7.

Table 7.6: Factor Loadings for Each Principal Component of the PCA

	F1	F2	F3	F4	F5	F6	F7	F8	F9
Elevation	**0.829**	0.232	-0.058	-0.160	-0.023	0.092	0.452	0.130	-0.007
Latitude	-0.158	0.224	**0.413**	**0.432**	0.748	-0.007	0.038	0.079	0.000
Longitude	**-0.520**	**0.756**	-0.080	-0.179	-0.179	0.013	-0.166	0.245	-0.003
Basin	**0.609**	**-0.718**	-0.006	0.101	-0.007	-0.005	-0.194	0.256	-0.002
Slope	0.146	0.158	0.366	**0.636**	-0.526	-0.367	0.057	0.008	0.000
Aspect	-0.049	-0.059	**0.751**	-0.108	-0.240	0.600	-0.021	-0.009	0.000
Curvature	-0.035	-0.116	**0.580**	**-0.602**	0.074	-0.529	0.014	0.011	0.000
SWE	**0.900**	0.351	0.047	-0.030	0.071	-0.008	-0.219	-0.088	-0.057
Depth	**0.911**	0.360	0.039	-0.051	0.058	0.005	-0.164	-0.050	0.062

Table 7.7: Variable Contributions (%) for Each Principal Component of the PCA

	F1	F2	F3	F4	F5	F6	F7	F8	F9
Elevation	**22.8**	3.62	0.274	2.46	0.059	1.08	58.5	10.6	0.629
Latitude	0.829	3.39	14.0	18.0	59.5	0.006	0.419	3.88	0.000
Longitude	8.98	**38.4**	0.527	3.10	3.40	0.021	7.87	37.6	0.091
Basin	12.3	**34.7**	0.003	0.991	0.005	0.003	10.7	41.3	0.037
Slope	0.706	1.69	11.0	**39.0**	29.4	17.2	0.940	0.038	0.000
Aspect	0.081	0.231	**46.3**	1.13	6.14	45.9	0.130	0.051	0.001
Curvature	0.040	0.911	**27.6**	**35.0**	0.581	35.7	0.053	0.072	0.000
SWE	**26.8**	8.29	0.185	0.084	0.537	0.009	13.7	4.90	45.5
Depth	**27.5**	8.72	0.128	0.255	0.352	0.003	7.71	1.58	53.8

Again in Table 7.6 & Table 7.7, the values in bold indicate the coefficients whose absolute value is equal to or greater than 50% of the maximum for the same column. The factor loadings have been computed in accordance with the mechanics introduced in Chapter 7.3, specifically Eq. (15). A similar pattern emerges in the variables that are highlighted as significant contributors, compared to the eigenvectors of Table 7.5. However, when the variable contributions are calculated in Table 7.7, it is evident that longitude and basin assignment are no longer major contributors to PC1 and latitude is neither a major contributor to PC3 nor PC4. In addition to the overall contribution of the variables, a closer look at the individuals (*i.e.* each SNODAS station values) and their *individual* contribution to each principal component was made. This check ensures that no single station represents a principal component by itself. Inclusive of PC1 through PC4, the highest percentage of contribution for a single individual is only 2.33% by station MOHC2. This result confirms the desired equal representation of all of the individual stations and justifies the overall usage of the PCA results.

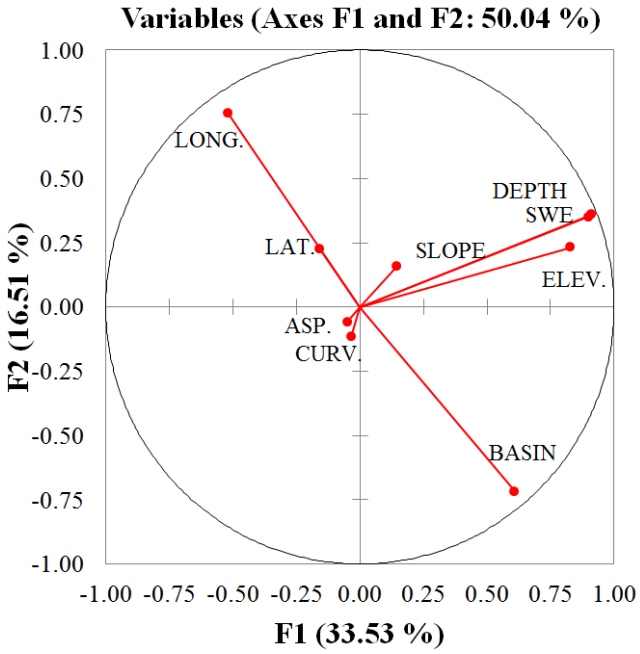

Figure 7.3: Biplot of PC1 Plotted Against PC2 Produced by the PCA.

Overall, the variable contribution table provides great insight into all of the key factors that underlie the data, specifically with respect to the groups of variables that collectively explain the variance and the order of these groups. These groups, listed by corresponding principal component, are:

(1) *Elevation*, *SWE* and snow *depth*
(2) *Longitude* and *basin* assignment
(3) *Aspect* and *curvature* of the terrain
(4) *Slope* and *curvature* of the terrain

Some of these results may be manually changed to eliminate duplicate variable consideration in preparation for the clustering analysis.

The results of the PCA, culminating with the variable contributions to each principal component, need to be translated into decisions about the clustering analysis to follow. Several nested clustering *operations* comprise the entire clustering analysis. The main contributing variables determined for each principal component become the only variables used for each clustering operation. Furthermore, the principal components in the order listed above represent the same order and clustering variables for each clustering operation. In other words, the variables in PC1 (elevation, SWE and snow depth) will be used in the first clustering operation, the variables of PC2 (longitude and basin) for the second, and so on. The variables in PC3 and PC4 will be merged into a single clustering operation, considering the close relationship between these variables (they are all descriptive topographic variables). A more detailed description of the clustering process followed is presented in Chapter 7.6.

7.5 Multivariate Cluster Analyses

As previously mentioned in Chapter 4.0, partitioning the state of Colorado into regions of stations with similar climatology will greatly assist in the development of ground snow density

relationships (snow depth-load equations) tailored to each region. Some form of regionalizing ground snow loads has been employed by several western U.S. states including Montana, Utah, California, Oregon, and Arizona. Colorado has also made use of this method, although only 'compacted' and 'settled' snow regions are currently distinguished, representing high and low-elevations, respectively (SEAC 2007). To the author's knowledge, neither SEAC nor the other Structural Engineering Associations of the mentioned western states currently utilize rigorous multivariate clustering as proposed here.

A multivariate cluster analysis is a statistical method for identifying homogenous subsets or classes of individuals; these individuals are assigned to a class based on similarity, as determined by a predefined criterion (Tan, Steinback and Kumar 2005). This criterion is defined for each of the clustering methods discussed later. The objective of any cluster analysis is to minimize within-class variance and conversely maximize between-class variance. Clustering analyses can be classified as either partitional or hierarchical, and each of these methods can be further defined as exclusive, overlapping, or fuzzy cluster analyses. The major classification, hierarchical versus partitional, essentially describes the structure of the clustering. In hierarchical clustering, the structure of the classes resembles a tree in which the root of the tree is a single class for the entire ensemble of individuals. Conversely, the furthest branch defines the last sub-class in which all individuals belong to their own class. In partitional clustering, there is no real clustering structure; the individuals are divided into one class or another. To visualize the distinction between these two types of analyses, Figure 7.4 illustrates a graphic describing the results of each type of analysis. It is clear that hierarchical clustering produces several levels of sub-classes that are related to each other via higher levels or branches. Partitional clustering, on

the other hand, simply divides individuals into mutually exclusive classes, analogous to a hierarchical clustering with only a single branch.

The other classifications described above as exclusive, overlapping, or fuzzy describe the individual memberships to each class. Exclusive cluster analysis is a clustering option wherein individuals are assigned a single class. An overlapping cluster analysis allows individuals to be members of multiple classes, based on the top choice(s). Finally, fuzzy clustering is an option where each individual belongs to every class, related by a probability from 0 to 1 (Tan, Steinback and Kumar 2005).

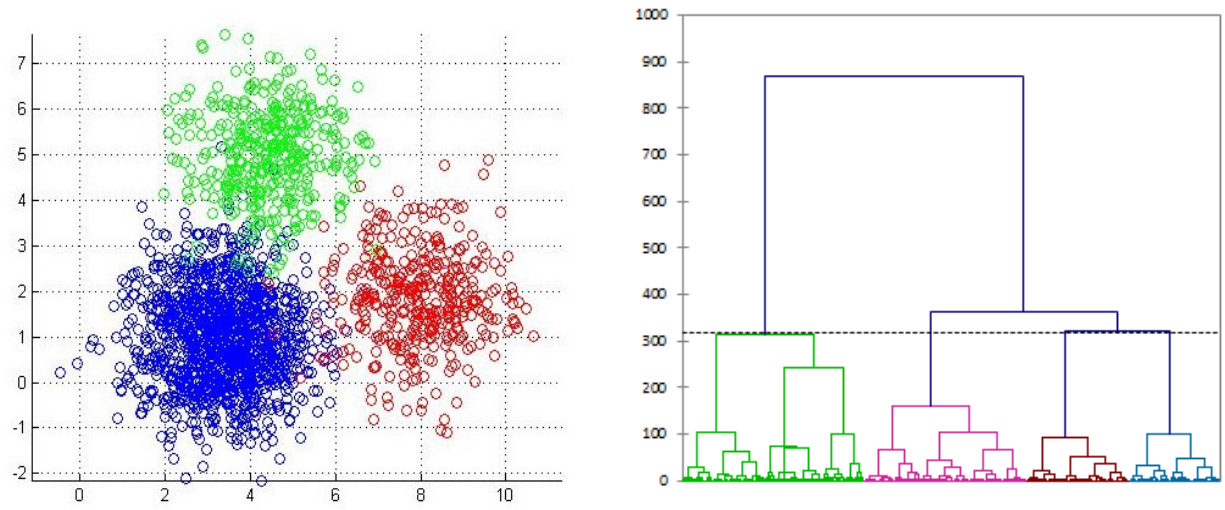

Figure 7.4: Illustrations of Clustering Analyses - Partitional Clustering, left, and Hierarchical Clustering, right. Adapted from Tan, Steinback and Kumar (2005).

In this study, the individual SNODAS weather stations represent the individuals. The descriptive items such as station properties, station locations, and modeled snow measurements are the variables used as the basis for the clustering (the variables listed at the end of Chapter 7.4). Both hierarchical and partitional clustering analysis methods will be evaluated since the natural clustering structure of the individuals is not known a priori. Therefore, it is inappropriate to assume either a hierarchical or non-hierarchical structure by employing either one alone. For prac-

tical purposes exclusive clustering is necessary since discrete partitions of SNODAS stations into statewide regions are desired. Fuzzy or overlapping memberships would complicate the production of mapped snow loads after the clustering is complete. The sections to follow describe the mechanics of each method of clustering discussed above. To avoid confusion, the term "class" will be used to refer to a cluster and the term "individuals" will be used to refer to SNODAS stations

7.5.1 Agglomerative Hierarchical Clustering

Agglomerative Hierarchical Clustering (AHC) is a clustering approach which aims to seek a sequence of nested classes of increasing homogeneity with increasing quantity of classes and conversely increasing heterogeneity with decreasing quantity of classes (Tufféry 2011). For instance, referring back to the right-hand graphic of Figure 7.4, the branches near the bottom represent more numerous classes with more similar members, whereas the first two branches represent only two classes with very dissimilar members. The term *agglomerative* specializes this type of hierarchical clustering as one in which the clustering process combines individuals into newly created nested classes as it progresses. In other words, for a sample space with n individuals, there are similarly n clusters at the beginning of the clustering process (*i.e.* the bottom branches of Figure 7.4). Also, at each agglomeration only two classes can be merged into one. The clustering process eventually groups all individuals into a single class. A related hierarchical approach, divisive hierarchical clustering, begins completely opposite to AHC by initializing with one cluster. AHC is by far the most widely used clustering technique for data mining so it is the method of choice for this investigation (Tufféry 2011).

The mechanics of AHC are rather simple but the computing time can be rather resource intensive when the sample size becomes rather large. In this investigation, the 588 SNODAS

stations represent all of the individuals, a rather small sample size relative to large databases analyzed in the financial industry (Tufféry 2011). The main goal, as previously mentioned, is to partition individuals into nested classes. The steps taken in an AHC process can be summarized by the following algorithm (Tan, Steinback and Kumar 2005).

(1) Compute the proximity matrix for the dataset.
(2) **LOOP**
    (a) Merge the closest two clusters.
    (b) Update the proximity matrix to reflect the changes.
(3) **END** when only one cluster remains.

Agglomerative Hierarchical Clustering initializes in step 1 by computing the effective distance between all of the individuals, thus creating a proximity matrix whose terms are the distances between the standardized variables of pairs of individuals. This proximity matrix is reconstructed, as seen in step 2b above, every time a new set of classes is created. The choice of the measure of proximity is left to the analyst and is either based on *similarities* (such as Pearson correlation coefficient) or *dissimilarities* (such as Euclidean distance) (Addinsoft 2013). For the purposes of this investigation, the dissimilarities metric is employed due to the fact that Euclidean distance is the simplest mathematical relationship between two individuals. Once the type of proximity matrix is chosen and constructed, an AHC analysis then begins the process of merging two sets of individuals into a class based one of several methods. An AHC analysis successively evaluates every individual and assigns its membership into a class during each loop of step 2. The various types of AHC methods are described and evaluated below.

Several methods exist, each of which possess different sets of criteria for assigning individuals class memberships. These clustering outcomes of each criterion begin to diverge after the second loop in step 2; prior to this every individual belongs to its own class. These methods include computing the distance between two of the closest individuals of two classes (MIN or sin-

gle linkage), the distance between two of the furthest individuals of two classes (MAX or complete linkage) or an average distance between all of the members (group average) (Tufféry 2011). Each of the above mentioned methods have particular sensitivities to properties of the data and also weaknesses in certain situations. For instance, the MAX method is highly sensitive to outliers and generally results in classes of equal diameter, in terms of the distance between the two individuals furthest from the class centroid. Many SNODAS stations at high-elevations have modeled output of SWE and snow depth that may resemble outliers, but are in fact the most important data points that describe the extreme value snow loads. These stations would introduce bias and would not be clustered properly when using the MAX method. The MIN method has a weakness that is highlighted in certain situations where the dataset may actually comprise two distinct classes but also other individuals that are equally spaced from and close to both. Known as the 'chain effect', it results in one heterogeneous cluster because the MIN method essentially followed a trail of individuals that connected the two classes (Johnson and Wichern 2007).

An alternative method, Ward's method aims to optimize an 'objective function' other than distance between classes during the clustering process (Ward 1963). For MAX, MIN, and group average methods the objective function is some type of distance measured between two classes. The objective function for Ward's method is the sum of squared error (SSE) that results from merging the pair.

$$SSE = \left[\sum_{i=1}^{n} {x_i}^2\right] - \left[\frac{1}{n} \cdot \left(\sum_{i=1}^{n} x_i\right)^2\right] \tag{17}$$

In Eq. (17), *i* is an index variable for each individual in the population *n* (size of each class), and *x* in each summation denotes the *i*th individual under consideration. At each successive cluster-

ing step, or branch on the dendrogram, every possible pair of individuals (or classes later on in the clustering process) is evaluated against this objective function and the pair which, when combined, results in the least SSE is merged. In other words, the goal of Ward's method is to cluster the pair that results in the smallest decrease in between-class variance, since SSE is a measure of variance (Ward 1963). Since AHC progresses from n clusters to a single cluster, the largest between-class variance is observed at initialization where every individual belongs to its own class. Mathematically, this situation where each individual in in its own class represents the best clustering, but, for practical purposes a quantity of clusters $k << n$ is desired. Each clustering step beyond the first reduces the between-class variance by some amount, this amount decreasing in magnitude with each step. Ward's method seeks to keep the between-class variance (SSE) as high as possible, thus creating the most homogenous classes. The philosophy behind Ward's method, described above, explains why it is the most popular method for AHC. The philosophy of this method is to maximize heterogeneity between classes and thus minimize it within classes, which speaks to the greater purpose of clustering. It is also more effective than the other described methods when applied to real world problems (Tufféry 2011).

Ward's method, and in general hierarchical clustering, is focused on locally optimizing the objective function at each clustering step. Globally, once the clustering has concluded, the analyst needs to manually cut-off the analysis at the most favorable point, leaving an appropriate number of classes. A Ward's method algorithm finds this point by determining the clustering step after which the largest loss of between-class SSE is observed. This can be graphically represented on a dendrogram, illustrated in Figure 7.5. The lengths of the branches on a dendrogram represent the loss of between-class SSE. The optimal cut-off point proceeding bottom up from the initialization of the analysis is at the dashed line denoted by point B, which results in

three classes. Truncating the analysis at point A results in an impractical number of classes while truncating it at point C results in the largest loss in between-class SSE. Thus, graphically the dendrogram should be trimmed at a rather large branch, which precedes the largest branch on the tree. Since Ward's method and other methods of AHC lack the ability to optimize a *global* objective function, care must be exercised after the process to ensure that the results are reliable and pass some tests of validity (discussed in the following sections).

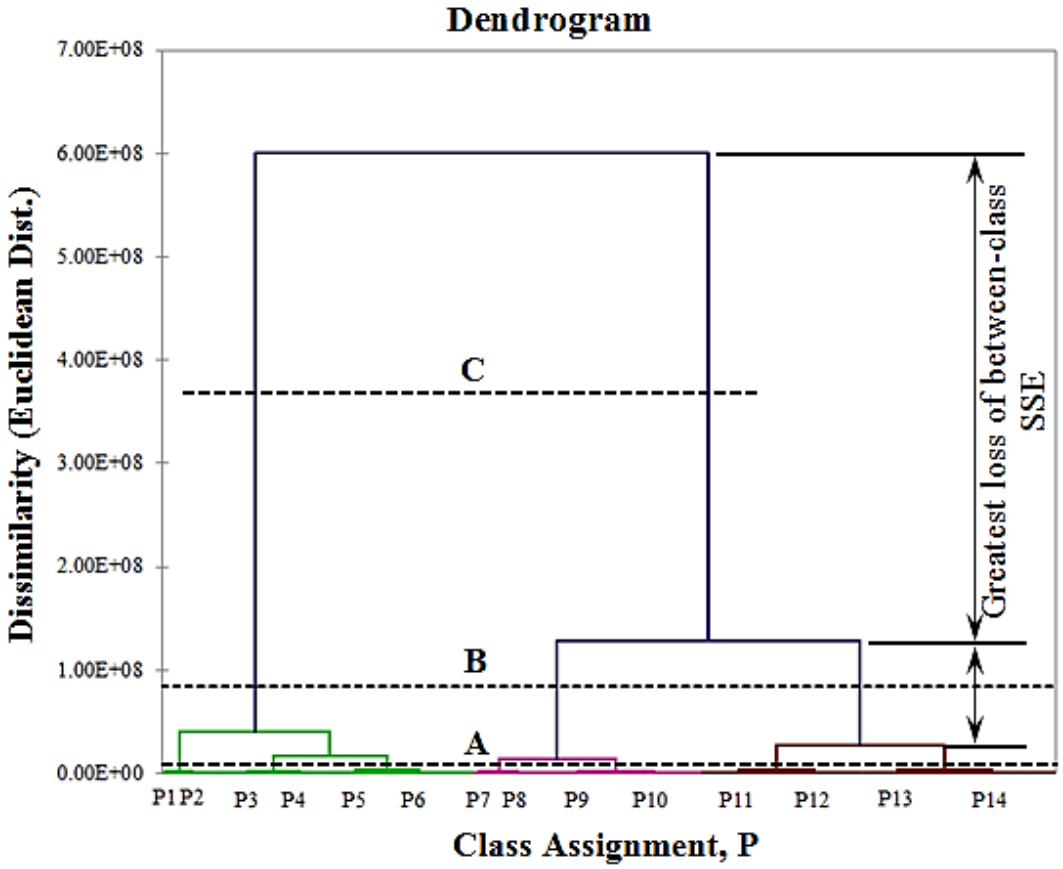

Figure 7.5: Dendrogram Produced by Agglomerative Hierarchical Clustering Analysis Showing the Optimal Point of Termination (Addinsoft 2013)

The applications of multivariate clustering in engineering are widespread. Clustering techniques were employed in Korea to regionalize precipitation gauges in order to better estimate regional flood characteristics (Kim, et al. 2004), in the United States to identify distinct subgroups of bridges so that long-term monitoring of them could be used to better describe degrada-

tion processes (Knight and Cooil 2005), and in the North Atlantic Ocean to group tidal gauge stations geographically by regional variability in order to understand sea level fluctuations (Scotto, Alonso and Barbosa 2010). Thus, clustering analyses have been established as reliable, versatile statistical tools that have broad applications.

Before any clustering is attempted, it is critical to define several indices of clustering validity. That way once a clustering analysis is complete, an assessment of its quality both within-classes and between-classes can be made. Between-class quality refers to the ability of the clustering algorithm (hierarchical, partitional) to differentiate classes into distinct subsets with minimal overlap of adjacent classes. Conversely, within-class quality refers to the ability of the algorithm to combine similar, proximate members into the same class. In both of these definitions, a measure of Euclidean distance is used to make a determination of quality. A few widely used indices that measure both are defined below.

The R^2 index measures the proportion of SSE explained by the classes themselves (*i.e.* between-class SSE / total SSE) (Tufféry 2011). Therefore, R^2 can be used to indicate between-class quality. The complementary index of this measure is that which measures the SSE explained by the members of the classes (*i.e.* within-class SSE / total SSE). The sum of both of these indices should equal 1.0. However, only the former (R^2) is reported in practice and in the literature. The closer R^2 is to 1, the higher the quality of clustering is for this index.

The *pseudo F* statistic measures the separation between all of the classes. It is not reported for each class but as an aggregate, weighted sum of all of the classes. The *pseudo F* statistic is defined by the following (Tufféry 2011).

$$F^* = \frac{R^2/(c-1)}{(1-R^2)/(n-c)} \tag{18}$$

In Eq. (18) F^* is the *pseudo F* statistic, R^2 is the weighted average index for all of the clusters, n is the total number of individuals in the population, and c is the number of classes. The greater this statistic is for a particular clustering operation, the greater the separation between all of the classes and thus the higher the quality. The *pseudo F* statistic is compared among all of the trials and all of the clustering methods. It is not to be used for single-linkage clustering; however, since this method of AHC is not considered in this analysis *pseudo F* can be used here.

7.5.2 K-means Clustering

A k-means clustering is a type of partitional clustering that seeks to subdivide a dataset into k classes based on the centroids, or arithmetic means, of newly established classes (Tan, Steinback and Kumar 2005). Unlike an AHC analysis, a k-means clustering analysis does not produce classes that are related to one another through hierarchical relationships since it only performs a single level of clustering. This is equivalent to always producing a clustering at the "C" level as indicated in the sample AHC dendrogram in Figure 7.5, with the exception that more than two classes can be produced for k-means. A k-means clustering analysis is iterative and is only complete once an objective function meets specified criteria, determined a priori. This objective function and the mechanics of k-means in general are described below.

A brief description of the k-means algorithm that describes how the analysis is implemented into statistical computer software is provided below (Tan, Steinback and Kumar 2005).

(1) Select k points as initial centroids (randomly or user defined)
(2) **LOOP**
    (a) Form k classes by assigning each individual to nearest centroid.
    (b) Re-compute centroids based on current assignments.
(3) **END** when defined criteria are met (*i.e.* convergence, minimal class change).

A k-means clustering analysis initiates in step (1) with the entire dataset and chooses a number of points as initial centroids of the dataset, chosen by the user. There are *k* of these initial centroids, and since the number of centroids is fixed at the start of the analysis it follows that the number of classes, *k*, must be chosen beforehand. Methods for choosing the appropriate number of classes are discussed later. These centroids are simply coordinates on a Cartesian plane; the number of variables being supplied for each clustering operation defines their dimensionality. For instance, in this investigation no more than three variables are clustered per operation so the k-means centroids have x-, y-, and z- coordinates. The locations of the centroids need not be individuals themselves. There are many methods for choosing the initial centroids each with advantages and disadvantages that must be weighed prior to performing the analysis. They can be chosen at random or determined by performing an AHC analysis first and analyzing its class centroids (Tan, Steinback and Kumar 2005).

The method of choosing initial class centroids randomly is logically the simplest and requires the least amount of time and resources. However, this method must be employed carefully to ensure that sufficient runs of the analysis are performed to generate enough variability (Tan, Steinback and Kumar 2005). Here the term *runs* refers to several complete k-means clustering operations performed end-to-end on the same dataset. These operations combined constitute a k-means clustering analysis (where the best clustering operation is chosen). Figure 7.6 illustrates the need to consider many runs. Here, stars denote the initial centroids of each class for four runs, or iterations. As Figure 7.6 illustrates, it is possible that centroids chosen at random may be very close to each other, which may result in the erroneous partitioning of a truly single cluster into multiple ones. Moreover, because centroids don't move significantly between iterations of a k-means analysis, self-correction isn't possible. To reduce the probability of very close ini-

tial centroids, a number of clustering iterations (perhaps several hundred) each with randomly selected initial centroids must be performed (Tufféry 2011). The iteration with the best quality, assessed by R^2 and *pseudo-F* statistic, is the chosen clustering.

Another method of determining initial centroids is to perform an agglomerative hierarchical clustering on the dataset and use the results of that analysis as the inputs to the k-means cluster analysis (Tan, Steinback and Kumar 2005). In this method class centroids obtained from the results of an AHC analysis are used as the starting centroids of the k-means analysis. The AHC analysis doesn't require manual input of class quantity at initialization since it optimizes this quantity during the analysis. One of the most common results from an AHC analysis performed by standard statistical software is, among other things, the centroids of each class. Once obtained, these centroids are used as the initial starting centroids for k-means. When used beforehand, AHC can provide the k-means analysis with a good starting point and reliable estimate of the natural structure of the dataset as well.

Once the initial centroids of the classes are chosen, step (2) in the k-means algorithm is executed. Individuals are incrementally assigned to classes based on the distance from these centroids, usually Euclidean distance (Johnson and Wichern 2007). In this clustering step all members are assigned to one of the *k* classes. The centroids are then re-computed based on the current assignments since they may change slightly as individuals are assigned. Once the tentative class memberships and re-computed centroids are determined, the entire process begins again. Class assignments are re-evaluated based on distance to the class centroids and the class centroids are re-computed again. Within this loop of step (2), some individuals roughly equidistant to two centroids might change classes. Ideally, the refinements of both class memberships and centroid coordinates would decrease as this step is repeated. In fact, experience with per-

forming many k-means analyses suggests that the majority of the reassignments occur during the first iteration (Johnson and Wichern 2007). The algorithm stops upon acceptance of a predefined criterion. Numerous types of stop criteria are available for commonly used statistical software and are discussed in detail below.

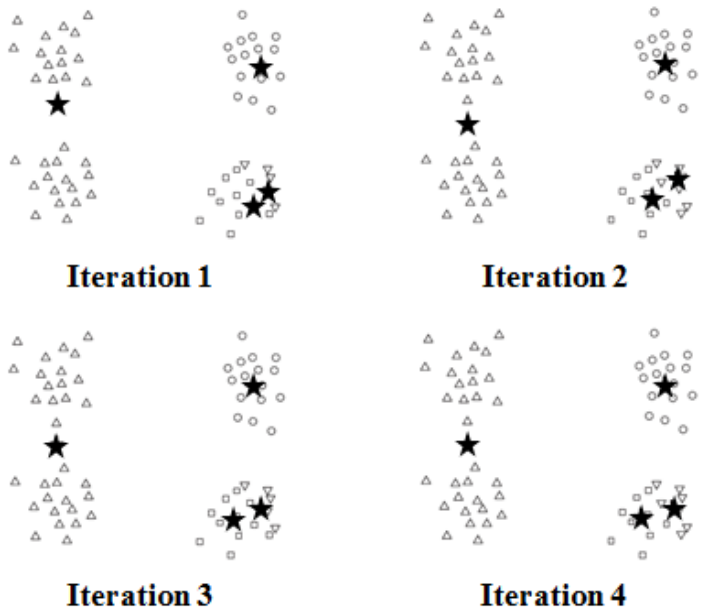

Figure 7.6: Four k-means *Clustering Runs Initializing with k Randomly Chosen Centroids (Tan, Steinback and Kumar 2005)*

The statistical software utilized in this investigation, XLSTAT Pro, offers a variety of stop criteria for its k-means clustering analysis. The most traditional is the *Trace(W)* criteria (Addinsoft 2013). The *Trace(W)* criteria essentially seeks to minimize the within-class SSE, thus maximizing between-class heterogeneity. It does this by re-arranging class memberships such that both the distance of each individual to the class centroid *and* the trace of the sum of squares and cross products (SSPC) matrix are minimized. The SSPC matrix is defined as follows (Johnson and Wichern 2007).

$$\text{SSPC} = \mathbf{W} = \sum_{j=1}^{p} \sum_{i=1}^{n} [X_{j,i}][X_{j,i}'] \tag{19}$$

In Eq. (19), n denotes the total number of individuals in each class, p denotes the total number of classes, and $X_{j,i}$ represents a matrix of Euclidean distances of each individual to the class centroids. The $X_{j,i}$ matrix is composed of these distances for the individuals displayed column wise and the different classes displayed row wise. The multiplication of this matrix with its transpose produces a square SSPC matrix. This matrix possesses within-class SSE along the diagonal and cross-product SSE values between different classes on the off-diagonals. Thus, minimizing the trace of this matrix minimizes the within-class sum of squares. The *Trace(W)* criterion is the proper partitional analog to Ward's hierarchical clustering method (Tufféry 2011). *Trace(W)* is sensitive to the effects of scaling, so the variables must be standardized otherwise the variables with the highest variance or standard deviation will be clustered together and the measures of clustering validity will be unreliable. Also, this criterion tends to produce classes of similar size and shape.

The second option of stop criterion offered by XLSTAT is *Determinant(W)*. This criterion seeks to minimize the determinant of the pooled within-class covariance matrix for each class (Addinsoft 2013). Since the variables are standardized, their means are equal to 0 and their standard deviations are equal to 1. Therefore, *Determinant(W)* minimizes the determinants of the within-class *correlation* matrix due to its equivalence to the standardized covariance matrix (refer to the latter portion of Chapter 7.3). When det(**W**) is zero, or close to zero, it indicates a linear dependency of the rows and the columns of the matrix. In other words, it signals that there are statistically significant interaction effects within the class among the variables used in the k-means clustering analysis (Johnson and Wichern 2007). Thus, it is a measure of within-class

homogeneity. The philosophy of this criterion is derived from the Wilk's Lambda statistic for multivariate analysis of variance, λ^*.

$$\lambda^* = \frac{|\mathbf{W}|}{|\mathbf{B} + \mathbf{W}|} \tag{20}$$

In Eq. (20), the matrix **B** is defined in a similar manner as **W** in Eq. (19) except that **B** accounts for the sum of squared error due to the clustering itself (*i.e.* total inertia). The Wilk's Lambda statistic therefore is the normalized form of the *Determinant(W)* criterion in XLSTAT that indicates a proportion of variance to total population variance. Both stop criteria are available in XLSTAT, the only difference being that *Determinant(W)* indicates an absolute value while the Wilk's Lambda criterion indicates a value between 0 and 1. These two criteria are considerably less susceptible to the detrimental effects of variable scale. Furthermore, they tend to produce class sizes that are less homogenous, which means that class sizes may better reflect the natural data structure if that structure possesses an uneven distribution of related individuals.

The measures of clustering validity for k-means are similar to those used in AHC. Accordingly, for each clustering operation the R^2 and *pseudo-F* statistic are reported to indicate quality of clustering.

7.6 Multivariate Cluster Analyses Performed on SNODAS Dataset

As previously mentioned, both hierarchical and partitional clustering methods are employed in this investigation. In particular, purely hierarchical, purely partitional, as well as hybrid clustering analyses are performed on the SNODAS dataset. A PCA-derived clustering is also performed in order to judge its efficacy alone, without applying clustering techniques. The results of the clustering analyses are evaluated based on statistical tests of clustering quality applicable to each of the different clustering methods. The results are then mapped using Geographical Information System (GIS) capable software and the classes are evaluated visually for

suitability in a state ground snow load map. This section is organized as follows. The results from the AHC analysis are presented first, followed by the k-means analysis, the PCA analysis, and finally the hybrid analysis. Results, discussion, and topographical GIS-produced mapped classes are presented together in the section for each method.

7.6.1 Results of Agglomerative Hierarchical Clustering

The Agglomerative Hierarchical Cluster analysis is performed with the assistance of the software program *XLSTAT Pro*. The AHC analysis is based on dissimilarities in the proximity matrix and the agglomeration method proposed by Ward. The clustering proceeds using the standardized SNODAS variables prepared in Chapter 7.2 and partially listed in Appendix K as the clustering variables. As previously mentioned the clustering process itself is phased into nested operations; each clustering operation is performed on the classes formed during the previous. Clustering variables are chosen according to the results of the PCA performed prior. In order to establish a minimum number of classes as a guideline, experimental AHC trials were performed in which an increasing quantity of classes was manually forced. The R^2 validity measure was computed for each so that a relationship between quantity of classes and clustering validity could be obtained (Tufféry 2011). The results are plotted in Figure 7.7. The quantity of classes after which there is an appreciable reduction in R^2 gain should be taken to be the minimum, which in this case is four. Four classes results in an acceptable level of between-class heterogeneity. These experimental trials assisted in the development of a process flowchart for AHC, illustrated in Figure 7.8. In total, four trials of clustering are performed; a single trace through the flowchart elements [1] through [5] represents one trial.

The first clustering operation in element [2] of Figure 7.8 is performed on the entire dataset using the clustering variables from set (a). For each of the four trials, set (a) includes the

variables SWE, snow depth, and elevation. Two classes are forced during the clustering operation in element [3] since there are generally great disparities in the standardized variables between high and low-elevation stations and it is desired to separate the stations as such. However, the clustering algorithm is not otherwise altered. The results are the first two classes produced by the clustering operation denoted by flowchart element [3] in Figure 7.8 (the circled numbers 1 and 2).

The individuals in these two classes are evaluated separately to determine patterns (*e.g.* high/low-elevations, SWE, snow depth). This evaluation determines which clustering input variables will be used for the clustering operations denoted by flowchart elements [4a] and [4b]. In performing several trials, one class generally contains low-elevation stations and so the clustering variables in set (b) are tailored to the low-elevations. Accordingly, they generally include longitude and basin occasionally combined with elevation, SWE, or snow depth (for some trial runs). The second class generally contains high-elevation stations (≈ 10,000 ft.). For this class, the clustering variables in set (c) are tailored to mountainous sites. Accordingly, they generally include slope, aspect, and curvature occasionally combined with elevation, SWE, or snow depth.

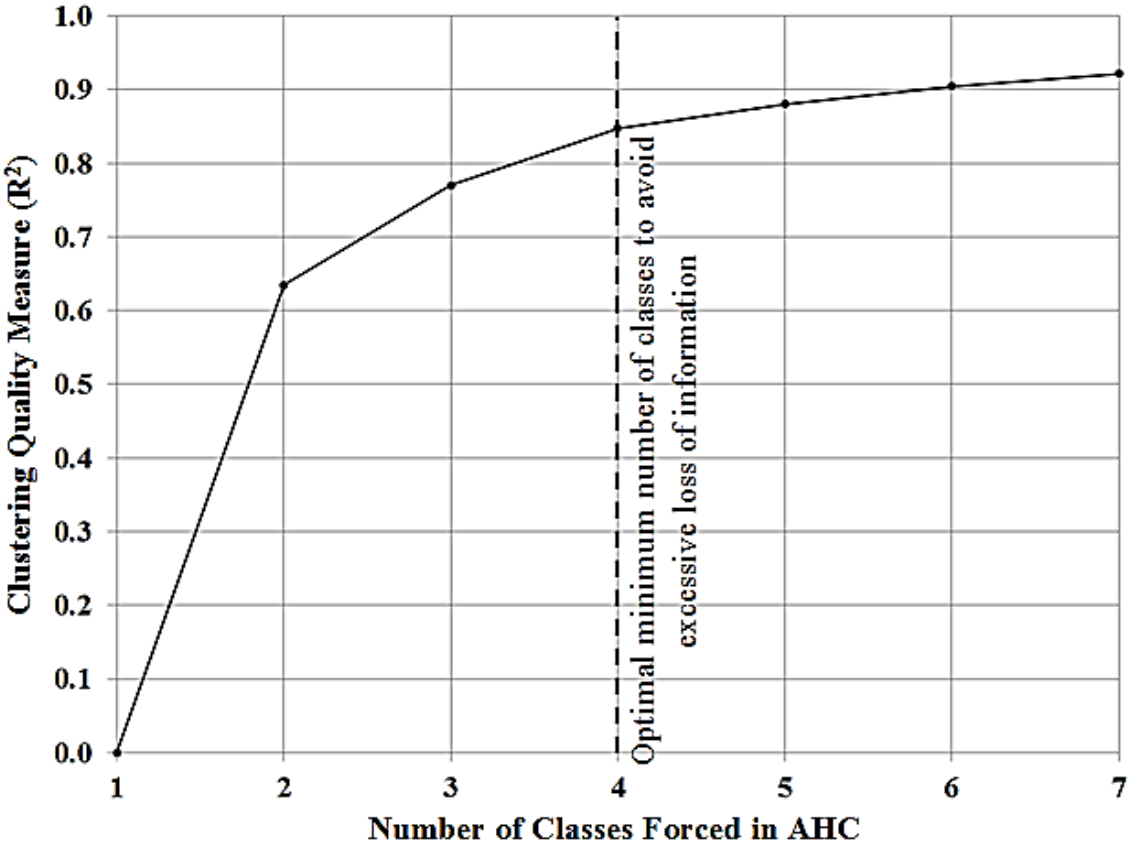

Figure 7.7: R^2 as a Function of the Number of Classes Manually Forced in AHC Experimental Trials.

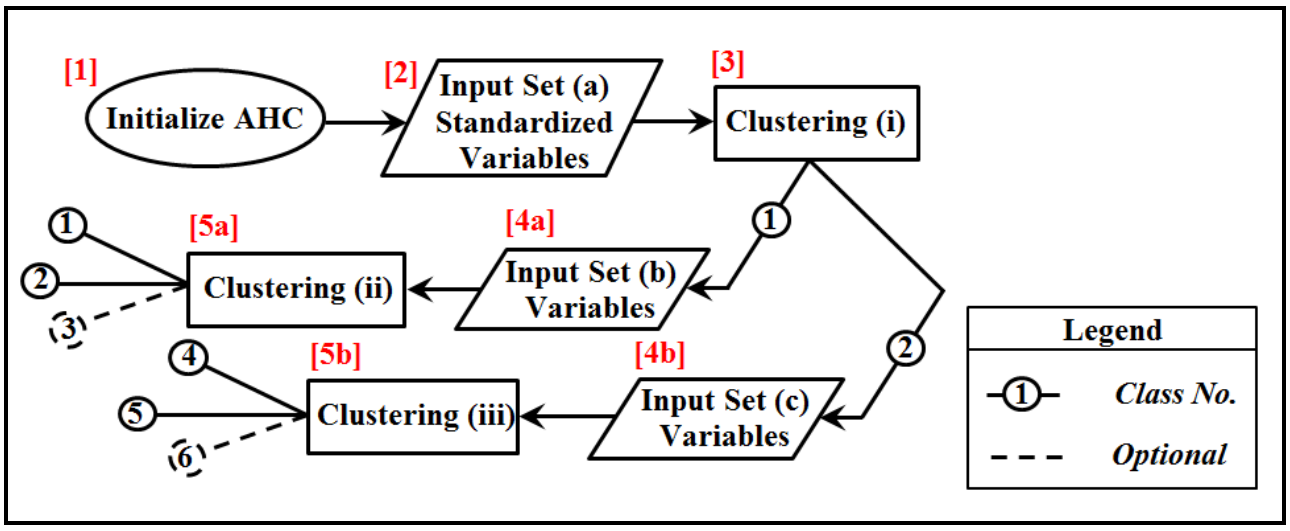

Figure 7.8: Process Flowchart for Agglomerative Hierarchical Clustering

The process laid out in Figure 7.8 is followed consistently throughout all AHC trials. The selected input variables for each clustering, however, are manually adjusted depending on

the quality of classes being achieved. If classes of poor quality are produced by the input variables, other combinations are chosen. This feedback mechanism results in trials with slightly different quantity/type of input variables and quantity of classes. This is why optional classes are denoted by dashed lines proceeding from elements [5a] and [5b]; in these instances the AHC algorithm determines the appropriate number of classes for clustering operations (ii) and (iii). Table 7.8 lists the trials of AHC analyses performed; input variables for sets (a), (b), and (c); the total number of resulting classes for each; and measures of clustering quality (R^2 and *pseudo F* statistic).

Table 7.8 indicates the clustering quality being achieved by various combinations of input variables. Each trial initiated with elevation, snow depth, and SWE as the input variables for clustering (i). These three variables were the major contributors to principal component PC1. In all trials, clustering operation (ii) ran with at least basin and longitude as input variables, since they were the major contributors to PC2. In trials 1 and 2, the additional variables of SWE or snow depth resulted in similar between-class variance but rather different *pseudo-F* scores. This indicates trial 2 is the more suitable of the two. Trial 3 illustrates that while aspect and curvature were major contributors of PC3 and moderately correlated with each other, neither produces good clustering results. Overall, as highlighted in bold, a combination of clustering results from trials 2 and 4 produces the best aggregate R^2 and *pseudo-F* score. A combination is possible since the class memberships produced by clustering (i) are identical for all four trials. Thus the classes produced using the inputs of elevation, SWE, and snow depth for clustering (i), basin, longitude, and snow depth for clustering (ii), and basin and longitude for clustering (iii) are the most suitable. This formation of classes is now referred to as the final AHC clustering. Graphical representations of each clustering are described below.

Table 7.8: Results of Agglomerative Hierarchical Clustering Trials

AHC Trial	Clustering (i) [3]			Clustering (ii) [5a]			Clustering (iii) [5b]			No. of Classes
	Input (a)	R^2	*F**	Input (b)	R^2	*F**	Input (c)	R^2	*F**	
1	E, SD, SWE,	0.635	203	BA, LG, SWE	0.831	572	AS, CV, SL	0.474	105	6
2	E, SD, SWE,	0.635	203	**BA, LG, SD**	**0.863**	**735**	BA, LG, SD	0.614	185	6
3	E, SD, SWE,	0.635	203	BA, E, LG	0.755	359	AS, CV	0.651	217	6
4	**E, SD, SWE,**	**0.635**	**254**	BA, LG	0.820	664	**BA, LG**	**0.848**	**813**	5

AS = aspect, BA = basin HUC, CV = curvature, E = elevation, LG = longitude,
SD = snow depth, SL = slope, SWE = snow water equivalent
*F** = *pseudo-F* statistic, R^2 = weighted average, between-class SSE
Note: red numbers in brackets denote flowchart elements from Figure 7.8.

The dendrograms for the final AHC clustering are presented in Figure 7.9. Recall from Figure 7.8 that the clustering process resulted in the subsequent clustering of the *original* classes P1 and P2 from flowchart element [3]; accordingly their indices are replaced by the final six classes P1 through P6 (center and bottom dendrograms). It can be seen that as the clustering operations progress, the range of dissimilarity (Euclidean distance) decreases, indicating that each operation is producing more homogenous classes of individuals than the previous. Also, for clustering (i) and (ii), the branches of the dendrogram are cut off before a significant loss of between-class SSE. This signifies that the practice of nesting the clustering operations employed is successful, as well as the AHC itself. While clustering (ii) could easily have been cut off at four classes, as noted by the branching in Figure 7.9, three classes are considered sufficient to explain the variability. Also for practical purposes it is not desired to have an additional class. A clustering that produces many classes may present as a very efficient and statistically robust clustering; however, analyses with too many clusters ultimately prove too cumbersome and time-

intensive to analyze and implement for the production of a ground snow load map. This highlights the need for manual supervision of the data. This is often accomplished by mapping the clusters on a topographical map using GIS-enabled software. Then, visual evaluation of the mapped classes provides the final step in assessment of the clustering.

The completed classes are then plotted on a topographical map, using the latitudes, longitudes, elevations, and station identifiers as input. Each class is input into ArcGIS and assigned a different colored pin to distinguish one class from another, as depicted in Figure 7.10. From the map it is clear that generally the AHC algorithm properly distinguishes the lower plains from the high-elevations, separating stations east of the Front Range from the stations to the west (defined by the boundary of red pins, class P5). Also, the mountain peaks of the Central Rockies, denoted as blue pins for P2, are well separated from others. Classes P3 and P6 (orange and yellow pins, respectively) overlap considerably, however, and don't clearly define distinct regions of the state. It is likely that these classes were separated early on in clustering (i) and were never recombined. Classes P4 and P5 (red and purple, respectively) appear to have been separated due to the physical distance between them. Lastly, class P1 only contains 36 stations and would be too small to constitute its own class. The intent of its creation is noted, though; this region defines the transition zone from relatively moderate snowfall and density in the plains to heavy deep snowfall in the mountains. It is believed by the author to be a crucial zone.

If chosen to be incorporated into a state snow load map, the arrangement of classes produced by the final AHC would need some modifications that would facilitate the formation of well-defined regions. First, overlapping and mistakenly assigned stations (*e.g.* the single green pin in the upper right of Figure 7.10) would be reassigned manually. Classes P4 and P5 would be combined into one.

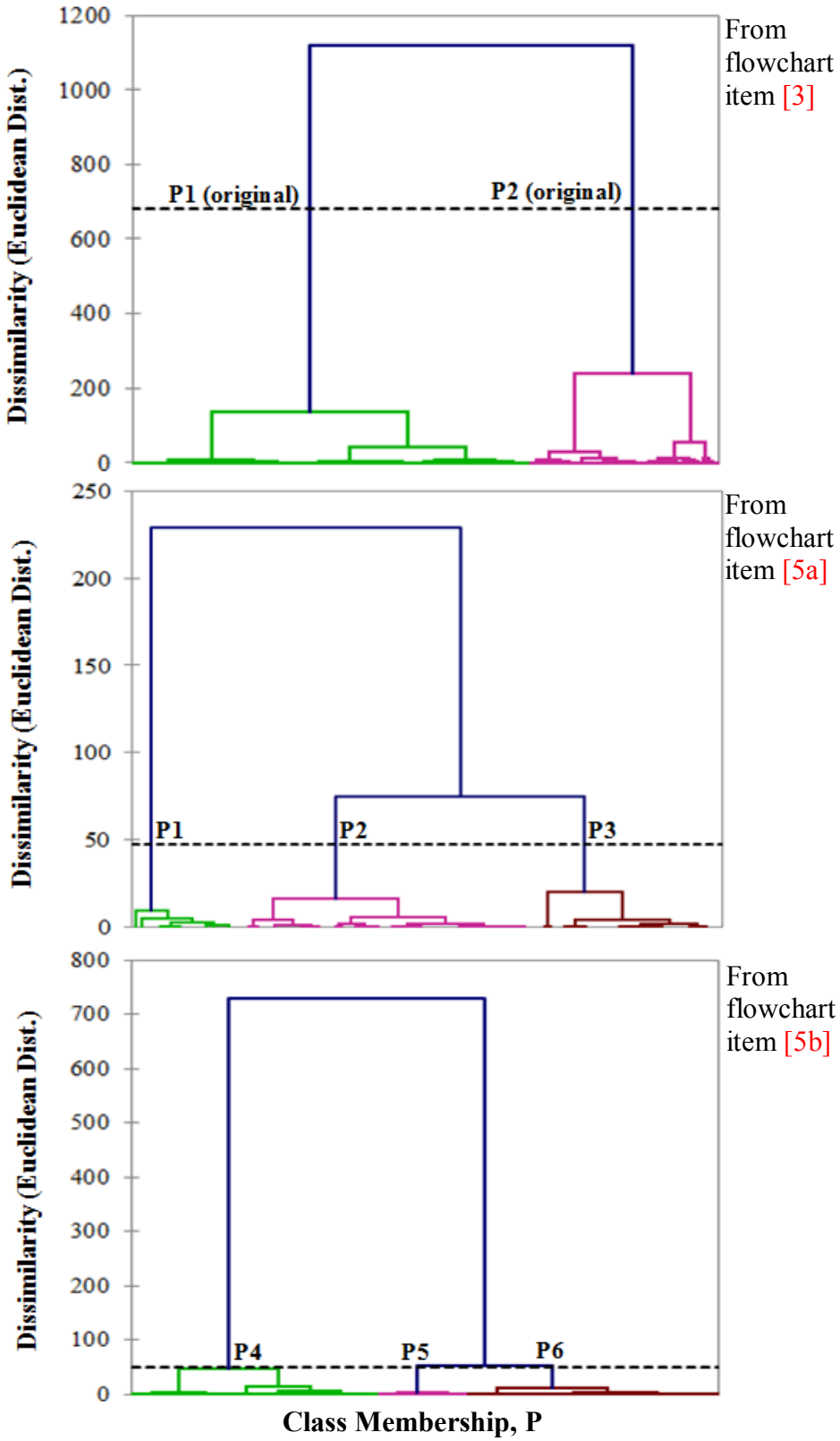

Figure 7.9: Dendrograms Created by Final Agglomerative Hierarchical Clustering Created with XLSTAT. From Top to Bottom, Dendrograms of Clustering (i), (ii), and (iii).

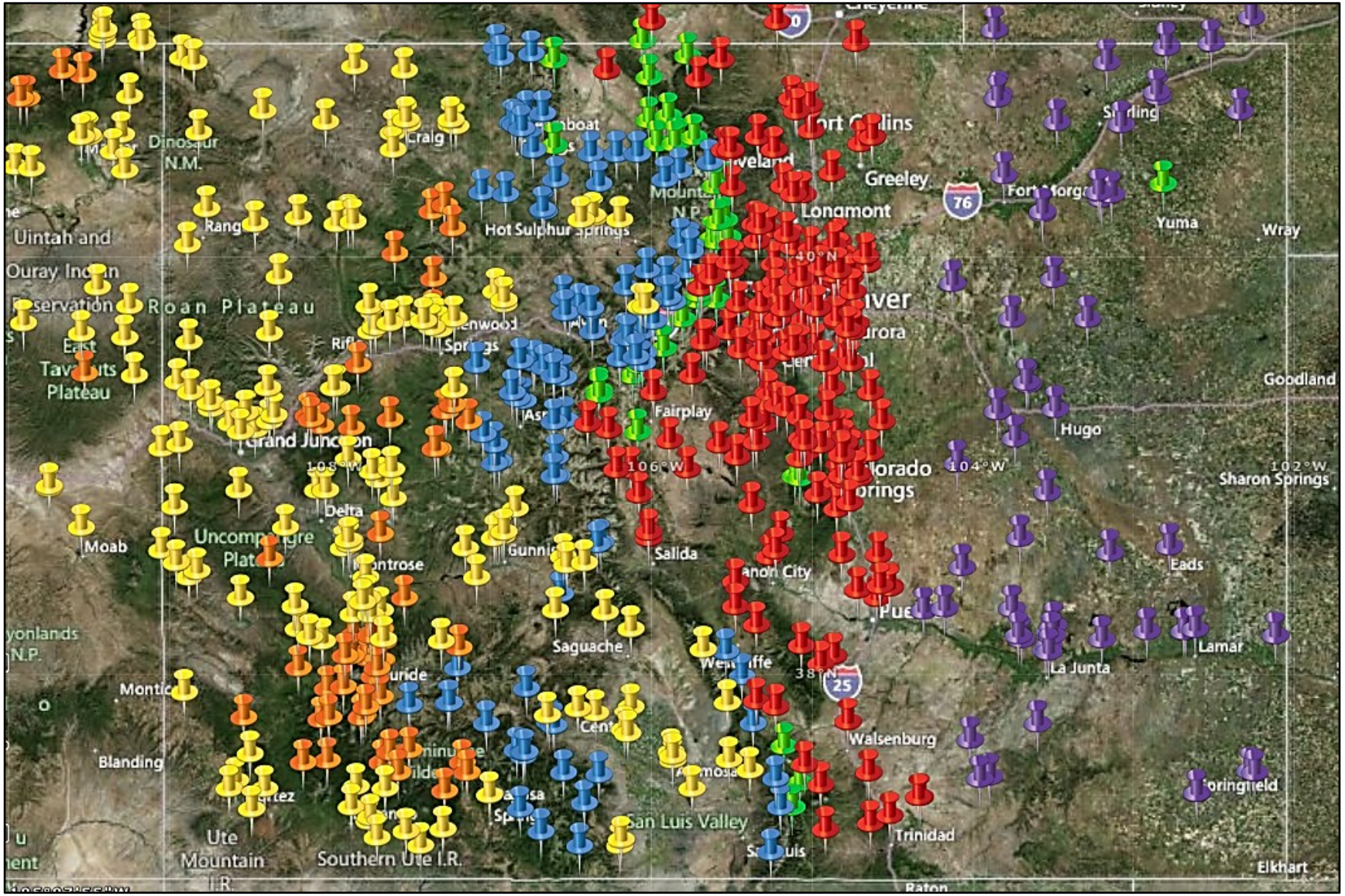

Figure 7.10: Topographical Map of Classes Created by Final Agglomerative Hierarchical Clustering Plotted With ArcGIS.
(Green - P1, Blue - P2, Orange - P3, Purple - P4, Red - P5, Yellow - P6)

7.6.2 *Results of* k-means *Clustering*

The k-means analysis is performed in the same manner as the previous AHC analysis. The process flowchart established for AHC and illustrated in Figure 7.8 is followed here as well. The nested clustering methodology is again employed since the clustering results thus far have proved successful. Similar to the AHC trials, several experimental k-means trials are performed prior to the analysis trials in order to formulate a relationship between clustering quality and the number of classes. This step is necessary for a k-means analysis since this method requires manual input of class quantity, *k*, at initialization. Also, it is unclear whether the quantity of classes determined Figure 7.7 for the AHC analysis is applicable here as well. The plot of R^2 vs. class quantity, is illustrated in Figure 7.11, indicates that the minimum quantity of classes is four. The plot, similar to that produced by the AHC experimental trials, indicates that the optimal number of classes is independent of the type of analysis performed.

The process followed in Chapter 7.6.1 is maintained for the k-means analysis, including the intermediate steps of choosing input variables for the various clustering operations. The stop criterion for the k-means analysis is *Determinant(W)*, described in Chapter 7.5.2. This stop criterion is appropriate since it does not produce homogenous class sizes, not anticipated to reflect the natural structure of the data. For initialization, centroids are chosen by performing a preliminary AHC analysis to determine the appropriate number of classes and their corresponding centroids. The results of this preliminary analysis, including the dendrogram and initial centers, are available in the upper portion of Appendix M. This technique eliminates the unfavorable effects of choosing poor initial centroids by random. Although initial centers are manually chosen at initialization, 500 iterations are performed during each operation for convergence of the stop criterion. The results of k-means are presented in Table 7.9.

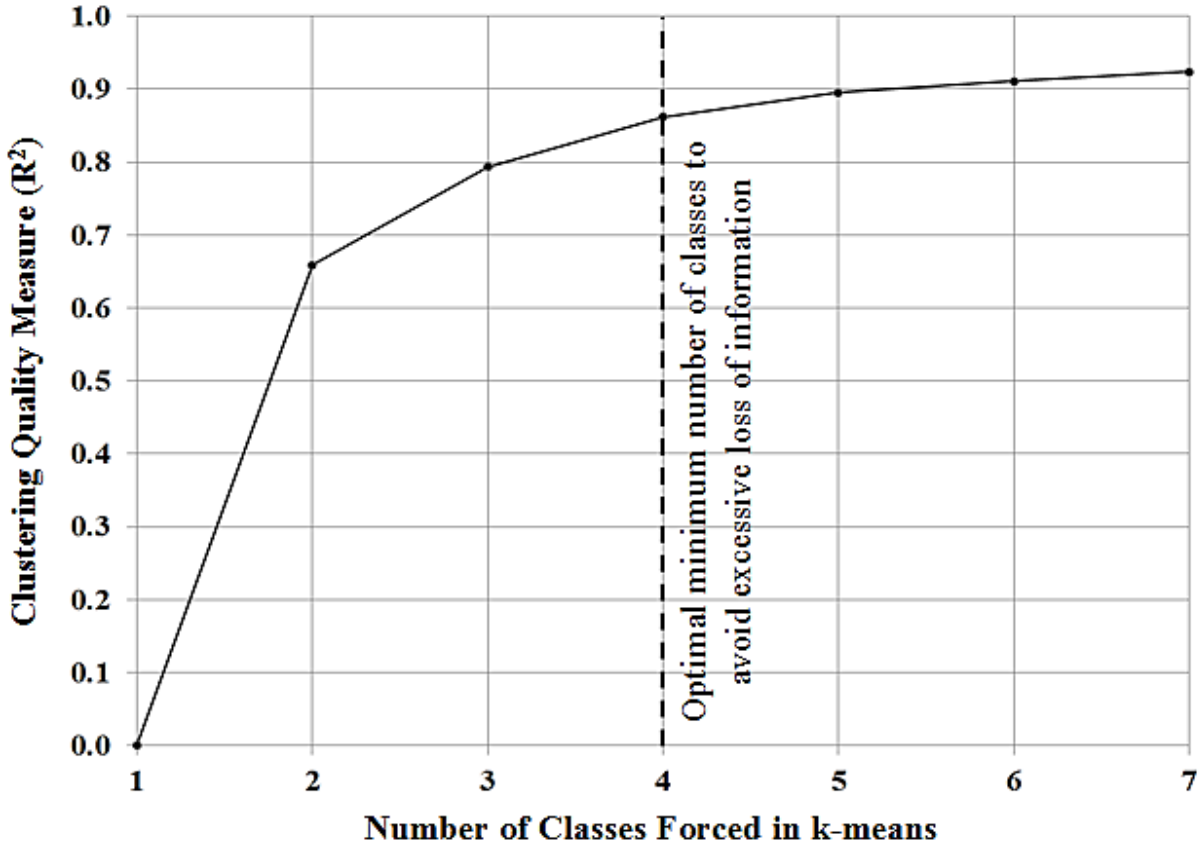

Figure 7.11: R^2 as a Function of the Number of Classes Manually Forced in k-means Experimental Trials

Table 7.9: Results of k-means Partitional Clustering Trials

k-means Trial	Clustering (i) [3]			Clustering (ii) [5a]			Clustering (iii) [5b]			No. of Classes
	Input (a)	R^2	*F**	Input (b)	R^2	*F**	Input (c)	R^2	*F**	
1	E, SD, SWE	0.789	544	BA, LG, SWE	0.740	415	AS,CV, SL	0.236	45	5
2	E, SD, SWE	0.789	544	BA, LG, SD	0.718	371	BA, LG, SD	0.449	119	5
3	E, SD, SWE	0.789	544	BA, E, LG	0.702	343	AS, CV	0.398	97	5
4	**E, SD, SWE**	**0.789**	**544**	**BA, LG**	**0.791**	**552**	**BA, LG**	**0.721**	**376**	**5**

AS = aspect, BA = basin HUC, CV = curvature, E = elevation, LG = longitude,
SD = snow depth, SL = slope, SWE = snow water equivalent
*F** = *pseudo-F* statistic, R^2 = weighted average, between-class SSE
Note: red numbers in brackets denote flowchart elements from Figure 7.8.

Table 7.9 indicates that the quality of clustering achieved by clustering operation (i) in all trials (F^*= 544) is moderately better than was achieved by the AHC analysis. For clustering operations (ii) and (iii) however, the highest measures of either R^2 or *pseudo-F* (0.791 and 552, respectively) are considerably lower compared to the AHC analysis. Also, there is a much greater range of quality values for clustering (iii) for the four trials of k-means. Nonetheless, the clustering analysis as a whole produced acceptable quality. For trial 4, selected as the final k-means clustering, all of the clustering operations achieved greater than 70% between-class variance.

For the clustering operation (ii), the results of the k-means analysis indicate that Basin and Longitude, when clustered alone, produce the highest quality clustering. This finding confirms the results of the PCA, which found that longitude and basin were primary contributors to PC2. Also, aspect and slope of the terrain do not appear to create suitable classes when included as variables for clustering operation (iii). Several additional trials not listed in Table 7.9 were performed; however, in no case did the inclusion of slope, aspect, or curvature produce a clustering quality higher than the trials presented in Table 7.9. For clustering operation (iii) the clear choice is again basin and longitude alone as the clustering variables. Overall, the validity measures of the k-means clustering analysis indicate that the best formation of classes results from using the inputs of elevation, SWE, and snow depth for clustering (i), and basin and longitude for both clustering (ii) and (iii). Represented entirely by trial 4, this formation of classes is now referred to as the final k-means clustering.

The final product of the k-means clustering analysis is a plot illustrating the value of the stop criterion, *Determinant(W)* as a function of each iteration performed. XLSTAT Pro computes the value of *Determinant(W)* after each k-means iteration using Eq. (19). These plots of stop criterion vs. iteration are used like biplots of a PCA to visually evaluate the efficacy of the

clustering. A convergence of the stop criterion value signals the end of the clustering operation. This plot for the final k-means clustering operation (i) is presented in Figure 7.12. The relatively low value of *Determinant(W)* compared to before any clustering (iteration 0) indicates that the clustering is successful. This particular k-means run converges after three iterations, indicating that no further class reassignments from the remaining 497 iterations would improve the clustering quality. Other plots for k-means clustering operations (ii) and (iii), not shown, provide similar results for those operations.

Figure 7.12: Plot of the Stop Criterion Determinant(W) as a Function of Iteration for the Final k-means Clustering. Plot was created using XLSTAT Pro.

The completed classes for the k-means analysis are plotted on a topographical map, illustrated in Figure 7.13, with colored pins for the members of the various classes produced. There are only four classes illustrated by Figure 7.13 because the original clustering produced an outlier class with very few SNODAS stations which were merged with another class. The stations from the outlier class were all SNOTEL stations high in the Rocky Mountains that were manually reassigned to a similar class composed mainly of other SNOTEL stations.

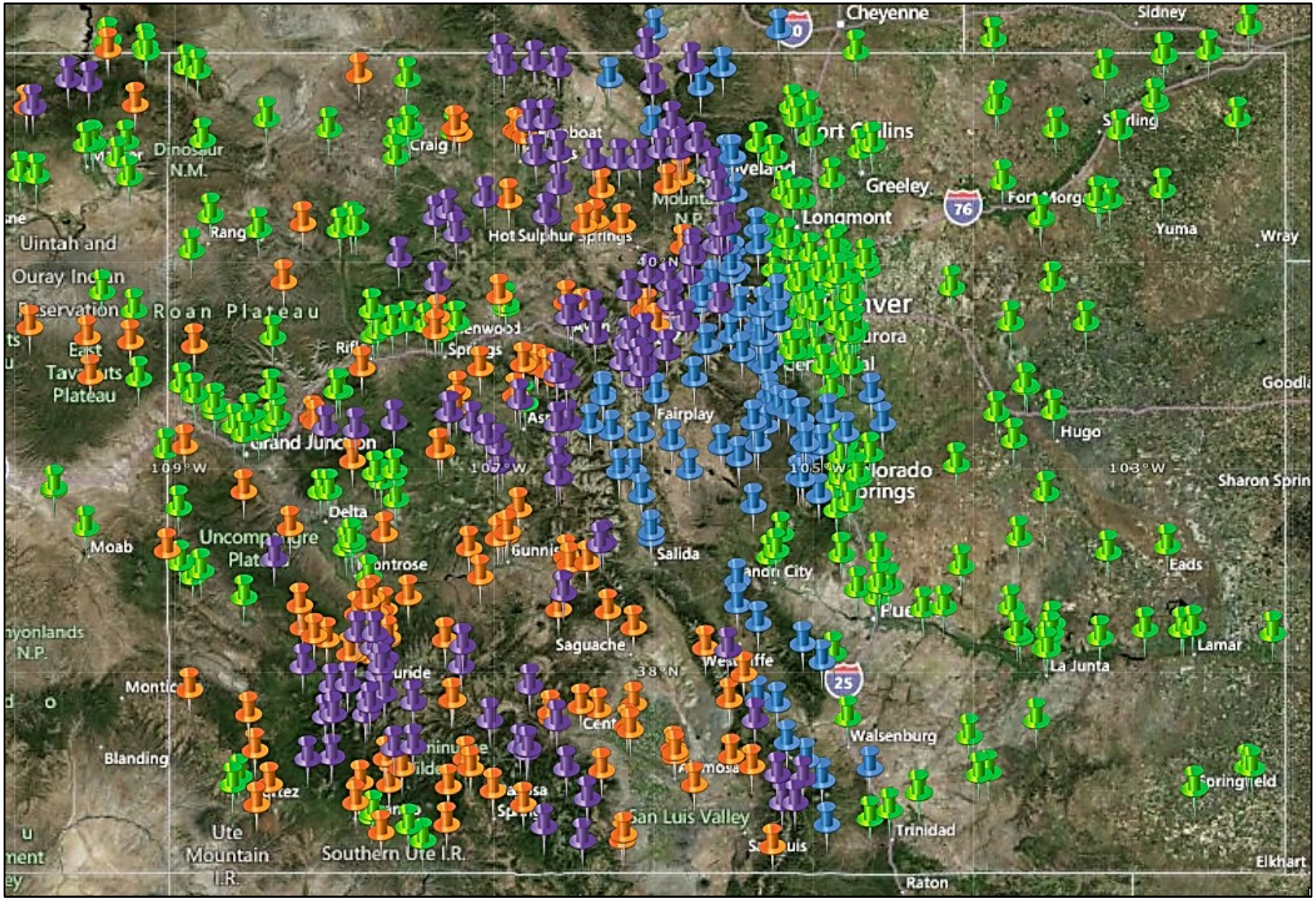

Figure 7.13: Topographical Map of Classes Created by Final K-means *Clustering Plotted With ArcGIS. (Green - P1, Blue - P2, Orange - P3, Purple - P4)*

From studying Figure 7.13 it is evident that the k-means clustering differentiated low and high-elevations well, specifically near the Front Range. However, for class P1, some low-lying stations on the eastern plains were clustered with stations west of the Great Divide. These two regions represented by P1 are expected to see different climatic patterns and snowfall so the merging of stations from these regions is undesirable. However, all of the low-elevation stations east of the Front Range were clustered together, which is appropriate since east of the Rocky Mountains, climatic patterns are relatively constant through to the border with Kansas.

Classes P2 and P4 appear to contain a mix of both high-elevation, alpine SNOTEL stations that probably experience deep snowfalls as well as lower elevations that appear to be in the shadows of other mountain peaks. It appears that the k-means algorithm had a difficult time differentiating between these two types of stations represented by the classes.

In general, classes P1, P3, and P4 do not seem to be well differentiated west of the Great Divide. This does not lend itself to a useful or practical ground snow load map since potential snow load isolines would cross over each other. It also does not appear that the mix of classes in the western portion of the state can be separated manually or corrected. In light of this and the fact that the measures of clustering validity were not extremely high, the k-means clustering analysis will not be considered further in this investigation.

7.6.3 Results of PCA-Based Clustering

PCA is very useful in reducing the dimensionality of a multivariate dataset (Jolliffe 2002, Johnson and Wichern 2007), and has been successfully shown to improve the quality of multivariate clustering methods when used a priori (Ben-Hur and Guyon 2003). However, few studies have attempted cluster or classification analyses based solely on the results of a PCA. While the

principal components themselves are not intended to be interpreted as classes, there is definitely a relationship between the principal components and the natural structure of the dataset.

For instance, in both the AHC and k-means analyses performed thus far, the input variables representing the first few principal components resulted in exceptional clustering variables. For instance, the major contributing variables to PC1 (SWE, snow depth, and elevation) and PC2 (longitude and basin) proved to be predictors of good clustering quality for clustering operations (i) and (ii), respectively. Due to the relationship between the principal components and the classes formed based on them, clustering based on the results of the PCA is investigated. Furthermore, by evaluating the performance of an unconventional PCA-based clustering analysis against the more traditional AHC and k-means methods, the efficacy of multivariate clustering methods in general can be gauged.

Since PCA is not an established method for clustering itself, there is no practical statistical measure of clustering quality, compared to the R^2 and *pseudo-F* statistics for AHC and k-means. Therefore, only a visual evaluation of the classes produced by the PCA-based clustering is used to measure the clustering quality. For the results presented thus far, the visual test has generally corroborated the statistical measures of quality. Visual evaluation of the clustering results is the most crucial element anyway since the method chosen to be implemented in a ground snow load map *must* pass the visual inspection.

The method of extracting classes from the results of the PCA proceeds as follows. First, a quantity of classes must be manually selected for the PCA-based method. Four classes are chosen since the first four PCs explain 75% of the total variance in the dataset, as described in Chapter 7.4. A matrix of the contributions of each individual to first four PCs is then created. This is similar to the variable contributions in Table 7.7, except that this matrix contains the con-

tributions of the *individuals* to each PC. This matrix, one of the products of XLSTAT output, indicates the PC to which each individual is the strongest contributor. By writing a simple code in MS Excel, this PC is determined for each individual, which then becomes the class to which the individual is assigned. An inventory of classes of individuals with geographic coordinates is then plotted on a topographical map of Colorado, illustrated in Figure 7.14, for the visual evaluation of the created classes.

It can clearly be seen from Figure 7.14 that there is great dispersion in the geographic locations of all of the classes. The only exception is class P2 which primarily is contained within the portion of the state to the west of the Front Range. In addition to crossing latitude and longitude boundaries, as observed for the multivariate clustering methods, the results of the PCA-based classes appear to cross elevation and even climatic boundaries as well. No class appears to exclusively represent regions of similar topography (longitude, elevation), climate (alpine vs. sub-alpine vs. prairie) or typical snowfall. This results in the significant spatial overlap between classes across the state. From a practical standpoint, it would be impossible to construct reasonable ground snow load isolines for the class structure depicted in Figure 7.14.

Due to the great spatial distribution of classes and the illogical assignment of stations to classes, the PCA-based clustering method is ruled out as a viable clustering technique. Therefore, this method will not be considered further. However, the assessment of this method is valuable to the regionalization of the SNODAS weather stations; its inefficiency supports the usage of the established multivariate clustering techniques such as k-means and AHC.

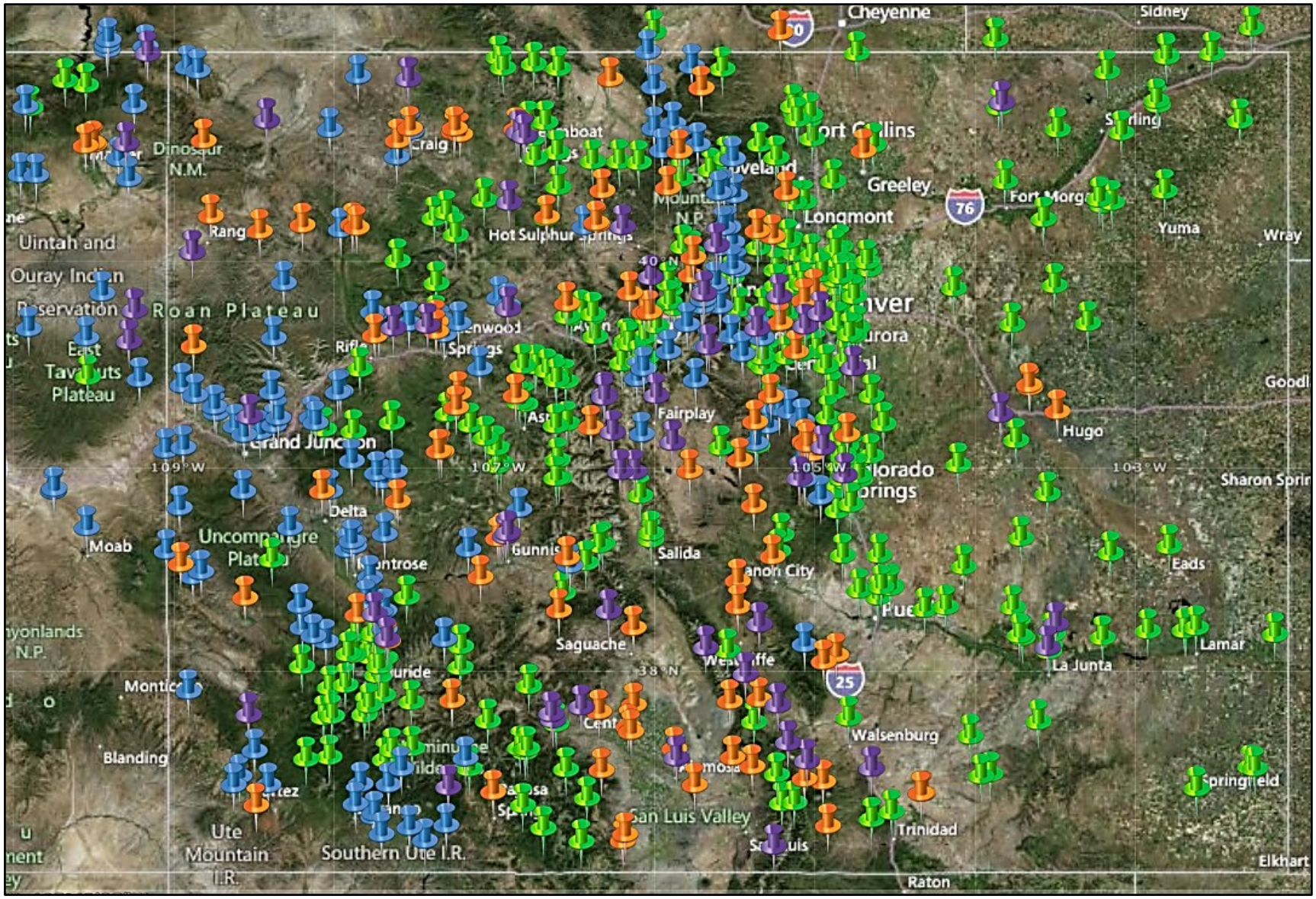

Figure 7.14: Topographical Map of Classes Created by Final PCA-Based Clustering Plotted With ArcGIS. (Green – P1, Blue – P2, Orange – P3, Purple – P4)

7.6.4 Results of Hybrid Clustering Analysis: K-means Followed by AHC

Hierarchical and partitional clustering techniques have been employed individually thus far to regionalize the SNODAS stations. While either of these methods is useful and effective on its own, a hybrid clustering method combines the strengths of both while minimizing their deficiencies. For instance, agglomerative hierarchical clustering methods suffer from the lack of a global objective function; at each step the algorithm merges the pair of classes that best suits local circumstances (Tufféry 2011). Conversely, the k-means clustering method evaluates memberships of the entire population at each iteration, but requires the quantity of classes and their centers beforehand. Also, it cannot effectively handle non-globular classes or those of varying densities (Tan, Steinback and Kumar 2005). The primary concern in applying one of these methods exclusively is that the natural structure of the data has not been ascertained. Both multivariate clustering methods have produced adequate clustering results individually, so neither one can be eliminated yet. Therefore, a hybrid clustering analysis is investigated, incorporating the strengths of both partitional and hierarchical methods in a step-wise manner.

The hybrid analysis process can be summarized in the following list of steps.

(1) Perform a preliminary AHC on entire dataset to obtain number of classes, k, and their centroids.
(2) Perform a k-means clustering using the inputs determined in the first step.
(3) Perform successive AHC analyses on each of the k classes; truncate the analyses at the optimal branch, per Ward's method.

Each phase of the hybrid analysis proceeds using the procedures for AHC and k-means analyses established in Chapters 7.6.1 and 7.6.2. The results of the hybrid analysis are presented in Table 7.10, which lists the clustering trials performed; input variables for sets (a), (b), and (c);

the total number of resulting classes for each; and measures of clustering quality (R^2 and *pseudo F* statistic).

Table 7.10: Results of the Hybrid Clustering Trials

Hybrid Trial	Clustering (i) [3]			Clustering (ii) [5a]			Clustering (iii) [5b]			No. of Classes
	Input (a)	R^2	*F**	Input (b)	R^2	*F**	Input (C)	R^2	*F**	
1	E, SD, SWE	0.608	181	BA, LG	0.838	602	BA, LG, SD	0.617	188	6
2	E, SD, SWE	0.608	226	BA, LG, SD	0.842	777	AS, CV	0.271	54	5
3	**E, SD, SWE**	**0.608**	**226**	**BA, LG, SWE**	**0.851**	**832**	**BA, LG**	**0.728**	**390**	**5**

AS = aspect, BA = basin HUC, CV = curvature, E = elevation, LG = longitude,
SD = snow depth, SL = slope, SWE = snow water equivalent
*F** = *pseudo-F* statistic, R^2 = weighted average, between-class SSE
Note: red numbers in brackets denote flowchart elements from Figure 7.8.

Table 7.10 demonstrates the progress of the hybrid analyses through all of the trials as the optimal clustering variables were isolated. The final hybrid clustering is highlighted in bold as trial 3. Overall, the statistical measures of quality for this clustering indicate that a good level of between-class variance is being attained, signifying that the hybrid analysis is successful.

In comparison to k-means and AHC, the hybrid analysis appears to have measures of quality that are slightly less than either, for clustering operation (i). However, the more important clustering operations (ii) and (iii) produce better classes. In terms of the *pseudo-F* statistic, the hybrid analysis (*F** = 832) scored better than either AHC (*F** = 735) or k-means (*F** = 552) for clustering operation (ii). However, for clustering operation (iii), the hybrid analysis scored less than AHC, but better than k-means. Recall that the *pseudo-F* statistic measures the separation between all of the clusters; it provides better contrast since its range of values is higher than R^2. These findings demonstrate that, statistically, the hybrid clustering analysis is one of the top performers of all of the methods considered thus far.

The class memberships for the hybrid analysis are plotted on a topographical map of Colorado, illustrated in Figure 7.15. It is evident that this method produces a well discretized arrangement of classes. Aside from aesthetics, several desirable qualities are noted about the spatial arrangement of classes.

First, the low-elevation and prairie SNODAS stations of class P3, denoted by orange pins, are well-separated from all other stations. They are even separated from the stations west of the Great Divide that are relatively similar in elevation. Recall that the k-means and PCA-based methods mixed these clearly separate climatic regions. The AHC method further clustered the low-elevation stations into two classes, though this action seemed unfounded.

Secondly, the intermediate region between low-elevation plains and high-elevation mountain peaks is distinguished by the hybrid analysis. The only other clustering method to appropriately separate this region into its own class is AHC. However, this transition class produced by AHC in Figure 7.10 is not as well-defined nor is it as organized as the class produced here. This transition region is believed to experience significantly greater snowfall than the plains but not the seasonal accumulation of snowpack like in the mountains (Doesken 2012). It is therefore a critical class that should be differentiated in the regionalization effort.

The hybrid analysis created the most uniform arrangement of classes in the mountains to the west of the Great Divide of all the clustering methods considered. Classes P2 and P4 (blue and purple pins, respectively) do not have excessive overlap except in minor cases where the alpine mountain stations of P2 are adjacent to sub-alpine stations of P4. Lastly, class P5 which represents the high desert of the San Luis Valley in the southern portion of the state was distinguished from other classes. This region is known historically to experience quite dry conditions year-round, and is in a precipitation shadow which makes it a rather unique region in itself

(Harris 2013). The hybrid analysis successfully captured this anomaly. The results of the hybrid clustering analysis, including the preliminary AHC dendrogram, k-means analysis results tables, and final AHC dendrograms are available in Appendix M.

With the above qualities in mind, the hybrid analysis outperforms the other clustering methods from a holistic perspective. It achieves very good statistical measures of clustering quality and produces classes that are well-differentiated and logically organized when plotted on a topographical map. This facilitates the creation of a ground snow load map. The spatial interpolation analysis to create snow load isolines, discussed in Chapter 8.0 would be the easiest for this method. After examining Figure 7.15 it is clear that there are few places where that analysis could err due to extensive overlap or mixing of many classes. Also, the class formation produced by the hybrid analysis would likely *not* result in a situation where two stations with extremely different elevations or snow loads are adjacent to one another. This situation, encountered in the ground snow load map production for Colorado by SEAC, forced the interpolation between two stations that likely overestimated the lower elevation station (SEAC 2007).

7.7 Developing Ground Snow Depth-Load Relationships for Each Class

In addition to the statistical and visual assessments of each clustering method, an analysis of the modeled snow load and snow depth data is performed. Specifically, annual maxima ground snow load data is derived from modeled SWE using Eq. (9), and is acquired along with the ground snow depth data from SNODAS output for every station. This output data from the clustered stations is plotted and a linear regression of the snow depths and snow loads is performed. The method of least squares is used to produce model equations, which are plotted with the data. The goodness-of-fit of each class is evaluated using the coefficient of determination, which is presented along with the model regression equation. By comparing these plots across

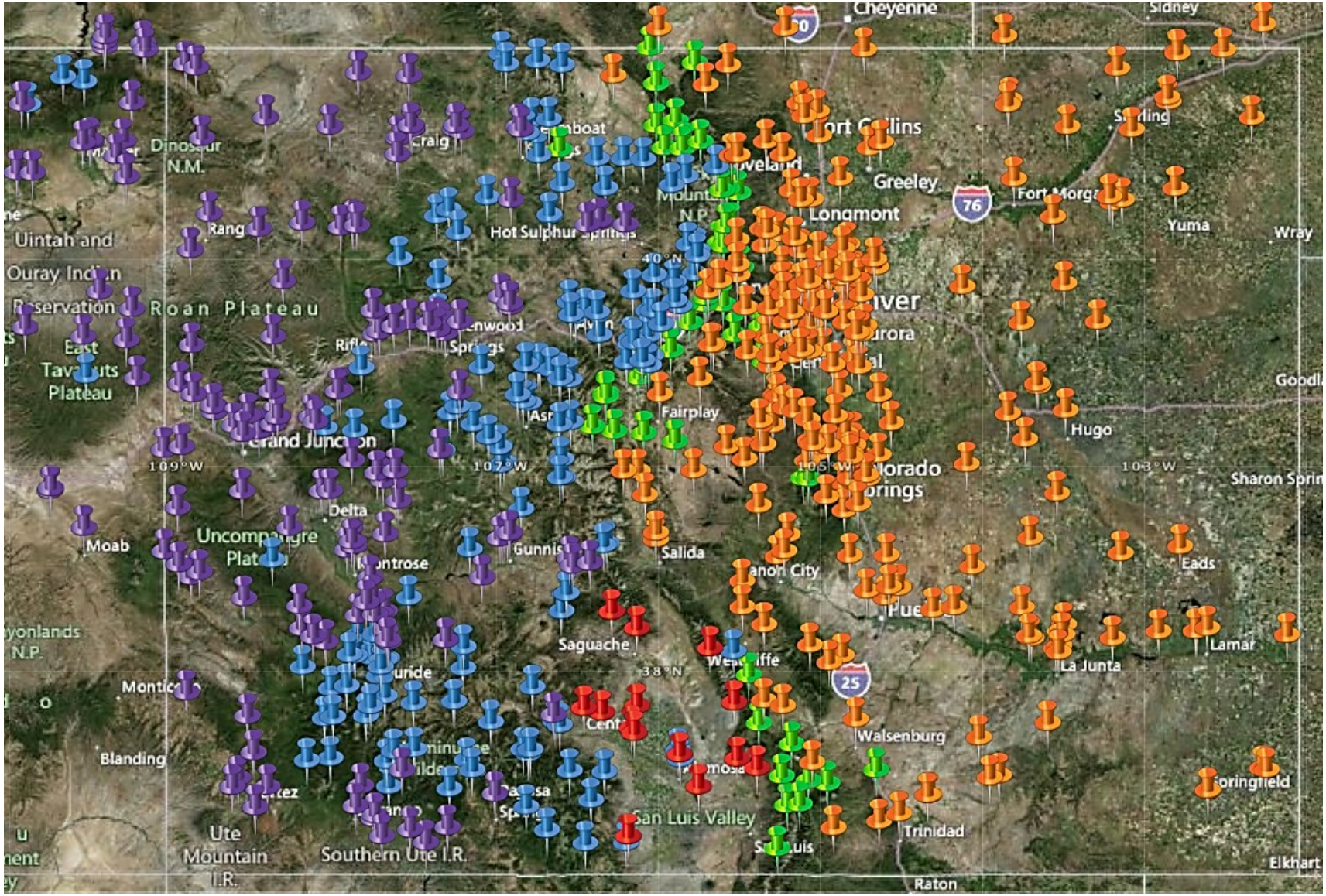

Figure 7.15: Topographical Map of Classes Created by Final Hybrid Clustering Plotted With ArcGIS. (Green – P1, Blue – P2, Orange – P3, Purple – P4, Red – P5)

all four methods (AHC only, k-means only, PCA-based, and hybrid), an additional measure of clustering efficacy can be used for evaluation. The ideal method for regionalization of SNODAS stations would not only produce statistically robust and practical clustering results, as determined in Chapter 7.6, but also distinct and closely correlated load vs. depth relationships for each class. The absence of visual outliers in each class and a high measure of correlation coefficient for the regression equations are desired. The regression equations for the SNODAS data assume the power form similar to the ASCE 7-10 equation, developed by Tobiasson and Geatorex (1996); in most cases this form resulted in the best fit for the data (compared to linear, polynomial, or other types of relationships).

For comparison, in every plot, the bi-linear RMCD and exponential ASCE 7-10 density equations are plotted for reference. Since these equations plot snow depths and snow loads at a 50-year recurrence interval (compared to the nine years of SNODAS output data), they are only plotted to provide a reference line for comparing different methods, not for direct comparison to the SNODAS data.

Due to the fact that each of these plots contains 588 individual data points and at least four different classes with separate regression equations, there is considerable obscurity when all of the data is plotted together. For clarity, the original data points are removed from the analysis plots presented in the body of this section. These plots for the AHC, k-means, PCA-based, and hybrid clustering methods are presented in Figure 7.16-Figure 7.19. All of the best-fit regression lines have been extended through 190 inches on the x-axis only for comparison purposes. Magnified plots for each method with all of the data points are available in Appendices N through Q. For each clustering method, two of these magnified plots are made; in each, different subgroups of data points are made partially transparent to improve clarity.

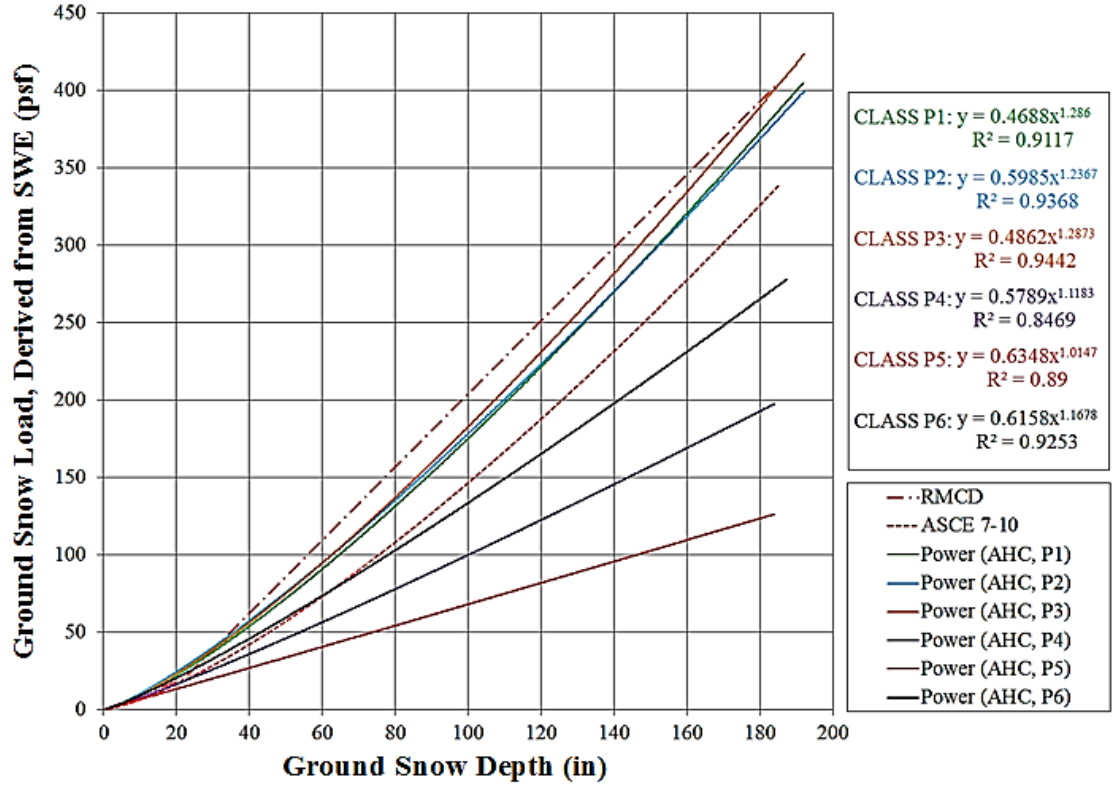

Figure 7.16:Regression of Snow Load on Snow Depth from AHC Clustering Method

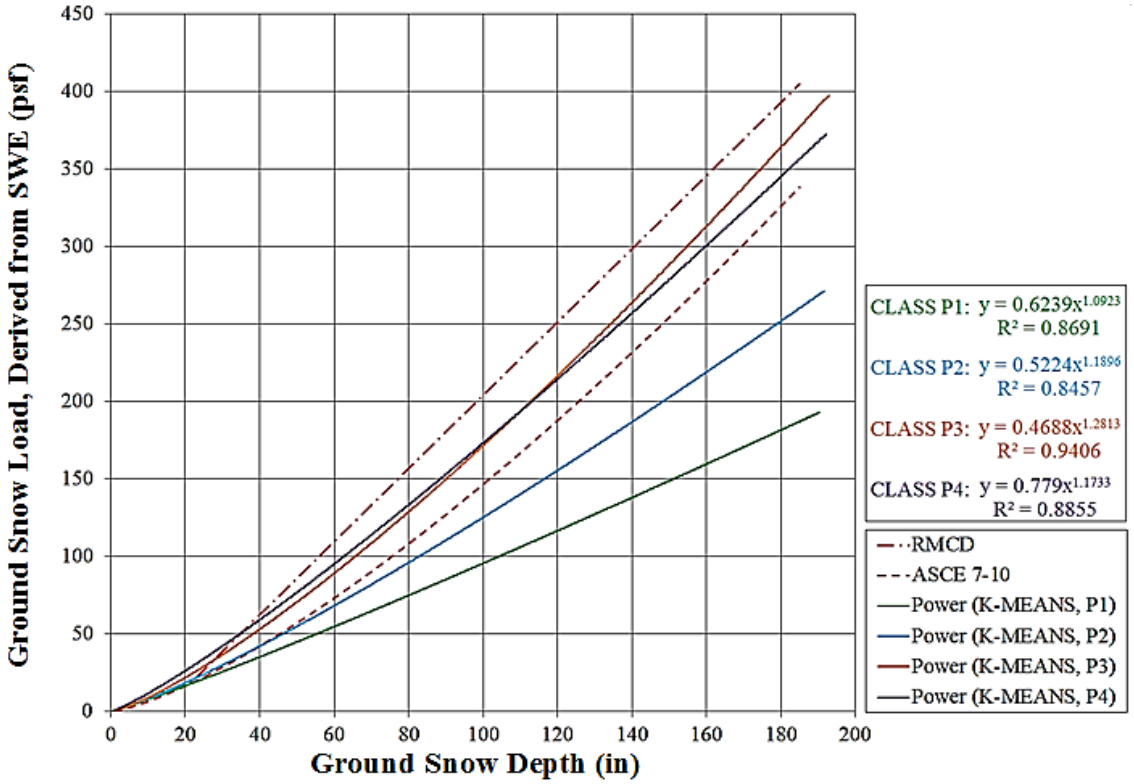

Figure 7.17: Regression of Snow Load on Snow Depth from k-means Clustering Method

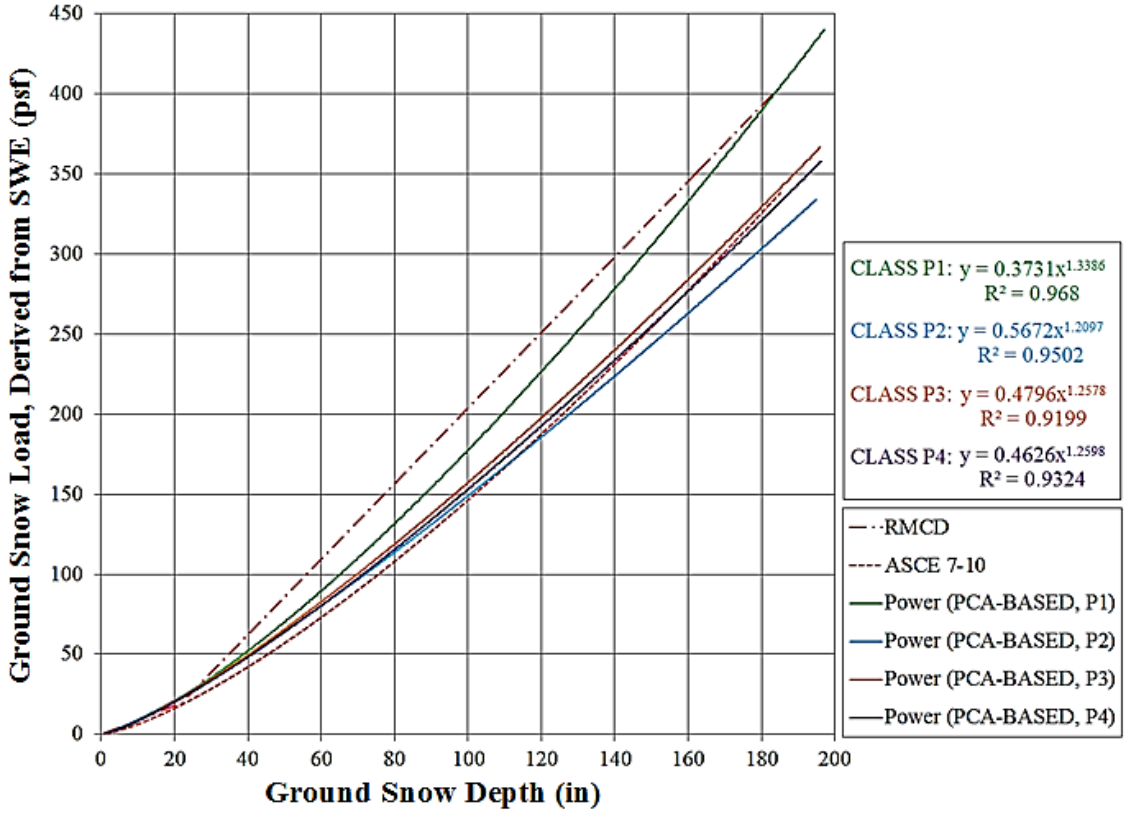

Figure 7.18: Regression of Snow Load on Snow Depth from PCA-Based Clustering

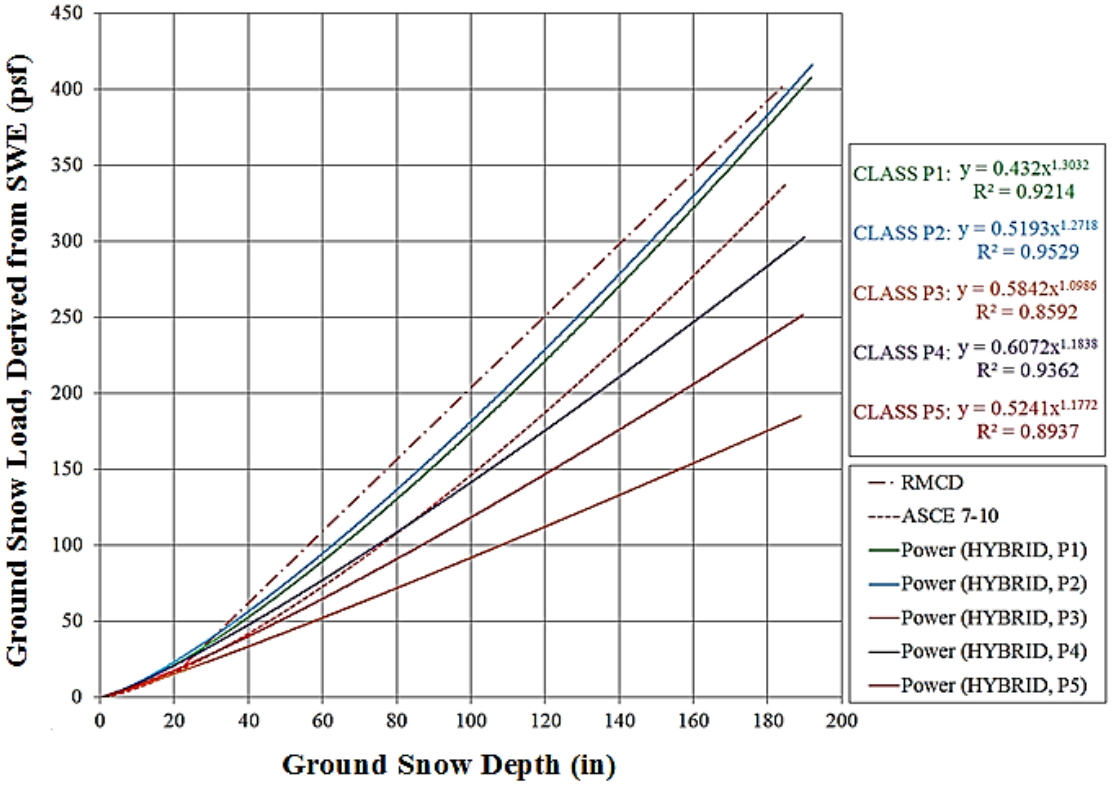

Figure 7.19: Regression of Snow Load on Snow Depth from Hybrid Clustering Method

Figure 7.16-Figure 7.19 show that each method generally produces good results in terms of the regression equations, with R^2 values generally greater than 0.84, but mostly above 0.90. Looking more closely between the methods, it is apparent that the PCA-based clustering method produces regression models that best fit the data within each class, with values between 0.92 and 0.97. However, from the results of Chapter 7.6.3 it is clear that this method is neither efficient from a clustering perspective nor practical from the perspective of producing a ground snow load map. Aside from the PCA-based method, the next best methods as evaluated from the regression analysis are the AHC-only and hybrid clustering methods. For these two methods, the majority of the classes have regression models that are well correlated to the data ($R^2 \geq 0.92$) with only a few that are less correlated ($R^2 \geq 0.85$). However, the hybrid method regression equations for each class are better differentiated (their regression equations do not overlap as much); this method also has one fewer class than the AHC-only method, resulting in a less complicated model. It is interesting to note that the regression models from these two methods, and in general from all of the methods, produce a better fit for the high-elevation stations in the Front Range and Rocky Mountain regions (*e.g.* classes whose model regression equations fall between the ASCE 7 and RMCD equations). Conversely, the classes that contained a mixture of low to mid-elevation stations from the plains and regions west of the Great Divide do not have as highly-correlated model equations.

To summarize the comparison between individual methods, all of the plots show some outliers (data points far from the majority in their class in Appendices N through Q) as well as overlap between classes. The AHC-only method, however, exhibits an extensive amount of overlap to the point where there is little differentiation between classes, particularly for the high-elevation classes. The k-means and PCA-based analysis plots show good separation between

classes representing high-elevation stations noted in Appendices O and P, respectively. However, k-means regression models do not show a high degree of correlation to the data and the PCA-based method has already been eliminated as a viable choice. The method that produces strong snow depth-load relationships throughout all classes consistently is the hybrid method, whose plots are illustrated in Appendix Q. The hybrid clustering technique is the method of choice based on the results of the regression analysis. However, one refinement that can be made to the results would be to merge classes P1 and P2 into one due to their similarities revealed by the regression analysis.

7.8 Comparison of SNODAS Regression Models to ASCE and RMCD Ground Snow Depth-Load Equations

As mentioned, no *direct* comparison can be made between the SODAS data and either of the two aforementioned density equations due to the disparity in recurrence intervals.[12] Bearing this in mind, the model equations for at least two of the classes in Figure 7.16-Figure 7.19 predict ground snow loads in excess of those predicted by the ASCE density equation and only slightly less than those predicted by the RMCD density equation for the same ground snow depth. These two classes consistently represent high-elevation mountainous regions where it is expected that measured ground snow loads should exceed those predicted by ASCE, but not RMCD.[13] Since only nine years of modeled output is available from SNODAS, it is impossible to extrapolate 50-year ground snow loads from the data for comparison to the RMCD. However, considering that the SNODAS model has *not* experienced many extreme events, it is likely that the current re-

[12] Plotted SNODAS data are annual maxima for nine years of modeled output compared to the RMCD and ASCE 7 equations which are representative of 50-year ground snow depths and loads.

[13] The ASCE 7-10 ground snow load map only includes statistical data from low-elevation NWS offices. As mentioned previously, the high mountain stations observe higher ground snow densities and loads due to the accumulation of snow over the winter season.

gression equations are rather under conservative. Extreme snow events result in significant accumulation of snow over a short period of time (generally a few days), which increases compaction due to self weight, as discussed in Chapter 4.2.

As an example, the mountainous SNOTEL station BURC2 (geographically located by Figure 3.3) experienced its greatest modeled SWE and snow depth of all modeled years (2003-2012) during the 2010-2011 water year. This particular winter season is well known for having brought nearly three feet of snowfall to the plains and several more to the mountains in late spring. The maximum modeled SWE and snow depth at station BURC2 for the 2010-2011 water year was 23.5 inches of water and 73.2 inches of snow, respectively (occurring on May 4). For reference, the average annual maximum SWE and snow depth *all* modeled water years at station BURC2 was 16.3 inches of water and 53.5 inches of snow depth, respectively. This extreme snow season represents nearly 150% of the average SWE and 140% of the average ground snow depth. It is likely that this single data point from station BURC2 for this extreme event greatly influenced the regression model for the class to which it was assigned.

As additional extreme winter storm events are captured by the model, all of the statistical parameters including the regression equations in Figure 7.16-Figure 7.19 will increase considerably. The extent of such increases is unknown but it can be argued that once extreme events are captured by the model, the snow depth-load relationships for the two leading classes (P1 and P2) of the hybrid clustering method will predict greater snow loads than the RMCD snow depth-load equation currently used in many western states.[14]

[14] Refer to Table 1.2 for states that currently employ the RMCD equation to develop ground snow loads.

By examining the plots in Appendices N through Q, it is obvious that the majority of the data points in low-elevation classes plot well above both the ASCE 7-10 and RMCD density equations. This is problematic since both of these density relationships were developed for these types of low-elevation stations with relatively normal snowfall events (*i.e.* no significant annual accumulation or extreme localized climatic effects). Furthermore, the future impact of extreme events mentioned above will only increase the disparity between the dataset and these density relationships.

7.9 Selection of Optimal Multivariate Clustering Method

The selection of the optimal multivariate clustering method is based on a holistic approach that seeks the best clustering method from assessing scores in the following categories.

(1) Examination of statistical measures of quality for overall clustering efficacy.
(2) Visual assessment of the arrangement of mapped classes for utility in a ground snow load map.
(3) Evaluation of the linear regression of the ground snow depth-load relationship for each class.

These three criteria evaluate various aspects of the clustering analyses, together describing the ability of each method to create well-separated, homogenous classes with closely correlated ground snow depth-load relationships. The final chosen method must also produce results that facilitate the construction of a ground snow load map.

To compare each method against one another, a qualitative scoring rubric is created and scores are assigned to each method for each of the three aforementioned categories. To simplify comparisons, a matrix of scores is constructed that will facilitate the final selection of the optimal multivariate clustering method, which is presented in Table 7.11. Individual scores for each category in this matrix are one of three possible values: a check denotes satisfactory results, a plus

denotes exemplary results, and a minus denotes poor results. The scores are assigned subjectively, however various categories rely heavily on statistical results from Chapter 7.6.

Table 7.11: Scoring Matrix for Evaluating Clustering Methods

Clustering Method	Statistical Measures	Visual Assessment	Regression
AHC-only	+	✓	✓
k-means	✓	✓	✓
PCA-based	N/A	–	+
Hybrid	✓	+	+

As Table 7.11 indicates, with the exception of the PCA-based method which is not considered further as a viable method, the scores are somewhat close among the other clustering methods. AHC ranks the best in the statistical measures category, although the R^2 and *pseudo-F* scores are very close between AHC and the hybrid methods. The hybrid is the clear choice in the visual assessment of the mapped classes. No other clustering method produces as homogenous classes nor clearly distinguishes the Front Range and San Luis Valley regions as does the hybrid method. Finally, the hybrid and PCA-based methods are both superior in terms of producing robust, well-correlated regression models for ground snow depth-load relationships. Since the PCA-based method has been eliminated, the hybrid method therefore ranks the highest in this category. The plotted data points for each class produced by the hybrid method are better-separated and there are fewer cases of overlapping model equations on the regression plots compared to the AHC method, the next highest scoring method in this category. The k-means method produced only satisfactory regression models when compared to the other methods that had model correlation coefficients well above 0.9 for most classes.

The ideal candidate method for regionalization of weather stations throughout Colorado possesses strengths in all of the above categories listed in Table 7.11. The AHC and k-means clustering techniques are good methods individually; however, it is clear that their strengths are highlighted and their weaknesses minimized by combining them into the hybrid method. The hybrid analysis therefore emerges as the premier clustering method. It has consistently performed well in *all* aspects of evaluation. It is therefore the proposed method for regionalization of weather stations.

7.10 Statistical Analysis of Ground Snow Depth Dataset

7.10.1 Preparation of CO-OP Station Dataset

Prior to developing ground snow loads at stations, the CO-OP depth data must first be prepared and 50-year ground snow depths be extrapolated. At that point, a ground snow load can be determined at each station.

Recall from Chapter 6.2 that the CO-OP station history datasets for all of the stations within Colorado were obtained from the GHCN database through the noted NOAA website. The datasets have undergone an extensive cleaning procedure to remove duplicate stations, entries with missing or invalid entries, *etc*. At this point, a single file now contains the entries of the remaining 492 stations, with monthly maximum values of ground snow depth. At this point, the historical records of the remaining stations vary from a single year to 64 years. The CO-OP station dataset must be truncated into an *annual* series maximum format and some minimum length of record must be established to eliminate stations with too sort a record. Within the hydrological community, where precipitation modeling and flood forecasting have necessitated an understanding of the proper sample size for extreme value prediction, a rule of thumb is to at least have 20-30 years of data (Doesken 2012, Balaji 2012). This window comes from recommenda-

tions from experts in the fields of snow climatology[15] and hydrology, specifically related to precipitation modeling and forecasting.[16] Furthermore, several studies evaluated by Takara and Stedinger (1994) compared various probability distribution fitting methods and the sample size required to achieve a good distribution fitting. A sample size of approximately 20 resulted in sufficient data for distribution fitting. Therefore, the dataset of CO-OP monthly maximum snow depth data is truncated to retain only those stations with at least 20 years of data. Furthermore, annual series data are extracted from the monthly series in preparation for the probability distribution fitting in Chapter 7.10.3. A list of the remaining 234 Colorado NWS CO-OP stations, with geographic locations, annual maximum ground snow depths, and years of data is available in Appendix R.

A topographical map of the hybrid clustering results, overlaid with the locations of the remaining 234 NWS CO-OP weather stations, is illustrated in Figure 7.20. This map is useful for assigning CO-OP stations to the nearest classes so that the appropriate ground snow depth-load equation can be applied to that CO-OP station's snow depth data.

Assignment of CO-OP stations to the classes produced by the hybrid clustering method should be done using GIS software such as ArcGIS, since the number of stations involved makes manual assignment too cumbersome. A rough sketch of class boundaries, drawn manually, creates an initial delineation of classes. An example of such an initial sketch, for the hybrid clustering method, is presented in Figure 7.21. These boundaries can be refined by considering stations on or close to the boundaries and adjusting the boundary lines accordingly.

---

[15] Dr. Doesken, the state climatologist, has extensively studied snowfall patterns at Colorado State University and is the founder of the CoCoRaHS cooperative precipitation survey program.

[16] Dr. Balaji is a hydrology professor at the University of Colorado at Boulder and has extensively studied flood frequency analysis and stream flow forecasting.

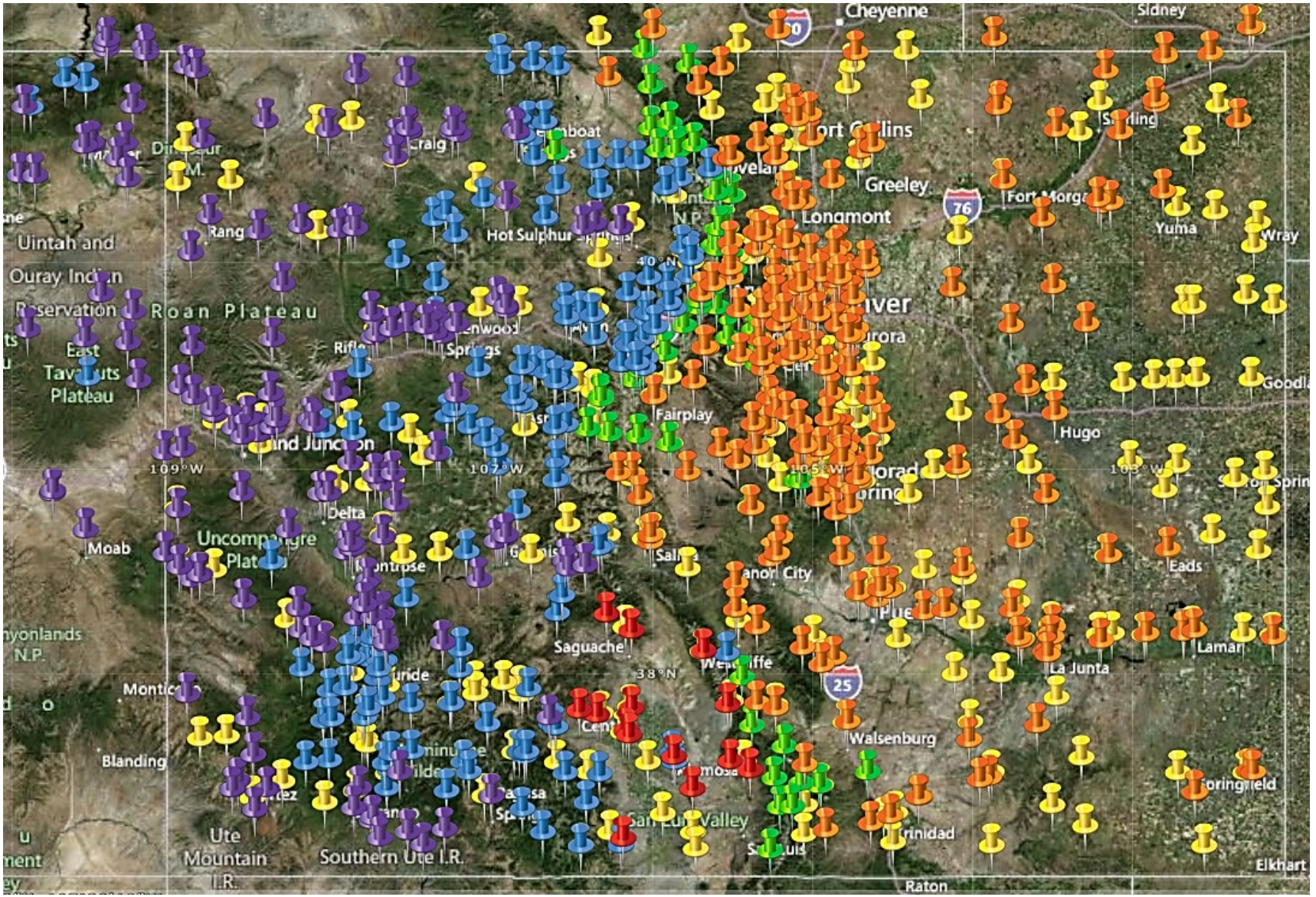

Figure 7.20: Topographical Map of Classes Similar to Figure 7.15 with Current NWS CO-OP Stations Superimposed. Map was produced by ArcGIS. (Yellow – CO-OP Stations)

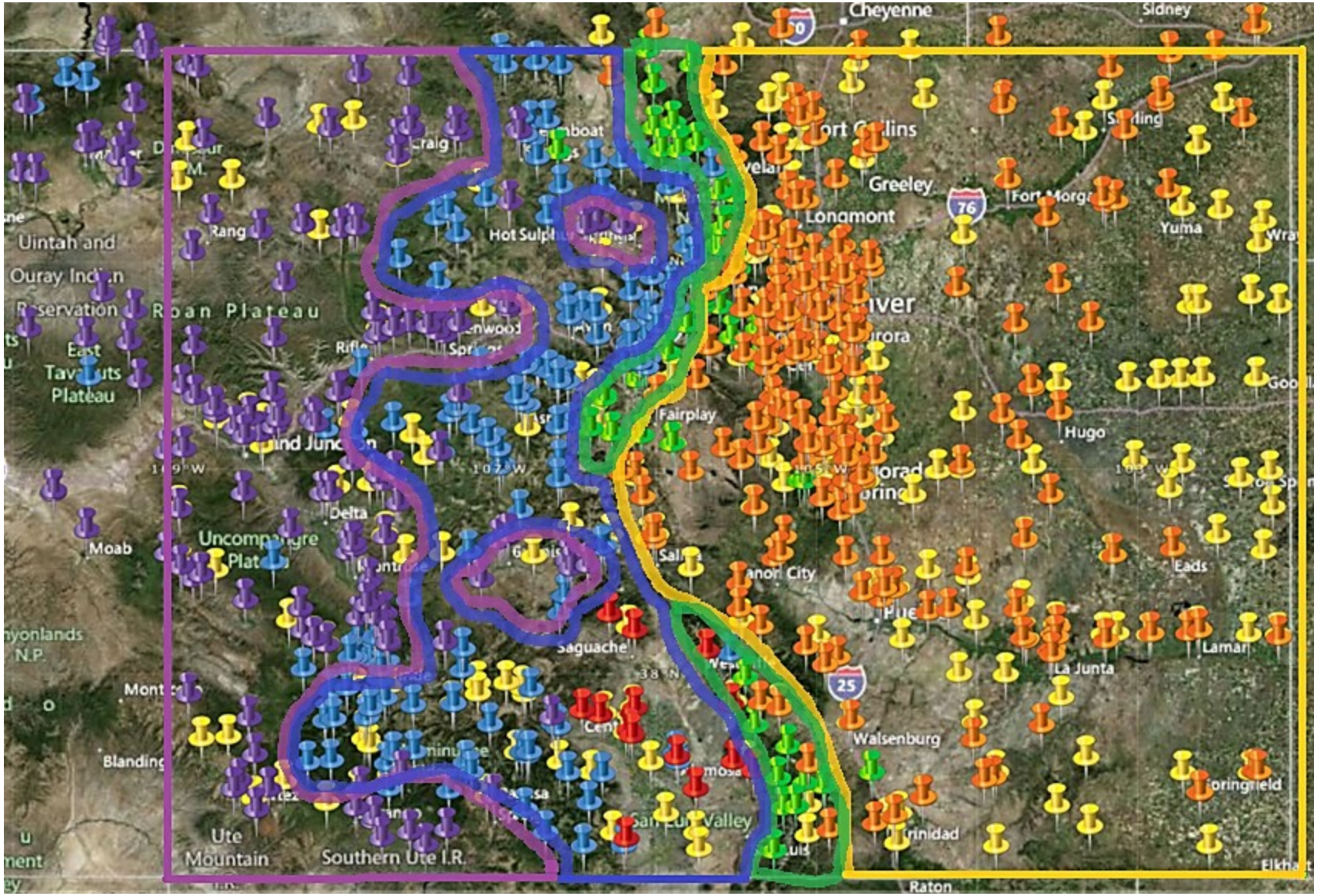

Figure 7.21: Topographical Map of Classes Similar to Figure 7.15 Annotated with Manually Drawn Class Boundaries.

Experience and professional judgment will dictate such refinements, including the possible re-assignment of individual stations manually or the exclusion of stations when drawing class boundaries. Once the boundaries are established, key points along these boundaries are located on the map and geographical coordinates approximated for input into ArcGIS. Several layers (one for each class) consisting of these key points connected by straight lines is then constructed in ArcGIS. Finally, using the extraction of points to layers command, the associated CO-OP stations are assigned a value in ArcGIS from 1 to *n* (in this case *n = 5*) depending on the class to which they are assigned.

7.10.2 Resolving Disparity between Annual Maximum Ground Snow Depth & Annual Maximum SWE

The difference in the pattern of snow depth accumulation between the high-elevation mountainous and on the low-elevation plains regions was discussed in Chapters 1.2 and further in Chapter 3.6. The accumulation of SWE exhibits a similar pattern. The typical triangular accumulation pattern, on a time-series plot of snow depth, in the mountains is illustrated in Figure 7.22 by the time-series output for SNODAS station BURC2 for the 2011-2012 water year.

In addition to the triangular accumulation/ablation pattern of snowfall in the mountains, Figure 7.22 illustrates that the maximum SWE occurs roughly half a month after the maximum snow depth. In fact, this pattern is exhibited by all of the mountainous SNODAS stations reviewed and is most likely due to the densification of the snowpack at maximum snow depth. The increasing amount of compaction due to the self-weight of the snowpack combined with surface ablation (from wind, transpiration, *etc*.) leads to diminished depth; the water content, however will steadily increase as the last spring winter storms pass through the mountains. Mountain snowpack can undergo drastic changes to its internal structure while retaining the majority of its water content until the rapid melt-off in late spring (Doesken 2012).

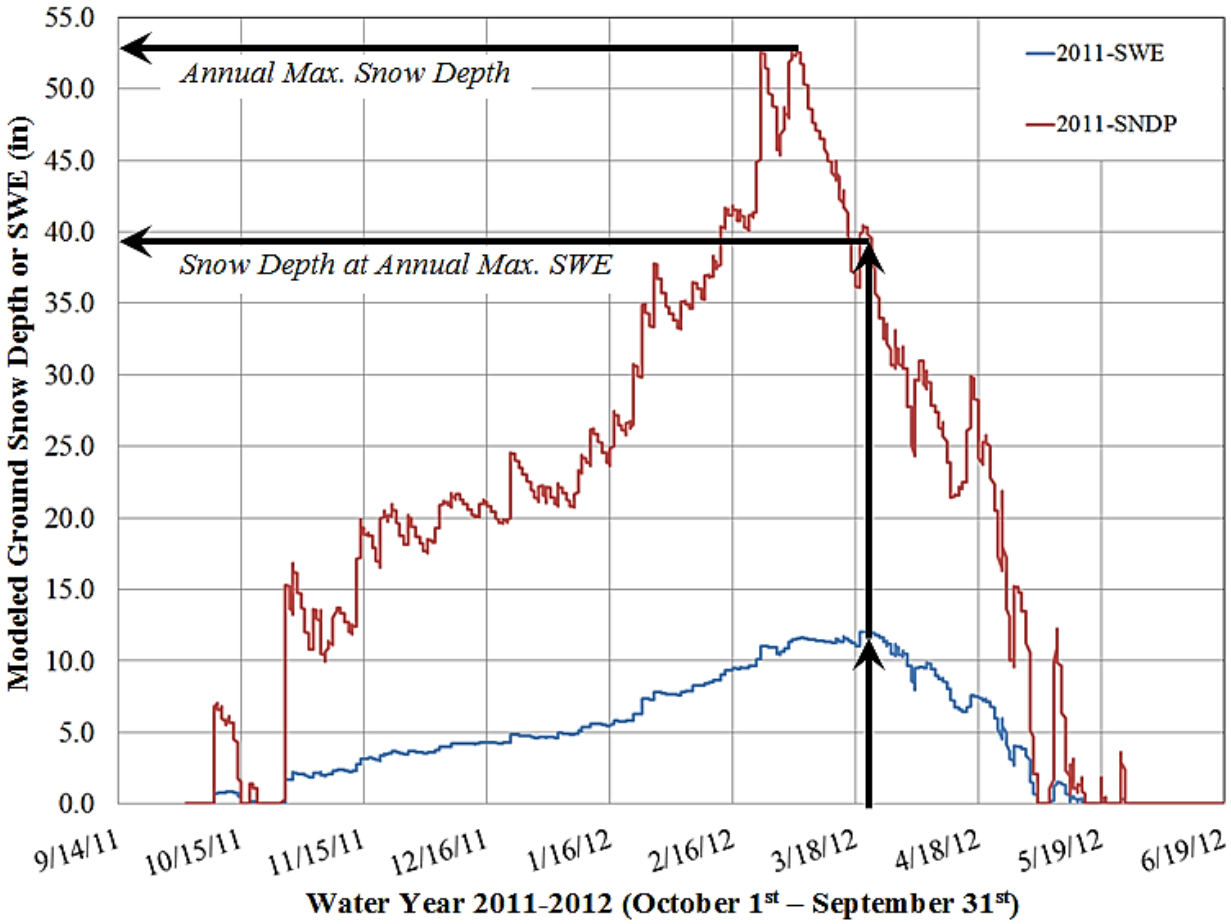

Figure 7.22: Time-Series Output of Ground Snow Depth and SWE for SNODAS Station BURC2 for WY 2011-2012.

Quite a different story is seen in the low-elevation SNODAS stations, either east or west of the Great Divide. Since there is nearly complete melting between winter snow storms the maximum SWE and maximum snow depth occur from the same storm, and are separated by just a few days. A typical pattern for low-elevation stations is illustrated by Figure 7.23.

This offset in the timing of the maximum snow depth and maximum SWE for *high-elevation* stations has significant implications to the statistical analysis. As apparent from Figure 7.22, the snow depth at maximum SWE is 39 inches of water while the maximum snow depth is 53 inches, more than a 30% increase. This significant disparity results in an issue between the ground snow depth-load equations developed in Chapter 7.7 (based on annual maximum SWE)

and the CO-OP dataset (based on annual maximum snow depth) on which the depth-load equations are to be applied. A snow depth-load model developed for the maximum SWE, coincident with a *lower* ground snow depth, would result in artificially inflated ground snow loads if this equation were to be applied to *higher* ground snow depths (the CO-OP annual maximums).

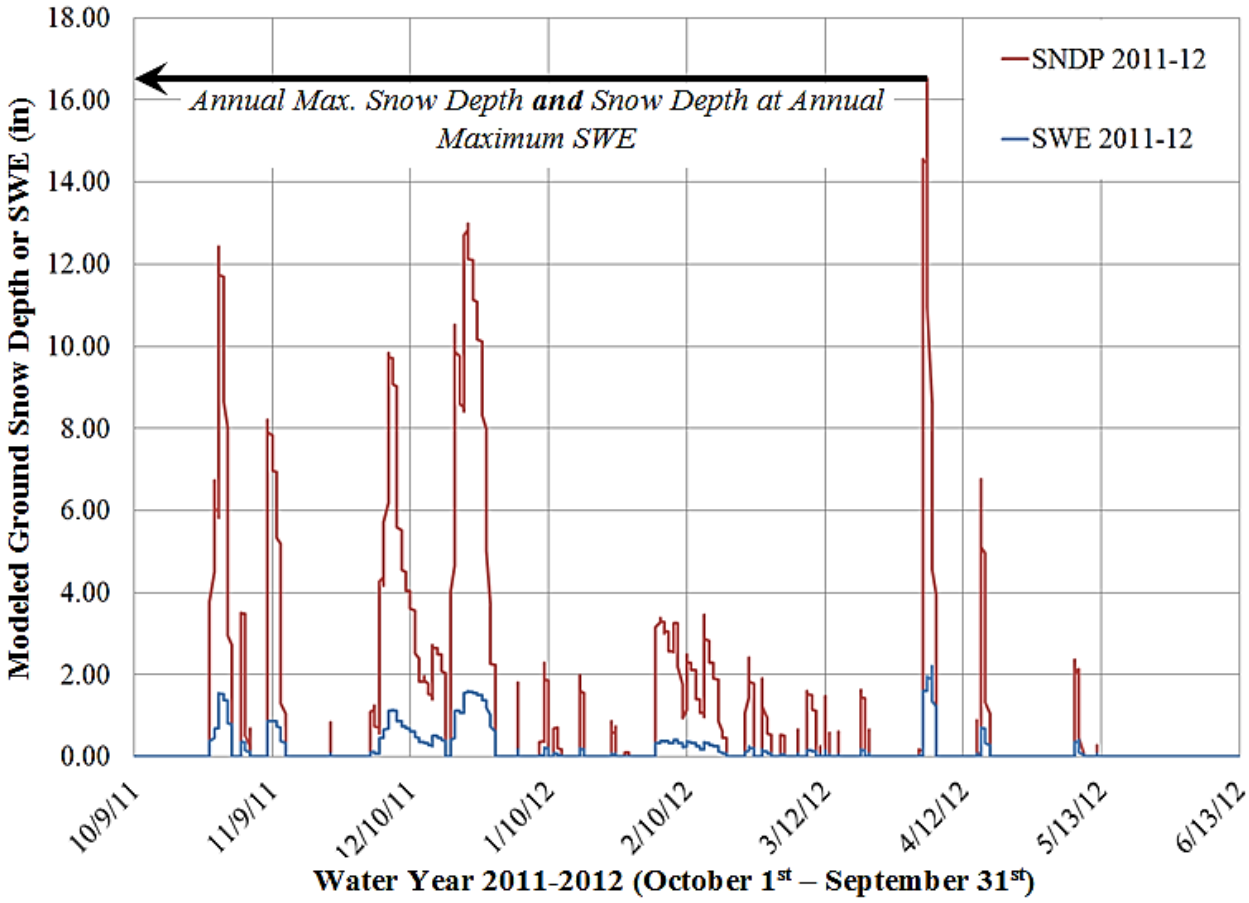

Figure 7.23: Time-Series Output of Ground Snow Depth and SWE for SNODAS Station AGRC2 for WY 2011-2012.

To correct for this inconsistency, a snow depth factor (SF) is computed from the modeled output of each of the 588 SNODAS stations. This factor, from item (6) in Table 7.1, is a ratio of the modeled snow depth at the date of maximum SWE to the annual maximum modeled snow depth. This factor is usually considerably less than unity for the mountainous stations and close to unity for the lower-elevation stations. This factor is to be applied to adjust the GHCN historical record of CO-OP annual maximum snow depths so that the snow depth used in the statistical

analysis in the following section is representative of what it would be at the date of maximum snow water content. Since the locations of most of the CO-OP stations coincide with SNODAS stations, the SF factor for each CO-OP station simply must be matched with its corresponding SNODAS station. For other CO-OP stations, the nearest SNODAS station SF factor is used.

7.10.3 Probability Distribution Fitting & Extrapolation of 50-Year Ground Snow Depths

The snow depth dataset, now transformed to an annual series maximum format and factored down by SF to better represent the snow depth at the date of maximum water content, can be used to compute the snow depth which occurs on average every 50 years. This task correlates to flowchart activity [2a] from Figure 5.1. In order to extract such values, a probability distribution must first be selected. The statistical nature of this objective necessitates extreme value theory as the appropriate philosophy for selecting a probability distribution. Extreme value theory identifies several families of distributions from which to choose: Gumbel (Type I), Weibull (Type II) and Frechet (Type III).

The philosophy of the regionalization of the SNODAS stations in Chapters 7.6 through 7.9 continues to be applied here for the selection of appropriate probability density functions (PDF) to fit the depth or load data at a particular site. Therefore, for each class produced by the hybrid clustering method an appropriate PDF is fit to the data from all the sites belonging to the same class. Various extreme value PDFs exhibit considerable differences in the nature of the tails. Similarly, there are considerable differences in the magnitudes of the extreme value ground snow depths and loads for SNODAS stations within each class. Therefore, the selection of an optimal PDF for *each* class is justified.

Criteria for determining the domain of attraction of a parent distribution (*i.e.* the PDF that describes the snow depths or loads) are proposed here. In particular, an overview of this meth-

odology is presented, including distribution types, testing procedures, and evaluation for goodness-of-fit. Details of parameter estimation, distribution plotting, and the actual implementation of this methodology are omitted. In practice, this method would then be used at each site to determine and appropriate PDF. Since there are hundreds of stations per class and therefore potentially multiple PDFs that can represent that class, the PDF which represents a *majority* of the stations within a class should be used to represent the entire class. Due to the sizeable effort required to evaluate and fit PDFs to hundreds of CO-OP stations, the distribution fitting is not carried out here.

The first step in distribution fitting is to decide on an initial selection criterion to narrow down potential PDF candidates. Prevalent methods for determining the domain of attraction include the Pickands III method, the Galambos method, the curvature method, and a plotting method where the tails of the data sample are plotted on probability paper and the concavity is established (Castillo 1988). A more comprehensive and practical method is to set up a system to test a wide range of extreme value theory distributions using the actual data and then use test statistics to determine the one with the best fit. The latter method, implemented in the 2007 Ground Snow Load Report for Colorado produced by the Structural Engineers Association of Colorado, (SEAC 2007) is proposed here. This system facilitates reproducibility since all distributions are tested each time the analysis is performed.

The proposed method for testing distribution fit includes choosing viable candidate extreme value PDFs and setting up code in computational software such as MathCAD, where each distribution is successively applied to the dataset and evaluated using appropriate test statistics. The candidate PDFs proposed in this paper are listed in Table 7.12. They were specifically chosen since they collectively represent many types of extreme value distributions with different pa-

rameters. Their associated parameters, which are required to describe the shape, scale, and more importantly the tail of the distributions, are also listed.[17]

Table 7.12: Proposed Families of Probability Distributions and their Parameters to be Evaluated for Usage with Snow Depth Dataset (Bury 1999).

No.	Distribution Family	Distribution Form	Required Parameters
(1)	Normal Distribution	2-Parameter	mean, $\mu(x)$; st. dev., $\sigma(x)$
(2)	Lognormal Distribution	2-Parameter	mean, $\mu(x)$; st. dev., $\sigma(x)$
(3)	Gamma Distribution	3-Parameter	mean, $\mu(x)$; st. dev., $\sigma(x)$; shape, λ
(4)	Log-Gamma Distribution	3-Parameter	mean, $\mu(x)$; st. dev., $\sigma(x)$; shape, λ
(5)	Type II GEV (Frechet)	3-Parameter	st. dev., $\sigma(x)$; 2-shape, λ
(6)	Type I GEV (Gumbel)	2-Parameter	mean, $\mu(x)$; st. dev., $\sigma(x)$

Estimation of the above parameters of the probability density functions is required in order to construct each of the distributions listed in Table 7.12. There are various methods to estimate parameters of distributions, with the most common methods being the method of moments and method of maximum likelihood (Ang and Tang 1984). The method of moments involves estimation of the parameters of interest from the sample moments of the data; the number of sample moments required is the same as the number of unknown parameters. The method of maximum likelihood involves estimating the value of parameters such that the likelihood function is maximized and therefore the slope of the function is zero. The likelihood function defines the likelihood that the data observed came from the distribution with varying values of the unknown parameters; those parameters that maximize the likelihood function are the parameters that define the distribution (Ang and Tang 1984). The method of moments is appropriate where

[17] The primary distribution parameters are location, μ, scale, σ, skewness, γ_1, and kurtosis, γ_2 (skewness and kurtosis are collectively referred to as shape factors, λ). These parameters for the distributions are related to the moments of the data (Bury 1999).

a small sample of the data (n<100) is available. Each method, however, is to be applied for each of the distributions listed in Table 7.12.[18]

Once the parameters have been estimated, the distributions can be constructed and several test statistics can be evaluated in order to determine the quality of the fit to the given dataset. There are several test statistics commonly employed in extreme value engineering for testing distribution fit. The most reliable and robust is the *Anderson-Darling* statistic, although others such as the *Modified Kolmogorov-Smirnov* statistic, *Chi-square* statistic, and *von-Mises* criterion are also frequently used. The evaluation of several test statistics is critical since one or two may produce equal results or may not be valid in certain situations (*e.g.* the *Chi-square* is not appropriate when the data lacks normality) (Bury 1999).[19]

Now that that the distributions have been constructed and the test statistics evaluated, an optimal PDF is chosen for each class of stations produced by the hybrid clustering method. Each optimal distribution is then applied to the snow depth dataset from the CO-OP stations that reside within each class.[20] Finally, a 50-year ground snow depth is extrapolated from the CO-OP dataset, modified by Chapter 7.10.2, using the corresponding PDF.

The final step is to apply the appropriate ground snow depth-load relationship defined by the hybrid method in Chapters 7.7 and 7.9 to the 50-year CO-OP ground snow depths in order to obtain 50-year ground snow loads. However, it is critical to note that as of the writing of this paper, only nine years of SNODAS data are available and the ground snow depth-load relation-

---

[18] Refer to *Extreme Value Theory in Engineering* for a description of both parameter estimation methods, including a definition of the likelihood function (Castillo 1988).

[19] Refer to *Statistical Distributions in Engineering* for a definition of the various test statistics and their appropriate usage (Bury 1999).

[20] Note that each station within the class will be defined by the same PDF, but different distribution parameters that define the data at that station.

ships determined in Chapter 7.7 do not represent depths and loads with a recurrence interval of 50 years. Therefore, they cannot directly be used with the 50-year snow depths from the CO-OP stations yet. More years of output from the SNODAS snowpack model will be required before it can be used reliably in practice. Refer to Chapter 10.0 for a discussion of future work.

8.0 GEOSPATIAL INTERPOLATION OF GROUND SNOW LOADS

The methodology for creating a ground snow load map is a crucial deliverable produced by this investigation. This last portion of the investigation is represented by flowchart element [6] on Figure 5.1. Structural engineers and designers rely on such maps as a basis for roof snow load design calculations and structural layouts. The effort and resources expended in the analysis phase of this investigation would be irrelevant if the point ground snow loads could not be properly mapped in a manner that best represents actual ground snow loads everywhere. The main issue is the uncertainty of ground snow load values at unsampled locations (*i.e.* locations without a modeled SNODAS or CO-OP station data point). Another issue is the uneven spatial distribution of stations that results in most of the weather stations clustered near population centers of the state. Therefore, in order to ensure that ground snow loads are mapped so that they best represent the actual values, some type of spatial interpolation method must be found that can resolve the issues above by providing the following.

(1) Accurate spatial interpolation of ground snow loads at unsampled locations.
(2) A methodology to account for unevenly distributed data points.

GIS software that utilize a variety of geospatial interpolation methods have emerged within the last several years to improve the accuracy of interpolation of point values on a digital elevation model (DEM). Currently there are several different methods of varying complexities that benefit specific applications. These methods include Nearest Neighbor or Thiessen Polygon (NN), Inverse Distance Weighting (IDW), and Kriging (K) (Zhang and Srinivasan 2009). NN and IDW methods are forms of pure spatial interpolation while Kriging involves statistical methods. Since each methodology produces different results and possesses unique strengths for cer-

tain applications (social sciences, hydrology, engineering) they must all be evaluated for suitability to the interpolation of extreme value ground snow loads.

8.1 Nearest Neighbor (Thiessen Polygons) Method

The Nearest Neighbor interpolation method (also known as Thiessen Polygons) is a rather simple spatial interpolation method. Specifically it is a local, deterministic method that seeks to interpolate values of variables in a continuous field based on the nearest sampled values (Burrough and McDonnell 1998). It considers only local variability based on some neighborhood of sampled points, *N*, ultimately developing an absolute value of some desired, spatially varying variable, *z(x)*. The value of *N* is determined by the analyst. The NN method takes the concept of using neighboring sampled points (*i.e.* a moving window of neighbors) to the extreme by estimating values at unsampled points using *only* the single nearest data point. This concept is graphically illustrated in Figure 8.1 whereby the dots represent sampling locations, such as weather stations, and the dark lines forming polygons represent the influence area around each sampling point, where the value of z(u) is equal to the value at the nearest sampled point z(x).

Since the Thiessen NN method assumes that values of any variable do not vary within the polygon, it is impossible to gauge within-tile variance (Burrough and McDonnell 1998). Therefore, this method is impractical if an insufficient number of sampled points is available or if the distribution is such that there are very sparse sampling locations. As a result, the Thiessen NN method may often mask small-scale spatial variability. Nonetheless, this method is commonly

used to produce a variety of descriptive maps; also computing time to produce such maps is minimized due to the simplicity of the interpolation method. [21]

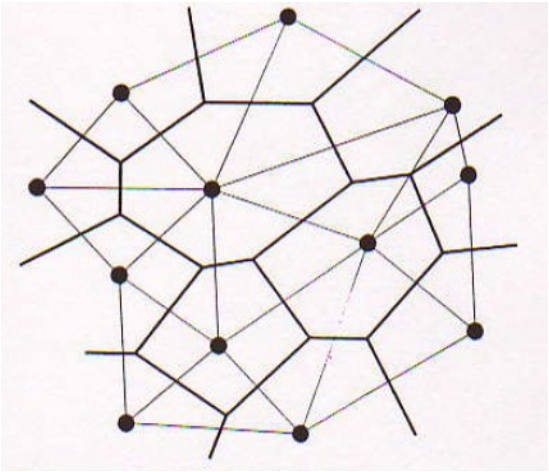

Figure 8.1: Thiessen Polygons for Randomly Distributed Sampling Points (Burrough and McDonnell 1998).

The simplicity of the Thiessen NN method is illustrated by its singular relationship for the value of the desired, unsampled variable *Z(u)* from the nearest sampled location *Z(x)* (the capital version *Z* refers to actual measured quantities of the variable).

$$Z(u) = Z(\mathbf{x}_i), \quad h_{ui} < h_{uj} \text{ for all i } \neq \text{j} \tag{21}$$

Eq. (21) simply states that the value of the desired, unsampled variable is equal to the value at the nearest sampled location, $Z(\mathbf{x}_i)$ when the separation distance between the unsampled location and *this* sampled location, h_{ui} is the least of the distances to any other sampled location, h_{uj} (Zhang and Srinivasan 2009).

A Nearest Neighbor variant, the Pycnophylactic Method was developed by Tobler to address the undesired effects of the NN method, specifically the tendency to produce sharp poly-

[21] The Thiessen Polygons NN method is often used to construct choropleth maps which illustrate quantities of variables, such as contaminant levels or population densities, delineated by colored or shaded regions on a map.

gons with little relief or smoothing (Zhang and Srinivasan 2009). A population density map, produced by Thiessen NN with Tobler's Pycnophylactic Method, would produce smooth, continuous surfaces at the edges of the polygons while preserving the mass or volume component (in this case the total population). This method relies on a 'mass preservation' condition that is imposed on each polygon to effectively smooth the boundaries between polygons while honoring the *sum* of the original quantities of the variables in each polygon. This condition fits a surface to the polygon regions and constrains its gradient to be flat near the interfaces with other polygons and maximized in the center, thereby smoothing values across the polygon.

This method, while efficient and simplistic, is specifically useful where exact values are not always required. Its applications include mapping population densities and contaminant levels using GIS for quick and rather rough estimates used in decision-making. Nearest Neighbor with the Tobler's Pycnophylactic Method tends to produce maximum and minimum values above and below actual measured quantities at sampled locations, and therefore is not an exact interpolator (Burrough and McDonnell 1998). This makes the Thiessen NN method rather unattractive for the purposes of this investigation.

8.2 Inverse Distance Weighting

An improvement on the Thiessen Polygon NN method is the inverse distance interpolation (IDW) method. This method takes into consideration more than just the single neighboring sampled location, weighting all sampled locations within some window of neighboring stations (Burrough and McDonnell 1998). This approach explicitly states that observations nearest to the unsampled location are to be weighted more heavily than observations farther away. The value of the variable at the unsampled location is computed as the weighted sum of the surrounding sampled locations:

$$Z(u) = \left(1 \Big/ \sum_{i=1}^{n} \lambda_{ui}\right) \times \sum_{i=1}^{n} \lambda_{ui} \cdot Z(\mathbf{x}_i), \qquad \text{where } \lambda_{ui} = \frac{1}{{h_{ui}}^{p}} \tag{22}$$

In Eq. (22), n and p refer to the neighborhood of sampled points considered around the unsampled location and the power associated to the distances of these sampled points, respectively (Zhang and Srinivasan 2009). The individual weights, λ_{ui} of each sampled location are computed based on the inverse weighting system.

The values of n and p must be chosen by the analyst rather arbitrarily and often times experience dictates these values. However, it is common to use inversely-squared distances, so p usually equals 2. As for the number of neighboring stations n, common practice is to use three or four stations, although there is no hard fast rule. This subjective selection of parameters speaks to a criticism of the IDW method and issues with its reproducibility. Other issues may arise with IDW, for instance, where solitary sampled data points exist with few nearby sampled locations. In this circumstance, the single sampled location value may appear to be an outlier or anomaly compared to the interpolated values around it, which may only be influenced by *other* sampled locations. This undesired effect, known as a 'duck-egg', is attributed to the analyst's choice of neighborhood size and is relatively easy to fix (Burrough and McDonnell 1998).

A recent research effort studied the effectiveness of various weighting interpolation methods, including IDW, in replacing missing rainfall gauge measurements throughout Kentucky (Teegavarapu and Bajaj 2008). This study used 15 rainfall gauges with data from 1971 to 2002 and compared IDW to other weighted distance models developed by Teegavarapu and Bajaj. Similar to the study performed by Murphy et al., cross-validation was employed in the assessment of the methods. The results of this study supported the conclusions drawn by Murphy et al. that IDW is inferior compared to other more complex spatial interpolation methods. None-

theless, IDW is very widely used in hydrology to estimate missing values between sampled locations, and is the premier method employed by the National Weather Service (Teegavarapu and Bajaj 2008).

8.3 Kriging

Kriging is a method of spatial interpolation in which moving, local weighted averages of the observed values in a neighborhood, *N* are used to predict values of a desired variable at unsampled locations (Oliver 2001). Unlike the preceding types of interpolation methods, Kriging is a type of geostatistical interpolation method that estimates the value of the desired variable based on an *unbiased descriptor* of the scale and pattern of spatial variation between sampling points. The other methods discussed thus far make assumptions regarding the pattern (*e.g.* Thiessen Polygons NN) or the scale (*e.g.* Inverse Distance Weighting) of variation. Kriging also provides an estimation of the quality of the prediction by way of an estimated variance for the predicted value. The Kriging interpolation equation has three main components, as depicted in its nominal form (Oliver 2001).

$$Z(u) = m(\mathbf{x}) + \epsilon'(\mathbf{x}) + \epsilon'' \tag{23}$$

In Eq. (23), $m(\mathbf{x})$ is a structural component describing the trend of Z whose form is determined by the specific type of Kriging chosen. Added to this are two terms, one of which describes the stochastic, spatially dependent residuals, $\epsilon'(\mathbf{x})$, the other accounting for the spatially independent background noise (or normally distributed random error), ϵ''. These last two terms take into consideration both short and long-range spatial variation.

Kriging is a generic term that embraces many different forms of geostatistical interpolation. Therefore the trend function, $m(\mathbf{x})$ from Eq. (23) can take on many forms, depending on the type of Kriging being performed: ordinary, simple, block, Kriging with local means, Kriging

with external drift, *etc*. (Burrough and McDonnell 1998). These numerous variants of Kriging will not be discussed in detail, but they all rely on the same universal fundamentals described below.

The aforementioned *unbiased descriptor* of the scale and pattern of the spatial variation, also referred to as the spatially dependent residual term $\epsilon'(\mathbf{x})$ in Eq. (23), is the semivariogram (Oliver 2001). As the most essential component of the Kriging formula, the semivariogram describes the degree of spatial correlation for a given region. It uniquely describes this spatial correlation between all of the sampling locations, **x**, at various "lag" distances from these sampling locations, h. The form of the semivariogram is defined as follows (Burrough and McDonnell 1998).

$$var\{Z(\mathbf{x}) - Z(\mathbf{x}+h)\} = \mathrm{E}[\{Z(\mathbf{x}) - Z(\mathbf{x}+h)\}^2] = 2 \cdot \gamma(h) \tag{24}$$

$$\gamma(h) = \left(\frac{1}{2n}\right) \times \sum_{i=1}^{n} \mathrm{E}[\{Z(\mathbf{x}) - Z(\mathbf{x}+h)\}^2] \tag{25}$$

In Eq. (25), E refers to expected value and n is the number of sampled locations, or stations. Conceptually, the semivariance term, $\gamma(h)$, in Eq. (25) is half of the variance of the differences between all possible values of the desired variable spaced a constant distance apart, h. By applying Eq. (25) successively for all sampled locations and incremental lag distances (inserting values of $Z(\mathbf{x})$ and $Z(\mathbf{x}+h)$), an ordered set of pairs (h,γ) is obtained. When plotted, these pairs comprise the experimental variogram, which is used to describe the spatial variation of the entire viewing area encompassing all sampled locations. A continuous mathematical model is then fit to these discrete, plotted pairs of data points in order to obtain a continuous variogram model. A few examples of experimental variograms are illustrated in Figure 8.2.

A few key components of any experimental variogram include the range, the nugget, and the sill. The range is the lag distance from any sampled location at which nearly all of the vari-

ance is explained; it is significant because it determines the critical number of sampled locations that contribute to the interpolation around any one station. The nugget is the residual semivariance at the y-intercept and is solely due to the background noise present in any spatially distributed dataset; it is accounted for by the rightmost term in Eq. (23). It is important to note the relative size of this nugget; if too large of a contribution is made by the nugget then there is too much background noise to even perform a spatial interpolation. The sill is the quantity of semivariance corresponding to a horizontal asymptote (if one exists) and can be thought of as nearly all of the total variance of the dataset.

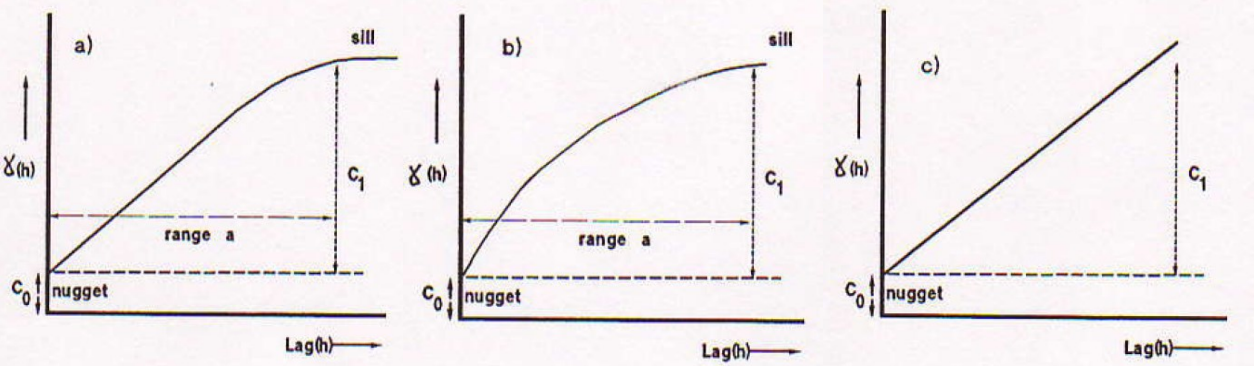

Figure 8.2: Examples of Common Types of Experimental Variograms. From Left to Right, Spherical, Exponential, and Linear (Burrough and McDonnell 1998).

With the known, fitted model of the experimental variogram, a Kriging analysis can be performed on any dataset given all of the values of $Z(\mathbf{x})$ and known distances h between all of the sampled locations. As mentioned, various forms of Kriging determine the exact form of the trend function, $m(\mathbf{x})$, and the manner by which weights are assigned to neighboring sampled locations. In general, however, the variogram is the key component that determines a) the size of the influence neighborhood, N, around a sampled location, and b) the semivariances between all of the sampled locations.

Kriging has been employed in numerous research efforts for various disciplines. Kriging is commonly employed in the field of hydrology where it has been shown to outperform many

other interpolation methods. For instance, Kriging was selected from an evaluation of various types of spatial interpolation methods, to represent long-term precipitation fields for the Luhoe tributary of the Yellow River in China (Zhang and Srinivasan 2009). That study evaluated several methods, such as IDW, Thiessen NN, and several variants of Kriging[22], using cross-validation to evaluate performance. Overall, Kriging produced the smallest coefficient of variation compared to the independent dataset (with the highest by the Thiessen NN method) and the least amount of absolute error (some 30% lower than the Thiessen NN method). The IDW method performed modestly but ultimately not much better than Thiessen NN.

Another research effort studied the distribution of water quality parameters in the Chesapeake Bay, the largest estuary in the United States extending from Maryland to Virginia, was studied using IDW as a potential method for interpolation (Murphy, Curriero and Ball 2010). Parameters including temperature, salinity, and dissolved oxygen were estimated using interpolation methods including IDW and Kriging. The authors found that IDW was intuitive and provided the benefits of efficiency and simplicity. Specifically, Murphy *et al.* (2010) collected data from May 1992 to July 1993 for a 40 km portion in the northern region of the Chesapeake Bay that contained numerous gauges. For two locations in this area (with corresponding depths of 2m and 8m, respectively), the authors removed the actual observed measurements of temperature, salinity, and dissolved oxygen and tested the efficacy of the two interpolation methods.[23] Once the validation between the actual and interpolated data was complete, the results showed that Kriging outperformed the IDW method overall. However, the validation results were rather

[22] The variants used in the study included Simple Kriging, Ordinary Kriging, Kriging with External Drift, and Kriging with Varying Local Means. For a description of the mechanics and specific applications of these variants, refer to Zhang and Srinivasan (2009).

[23] This method, referred to as cross-validation, has been used extensively in the field of hydrology for performance evaluation of various types of models (Zhang and Srinivasan 2009, Murphy, Curriero and Ball 2010).

close, with both methods presenting above a 0.98 correlation coefficient with the actual dataset. However, the RMSE/SD (root-mean-square error divided by the standard deviation) evaluation parameter was considerably lower for Kriging than for the IDW method (0.20 and 0.26, respectively), indicating better overall performance for Kriging.

8.4 Implementation of Optimal Geospatial Interpolation Method in the Production of a 50-Year Ground Snow Load Map

Though there exist other spatial interpolation methods not discussed in this paper, an accurate and suitable method is all that is needed for the purposes of this investigation. Of the interpolation methods discussed thus far, Kriging fits this criterion the best. First of all, it is the only geostatistical method introduced; it appropriately optimizes the number and weights of the neighboring sampled locations considered for each interpolation while providing unbiased estimates (Burrough and McDonnell 1998). Also, it considers all sources of spatial variation (*e.g.* local, regional, and background noise) in the values of such variables. The Kriging analysis itself provides estimates of errors, or variances, which can be used to assess individual interpolation operations (Oliver 2001). Kriging has been shown in numerous research studies to outperform other less complex interpolation techniques (Murphy, Curriero and Ball 2010, Zhang and Srinivasan 2009, Teegavarapu and Bajaj 2008). Lastly, Kriging is a common interpolation algorithm built into many GIS software platforms and therefore is readily available.

To implement Kriging with the proposed method in this paper for mapping ground snow loads all that are needed are the ground snow loads at each sampled location[24] (SNODAS and CO-OP stations), the geographical coordinates of these stations, and a GIS-based application

[24] These ground snow loads have been determined in accordance with Chapter 7.10.3. These snow loads, derived from SNODAS output, should only be implemented once there is sufficient modeled data from which to extrapolate a relationship between 50-year modeled snow depths and 50-year modeled snow loads.

such as ArcGIS. First, a terrain map of the area of interest is initiated in GIS with a digital elevation map overlaid, in order to provide elevation details. A raster file is then constructed within the GIS software using the latitudes and longitudes of each SNODAS station coupled with the corresponding 50-year ground snow load values determined in accordance with Chapter 7.10.3. A raster file converts a dataset composed of geographical locations and snow loads into a digitally encoded format recognizable by the GIS software. At this point, SNODAS stations are located geographically, each with a corresponding ground snow load value.

A Kriging analysis is then performed by the GIS software so that a continuous field of interpolated ground snow loads is computed for the terrain map. Once the analysis is complete, the GIS software can provide an extraction of values for any point(s) at any desired spatial distribution. The extraction is performed either by an extract to layer or extract to points command. For instance, a user can either construct a layer in the GIS software composed of a regularly-spaced grid of points (besides the sampled locations) *or* provide geographical coordinates of pre-defined points and the GIS software will populate a spreadsheet with the coordinates and associated interpolated values (50-year ground snow loads).

The optimal method extraction would utilize a fine enough mesh of points such that after the GIS Kriging interpolation is complete, a series of straight splines, or isolines connecting equal ground snow load points, can be constructed with sufficient resolution for map production. Isolines at equally-spaced snow load intervals of 5 psf are then retained while the rest of the data points and lines are removed for clarity. The final step in the production of a ground snow load map is the delineation of county, road, and natural landmark markings.

9.0 CONCLUDING REMARKS

This thesis develops an innovative approach for determining ground snow loads based on a hydrological snowpack model that assimilates various sources of climatological data, a robust statistical analysis of the output to regionalize those sources, and a geostatistical interpolation method that is able to produce mapped ground snow loads. Using the state of Colorado as a case study, a proposal to unify the methodology for developing ground snow loads in the West has been offered. This thesis is summarized as follows.

Chapter 1.0 examined the current philosophies in place for developing ground snow loads at the national level prescribed by the ASCE 7 Standard, as well as various efforts in the West to develop state-level snow loads where excluded by ASCE 7. Also, various discrepancies in methodology and agreement at state borders revealed the need to update and unify the ground snow load regimes of the western United States. Chapter 2.0 introduced the types of weather measurement stations whose datasets are often employed in snow load analyses. The evaluation of all sources led to the conclusion that a union of all types of measurement techniques would provide the most benefit, highlighting the strengths and mitigating the biases and limitations of each. Chapter 3.0 described how various types of measurements could be used by employing a relatively new hydrological tool used to forecast the availability of water, the SNODAS snow-pack model developed by NOAA. SNODAS is a validated model that can predict SWE and snow depth at sites throughout the state, providing an ideal data source for the investigation. Chapter 4.0 reviewed several pertinent research efforts studying the correlation between ground snow depth and snow water equivalent. These research efforts often employed several predictor variables such as season, altitude, region, temperature, *etc*. into regression analyses. These stud-

ies greatly influenced the decision to regionalize weather stations across the state into distinct climate regions using parameters such as elevation, snow depth, and various other variables.

Chapter 5.0 provided a road map for the proposed method for determining ground snow loads and a description of the necessary data analysis. It introduced a process flowchart that dictated how data was to be acquired, whether it be SNODAS or NWS CO-OP data, and also the order and type of statistical analyses to be performed on the data. This flowchart provided the framework for the rest of the analysis in this investigation. Chapter 6.0 detailed the procedure for acquiring the SNODAS and NWS CO-OP data, including datasets, modeled output, and descriptive station variables such as aspect, slope, basin HUC number, *etc*. Chapter 7.0 provided the description and results of all the statistical analyses performed on the data in order to regionalize the SNODAS stations, from the principal component analysis to the various cluster analyses. The principal component analysis facilitated the selection of clustering variables to be used in various clustering analyses. After an evaluation of several clustering methods, a hybrid method was selected as the most appropriate clustering method and ground snow depth-load relationships were developed. Chapter 7.0 concluded with a proposed method for selecting probability distributions so that 50-year ground snow depths can be extrapolated at the depth-only CO-OP stations. Finally, the snow depth-load relationships developed earlier in the chapter are coupled with the 50-year ground snow depths to produce 50-year ground snow loads. Chapter 8.0 evaluated three different types of spatial interpolation methods, Thiessen Polygon Nearest Neighbor, Inverse Distance Weighting, and Kriging. Ultimately, Kriging was determined to be the most accurate interpolation method, and was proposed as the method for mapping ground snow loads.

The overall objective of this investigation was to propose a sound methodology for determining probabilistic ground snow loads using modern tools and resources from other disci-

plines in an effort to improve the quality of design snow loads. This objective was accomplished in several ways.

First, the methodology developed in Chapter 5.0 and incorporated throughout the rest of the paper is intuitive and based on the principles of the scientific method. The components of this method are embodied in the process flowchart in Figure 5.1. Initially, a theory of the relevant factors that affect ground snow depth and snow load at a particular site were developed using support from previous studies and research efforts. These factors, such as site elevation, terrain slope and aspect, HUC number, *etc*. were then tested by constructing trials of various statistical analyses such as PCA and clustering. Finally, analyses of the results of the quantitative and qualitative measures of performance were made, facilitating the determination of the optimal solution. This proposed model is intuitive and simple to follow, which will promote widespread usage. This flowchart has provided a model for developing ground snow loads that can readily be adopted in any region. Moreover, this model can be used as a standard for ensuring the consistency of every aspect of ground snow load development, from initial procurement of raw data to the final snow load map. Having a comprehensive model such as this allows continual improvements to be made to it by modifying certain aspects while holding the rest constant.

Second, the resources chosen to augment the proposed methodology have proven to be valuable tools that demonstrate the significant advancements in technology as well as enhance the capabilities of traditional structural engineering methods. For instance, the SNODAS model utilized in this study represents tens of years of research in hydrology, climatology, and thermodynamics, coupled with numerical methods and modern computing capabilities. The snowpack model itself has been validated and provides a continuous field of modeled ground snow depths and loads at a much finer spatial resolution than current methods. Current methods in use by the

western states to determine ground snow loads only utilize historical point source data that often results in large unsampled regions; this eventually translates into errors in mapping the ground snow loads. The usage and endorsement of the SNODAS model in this paper promotes a multiple-disciplinary approach.

Lastly, the quality of design loads can be improved by implementing the methodology proposed in this paper. The model developed herein is supported by mathematical techniques that ensure a high level of quality and reproducibility. These techniques are not subject to the bias that would result from using subjective methods alone such as manual clustering or manual selection of clustering variables. However, this model also recognizes and accounts for the shortcomings of any approach rooted purely in mathematics. The dual approach presented in this paper allows cross-validation, using the mathematical PCA and clustering techniques to provide an initial solution that can either be confirmed or rejected by the subjective, visual assessment.

10.0 FUTURE WORK

This thesis provides a framework for improving the process by which snow loads are developed. The approach developed herein is innovative and unique; hydrological water forecasting models have never been used in this particular fashion. Accordingly, the methodology established in this investigation has not gone through an assessment and review process from the engineering community as have the methodologies currently in practice. Nonetheless, this proposal is crucial to updating aging snow load design philosophies both on a state and national level. Below are some considerations for future improvements to the proposed framework.

The SNODAS snowpack model output incorporated into this investigation utilized nine years of modeled data from the water years of 2003 through 2012. This record length is limited by the fact that the model has only been operational since 2002 and its records are only available since 2003. The recommended minimum length of record for the purposes of SNODAS validation and statistical robustness is at least 20 years, as established by climatologists and hydrologists in this paper. Efforts to utilize SNODAS datasets in the same fashion as this investigation should therefore wait until at least 20 years of modeled output is available, or until additional validation studies have been performed similar to Clow et al. (2012). Additionally, there are numerous other stations modeled by SNODAS that were omitted due to record lengths less than the full nine years. This inconsistency would have presented unique challenges to the statistical analysis. The complete inventory of SNODAS stations should be utilized for future efforts since additional stations are constantly being added to the model, improving the spatial coverage.

The multivariate statistical analyses performed in this investigation were based on several descriptive station properties that were considered influential in describing patterns of snow depth, density, and SWE. The majority of the properties such as elevation, latitude, longitude,

slope, aspect, and curvature were derived from geographical characteristics while the remaining three (basin HUC number, modeled snow depth, modeled SWE) describe other characteristics. The introduction of more variables related to climatological processes or patterns may permit development of an increasingly accurate model for ground snow depth and density. For instance, variables derived from long-term weather patterns or regional climatological characteristics could provide insight into describing patterns of snowfall depth or density. Future efforts to improve the work of this investigation should consider the assignment of climatological properties to SNODAS stations, perhaps based on long-term climatic patterns as studied by Changnon, McKee, and Doesken (1993). Consideration of climatological processes in developing ground snow loads will prove increasingly important in the future, especially considering the potential effects of global climate change.

The most critical component of a ground snow load analysis is the dataset used in the analysis. Increasing either the spatial or temporal coverage of an ensemble of weather stations provides by far the greatest benefit to the analysis. A dataset archived by the Colorado Avalanche Information Center (CAIC) could perhaps augment or help validate the SNODAS snowpack model.[25] The CAIC network consists of stations that record information vital to predicting and mitigating avalanches. Most of these stations are independent of the stations assimilated into the SNODAS model. Furthermore, routine recordings of climatological variables are available for modest lengths of uninterrupted measurements. These records could eventually be used validate SNODAS at specific temporal intervals, once there are sufficient years of CAIC measurements.

---

[25] Records from CAIC avalanche stations can be obtained from the following website: https://avalanche.state.co.us/obs_stns/stns.php

LIST OF REFERENCES

Addinsoft. *XLSTAT Pro - Core Statistical Software.* Vol. v. 2013.1.01. New York, NY, 2013.

Alcott, T., and J. Steenburgh. "Snow-to-Liquid Ratio Variability and Prediction at a High-Elevation Site in Utah's Wasatch Mountains." *Weather and Forecasting* 25 (February 2010): 323-337.

Ang, Alfredo, and Wilson Tang. *Probability Concepts in Engineering Planning and Design.* New York, NY: John Wiley & Sons, Inc., 1984.

ASCE/SEI. *Minimum Design Loads for Buildings and Other Structures.* Standard, Reston, VA: American Society of Civil Engineers & Structural Engineering Institute, 2010.

Balaji, Rajagopalan, interview by Michael R. DePaolo. *Hydrology Professor, University of Colorado at Boulder* (November 9, 2012).

Barlage, Michael, et al. "Noah Land Surface Model Modifications to Improve Snowpack Prediction in the Colorado Rocky Mountains." *Journal of Geophysical Research* (American Geophysical Union) 115 (November 2010): 1-15.

Barrett, A. *National Operational Hydrologic Remote Sensing Center SNOw Data Assimilation System (SNODAS) Products at NSIDC.* Special Report #11, University of Colorado at Boulder, Boulder, CO: National Snow and Ice Data Center, 2003.

Baxter, Martin A. *Snow to Liquid Ratio: Climatology and Forecast Methodologies.* Short Course Proceeding, Department of Earth and Atmospheric Sciences, Saint Louis University, St. Louis, MO: Cooperative Institude for Precipitation Systems, 2005.

Ben-Hur, Asa, and Isabelle Guyon. "Detecting Stable Clusters Using Principal Component Analysis." *Functional Genomics: Methods and Protocols* (Humana Press), 2003: 159-182.

Bocchiola, D, and B. Groppelli. "Spatial Estimation of Snow Water Equivalent at Different Dates Within the Adamello Park of Italy." *Cold Regions Science and Technology* 63 (2010): 97-109.

Bocchiola, Daniele, and Renzo Rosso. "The Distribution of Daily Snow Water Equivalent in the Central Italian Alps." *Advances in Water Resources* (Elsevier Ltd.) 30 (2007): 135-147.

Burrough, Peter, and Rachael McDonnell. *Principles of Geographical Information Systems.* Oxford: Oxford University Press, 1998.

Bury, Karl. *Statistical Distributions in Engineering.* Cambridge: Cambridge University Press, 1999.

Caltech. *A Snowflake Primer: The Basic Facts About Snowflakes and Snow Crystals.* February 1, 1999. http://www.its.caltech.edu/~atomic/snowcrystals/primer/primer.htm (accessed March 23, 2013).

Castillo, Enrique. *Extreme Value Theory in Engineering.* San Diego, CA: Academic Press, Inc., 1988.

Changnon, D., T. McKee, and N. Doesken. "Annual Snowpack Patterns Across the Rockies: Long-Term Trends and Associated 500-mb Synoptic Patterns." *Monthly Weather Review* 121 (March 1993): 633-647.

Cifelli, Robert, et al. "The Community Collaborative Rain, Hail, and Snow Network." *Bulletin of the American Meteorological Society*, August 1, 2005: 1069-1077.

Clow, David W., Leora Nanus, Kristine L. Verdin, and Jeffrey Schmidt. "Evaluation of SNODAS Snow Depth and Snow Water Equivalent Estimates for the Colorado Rocky Mountains, USA." *Hydrological Processes* (Wiley Online Library) 26 (2012): 2583-2591.

CoCoRaHS. *Community Collaborative Rain, Hail, & Snow Network.* Colorado Climate Center. 2011. http://www.cocorahs.org/ (accessed April 2, 2013).

CRREL. *A One-Dimensional Temperature Model for a Snow Cover: Technical Documentation for SNTHERM.89.* Special Report 91-16, Cold Regions Research & Engineering Laboratory, U.S. Army Corps of Engineers , 1991.

Daly, C., R. Neilson, and D. Phillips. "A Statistical-Topographic Model for Mapping Climatological Precipitation over Mountainous Terrain." *Journal of Applied Meteorology* 33 (February 1994): 140-158.

De Lannoy, Gabriëlle, et al. "Multiscale Assimilation of Advanced Microwave Scanning Radiometer-EOS Snow Water Equivalent and Moderate Resolution Imaging Spectroradiometer Snow Cover Fraction Observations in Northern Colorado." *Water Resources Research* (American Geophysical Union) 48 (January 2012): 1-17.

Doesken, Nolan, interview by Michael R. DePaolo. *Colorado State Climatologist* (November 5, 2012).

Durand, M, N.P. Molotch, and S.A. Margulis. "Merging Complementary Remote Sensing Datasets in the Context of Snow Water Equivalent Reconstruction." *Remote Sensing of Environment* 112 (2008): 1212-1225.

Eichenlaub, V.L. "Lake Effect Snowfall to the Lee of the Great Lakes: Its Role in Michigan." *Bulletin of the American Meteorological Society* 51, no. 5 (May 1970): 403-412.

Ellingwood, B., and R. Redfield. "Ground Snow Loads for Structural Design." *Journal of Structural Engineering* (American Society of Civil Engineers) 109, no. 4 (April 1983): 950-964.

Ellingwood, B., and R. Redfield. "Probability Models for Annual Extreme Water-Equivalent Ground Snow." *Monthly Weather Review* 112 (June 1984): 1153-1159.

Erickson, Tyler, and Mark Williams. "Persistence of Topographic Controls on the Spatial Distribution of Snow in Rugged Mountain Terrain, Colorado, United States." *Water Resources Research* (American Geophysical Union) 41, no. W04014 (April 2005): 1-17.

Ferris, Ritchey. *The Statistical Imagination.* 2nd Ed. Birmingham, AL: McGraw-Hill, 2008.

Formichi, Paolo. "EN1991 - Eurocode 1: Actions on Structures. Part 1-3 General Actions - Snow Loads." *Eurocodes Background and Applications: Dissemination of Information Workshop.* Pisa: University of Pisa - Italy, 2008. 1-60.

Gulvanessian, Haig, J. A. Calgaro, and Milan Holickây. *Designers' Guide to EN1990 Eurocode: Basis of Structural Design.* Bodmin: MPG Books, 2002.

Harris, James, interview by Michael R. DePaolo. *Chairman, Snow Load Committee, Structural Engineers Association of Colorado* (March 9, 2013).

IBC. *International Building Code.* Standard, Country Club Hills, IL: International Code Council, Inc., 2009.

Johnson, Richard, and Dean Wichern. *Applied Multivariate Statistical Analysis.* 6th. Upper Saddle River, NJ: Pearson Prentice Hall, 2007.

Jolliffe, I.T. *Principal Component Analysis, Second Edition.* Aberdeen: Springer, 2002.

Jonas, T., C. Marty, and J. Magnusson. "Estimating the Snow Water Equivalent from Snow Depth Measurements in the Swiss Alps." *Journal of Hydrology*, 2009: 161-167.

Judson, A., and N. Doesken. "Density of Freshly Fallen Snow in the Central Rocky Mountains." *Bulletin of the American Meteorological Society* 81, no. 7 (January 2000): 1577-1587.

Kayihan, F., A. Cinar, and A. Palazoglu. *Chemical Process Performance Evaluation.* Boca Raton, FL: CRC Press, 2007.

Kennedy, Joseph C.G. *Agriculture of the United States. 1860; The Eighth Census.* Census, Secretary of the Interior, Washington, D.C.: Government Printing Office, 1864.

Kim, K., J. Heo, W. Nam, and E. Shin. "Applicability of Various Clustering Techniques for Regional Frequency Analysis ." *Critical Transitions in Water and Environmental Resources Management* (American Society of Civil Engineers), 2004: 1-9.

Knight, M., and B. Cooil. "Infrastructure Investigation Using Latent Class Cluster Analysis." *Computing in Civil Engineering* (American Society of Civil Engineers), July 2005: 1-10.

Kumar, Sujay, Christa Peters-Lidard, David Mocko, and Yudong Tian. "Multiscale Evaluation of the Improvements in Surface Snow Simulation through Terrain Adustments to Radiation." *Journal of Hydrometeorology* (American Meteorological Society) 14 (February 2013): 220-232.

Leyk, Stefan. "GIS Modeling: Terrain Analysis." Department of Geography, University of Colorado. 2008. http://www.colorado.edu/geography/class_homepages/geog_4203_s08/class6_TerrainAnSlopeAspect.pdf (accessed April 18, 2013).

Murphy, Rebecca, Frank Curriero, and William Ball. "Comparison of Spatial Interpolation Methods for Water Quality Evaluation in the Chesapeake Bay." *Journal of Environmental Engineering* (American Society of Civil Engineers) 136 (February 2010): 160-171.

NASA. *The MODIS Snow & Sea Ice Global Mapping Project.* June 5, 2012. http://modis-snow-ice.gsfc.nasa.gov/ (accessed February 20, 2013).

NCAR. *How Deep is the Snow?* May 6, 2011. http://www2.ucar.edu/atmosnews/features/4477/how-deep-snow (accessed January 29, 2013).

NCDC. *Annual Climatological Summaries for GHCN Database.* Documentation, Washington, DC: National Oceanic and Atmospheric Administration - National Climatic Data Center, 2013.

—. *Global Historical Climatology Network.* 2012a. http://www.ncdc.noaa.gov/oa/climate/ghcn-daily/ (accessed January 29, 2013).

—. *NOAA's National Climatic Data Center.* 2012b. http://www.ncdc.noaa.gov/ (accessed January 28, 2013).

—. *NOAA's National Climatic Data Center.* 2012c. http://www.ncdc.noaa.gov/homr/ (accessed February 22, 2013).

NOAA. *NOAA History.* June 8, 2006. http://www.history.noaa.gov/ (accessed Jan. 21, 2012).

NOHRSC. "SNODAS Snow Model Time Series Output." *NOAA's National Operational Hydrologic Remote Sensing Center.* February 16, 2012. http://www.nohrsc.noaa.gov/interactive/html/graph.html (accessed November 1, 2012).

Nolin, Anne. "Recent Advances in Remote Sensing of Seasonal Snow." *Journal of Glaciology* 56, no. 200 (2010): 1141-1150.

NRCS. *National Water and Climate Center.* 2012. http://www.wcc.nrcs.usda.gov/snowcourse/ (accessed January 30, 2013).

—. *SNOTEL And Snow Survey & Water Supply Forecasting.* U.S. Department of Agriculture. 2009. www.wcc.nrcs.usda.gov/snow/about.html (accessed October 16, 2012).

—. "Snow Surveys and Water Supply Forecasting: Agriculture Information Bulletin 536." *USDA Natural Resources Conservation Service.* United States Department of Agriculture. 2012. http://www.wcc.nrcs.usda.gov/factpub/aib536.html (accessed January 26, 2013).

NSIDC. *Snow Data Assimilation System (SNODAS) Data Products at NSIDC.* Digital Media. Boulder, CO: National Snow and Ice Data Center, 2004.

NWS. "Latitude/Longitude Distance Calculator." *NOAA National Weather Service - National Hurricane Center.* October 27, 2010. http://www.nhc.noaa.gov/gccalc.shtml (accessed March 20, 2013).

—. "NOAA's National Weather Service." *What is the COOP Program.* April 25, 2012a. www.nws.noaa.gov (accessed October 12, 2012).

—. *NOAA's National Weather Service.* 2012b. www.nws.noaa.gov (accessed January 16, 2013).

NWS. *Standard Hydrometeorological Exchange Format (SHEF) Code Manual.* Manual, Office of Climate, Water and Weather Services, National Weather Service, 2012c.

Oliver, Margaret. "Determining the Spatial Scale of Variation in Environmental Properties using the Variogram." In *Modeling Scale in Geographical Information Science*, edited by Nicholas Tate and Peter Atkinson, 193-219. John Wiley & Sons, Ltd., 2001.

Olsen, R. C. *Remote Sensing from Air and Space.* Bellingham, WA: SPIE Press, 2007.

Paniconi, Claudio, Marino Marrocu, Mario Putti, and Mark Verbunt. "Newtonian Nudging for a Richards Equation-Based Distributed Hydrological Model." *Advances in Water Resources* (Elsevier Science Ltd.) 26 (2003): 161-178.

Parajka, Bloschl. "MODIS-Based Snow Cover Products, Validation, and Hydrologic Applications." *Multiscale Hydrologic Remote Sensing: Perspectives and Applications* (Austrian Academy of Sciences), 2012: 185-212.

Quayle, Lazar, Cram. "Land Station Definitions." *University Corporation for Atmospheric Research.* 2013. http://rda.ucar.edu/docs/definitions/stations.html (accessed January 30, 2013).

Robinson, D. A. "Evaluation of the Collection, Archiving, and Publication of Daily Snow Data in the United States." *Physical Geography* (V. H. Winston & Son) 10, no. 2 (1989): 120-130.

Romanov, Peter, and Dan Tarpley. "Estimation of Snow Depth Over Open Prairie Environments Using GOES Imager Observations." *Hydrological Processes* (John Wiley & Sons) 18 (2004): 1073-1087.

Sack, R.L., and A. Sheikh-Taheri. *Ground and Roof Snow Loads for Idaho.* Moscow, ID: University of Idaho, Department of Civil Engineering, 1986.

Sack, Ronald. "Western States Ground Snow Loads - Border Comparisons." Document, College of Engineering & Architecture, Washington State University Pullman, Pullman, WA, 2011, 3.

Sack, Ronald. "Western States Ground Snow Loads." Report, College of Engineering & Architecture, Washington State University Pullman, Pullman, WA, 2012, 3.

Samelson, D, and D.S. Wilks. "A Simple Method for Specifying Snowpack Water Equivalent in the Northeastern United States." *Journal of Applied Meteorology* 32 (1992): 965-974.

Schmidlin, Thomas. "A Critique of the Climatic Record of "Water Equivalent Snow on the Ground" in the United States." *Journal of Applied Meteorology*, 1990: 1136-141.

Scotto, M., A. Alonso, and S. Barbosa. "Clustering Time Series of Sea Levels: Extreme Value Approach." *Journal of Waterway, Port, Coastal, and Ocean Engineering* (American Society of Civil Engineers) 136, no. 4 (August 2010): 215-225.

SEAC. *Colorado Ground Snow Loads.* Report, Denver, CO: Structural Engineers Association of Colorado, 2007.

Soil Conservation Service. *Snow Survey Sampling Guide.* Instructional Report, Washington, DC: West National Technical Center, 1984.

Sturm, Matthew, Brian Taras, Glen Liston, Chris Derksen, and Jon Lea. "Estimating Snow Water Equivalent Using Snow Depth Data and Climate Classes." *Journal of Hydrometeorology*, 2010: 1380-394.

Takara, K, and J. R. Stedinger. "Recent Japanese Contributions to Frequency Analysis and Quantile Lower Bound Estimators." *Stochastic and Statistical Methods in Hydrology and Environmental Engineering* 1 (1994): 217-234.

Tan, Pang-Ning, Michael Steinback, and Vipin Kumar. *Introduction to Data Mining.* Boston, MA: Addison-Wesley, 2005.

Teegavarapu, Ramesh, and Pankaj Bajaj. "Optimal Spatial Weighting Methods for Estimation of Missing Rain Gage Records." *World Environmental and Water Resources Congress 2008.* Ahupua'a, Hawaii: American Society of Civil Engineers, 2008. 1-9.

Tobiasson, W., and A. Greatorex. "Database and Methodology for Conducting Site Specific Snow Load Case Studies for the United States." *Proceedings from the Third International Conference on Snow Engineering.* Sendai, Japan, 1996. 249-256.

Tobiasson, Wayne, James Buska, and Alan Greatorex. "Developing Ground Snow Loads for New Hampshire." In *Snow Engineering*, by Holand, Løset, Norem Hjorth-Hansen, 313-321. Balkema, Rotterdam, 2000.

Tufféry, Stéphane. *Data Mining and Statistics for Decision Making.* Hoboken, NJ: Wiley, 2011.

USDA. *United States Department of Agriculture.* 2012. http://www.usda.gov (accessed January 30, 2013).

USGS. "Hydrologic Unit Maps." *United States Geodetic Survey: Water Resources of the United States.* February 20, 2013. http://water.usgs.gov/GIS/huc.html (accessed April 19, 2013).

Varmuza, K., and P. Filzmoser. *Introduction to Multivariate Statistical Analysis in Chemometrics.* Boca Raton, FL: CRC Press, 2009.

Ward, Joe Jr. "Hierarchal Grouping to Optimize an Objective Function." *Journal of the American Statistical Association* (American Statistical Association) 58, no. 301 (March 1963): 236-244.

WMO. *Observing Stations and WMO Catalogue of Radiosondes.* March 2013. http://www.wmo.int/pages/prog/www/ois/volume-a/vola-home.htm (accessed March 19, 2013).

—. "WMO Publication No. 9, Vol. A: Record Layout of the Master Flat File." *World Meteorological Organization.* May 1998. http://www.wmo.int/pages/prog/www/ois/volume-a/9ALayoutGuide9805.html (accessed March 19, 2013).

Wood, Louvan E. "Automatic Weather Stations." *Journal of Meteorology*, 1946: 115-121.

WRCC. *COOP Sites.* April 11, 2006. http://www.wrcc.dri.edu/summary/Climsmco.html (accessed March 19, 2013).

Zhang, X., and R. Srinivasan. "GIS-Based Spatial Precipitation Estimation: A Comparison of Geostatistical Approaches." *Journal of the American Water Resources Association* (American Water Resources Association) 45, no. 4 (August 2009): 894-906.

Zhang, X., N. A. Drake, J. Wainwright, and M. Mulligan. "Global Scale Overland Flow and Soil Erosion Modelling using Remote Sensing and GIS Techniques: Model Implementation and Scaling." *Proceedings of RSS 1997 Remote Sensing in Action.* Remote Sensing Society, 1997. 379-384.

Zhang, Y., J. Li, and Y. Chae. "Hysteresis-Based Structural Damage Detection Using Multi-Resolution Sensor Data." Edited by M. Tomizuka, R. W. Chen, C. B. Yun, B. F. Spencer and W. M. Chen. *World Forum on Smart Materials and Smart Structures Technology.* China: CRC Press, 2007.

Zhang, Z. M., B. K. Tsai, and G. Machin. *Radiometric Temperature Measurements: Experimental Methods in the Physical Sciences.* Vol. 42. Oxford: Elsevier, 2010.

APPENDIX

A Ground Snow Load Map for the Conterminous U.S. (ASCE 7, Fig.7-1)

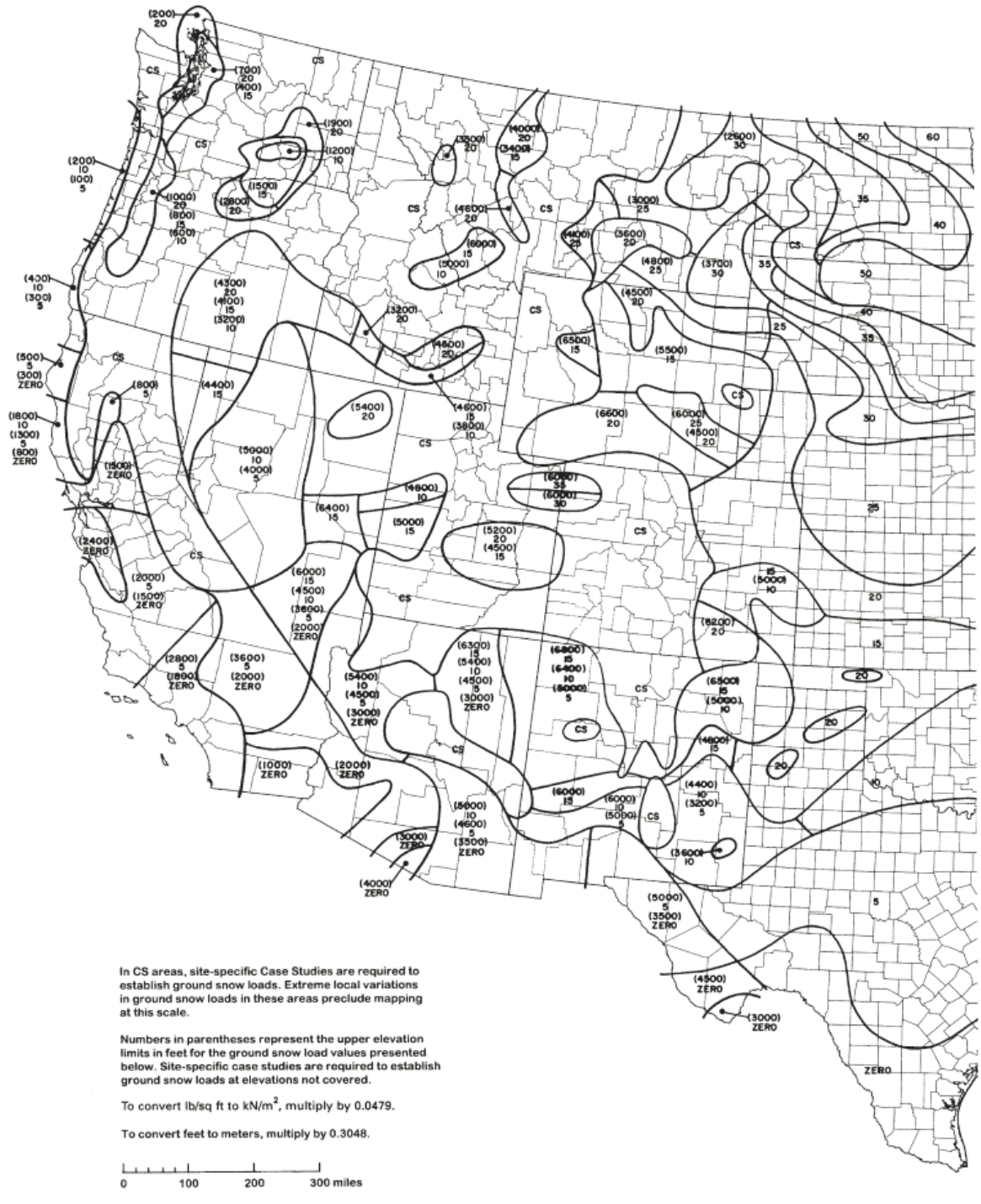

FIGURE 7-1 Ground Snow Loads, P_g, for the United States (Lb/Ft^2).

A *(Continued)*

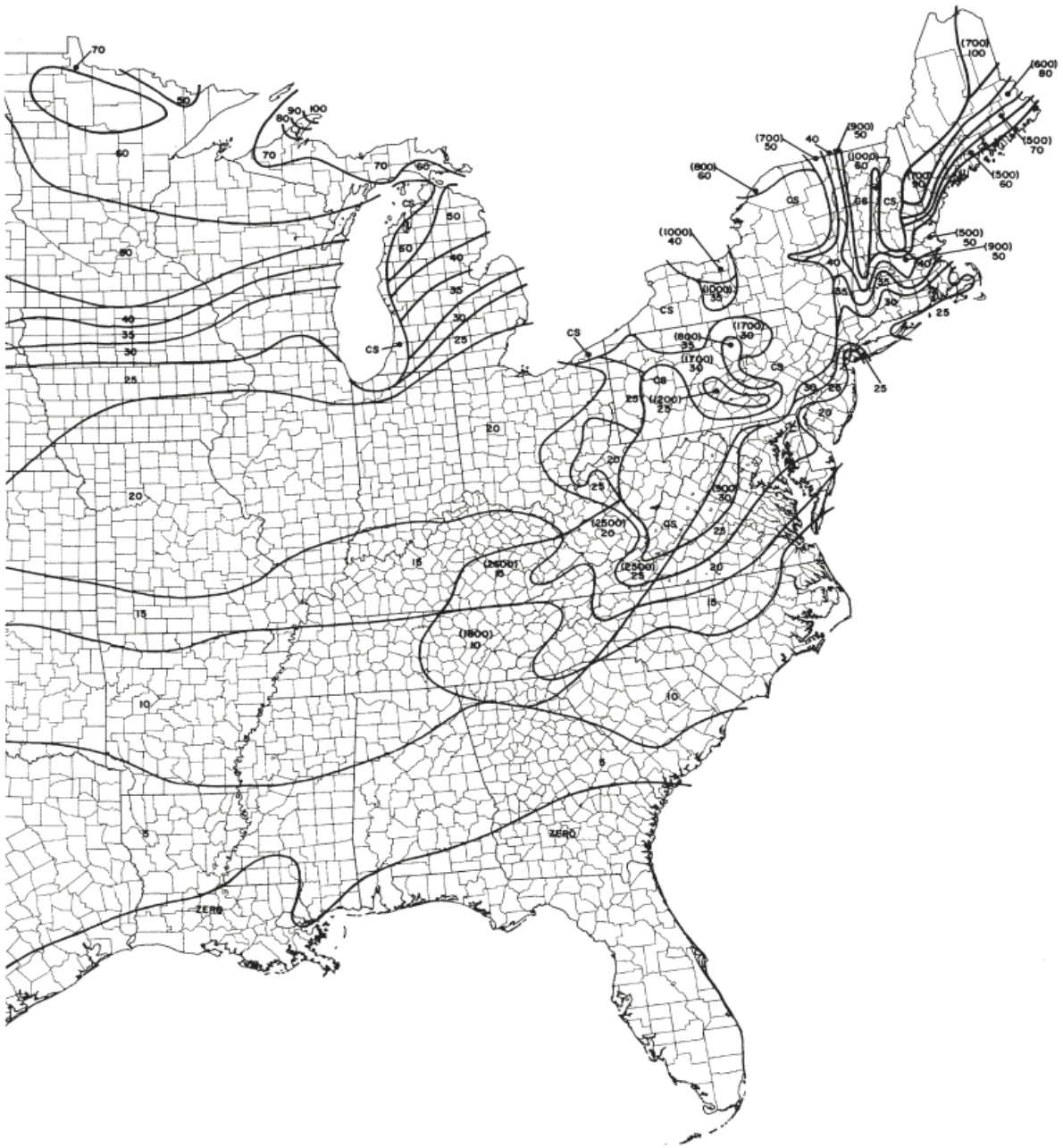

FIGURE 7-1. (*Continued*)

Reproduced with permission from the American Society of Civil Engineers

B Colorado State Ground Snow Load Map Produced by the Structural Engineers Association of Colorado (SEAC 2007)

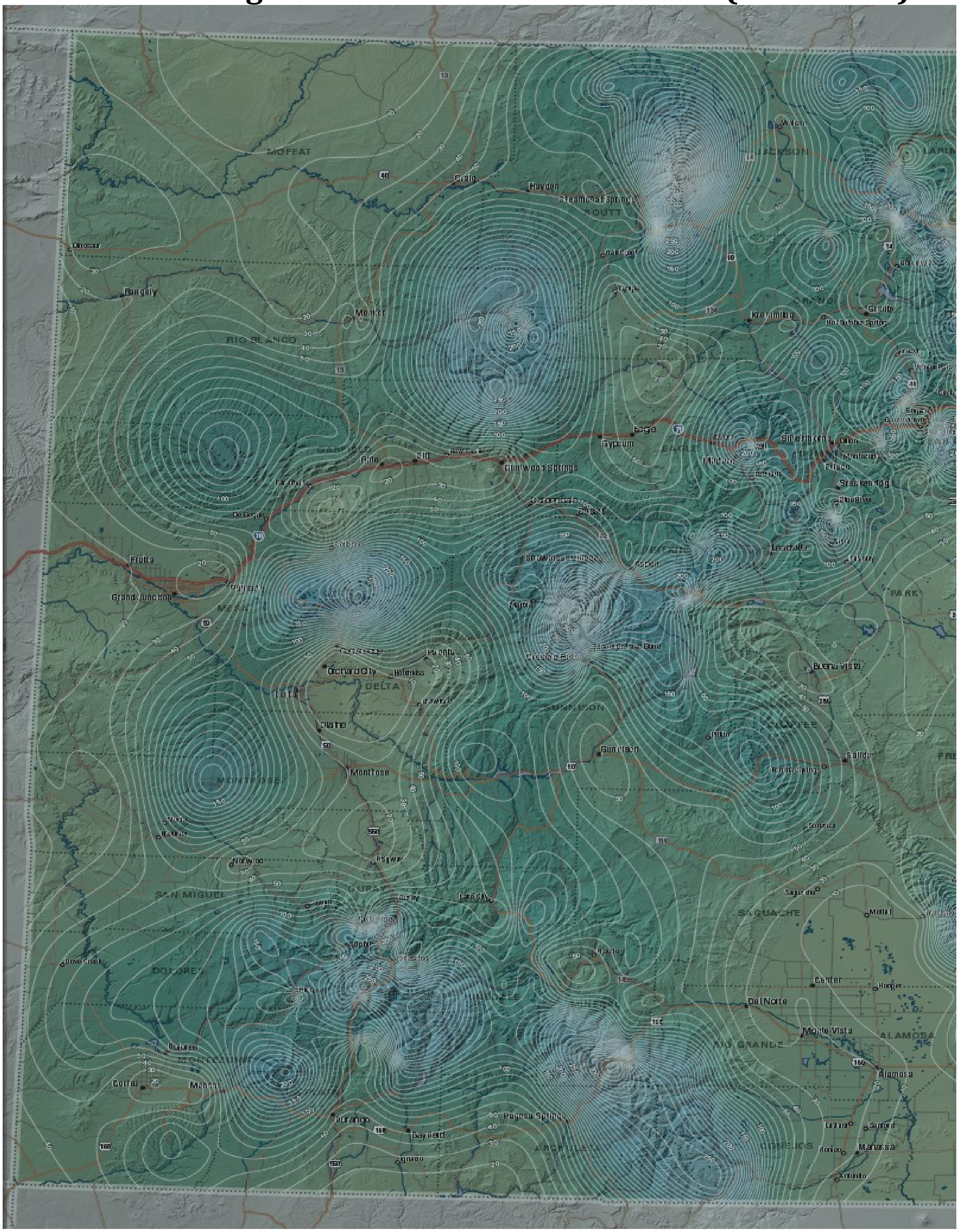

B *(Continued)*

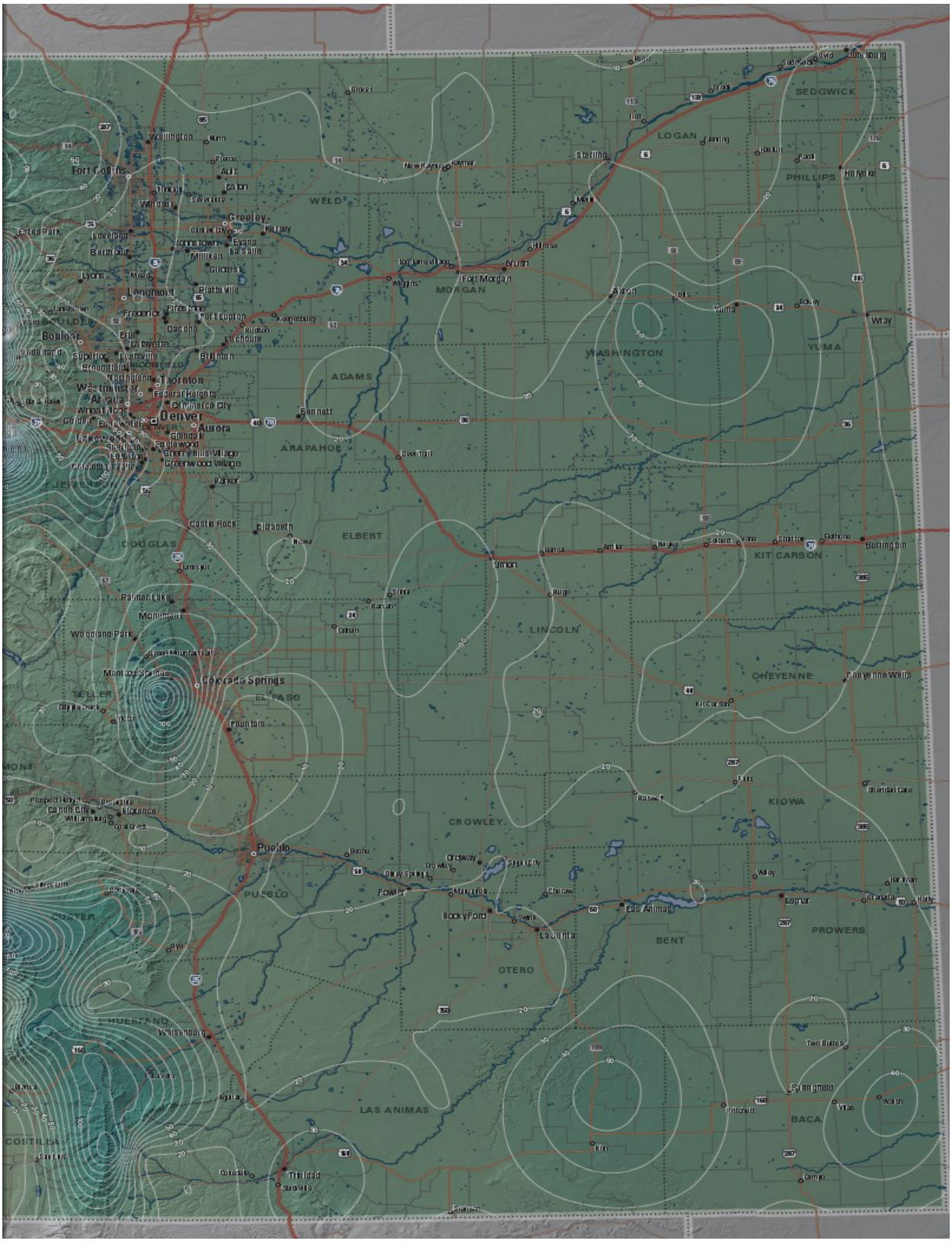
SEDGWICK
LOGAN
PHILLIPS
WELD
MORGAN
WASHINGTON
YUMA
ADAMS
ARAPAHOE
DOUGLAS
ELBERT
KIT CARSON
LINCOLN
CHEYENNE
EL PASO
TELLER
CROWLEY
KIOWA
PUEBLO
CUSTER
HUERFANO
LAS ANIMAS
BENT
PROWERS
OTERO
BACA
Fort Collins
Greeley
Denver
Aurora
Colorado Springs
Pueblo
Trinidad
Sterling
Fort Morgan
Brush
Wray
Burlington
Limon
Castle Rock
Elizabeth
Parker
Monument
Fountain
Cheyenne Wells
La Junta
Las Animas
Lamar
Springfield
Two Buttes

C SNODAS Stations in Colorado Used for Snow Load Analysis (AGLC2 through BRTC2 shown)

SNODAS ID	STATION TYPE	ELEV. (feet)	LAT. (deg-N)	LONG. (deg-W)
AGLC2	COOPB	6690	37.38	-104.65
AGRC2	COOPB	8652	37.32	-104.95
AKNC2	UCOOP	4590	40.14	-103.20
AKO	ASOS	4678	40.17	-103.21
AKRC2	COOPBC	4541	40.16	-103.14
ALAC2	AHOS, COOPB, GOES, RFCSIM	7546	37.48	-105.88
ALEC2	COOPB, GOES	8045	38.66	-106.85
ALKC2	COOPB, GOES	8314	40.19	-105.50
ALS	ASOS, COOPAB	7543	37.44	-105.87
ANTC2	COOPABC, GOES	8944	38.99	-105.89
APA	ASOS	5869	39.56	-104.85
APNC2	COOPB, GOES	8054	39.18	-106.80
APSC2	SNOTEL	10039	37.33	-105.07
ARBC2	COOPAB	6181	37.02	-107.44
ARGC2	GOES	8944	39.04	-106.27
AROC2	SNOTEL	9672	39.92	-105.76
ARPC2	SNOTEL	11004	40.35	-106.38
ASE	AHOS, ASOS, LAWRS, SAWRS	7759	39.22	-106.87
ASIC2	UCOOP	9213	39.83	-105.48
ASPC2	COOPAB	8054	39.19	-106.84
ATBC2	AHOS, COOPAB	5699	39.50	-108.38
AVNC2	UCOOP	8458	39.67	-106.55
BALC2	AMRAD, GOES	8766	39.51	-105.52
BAWC2	AMOS, GOES	7877	39.38	-105.34
BAYC2	UCOOP	7933	37.30	-107.66
BCKC2	GOES	4281	38.18	-103.76
BCRU1	GOES	5531	39.30	-109.22
BCVC2	SNOTEL	8543	39.60	-106.51
BEDC2	COOPAB	5000	38.33	-108.88
BHRC2	GOES	8593	37.02	-106.20
BKFC2	COOPAB	6975	39.03	-104.80
BKRC2	COOPB, GOES	10256	39.41	-106.05
BLKC2	SNOTEL	9452	40.31	-105.64
BLNC2	COOPAB	7762	37.44	-105.52
BLPC2	GOES	10367	37.79	-106.78
BLRC2	GOES	8802	39.63	-106.07
BLSC2	AHOS, SNOTEL	10955	39.76	-107.36
BMKC2	COOPAB	7602	38.47	-107.16
BNVC2	COOPAB	7979	38.85	-106.13
BOSC2	COOPB	4603	38.17	-104.31
BOUC2	COOPAB	5515	39.99	-105.27
BPRC2	COOPB, GOES	5367	40.80	-108.92
BREC2	UCOOP	9531	39.51	-106.06
BRIC2	COOPAB	5036	39.94	-104.84
BRMC2	AHOS, SNOTEL	10633	39.09	-106.54
BRTC2	AHOS, SNOTEL	11598	37.71	-107.51

D Description of SNODAS Station Types (NWS 2012b)

STATION TYPE	DESCRIPTION OF STATION TYPE
AHOS	AUTOMATED HYDROLOGICAL OBSERVING STATION
ALERT	AUTOMATED LOCAL EVALUATION IN REAL TIME (EVENT)
AMOS	AUTOMATED METEOROLOGICAL OBSERVING STATION
ARC	AUTOMATIC REMOTE COLLECTOR
ASOS	AUTOMATED SURFACE OBSERVING SYSTEM
AUTOB	AUTOMATED METEOROLOGICAL OBSERVING SYSTEM
AWIPS	ADVANCED WEATHER INTERACTIVE PROCESSING SYSTEM
AWOS	AUTOMATED WEATHER OBSERVING SYSTEM
BASIC	BASIC (CONTRACT OBSERVING STATION)
BSAWRS	SUPPLEMENTAL AVIATION WEATHER REPORTING STATION (AWOS BACKUP)
CADAS	CENTRALIZED AUTOMATIC DATA ACQUISITION SYSTEM
COOPA	COOPERATIVE OBSERVER STATION CLIMATE
COOPAB	COOPERATIVE OBSERVER STATION CLIMATE: HYDRO.
COPABC	COOPERATIVE OBSERVER STATION CLIMATE: HYDRO./METEOR.
COOPAC	COOPERATIVE OBSERVER STATION CLIMATE: METEOR.
COOPB	COOPERATIVE OBSERVER STATION: HYDRO.
COOPBC	COOPERATIVE OBSERVER STATION: HYDRO./METEOR.
COOPC	COOPERATIVE STATION HYDRO. OR METEOR.
CRS	CONSOLE REPLACEMENT SYSTEM
GOES	GEOSTATIONERY OPERATIONAL ENVIRONMENTAL SATELLITE
LAWRS	LIMITED AVIATION WEATHER REPORTING STATION
NWR	NOAA WEATHER RADIO TRANSMITTER
NWRP	NOAA WEATHER RADIO PERIPHERAL EQUIPMENT
NWRTS	NOAA WEATHER RADIO VHF TRANSMITTING STATION
NWW	NOAA WEATHER WIRE
OTHER	ALL OTHER PROGRAMS
RAMOS	REMOTE AUTOMATED METEROLOGICAL SYSTEM
RFCSIM	RIVER FORECAST CENTER SIMULATION STATION
S	SYNOPTIC OBSERVATION
SAWRS	SUPPLEMENTARY AVIATION WEATHER REPORTING STATION
SAWRS II	SUPPLEMENTAL AVIATION WEATHER REPORTING STATION (ASOS BACKUP)
SCAN	SOIL CLIMATE ANALYSIS NETWORK
SNOCOR	SNOW COURSE
SNOTEL	SNOW TELEMETRY
UA	UPPER AIR OBSERVATION
UCOOP	UNOFFICIAL COOPERATIVE STATION
WSF	WATER SUPPLY FORECAST
WSR88D	WEATHER SURVEILLANCE RADAR (NEXRAD)

E Landsat Remote Sensing Analysis for Station BOUC2 Used to Obtain Driving Variables for SNODAS (NOHRSC 2012)

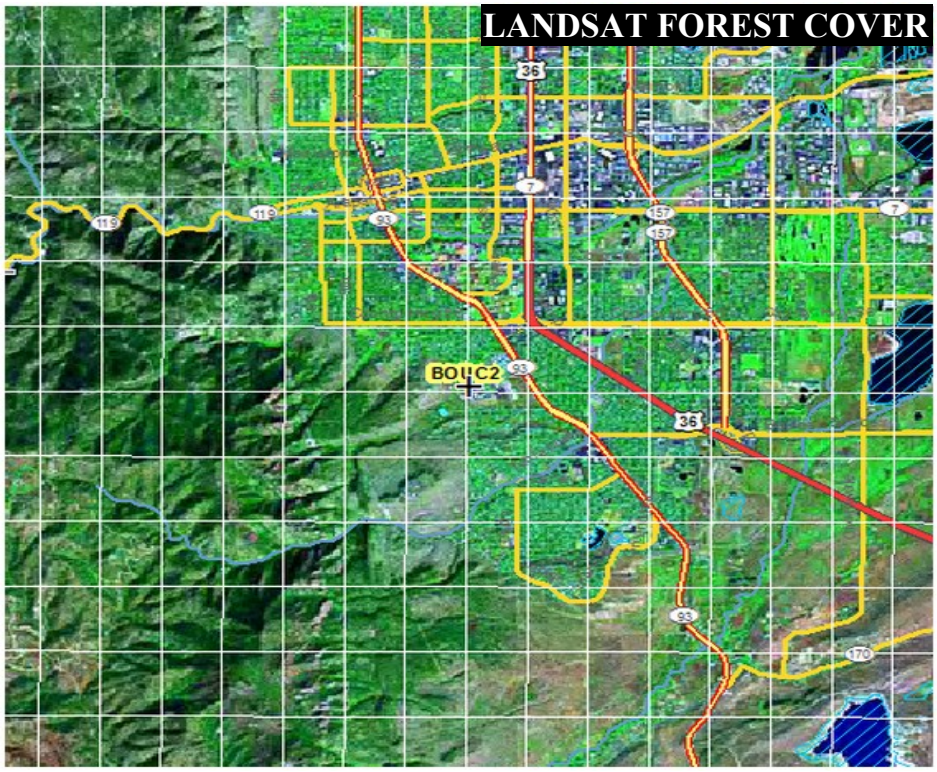

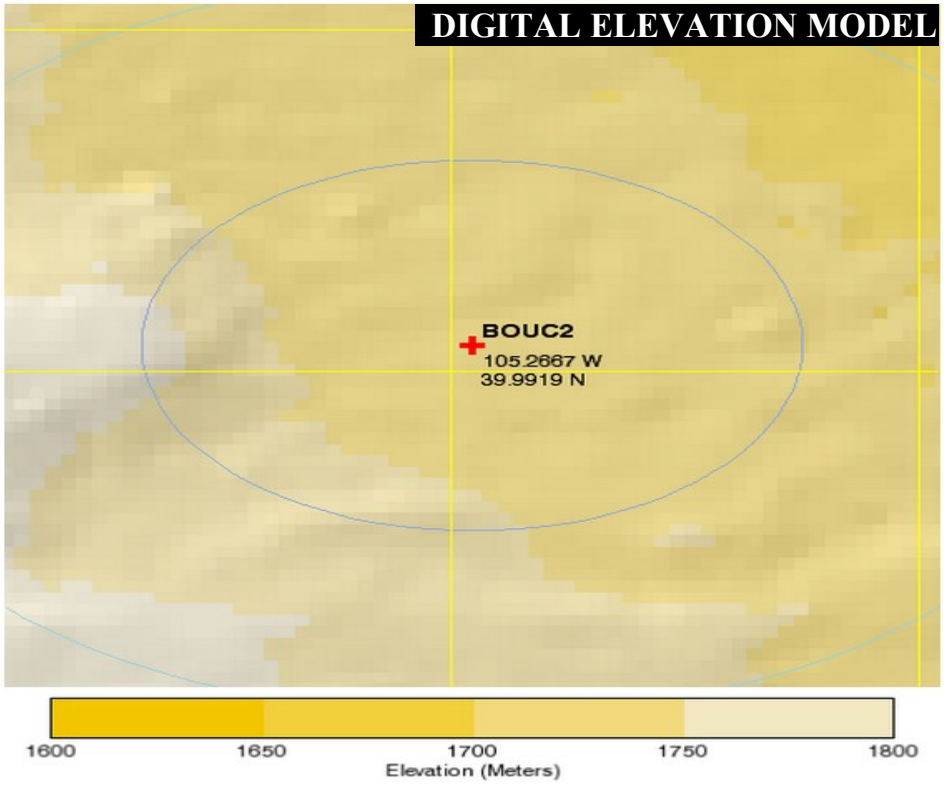

F SNODAS Output Plots for Station 'BURC2' for WY 2005-2006 (NOHRSC 2012)

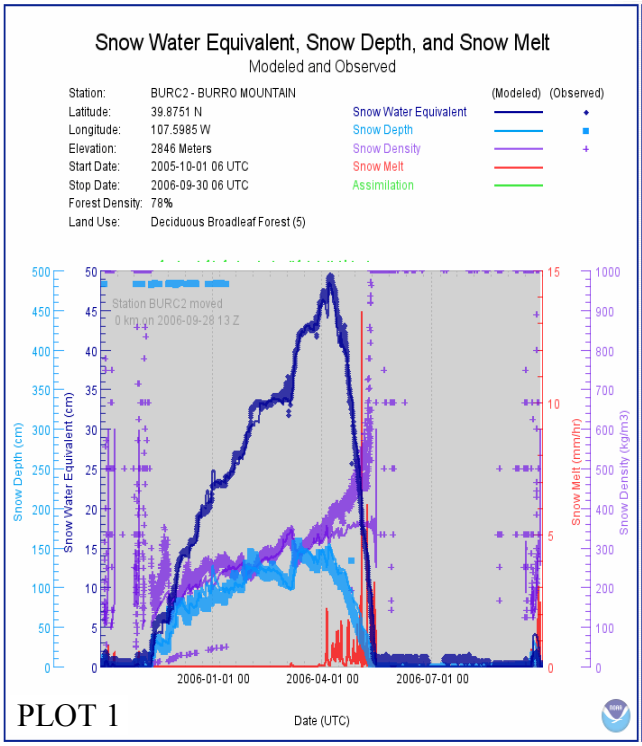

PLOT 1

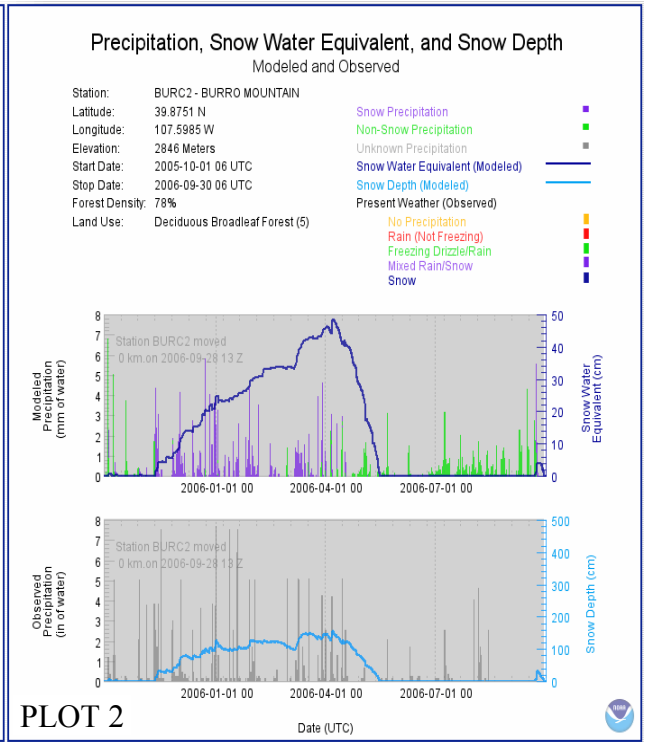

PLOT 2

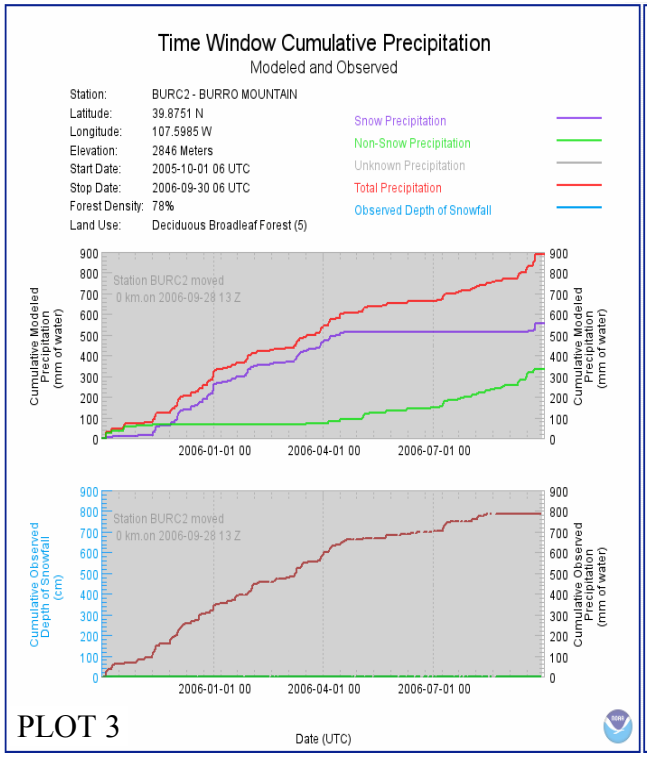

PLOT 3

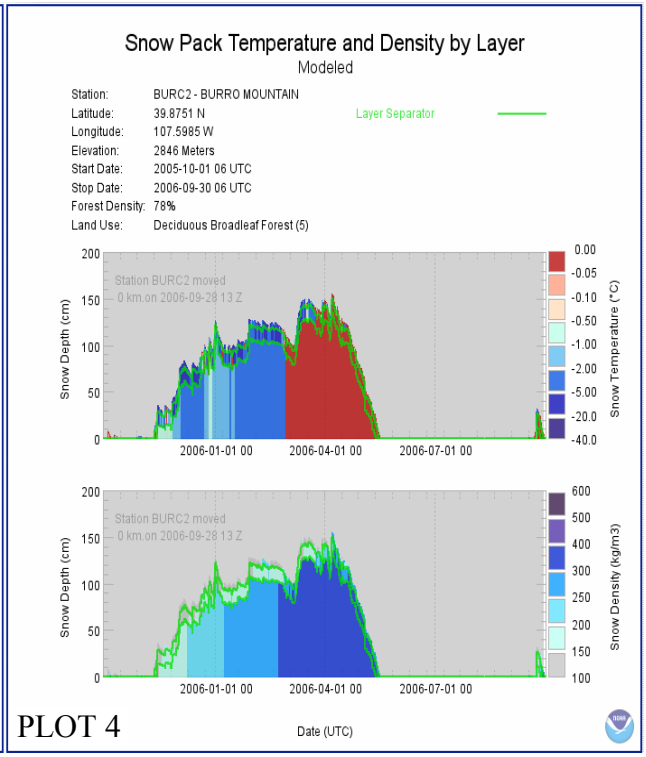

PLOT 4

F *(Continued)*

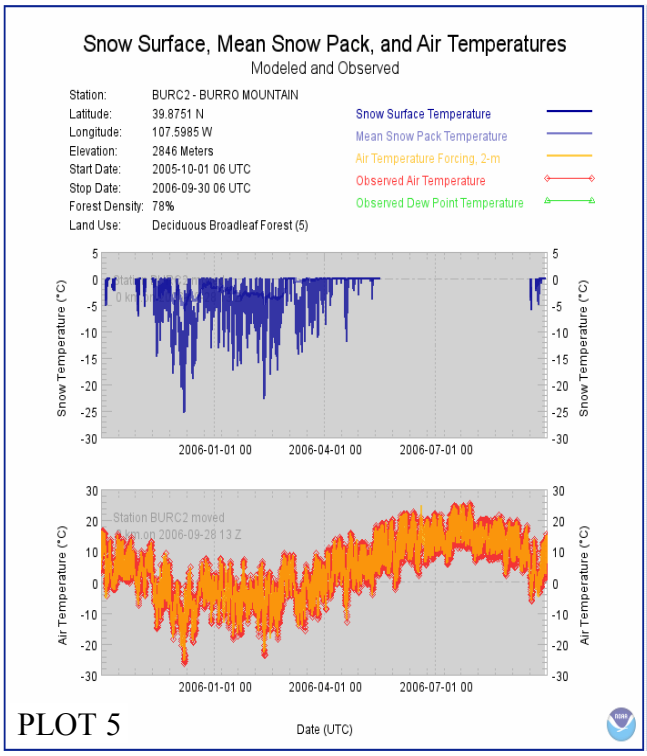

PLOT 5

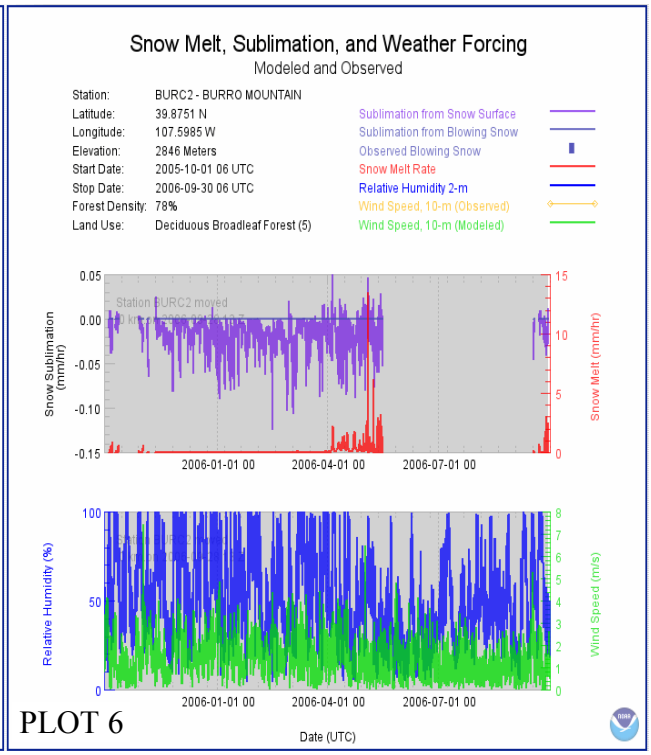

PLOT 6

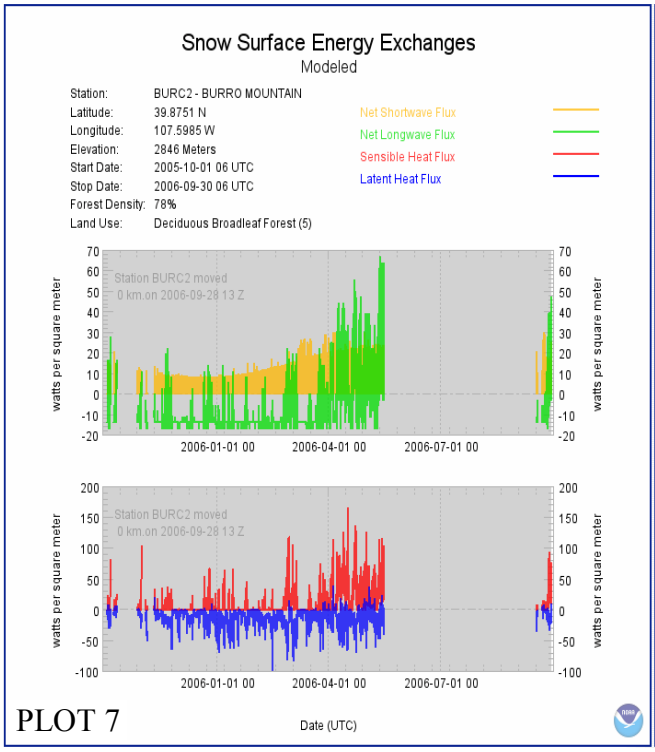

PLOT 7

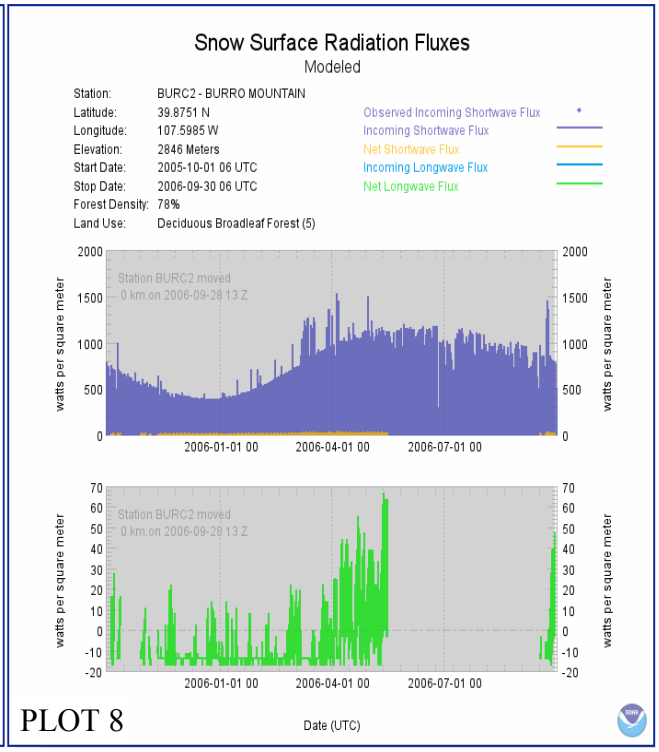

PLOT 8

G Plot 2 CSV File of SNODAS Model Output for Station 'BURC2' for WY 2005-2006 (April 2-May 1 Shown)

Date	(Modeled) Snow Precipitation (in)	(Modeled) Snow Water Equivalent (in)	(Modeled) Snow Depth (in)	Date w/o Time (m/d/yyyy)	Hour
4/2/2006 6:00	0.02	18.19	57.37	4/2/2006	6
4/3/2006 6:00	0.00	18.16	56.84	4/3/2006	6
4/4/2006 6:00	0.00	18.07	54.21	4/4/2006	6
4/5/2006 6:00	0.00	17.79	52.05	4/5/2006	6
4/6/2006 6:00	0.03	17.40	50.99	4/6/2006	6
4/7/2006 6:00	0.00	17.69	56.52	4/7/2006	6
4/8/2006 6:00	0.00	19.00	60.36	4/8/2006	6
4/9/2006 6:00	0.00	18.90	57.70	4/9/2006	6
4/10/2006 6:00	0.00	18.49	55.18	4/10/2006	6
4/11/2006 6:00	0.00	18.13	53.58	4/11/2006	6
4/12/2006 6:00	0.00	17.98	53.64	4/12/2006	6
4/13/2006 6:00	0.00	17.54	51.28	4/13/2006	6
4/14/2006 6:00	0.00	16.84	48.60	4/14/2006	6
4/15/2006 6:00	0.00	16.17	46.36	4/15/2006	6
4/16/2006 6:00	0.00	16.28	48.82	4/16/2006	6
4/17/2006 6:00	0.00	15.90	46.34	4/17/2006	6
4/18/2006 6:00	0.01	16.07	47.20	4/18/2006	6
4/19/2006 6:00	0.00	15.89	48.16	4/19/2006	6
4/20/2006 6:00	0.00	15.78	47.78	4/20/2006	6
4/21/2006 6:00	0.00	15.70	46.36	4/21/2006	6
4/22/2006 6:00	0.00	15.46	44.62	4/22/2006	6
4/23/2006 6:00	0.00	14.82	41.91	4/23/2006	6
4/24/2006 6:00	0.00	14.01	39.25	4/24/2006	6
4/25/2006 6:00	0.00	13.55	38.61	4/25/2006	6
4/26/2006 6:00	0.00	13.35	37.85	4/26/2006	6
4/27/2006 6:00	0.00	13.08	36.61	4/27/2006	6
4/28/2006 6:00	0.00	11.62	32.21	4/28/2006	6
4/29/2006 6:00	0.00	11.22	31.53	4/29/2006	6
4/30/2006 6:00	0.00	11.00	30.62	4/30/2006	6
5/1/2006 6:00	0.00	10.53	29.34	5/1/2006	6

H Digital Elevation Model of Colorado Generated by ArcGIS

Note: white indicates very high elevations whereas green indicates low elevations

I Spatial Analysis of Colorado with Aspect & Slope Relief Imagery Generated by ArcGIS

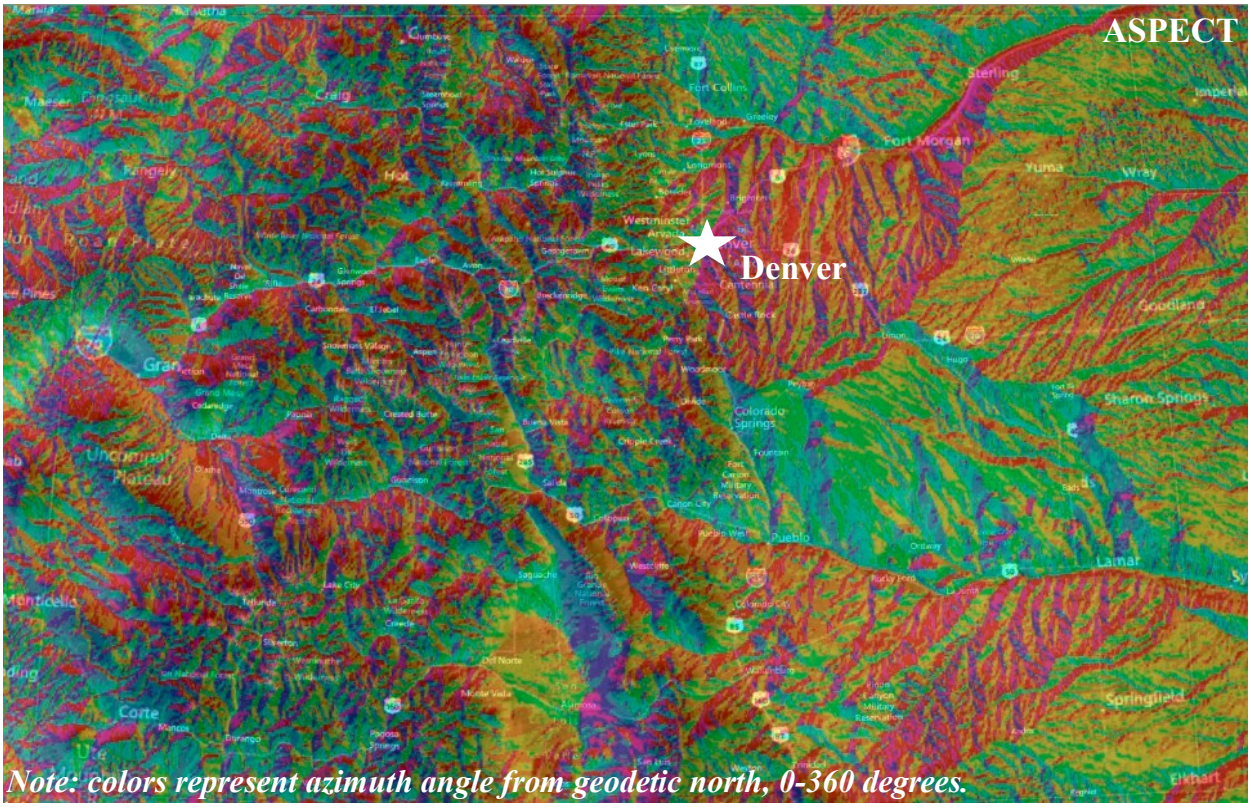

Note: colors represent azimuth angle from geodetic north, 0-360 degrees.

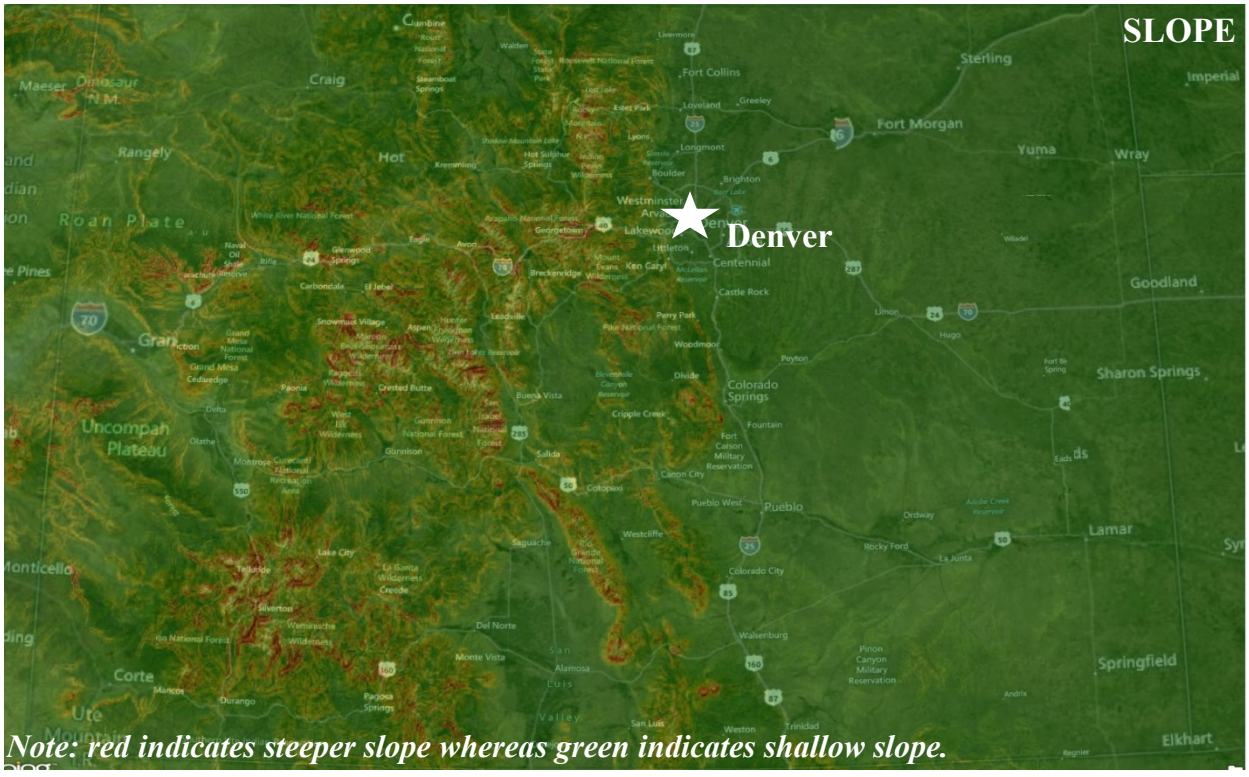

Note: red indicates steeper slope whereas green indicates shallow slope.

J Descriptive Summaries & Basic Statistics for SNODAS Station 'AGLC2' (WY2003-WY2012)

SNODAS MODEL OUTPUT SUMMARY - STATION 'AGLC2'											
WATER YEAR	MAX SWE		DATE	SNOW LOAD	SNDP AT DATE OF MAX SWE		SWE / SNDP	SNOW DENSITY	MAX SNDP	DATE	$\frac{SNDP_{SWE}}{SNDP_{MAX}}$
	(ft)	(in)	(m/d/yyyy)	(psf)	(ft)	(in)	(--)	(pcf)	(in)	(m/d/yyyy)	(--)
2003-2004	0.053	0.63	4/12/2004	3.28	0.396	4.75	0.133	8.28	4.77	4/12/2004	0.996
2004-2005	0.124	1.49	3/15/2005	7.75	1.112	13.3	0.112	6.97	13.3	3/15/2005	1.000
2005-2006	0.063	0.75	1/23/2006	3.90	0.463	5.55	0.135	8.43	5.55	1/23/2006	1.000
2006-2007	0.367	4.40	1/8/2007	22.9	1.458	17.5	0.251	15.7	24.2	1/3/2007	0.724
2007-2008	0.115	1.38	3/6/2008	7.18	0.929	11.2	0.124	7.72	11.2	3/6/2008	0.999
2008-2009	0.105	1.26	3/27/2009	6.55	0.948	11.4	0.111	6.91	11.4	3/27/2009	1.000
2009-2010	0.202	2.42	3/1/2010	12.6	1.330	16.0	0.152	9.46	16.0	3/1/2010	0.999
2010-2011	0.217	2.60	2/9/2011	13.5	1.500	18.0	0.144	9.01	19.3	2/6/2011	0.935
2011-2012	0.157	1.88	4/4/2012	9.78	1.279	15.4	0.122	7.64	15.4	4/4/2012	0.997
MEAN:		1.87		9.71		12.6		8.90	13.4		0.961
ST. DEVIATION:		1.16		6.04		4.84		2.69	6.19		0.091
VARIANCE:		1.35		36.5		23.4		7.21	38.3		0.008

K Standardized SNODAS Station Variables for Cluster Analysis (stations AGLC2-BRTC2 shown)

SNODAS ID.	STATION TYPE	ELEV	LAT	LONG	BASIN	SLOPE	ASP.	CURV.	SWE	DEPTH
AGLC2	COOPB	-0.33	-1.62	0.96	-0.73	0.36	-1.62	1.27	-0.55	-0.49
AGRC2	COOPB	0.62	-1.69	0.78	-0.73	-0.96	-0.67	-0.09	-0.40	-0.38
AKNC2	UCOOP	-1.35	0.99	1.83	-1.29	-0.92	-0.67	-0.28	-0.64	-0.62
AKO	ASOS	-1.31	1.02	1.82	-1.29	-0.90	-0.67	0.34	-0.64	-0.63
AKRC2	COOPBC	-1.37	1.01	1.87	-1.29	-0.80	-1.62	-1.22	-0.64	-0.63
ALAC2	AHOS, COOPB †	0.08	-1.53	0.22	0.40	-0.59	-0.67	-1.27	-0.69	-0.83
ALEC2	COOPB, GOES	0.33	-0.41	-0.36	0.96	-0.95	-0.67	0.04	-0.20	-0.16
ALKC2	COOPB, GOES	0.46	1.04	0.45	-1.29	-0.40	1.22	-0.07	-0.32	-0.18
ALS	ASOS, COOPAB	0.08	-1.58	0.23	0.40	-0.81	1.22	-0.41	-0.69	-0.83
ANTC2	COOPABC, GOES	0.76	-0.10	0.22	-1.29	-0.92	1.22	0.04	-0.64	-0.69
APA	ASOS	-0.73	0.44	0.84	-1.29	0.84	-0.67	0.22	-0.59	-0.61
APNC2	COOPB, GOES	0.33	0.08	-0.33	0.96	-0.25	0.28	-0.73	0.68	0.85
APSC2	SNOTEL	1.29	-1.67	0.71	-0.73	-0.55	-0.67	-2.06	0.42	0.60
ARBC2	COOPAB	-0.58	-1.97	-0.71	0.96	-0.79	-0.67	-0.06	-0.59	-0.63
ARGC2	GOES	0.76	-0.05	-0.01	-0.73	-0.63	-1.62	0.95	-0.48	-0.46
AROC2	SNOTEL	1.12	0.78	0.30	0.96	0.06	1.22	0.18	1.40	1.56
ARPC2	SNOTEL	1.76	1.19	-0.08	0.96	-0.22	-0.67	-0.07	2.53	2.36
ASE	AHOS, ASOS †	0.19	0.12	-0.37	0.96	2.68	1.22	0.00	0.31	0.43
ASIC2	UCOOP	0.89	0.70	0.46	-1.29	-0.96	-0.67	-0.04	-0.40	-0.20
ASPC2	COOPAB	0.33	0.09	-0.35	0.96	-0.70	-0.67	0.14	0.60	0.71
ATBC2	AHOS, COOPAB	-0.81	0.39	-1.27	0.96	0.23	0.28	0.14	-0.51	-0.53
AVNC2	UCOOP	0.53	0.54	-0.18	0.96	-0.96	-0.67	-0.11	0.02	0.11
BALC2	AMRAD, GOES	0.68	0.39	0.44	-1.29	-0.73	1.22	-0.12	-0.37	-0.23
BAWC2	AMOS, GOES	0.24	0.27	0.55	-1.29	-0.82	1.22	0.00	-0.43	-0.38
BAYC2	UCOOP	0.27	-1.70	-0.85	0.96	-0.98	-0.67	0.05	-0.23	-0.12
BCKC2	GOES	-1.50	-0.87	1.50	-0.73	-0.85	1.22	0.13	-0.70	-0.80
BCRU1	GOES	-0.89	0.19	-1.78	0.96	-0.75	1.22	-0.18	-0.61	-0.72
BCVC2	SNOTEL	0.57	0.48	-0.15	0.96	-0.66	0.28	-0.04	0.86	1.00
BEDC2	COOPAB	-1.15	-0.72	-1.58	0.96	-0.72	0.28	-0.01	-0.75	-0.96
BHRC2	GOES	0.59	-1.97	0.03	0.40	-0.40	-0.67	-0.24	-0.31	-0.29
BKFC2	COOPAB	-0.19	-0.06	0.87	-0.73	-0.80	-1.62	-1.38	-0.62	-0.62
BKRC2	COOPB, GOES	1.40	0.30	0.12	0.96	-0.84	-0.67	-0.84	0.67	0.90
BLKC2	SNOTEL	1.01	1.15	0.37	0.96	1.42	1.22	-0.22	1.91	1.77
BLNC2	COOPAB	0.19	-1.57	0.44	0.40	-0.67	0.28	-1.00	-0.63	-0.67
BLPC2	GOES	1.45	-1.24	-0.31	0.40	-0.85	1.22	0.06	0.69	0.73
BLRC2	GOES	0.69	0.50	0.11	0.96	-0.89	-0.67	-1.05	-0.19	-0.04
BLSC2	AHOS, SNOTEL	1.74	0.64	-0.66	0.96	-0.80	1.22	-0.39	3.26	2.76
BMKC2	COOPAB	0.11	-0.60	-0.55	0.96	-0.86	1.22	-0.09	-0.24	-0.21
BNVC2	COOPAB	0.29	-0.23	0.08	-0.73	-0.86	-1.62	3.34	-0.66	-0.71
BOSC2	COOPB	-1.34	-0.88	1.17	-0.73	-0.74	1.22	-0.08	-0.71	-0.84
BOUC2	COOPAB	-0.90	0.85	0.59	-1.29	-0.88	1.22	2.20	-0.58	-0.52
BPRC2	COOPB, GOES	-0.97	1.62	-1.60	0.96	-0.68	-0.67	0.24	-0.69	-0.83
BREC2	UCOOP	1.05	0.39	0.12	0.96	0.09	-0.67	0.25	0.57	0.85
BRIC2	COOPAB	-1.13	0.81	0.85	-1.29	-0.39	1.22	1.39	-0.65	-0.72
BRMC2	AHOS, SNOTEL	1.58	-0.01	-0.17	0.96	-0.92	1.22	-0.24	0.85	1.12
BRTC2	AHOS, SNOTEL	2.05	-1.31	-0.75	0.40	-0.84	1.22	-0.29	2.47	2.59

† Station operated and maintained by numerous authorities; some assignments have been omitted for clarity

L Biplots for All Factor Axes Produced by the PCA

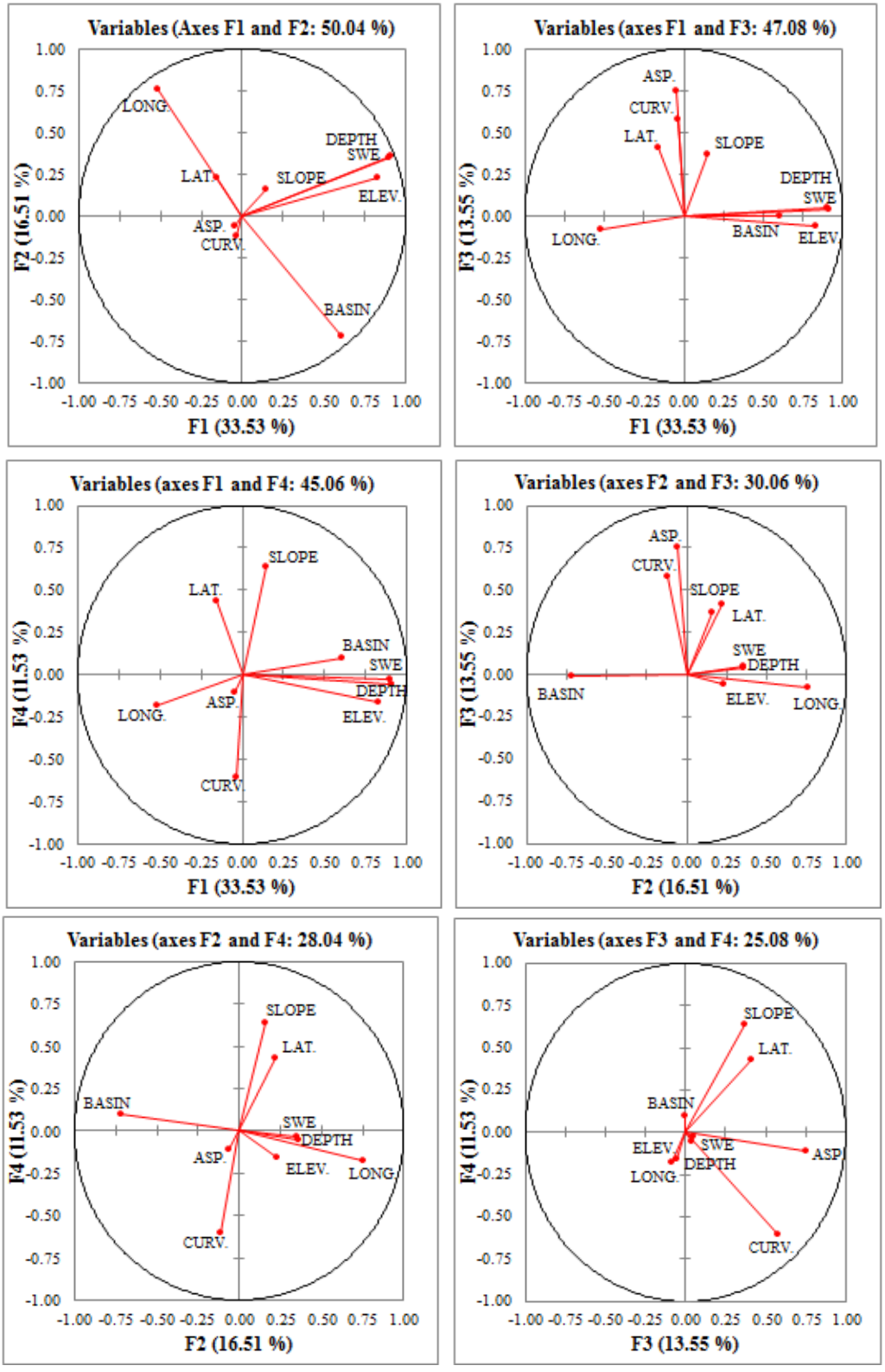

Prepared using XLSTAT Pro Statistical Software (Addinsoft 2013)

M Results from Hybrid Clustering Analysis

(1) Prelim. AHC Analysis

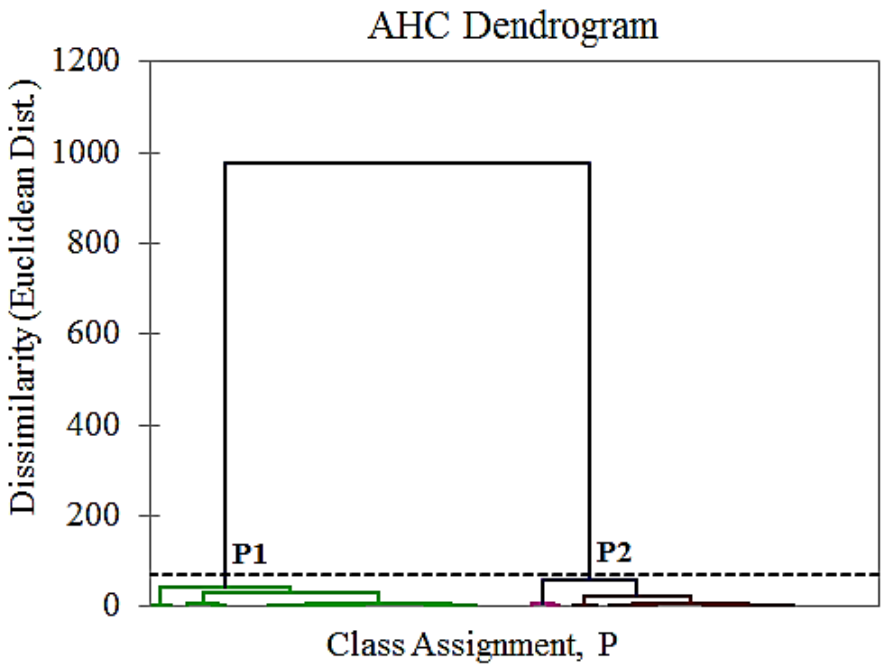

Class Centroids from Preliminary AHC:

Class	ELEV.	SWE	DEPTH
1	0.404	-0.236	-0.198
2	-0.422	0.136	0.087

(2) k-means Analysis

Statistics for Each k-means Iteration:

Iteration No.	Within-Class Var	Trace(W)	Det(W)	Wilks' Lambda
0	1.177	690	360280	0.265
1	1.177	690	360280	0.265

Variance decomposition for the optimal classification:

	Absolute	Percent
Within-class	1.18	0.392
Between-classes	1.83	0.608
Total	3.01	1.000

M (*Continued*)

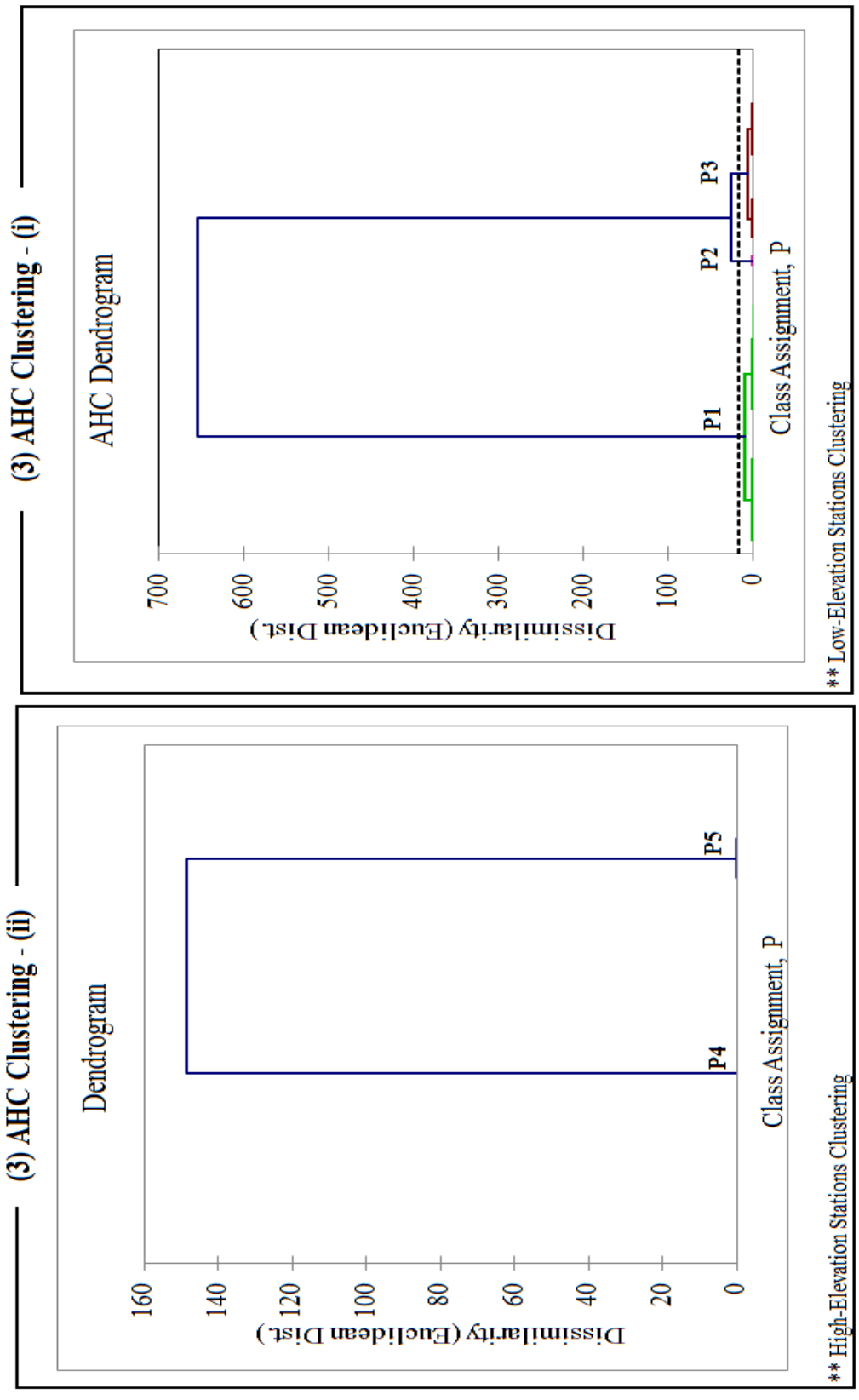
(3) AHC Clustering - (i)
AHC Dendrogram
Dissimilarity (Euclidean Dist.)
700
600
500
400
300
200
100
0
P1
P2
P3
Class Assignment, P
** Low-Elevation Stations Clustering
(3) AHC Clustering - (ii)
Dendrogram
Dissimilarity (Euclidean Dist.)
160
140
120
100
80
60
40
20
0
P4
P5
Class Assignment, P
** High-Elevation Stations Clustering

N Supplemental Plots of Snow Depth-Load Regression Analysis for AHC Method

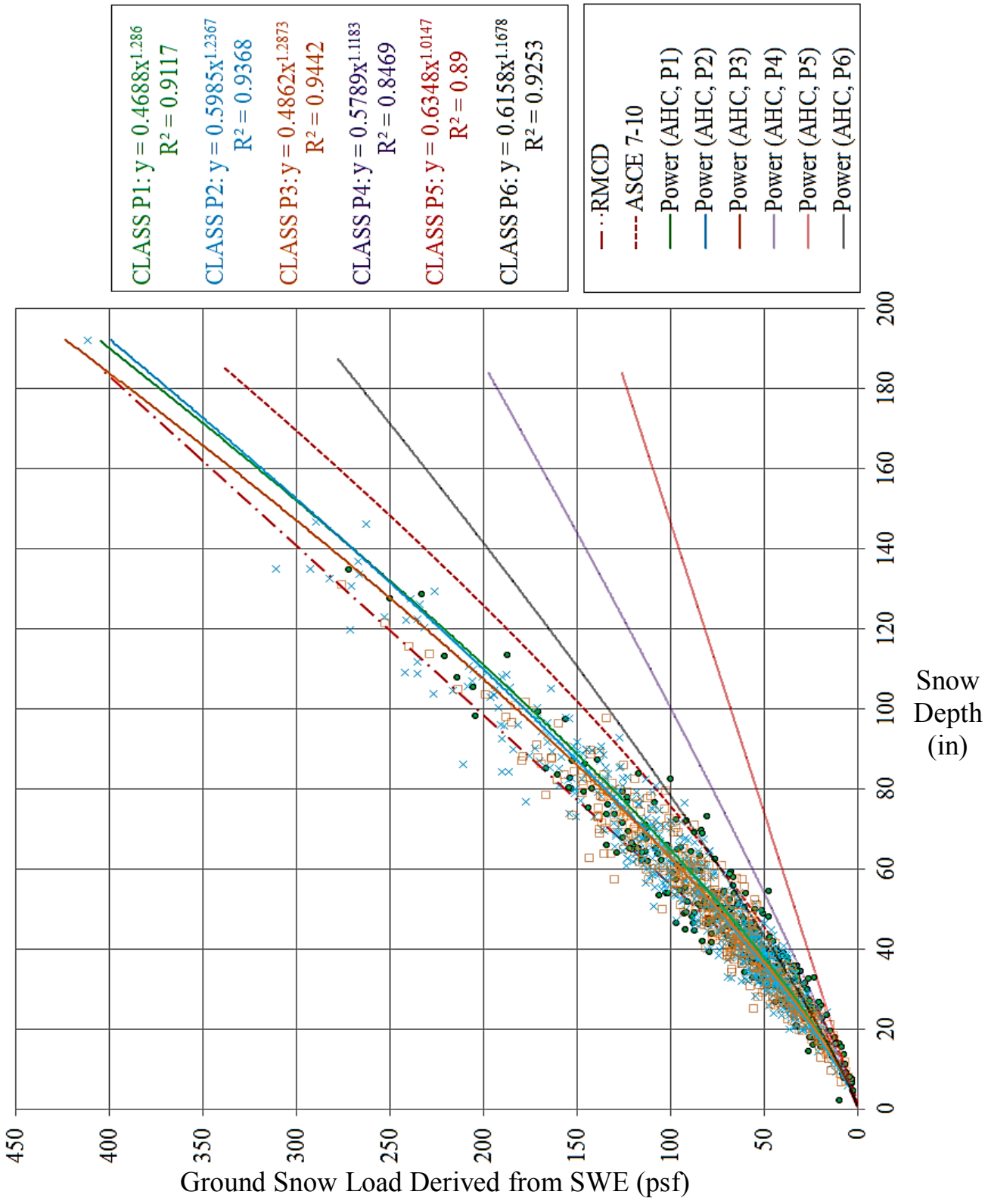

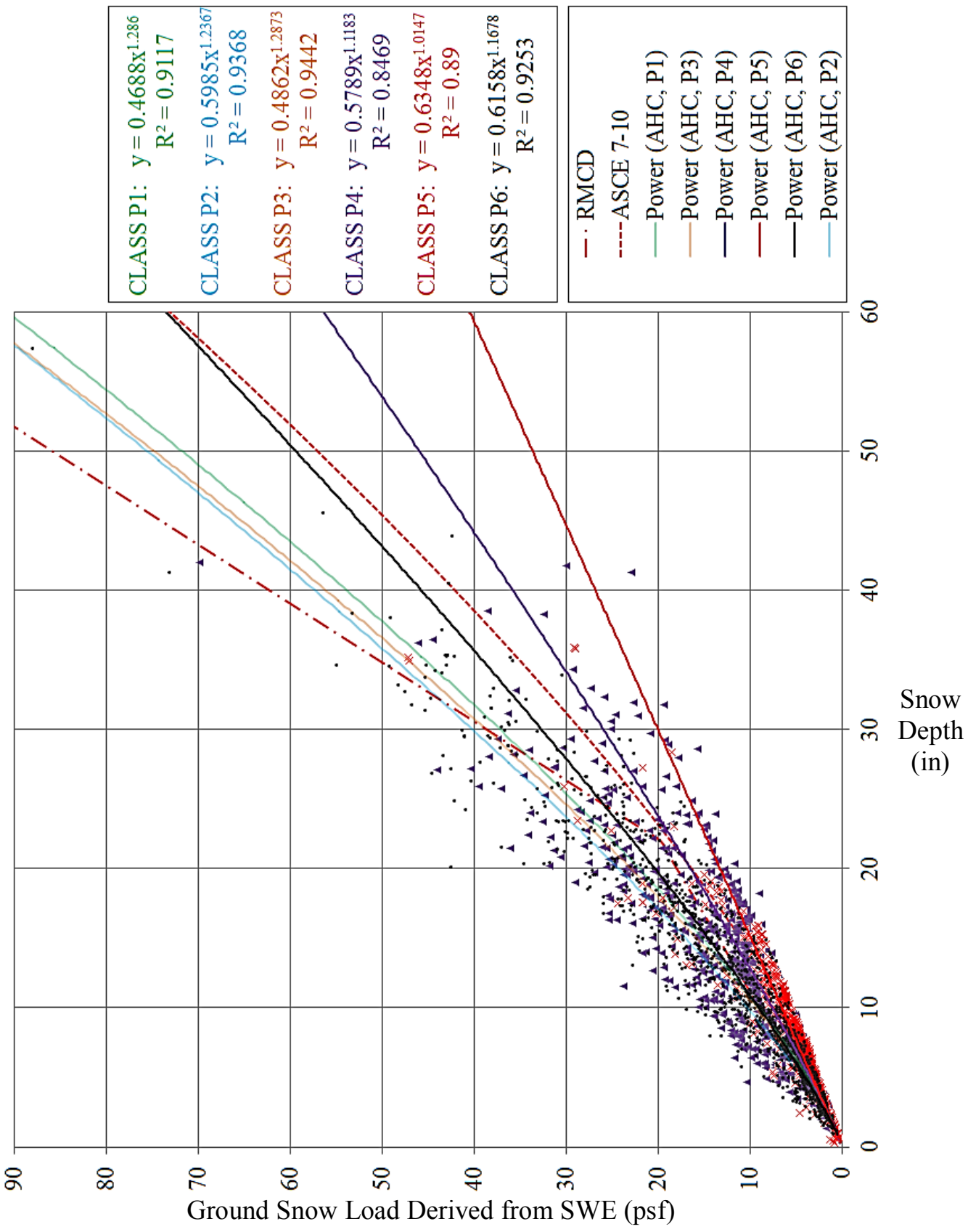
CLASS P1: y = 0.4688x^1.286 R² = 0.9117
CLASS P2: y = 0.5985x^1.2367 R² = 0.9368
CLASS P3: y = 0.4862x^1.2873 R² = 0.9442
CLASS P4: y = 0.5789x^1.1183 R² = 0.8469
CLASS P5: y = 0.6348x^1.0147 R² = 0.89
CLASS P6: y = 0.6158x^1.1678 R² = 0.9253
RMCD
ASCE 7-10
Power (AHC, P1)
Power (AHC, P3)
Power (AHC, P4)
Power (AHC, P5)
Power (AHC, P6)
Power (AHC, P2)
0
10
20
30
40
50
60
70
80
90
Ground Snow Load Derived from SWE (psf)
0
10
20
30
40
50
60
Snow Depth (in)

O Supplemental Plots of Snow Depth-Load Regression Analysis for k-means Clustering Method

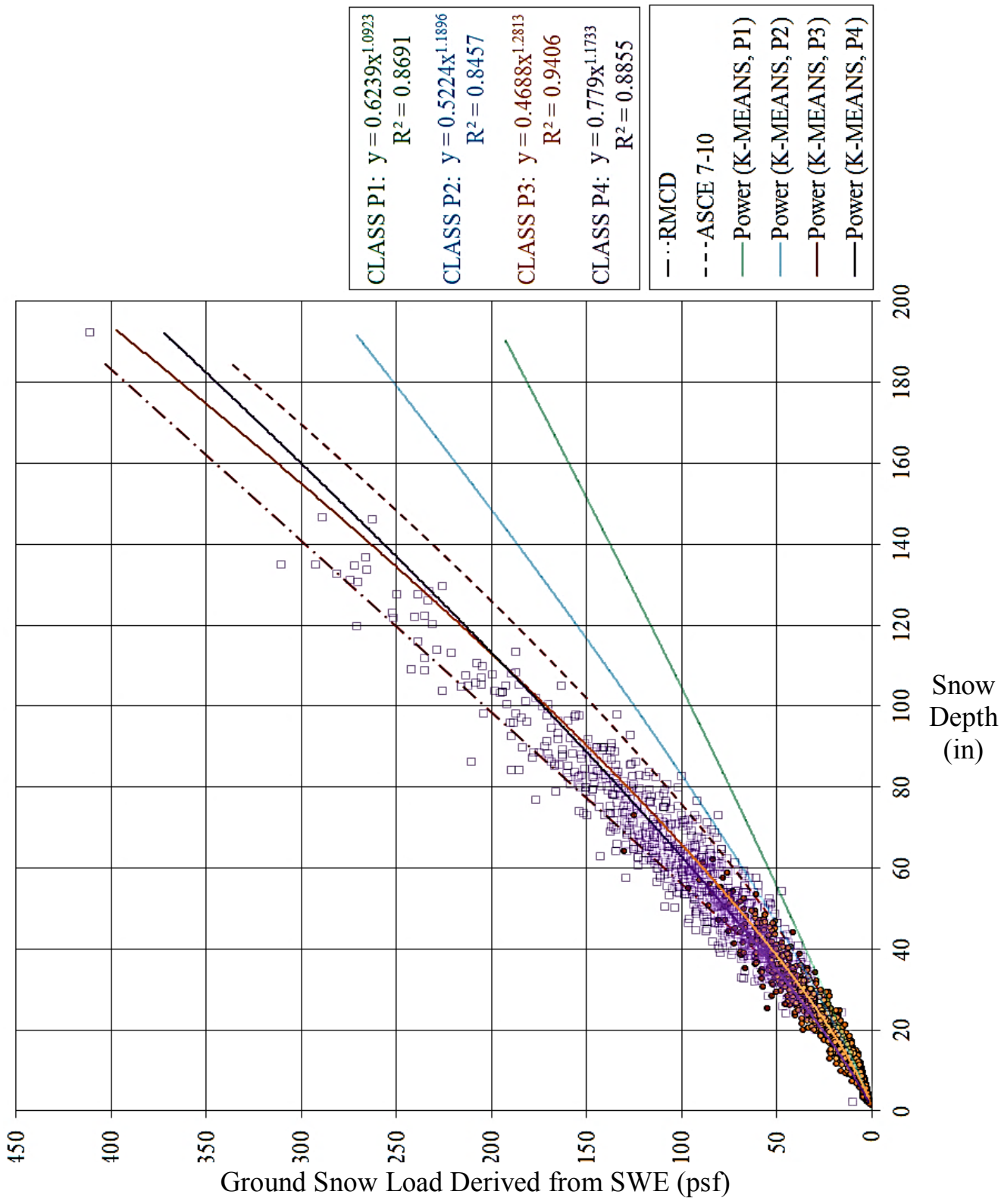

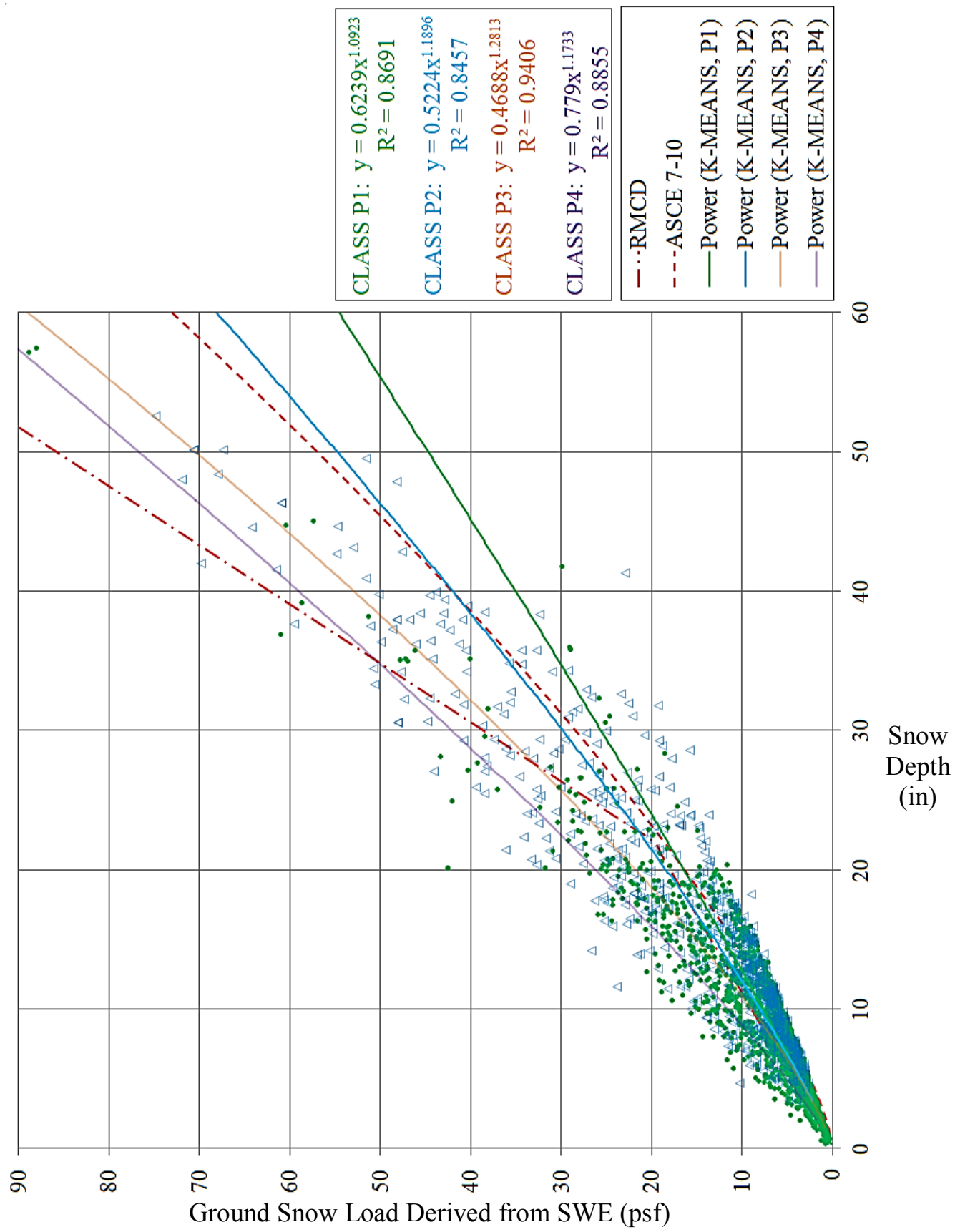
CLASS P1: y = 0.6239x^1.0923
R² = 0.8691
CLASS P2: y = 0.5224x^1.1896
R² = 0.8457
CLASS P3: y = 0.4688x^1.2813
R² = 0.9406
CLASS P4: y = 0.779x^1.1733
R² = 0.8855
RMCD
ASCE 7-10
Power (K-MEANS, P1)
Power (K-MEANS, P2)
Power (K-MEANS, P3)
Power (K-MEANS, P4)
0
10
20
30
40
50
60
70
80
90
Ground Snow Load Derived from SWE (psf)
0
10
20
30
40
50
60
Snow Depth (in)

P Supplemental Plots of Snow Depth-Load Regression Analysis for PCA-Based Clustering Method

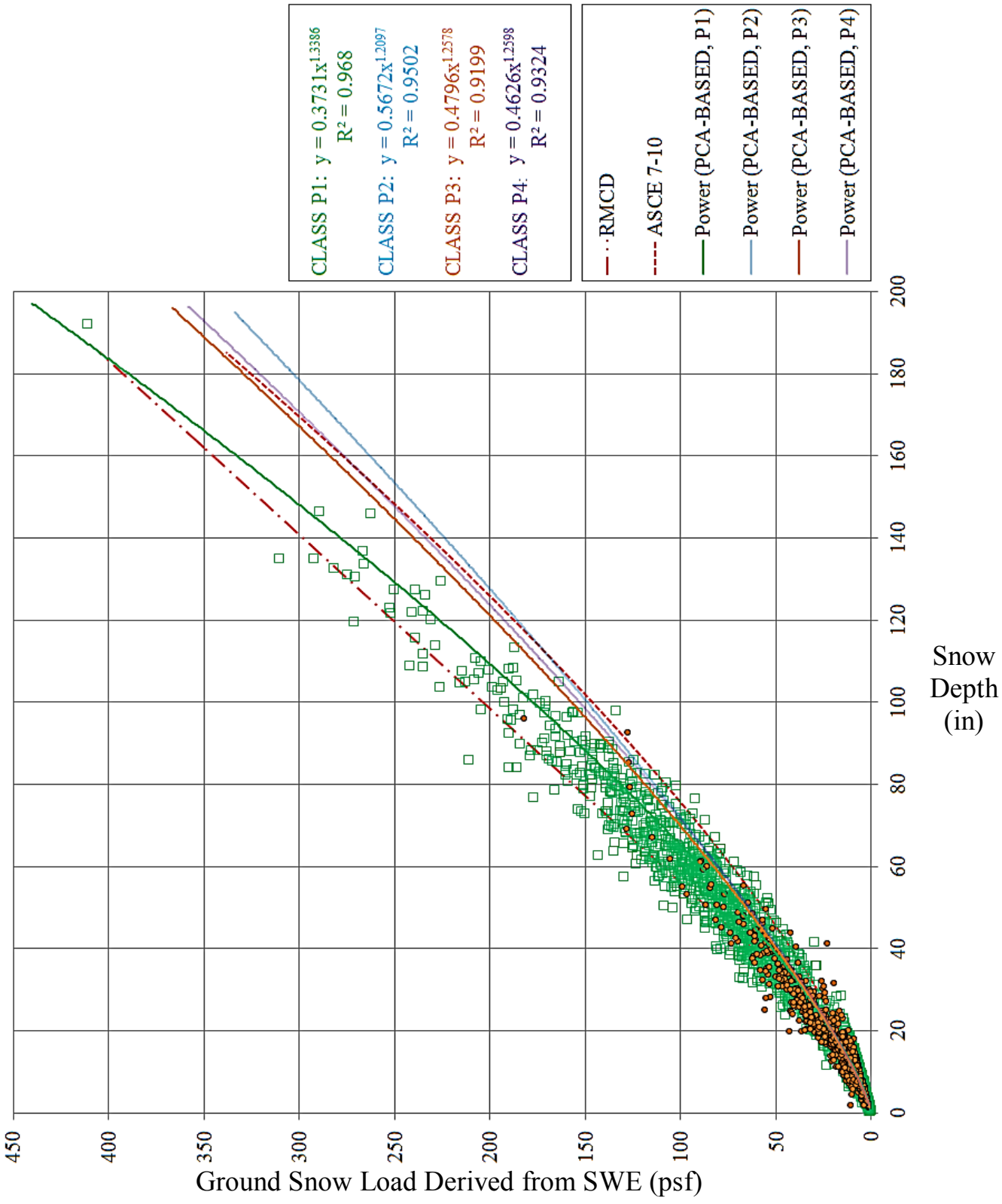

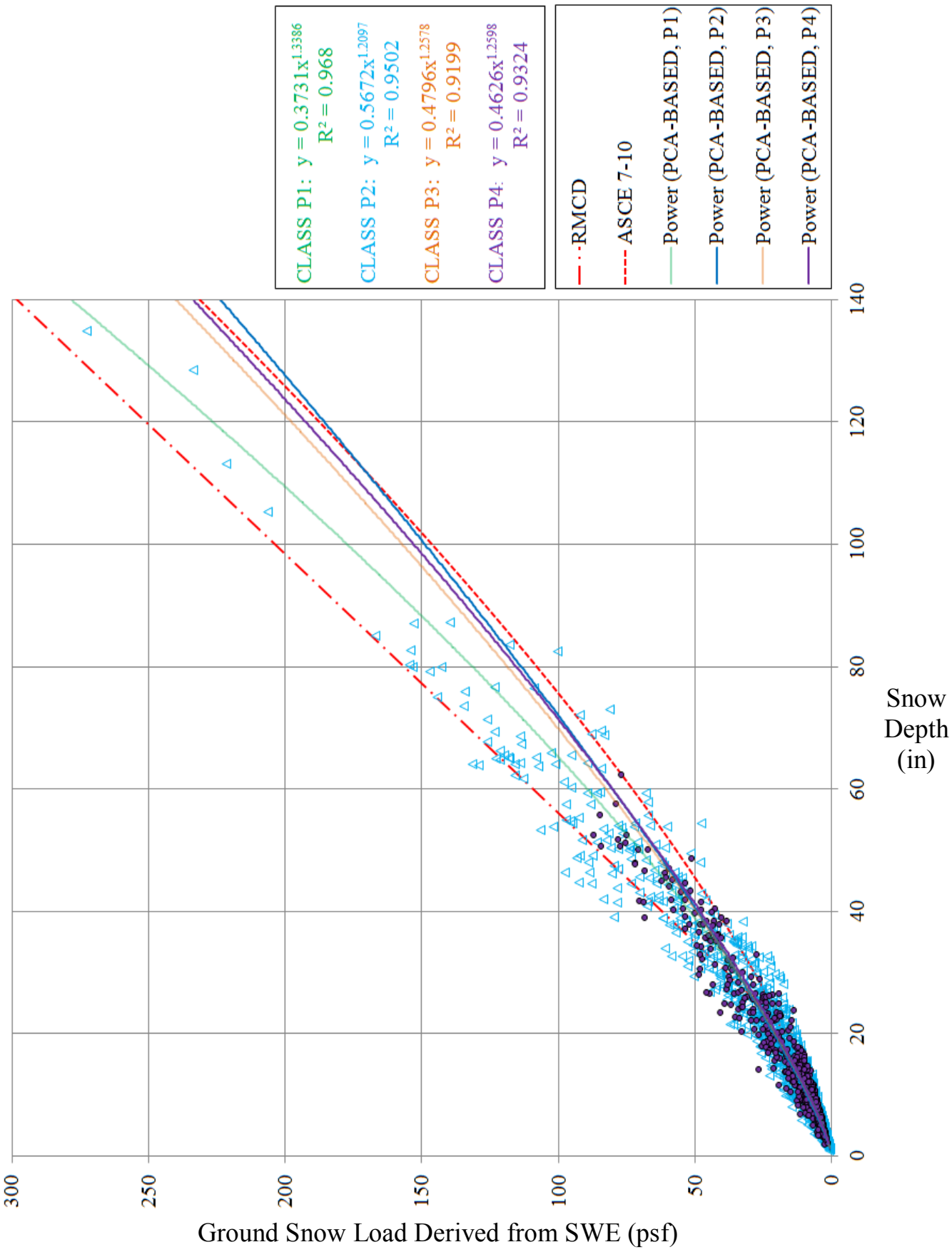
CLASS P1: y = 0.3731x^1.3386 R² = 0.968
CLASS P2: y = 0.5672x^1.2097 R² = 0.9502
CLASS P3: y = 0.4796x^1.2578 R² = 0.9199
CLASS P4: y = 0.4626x^1.2598 R² = 0.9324
RMCD
ASCE 7-10
Power (PCA-BASED, P1)
Power (PCA-BASED, P2)
Power (PCA-BASED, P3)
Power (PCA-BASED, P4)
0
20
40
60
80
100
120
140
Snow Depth (in)
0
50
100
150
200
250
300
Ground Snow Load Derived from SWE (psf)

Q Supplemental Plots of Snow Depth-Load Regression Analysis for Hybrid Clustering Method

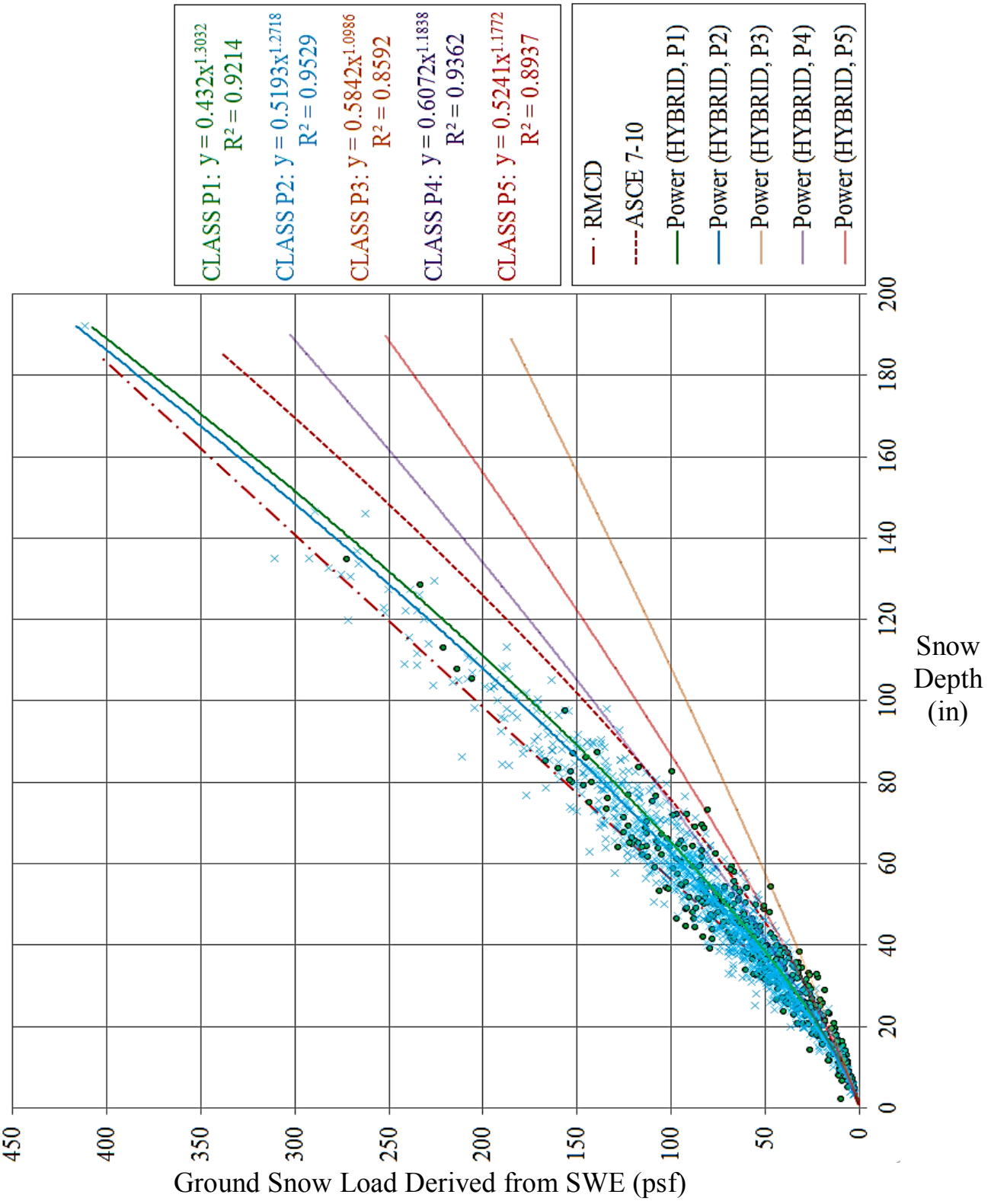

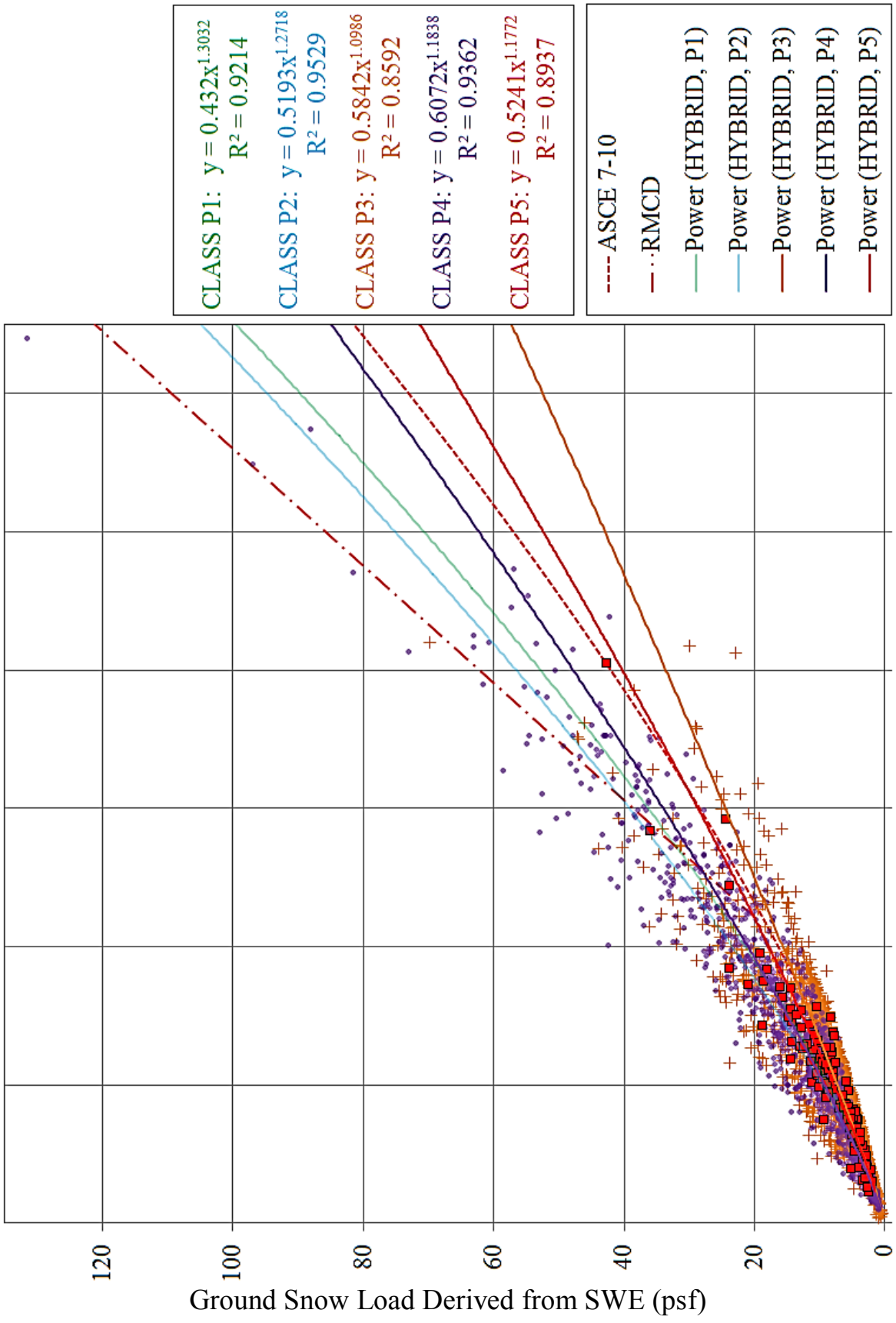
CLASS P1: y = 0.432x^1.3032 R² = 0.9214
CLASS P2: y = 0.5193x^1.2718 R² = 0.9529
CLASS P3: y = 0.5842x^1.0986 R² = 0.8592
CLASS P4: y = 0.6072x^1.1838 R² = 0.9362
CLASS P5: y = 0.5241x^1.1772 R² = 0.8937
ASCE 7-10
RMCD
Power (HYBRID, P1)
Power (HYBRID, P2)
Power (HYBRID, P3)
Power (HYBRID, P4)
Power (HYBRID, P5)
0
20
40
60
80
100
120
Ground Snow Load Derived from SWE (psf)
0
10
20
30
40
50
60
Snow Depth (in)

R NWS Cooperative Observer Stations in Colorado with Greater than 20 Years of Measured Snow Depths

No.	CO-OP ID #	STATION NAME	ELEV.	LAT.	LONG.	YEARS
1	050102	AGUILAR CO US	1951	37.4	-104.7	25
2	050114	AKRON 4 E CO US	1385	40.2	-103.2	40
3	050114	AKRON WASHINGTON CO	1421	40.2	-103.2	48
4	050130	ALAMOSA SAN LUIS VALLEY	2296	37.4	-105.9	64
5	050185	ALLENSPARK 3 NW CO US	2591	40.2	-105.5	56
6	050214	ALTENBERN CO US	1730	39.5	-108.4	64
7	050228	AMES CO US	2652	37.9	-107.9	38
8	050242	AMY CO US	1598	38.9	-103.7	25
9	050263	ANTERO	2719	39.0	-105.9	46
10	050310	ARBOLES 1 W CO US	1891	37.0	-107.4	49
11	050372	ASPEN 1 SW CO US	2456	39.2	-106.8	64
12	050437	AYER RANCH CO US	2205	39.0	-104.6	22
13	050454	BAILEY CO US	2356	39.4	-105.5	64
14	050674	BERTHOUD PASS CO US	3448	39.8	-105.8	35
15	050776	BLANCA 4 NW CO US	2390	37.5	-105.5	58
16	050797	BLUE MESA LAKE CO US	2307	38.5	-107.2	45
17	050825	BONHAM RESERVOIR CO US	3003	39.1	-107.9	49
18	050834	BONNY DAM 2 NE CO US	1142	39.6	-102.2	46
19	050848	BOULDER CO US	1672	40.0	-105.3	64
20	050895	BRANDON CO US	1196	38.5	-102.4	44
21	050898	BRANSON CO US	1914	37.0	-103.9	26
22	050909	BRECKENRIDGE CO US	2920	39.5	-106.0	64
23	050945	BRIGGSDALE CO US	1473	40.6	-104.3	48
24	050950	BRIGHTON 3 SE CO US	1529	39.9	-104.8	39
25	051017	BROWNS PARK REFUGE CO	1632	40.8	-108.9	31
26	051060	BUCKHORN MOUNTAIN 1 E	2256	40.6	-105.3	23
27	051071	BUENA VISTA 2 S CO US	2422	38.8	-106.1	64
28	051121	BURLINGTON CO US	1266	39.3	-102.3	48
29	051157	BUTLER RANCH CO US	1479	38.0	-104.5	25
30	051179	BYERS 5 ENE CO US	1595	39.7	-104.2	22
31	051179	BYERS 5 ENE CO US	1555	39.7	-104.1	42
32	051186	CABIN CREEK CO US	3054	39.7	-105.7	44
33	051268	CAMPO 7 S CO US	1255	37.0	-102.6	45
34	051294	CANON CITY CO US	1636	38.5	-105.2	64
35	051401	CASTLE ROCK CO US	1936	39.4	-104.8	43
36	051443	CEDAREDGE 3 E CO US	2075	38.9	-107.9	64
37	051458	CENTER 4 SSW CO US	2339	37.7	-106.1	61
38	051528	CHEESMAN CO US	2097	39.2	-105.3	64
39	051547	CHERRY CREEK DAM CO US	1721	39.6	-104.8	52
40	051564	CHEYENNE WELLS CO US	1314	38.8	-102.4	64
41	051609	CIMARRON CO US	2137	38.4	-107.6	45
42	051660	CLIMAX CO US	3442	39.4	-106.2	63
43	051713	COCHETOPA CREEK CO US	2439	38.4	-106.8	64
44	051745	COLLBRAN 3 ENE CO US	1970	39.3	-107.9	22
45	051772	COLORADO NATIONAL	1762	39.1	-108.7	64
46	051778	COLORADO SPRINGS AIR.	1884	38.8	-104.7	64
47	051886	CORTEZ CO US	1880	37.3	-108.6	64

48	051928	CRAIG CO US	1914	40.5	-107.6	28
49	051932	CRAIG 4 SW CO US	1980	40.5	-107.6	35
50	051948	CREEDE WATER TREATMENT	2629	37.8	-106.9	33
51	051959	CRESTED BUTTE CO US	2702	38.9	-107.0	64
52	051964	CRESTONE 2 SE CO US	2440	38.0	-105.7	30
53	051977	CRIPPLE CREEK 3 NNW CO US	2815	38.8	-105.2	64
54	052178	DELHI CO US	1552	37.6	-104.0	26
55	052184	DEL NORTE 2 E CO US	2397	37.7	-106.3	64
56	052196	DELTA 3 E CO US	1532	38.8	-108.0	44
57	052220	DENVER STAPLETON CO US	1611	39.8	-104.9	64
58	052281	DILLON 1 E CO US	2763	39.6	-106.0	64
59	052286	DINOSAUR NATIONAL MNMT	1820	40.2	-109.0	47
60	052312	DOHERTY RANCH CO US	1564	37.4	-103.9	32
61	052326	DOLORES CO US	2118	37.5	-108.5	56
62	052441	DURANGO CO US	2061	37.3	-107.9	64
63	052446	EADS CO US	1284	38.5	-102.8	64
64	052454	EAGLE CO AIRPORT CO US	1980	39.7	-106.9	46
65	052761	ESTES PARK 1 SSE CO US	2373	40.4	-105.5	64
66	052790	EVERGREEN CO US	2129	39.6	-105.3	51
67	052932	FLAGLER 1 S CO US	1516	39.3	-103.1	49
68	052947	FLEMING 3 SW CO US	1297	40.6	-102.9	64
69	052965	FLORISSANT FOSSL BED CO	2554	38.9	-105.3	23
70	052997	FORDER 8 S CO US	1458	38.6	-103.7	31
71	053002	FORT CARSON BUTTS ARMY	1781	38.7	-104.8	22
72	053005	FORT COLLINS CO US	1525	40.6	-105.1	64
73	053016	FORT LEWIS CO US	2329	37.2	-108.1	64
74	053027	FORT LUPTON 2 SE CO US	1531	40.1	-104.8	27
75	053038	FORT MORGAN CO US	1329	40.3	-103.8	64
76	053063	FOUNTAIN CO US	1695	38.7	-104.7	49
77	053079	FOWLER 1 SE CO US	1320	38.1	-104.0	64
78	053116	FRASER CO US	2609	39.9	-105.8	64
79	053146	FRUITA CO US	1373	39.2	-108.7	64
80	053222	GARDNER CO US	2123	37.8	-105.2	23
81	053246	GATEWAY CO US	1401	38.7	-109.0	64
82	053258	GENOA CO US	1709	39.3	-103.5	64
83	053261	GEORGETOWN CO US	2597	39.7	-105.7	64
84	053359	GLENWOOD SPGS NUMBER 2	1797	39.5	-107.3	62
85	053489	GRAND JUNCTION 6 ESE CO	1451	39.0	-108.5	49
86	053500	GRAND LAKE 6 SSW CO US	2526	40.2	-105.9	58
87	053530	GRANT CO US	2644	39.5	-105.7	49
88	053541	GREAT SAND DUNES NAT CO	2494	37.7	-105.5	62
89	053553	GREELEY UNC CO US	1437	40.4	-104.7	64
90	053592	GREEN MOUNTAIN DAM CO	2359	39.9	-106.3	64
91	053629	GROSS RESERVOIR CO US	2429	39.9	-105.4	34
92	053643	GROVER 10 W CO US	1551	40.9	-104.4	22
93	053656	GUFFEY 10 SE CO US	2620	38.7	-105.4	56
94	053662	GUNNISON 3 SW CO US	2323	38.5	-107.0	64
95	053742	HAMILTON 1 SSE CO US	1945	40.4	-107.6	64
96	053828	HASWELL CO US	1378	38.4	-103.2	64
97	053850	HAWTHORNE CO US	1806	39.9	-105.3	27
98	053867	HAYDEN CO US	1971	40.5	-107.3	64
99	053951	HERMIT 7 ESE CO US	2758	37.8	-107.1	64
100	053982	HIGBEE 2 SW CO US	1296	37.8	-103.5	32
101	054054	HOHNHOLZ RANCH CO US	2365	41.0	-106.0	26

102	054078	HOLLY 1 NW CO US	1039	38.1	-102.1	64
103	054129	HOT SULPHUR SPRINGS 2 SW	2318	40.1	-106.2	28
104	054135	HOURGLASS RESERVOIR CO	2902	40.6	-105.6	23
105	054172	HUGO 1 NW CO US	1532	39.1	-103.5	22
106	054234	IDAHO SPRINGS CO US	2303	39.8	-105.5	26
107	054242	IDALIA CO US	1209	39.7	-102.3	64
108	054250	IGNACIO 1 N CO US	1969	37.1	-107.6	44
109	054270	INDEPENDENCE PASS 5 SW	3200	39.1	-106.6	32
110	054293	INTER CANYON CO US	2146	39.6	-105.2	34
111	054380	JOES CO US	2309	37.0	-105.6	32
112	054380	JOES CO US	1296	39.7	-102.7	32
113	054388	JOHN MARTIN DAM CO US	1163	38.1	-102.9	64
114	054413	JULESBURG CO US	1057	41.0	-102.3	64
115	054444	KARVAL CO US	1547	38.7	-103.5	64
116	054452	KASSLER CO US	1703	39.5	-105.1	64
117	054460	KAUFFMAN 4 SSE CO US	1600	40.9	-103.9	37
118	054538	KIM 15 NNE CO US	1582	37.5	-103.3	32
119	054546	KIM 10 SSE CO US	1615	37.1	-103.3	23
120	054584	KIOWA 5 SE CO US	1937	39.3	-104.4	46
121	054603	KIT CARSON CO US	1306	38.8	-102.8	29
122	054664	KREMMLING CO US	2274	40.1	-106.4	64
123	054720	LA JUNTA MUNICIPAL	1278	38.0	-103.5	64
124	054726	LA JUNTA 20 S CO US	1283	37.8	-103.5	30
125	054735	LAKE CITY NUMBER 2 CO US	2644	38.0	-107.3	64
126	054742	LAKE GEORGE 8 SW CO US	2606	38.9	-105.5	52
127	054762	LAKEWOOD CO US	1719	39.7	-105.1	50
128	054770	LAMAR CO US	1106	38.1	-102.6	64
129	054834	LAS ANIMAS CO US	1186	38.1	-103.2	64
130	054885	LEADVILLE LAKE CO	3029	39.2	-106.3	60
131	054934	LEMON DAM CO US	2550	37.4	-107.7	30
132	054945	LEROY 9 WSW CO US	1363	40.5	-103.0	58
133	055001	LIME 3 SE CO US	1387	40.5	-103.1	58
134	055017	LIMON CO US	1637	39.3	-103.7	23
135	055018	LIMON WSMO CO US	1695	39.2	-103.7	24
136	055020	LIMON HASS RANCH CO US	1678	39.0	-103.7	56
137	055040	LITTLE DOLORES CO US	1479	39.8	-103.5	54
138	055048	LITTLE HILLS CO US	1872	40.0	-108.2	43
139	055116	LONGMONT 2 ESE CO US	1509	40.3	-105.2	48
140	055236	LOVELAND 2 N CO US	1548	40.4	-105.1	22
141	055327	MANCOS CO US	2105	37.4	-108.4	47
142	055408	MARVINE CO US	2195	40.0	-107.6	53
143	055414	MARVINE RANCH CO US	2377	40.0	-107.4	26
144	055446	MAYBELL CO US	1812	40.5	-108.1	54
145	055484	MEEKER CO US	1884	40.0	-108.0	59
146	055489	MEEKER 10 NW CO US	1935	40.0	-107.9	59
147	055507	MEREDITH CO US	2385	39.4	-106.7	44
148	055520	MESA LAKES RESORT CO US	2989	39.1	-108.1	26
149	055531	MESA VERDE NATIONAL	2160	37.2	-108.5	64
150	055706	MONTE VISTA 2 W CO US	2336	37.6	-106.2	33
151	055722	MONTROSE NUMBER 2 CO US	1765	38.5	-107.9	64
152	055922	NEW RAYMER CO US	1458	40.6	-103.8	38
153	055970	NORTHDALE CO US	2036	37.8	-109.0	54
154	055984	NORTHGLENN CO US	1648	39.9	-105.0	27
155	055990	NORTH LAKE CO US	2684	37.2	-105.1	32

156	056013	NORWOOD NUMBER 2 CO US	2137	38.1	-108.3	64
157	056116	OLATHE 4 SSW CO US	1706	38.6	-108.0	28
158	056131	ORDWAY 2 ENE CO US	1315	38.2	-103.7	64
159	056136	ORDWAY 21 N CO US	1453	38.5	-103.7	32
160	056192	OTIS 11 NE CO US	1274	40.3	-102.8	36
161	056205	OURAY NUMBER 2 CO US	2352	38.0	-107.7	23
162	056259	PAGOSA SPRINGS 2 W CO US	2320	37.3	-107.1	62
163	056266	PALISADE CO US	1448	39.1	-108.4	64
164	056271	PALISADE LAKES 6 SSE CO US	2467	37.4	-107.2	23
165	056280	PALMER LAKE CO US	2213	39.1	-104.9	47
166	056306	PAONIA 1 SW CO US	1700	38.9	-107.6	55
167	056320	PARADOX 2 N CO US	1660	38.4	-108.9	64
168	056326	PARKER 6 E CO US	1923	39.5	-104.7	49
169	056342	PARSHALL 10 SSE CO US	2522	39.9	-106.1	21
170	056410	PENROSE CO US	1650	38.5	-105.1	24
171	056513	PITKIN CO US	2804	38.6	-106.5	35
172	056559	PLATORO CO US	2997	37.4	-106.5	40
173	056740	PUEBLO MEMORIAL AIRPORT	1439	38.3	-104.5	58
174	056743	PUEBLO CITY RESERVOIR CO	1430	38.3	-104.7	22
175	056765	PUEBLO RESERVOIR CO US	1480	38.3	-104.7	37
176	056797	PYRAMID CO US	2441	40.2	-107.1	57
177	056816	RALSTON RESERVOIR CO US	1798	39.8	-105.2	34
178	056832	RANGELY 1 E CO US	1611	40.1	-108.8	62
179	056930	RED FEATHER LAKES 6 CO US	2318	40.7	-105.5	30
180	057017	RICO CO US	2682	37.7	-108.0	53
181	057020	RIDGWAY CO US	2144	38.2	-107.8	30
182	057031	RIFLE CO US	1657	39.5	-107.8	43
183	057050	RIO GRANDE RESERVOIR CO	2953	37.7	-107.3	35
184	057167	ROCKY FORD 2 SE CO US	1271	38.0	-103.7	64
185	057287	RUSH 1 N CO US	1862	38.9	-104.1	39
186	057287	RUSH 1 N CO US	1845	38.9	-104.1	23
187	057309	RUXTON PARK CO US	2758	38.8	-105.0	51
188	057430	SAN LUIS 1 S CO US	2421	37.2	-105.4	26
189	057455	SAPINERO 8 E CO US	2953	37.8	-107.1	59
190	057460	SARGENTS CO US	2579	38.4	-106.4	52
191	057510	SEDALIA 4 SSE CO US	1821	39.4	-105.0	56
192	057513	SEDGWICK CO US	1092	40.9	-102.5	58
193	057515	SEDGWICK 5 S CO US	1216	40.9	-102.5	54
194	057572	SHEEP MOUNTAIN CO US	2363	37.7	-105.2	24
195	057618	SHOSHONE CO US	1826	39.6	-107.2	64
196	057656	SILVERTON CO US	2830	37.8	-107.7	62
197	057862	SPRINGFIELD CO US	1345	37.4	-102.6	37
198	057866	SPRINGFIELD 7 WSW CO US	1409	37.4	-102.7	46
199	057936	STEAMBOAT SPRINGS CO US	2093	40.5	-106.8	64
200	057950	STERLING CO US	1211	40.6	-103.2	62
201	057992	STONINGTON CO US	1165	37.3	-102.2	29
202	058008	STRATTON CO US	1341	39.3	-102.6	64
203	058022	STRONTIA SPRINGS DAM CO	1780	39.4	-105.1	27
204	058064	SUGARLOAF RESERVOIR CO	2968	39.2	-106.4	64
205	058154	TACOMA CO US	2225	37.5	-107.8	38
206	058157	TACONY 13 SE CO US	1512	38.4	-104.1	48
207	058184	TAYLOR PARK CO US	2798	38.8	-106.6	64
208	058204	TELLURIDE 4 WNW CO US	2643	37.9	-107.9	60
209	058431	TRINIDAD RIVER CO US	1844	37.2	-104.5	44

210	058434	TRINIDAD PERRY STOKES	1751	37.3	-104.3	53
211	058436	TRINIDAD LAKE CO US	1923	37.2	-104.6	21
212	058454	TROUT LAKE CO US	2956	37.8	-107.9	38
213	058468	TROY 1 SE CO US	1710	37.1	-103.3	39
214	058510	TWO BUTTES CO US	1260	37.6	-102.4	24
215	058560	URAVAN CO US	1530	38.4	-108.7	51
216	058582	VALLECITO DAM CO US	2531	39.6	-106.4	38
217	058582	VALLECITO DAM CO US	2365	37.4	-107.6	64
218	058722	VONA CO US	1373	39.3	-102.7	34
219	058742	WAGON WHEEL GAP 3 N CO	2593	37.8	-106.8	23
220	058756	WALDEN CO US	2456	40.7	-106.3	40
221	058781	WALSENBURG 1 NW CO US	1920	37.6	-104.8	64
222	058793	WALSH 1 W CO US	1213	37.4	-102.3	61
223	058839	WATERDALE CO US	1594	40.4	-105.2	64
224	058931	WESTCLIFFE CO US	2396	38.1	-105.5	64
225	059058	WILD HORSE 6 N CO US	1437	40.2	-104.2	43
226	059096	WILLIAMS FORK DAM CO US	1337	38.7	-103.0	22
227	059147	WINDSOR CO US	2322	40.0	-106.2	34
228	059213	WOODROW 6 NNE CO US	2876	37.5	-106.9	45
229	059243	WRAY CO US	2310	37.0	-104.5	31
230	059246	WRAY 19 N CO US	1122	40.1	-102.2	43
231	059265	YAMPA CO US	1151	40.3	-102.3	56
232	059278	YELLOW JACKET 4 NE CO US	2091	37.5	-108.8	43
233	059297	YUMA 10 NW CO US	1262	40.1	-102.7	42